Cooperative Asymmetric Catalysis with Squaramide H-Bond Donors and Lewis Acids

Cooperative Asymmetric Catalysis with Squaramide H-Bond Donors and Lewis Acids

A dissertation presented

by

Anna Levina

to

The Department of Chemistry and Chemical Biology

in partial fulfillment of the requirements

for the degree of

Doctor of Philosophy

in the subject of

Chemistry

Harvard University

Cambridge, Massachusetts

June 2016

Dissertation Advisor: Eric N. Jacobsen *Anna Levina*

Cooperative Asymmetric Catalysis with Squaramide H-Bond Donors and Lewis Acids

Abstract

A new mode of cooperative catalysis with chiral squaramide hydrogen-bond donors and trialkylsilyl trifluoromethanesulfonates (triflates) for asymmetric nucleophilic additions to oxocarbenium ions was explored. Evidence is provided for a dual role of the squaramide catalyst: rate acceleration through activation of the silicon Lewis acid and enantioinduction through triflate anion-binding. In the first chapter, we present examples of current methodologies used for activation of Brønsted and Lewis acids in organocatalysis. In the rest of this thesis, we explore the mechanism and applications of cooperative catalysis with chiral squaramide hydrogen-bond donors and trialkylsilyl triflates.

In Chapter 2, we show that in the presence of trialkylsilyl triflate, chiral squaramides can catalyze highly enantioselective (4+3) cycloaddition reactions of pyruvic aldehyde dimethyl acetal derivatives with furans. Detailed mechanistic studies reveal the formation of a resting state complex between the squaramide catalyst and the trialkylsilyl triflate, which leads to enhanced Lewis acidity of silicon. The chiral squaramide catalyst then controls the stereoselectivity of the subsequent nucleophilic addition to the oxocarbenium through binding of the triflate anion.

Chapter 3 describes the development of an asymmetric squaramide and trialkylsilyl triflate co-catalyzed nucleophilic substitution of acetals. High enantioselectivities are achieved in this transformation with a range of nucleophiles spanning five orders of magnitude in

nucleophilicity parameter, from methallyltrimethylsilane to silyl ketene acetal. In Chapter 4, we expand this new reactivity concept to aldehyde substrates. A synthetically practical chiral squaramide is shown to catalyze an asymmetric Mukaiyama aldol reaction with moderate enantioselectivities.

Table of Contents

Abstract iii

Table of Contents v

Acknowledgement ix

List of Abbreviations xii

Chapter 1: Acid Activation Strategies for Asymmetric Organocatalysis 1

1.1. Introduction 1

1.2. Brønsted Acid Activation Strategies 2

1.2.1. Lewis Acid Activation of Brønsted Acids 2

1.2.2. Brønsted Acid Activation via Coordination to Hydrogen-Bond Donor 4

1.2.3. Enhancing Acidity of Hydrogen-Bond Donors via Coordination to Lewis and Brønsted Acids 6

1.3. Lewis Acid Activation Strategies 10

1.3.1. Lewis Base Activation of Lewis Acids 10

1.3.2. Brønsted Acid Activation of Lewis Acids 12

1.4. Conclusions and Outlook 13

Chapter 2: Development and Mechanistic Elucidation of an Squaramide-Catalyzed and Silyl Trifluoromethanesulfonate-Promoted Enantioselective (4+3) Cycloaddition 14

2.1. Introduction 14

2.2. Results and Discussion 17

2.2.1. Initial Findings 17

2.2.2. Elucidation of Squaramide-TESOTf Interactions 18

2.2.3. Catalyst Optimization 25

2.2.4. Investigation of Substrate Scope 28

2.3. Conclusion 30

2.4. Experimental Section 31

2.4.1. General Information 31

2.4.2. Preparation and Characterization of Squaramide Catalysts 32

2.4.3. Preparation and Characterization of Substrates 44

2.4.4. General Procedure for Squaramide-Catalyzed (4+3) Cycloaddition 48

2.4.5. Characterization of Products **2a**-**2l** 49

2.4.6. X-Ray Crystallographic Report 85

2.4.6.1. X-Ray Crystallographic Report for compound **2b** 85

2.4.6.2. X-Ray Crystallographic Report for compound **S4** 90

2.4.7. Procedure for ^{1}H NMR Studies on Starting Material Ionization 98

2.4.8. Examination of Solvent and Promoter 100

2.4.9. Catalyst Structure Investigation 101

2.4.10. Data for Kinetics Analysis with In Situ IR Spectroscopy and Derivation of Empirical Rate Laws 103

2.4.11. Procedure for In Situ IR Spectroscopy for Resting State B Characterization 118

2.4.12. NMR Binding Studies 119

2.4.13. Non-Linear Effects Study 125

2.4.14. Computational Studies 126

Chapter 3: Squaramide and Silyl Trifluoromethanesulfonate co-Catalyzed Asymmetric Additions of π-Nucleophiles to Acetals **131**

3.1. Introduction 131

3.2. Results and Discussion 132

3.2.1. Preliminary Experiments 132

3.2.2. Investigation of Acetal Structure 136

3.2.3. Investigation of Catalyst Structure 138

3.2.4. Optimization of Reaction Conditions 141

3.2.5. Acetal Scope and Limitations 143

3.2.6. Nucleophile Scope 147

3.3. Conclusion 149

3.4. Experimental Section 150

3.4.1. General Information 150

3.4.2. Characterization Data for Substrates **3a-3i** 151

3.4.3. General Procedure for Squaramide-Catalyzed (4+3) Nucleophilic Substitution of Acetals 156

3.4.4. Characterization of Products **4a-9g** 157

3.4.5. Additional Substrate Scope Studies 205

3.4.6. Additional Reaction Optimization Data 207

3.4.7. Absolute Confirmation Determination 209

Chapter 4: Squaramide and Silyl Trifluoromethanesulfonate co-Catalyzed Asymmetric Mukaiyama Aldol **211**

4.1. Introduction 211

4.2. Results and Discussion 212

4.2.1. Catalyst Optimization 212

4.2.2. Optimization of Reaction Conditions 215

4.2.3. Aldehyde Scope 218

4.2.4. Nucleophile Scope 220

4.2.5. Preparative Scale Reactions 222

4.3. Conclusion 223

4.4. Experimental Section 224

4.4.1. General Information 224

4.4.2. Synthesis and Characterization of Catalyst **3g** 225

4.4.3. General Procedure for Squaramide-Catalyzed Mukaiyama Aldol Reaction 226

4.4.4. Characterization of Products **2a**, **2r** and (*S*)-1-(4-bromophenyl)-3-methylbut-3-en-1-ol 227

4.4.5. Absolute Configuration Determination 235

4.4.6. Catalyst Optimization Studies 236

4.4.7. Reaction Optimization Studies 239

Acknowledgement

I would like to thank Eric Jacobsen for creating a unique working environment where I could feel both challenged and supported. I thank him for reminding me to constantly question my research direction and take a step back to see the big picture. Over the past four years, Eric has taught me not only how to be a better scientist, but also about how to best present my work. His focus on feedback regarding presentation style is truly unique and I will no doubt benefit from it in my further career.

I would also like to thank my committee members, Emily Balskus and Ted Betley. I was incredibly fortunate to have committee members who always came prepared to my GAC meetings, were supportive and asked insightful questions that helped redefine the direction of my research. I wanted to thank both Emily and Ted for encouraging me to focus on the mechanistic aspects of the research described in Chapter 2 of this thesis during my first GAC meeting. I am grateful for your thoughtful advice and support during my PhD.

Nicole Minotti is an unsung hero of the Jacobsen group! I want to take this opportunity to thank her for all the work she does to make sure Jacobsen lab runs smoothly.

I owe much of success in my PhD career to the amazing mentors I had during my undergrad. Greg Fu was very kind to find a spot for me in his lab. Through an amazing class (5.43) I took with him and his guidance in my research, Greg taught me how to think about chemistry and approach problems. My mentor in the Fu lab, Dr. Alex Bissember, patiently taught me proper chemistry techniques and how to utilize my time in the lab efficiently. Apart from doing research in the Fu group during my undergrad, I was lucky to have an opportunity to do two summer internships at Biogen. I would like to thank my mentors there: Dr. Adam Littke, Dr. Xianglin Shi and the whole Biogen Process Chemistry Department for giving me a chance to

experience research in the industry setting, teaching me about reaction optimization and for all the great time we had together.

I would like to thank all of the members of the Jacobsen group that overlapped with my time here. Special thanks to Steven Banik, who helped me transition into the Jacobsen group during my rotation, tried to keep his hood clean for me during that time and was an invaluable collaborator during my entire PhD career. Steven's contribution to the (4+3) cycloaddition project was instrumental to its success. I admire Steven for his creativity and fearless approach to science and I have learnt so much from him. Thanks to Andy Rötheli for being a great office mate and for finding time to help me set up and analyze biding studies and low-temperature NMR experiments. A very special thanks to my bay mate: Libby Hennessy, for tirelessly reading my thesis, being a great friend and getting me hooked on barre. Without Libby, both this thesis and I would be in a much worse shape.

I greatly benefited from advice and kindness of the Jacobsen group members over the past four years. Thank you Gary Zhang, Yongho Park, Charles Yeung, Rose Kennedy, Shauna Paradine and Chris Kim for letting me borrow catalysts and fragments. Thanks to all of the Tuesday subgroup members for their patience with my presentations and thoughtful advice.

I would like to thank my family back home and my family of Boston friends here. Thank you all for putting up with me! Huge thanks to my brother, Sergey, who being a PhD chemist himself, always had a practical advice, a sarcastic remark or a juicy chemistry gossip to offer depending on what I needed at the moment. I am so lucky to have you as a role model.

Finally, I would like to thank my husband Ivan for his love, support and endless understanding. You make everything more fun, including grad school.

For Ivan, who walked to the lab with me every day

List of Abbreviations

Ac	Acetyl
Ar	Aryl
Bn	Benzyl
Boc	*tert*-butoxycarbonyl
Bu	butyl
conv	conversion
DIPEA	*N,N*-diisopropylethylamine
ee	enantiomeric excess
ent	enantiomer
Et	ethyl
equiv	equivalents
ESI	electrospray ionization
Fmoc	9-fluorenylmethoxycarbonyl
FTIR	Fourier transform infrared spectroscopy
g	grams
GC	gas chromatography
h	hours
HBTU	O-(Benzotriazol-1-yl)-N,N,N’,N’-tetrameth
HPLC	high-performance liquid chromatography
Hz	hertz
i-Pr	isopropyl
IR	infrared

LDA	lithium *N,N*-diisopropylamide
M	molar
Me	methyl
min	minutes
mol	mole
MS	mass spectrometry
MTBE	methyl *tert*-butyl ether
NMR	nuclear magnetic resonance
n.r.	no reaction
Ph	phenyl
s	second
s-Bu	*sec*-butyl
t-Bu	*tert*-buty
TBS	*tert*-butyldimethylsilyl
TBSOTf	*tert*-butyldimethylsilyl trifluoromethanesulfonate
TES	triethylsilyl
TESOTf	triethylsilyl trifluoromethanesulfonate
Tf	trifluoromethanesulfonyl
TFA	trifluoroacetic acid
TfOH	trifluoromethanesulfonic acid
THF	tetrahydrofuran
TIPS	triisopropylsilyl
TIPSOTf	triisopropylsilyl trifluoromethanesulfonate

TMS	trimethylsilyl
TMSCl	trimethylsilyl chloride
TMSOTf	trimethylsilyl trifluoromethanesulfonate

Chapter 1

Acid Activation Strategies for Asymmetric Organocatalysis

1.1. Introduction

Brønsted and Lewis acids are important classes of catalysts in modern organic chemistry and with the growing interest in the development of catalytic enantioselective reactions, chiral versions of such catalysts have become ubiquitous in recent years. However, both Brønsted and Lewis acids often suffer from reduced reactivity when chiral information is incorporated into their structure. A number of methods to enhance the acidity of these catalysts have been developed over the past 25 years. These methods include structural modifications to the acid catalyst itself as well as the use of acidic and basic additives to activate acid catalysts.[1,2] In this Chapter we focus on Lewis and Brønsted acid activation strategies that involve the use of acid or base promoters in the context of asymmetric catalysis. In particular, strategies for increasing the acidity of hydrogen-bond donor catalysts via the addition of Lewis and Brønsted acids are highlighted.

[1] For a review on enhancing acidity of Brønsted acid catalysts, see: (a) James, T.; Gemmeren, M.; List, B. *Chem. Rev*. **2015**, *115*, 9388–9409. (b) Akiyama, T.; Mori, K. *Chem. Rev*. **2015**, *115*, 9277–9306. (c) Akiyama, T. *Chem Rev.* **2007**, *107*, 5744–5758.

[2] For a review on combined acid catalysis for asymmetric synthesis, see: Yamamoto, H.; Futatsugi, K. *Angew. Chem. Int. Ed.* **2005**, *44*, 1924–1942.

1.2. Brønsted Acid Activation Strategies

1.2.1. Lewis Acid Activation of Brønsted Acids

The Lewis acid-assisted Brønsted acid (LBA)[3] catalyst system is a convenient method to access highly active, yet synthetically simple chiral Brønsted acid catalysts. Yamamoto and Ishihara reported a LBA system that combined a chiral phenol derivative with $SnCl_4$ (Figure 1.1).[4] This system was shown to catalyze enantioselective protonation of silyl enol ethers and later biomimetic cyclization of polyprenoids. In this approach, a weak chiral Brønsted acid is activated via coordination of a Lewis acid.

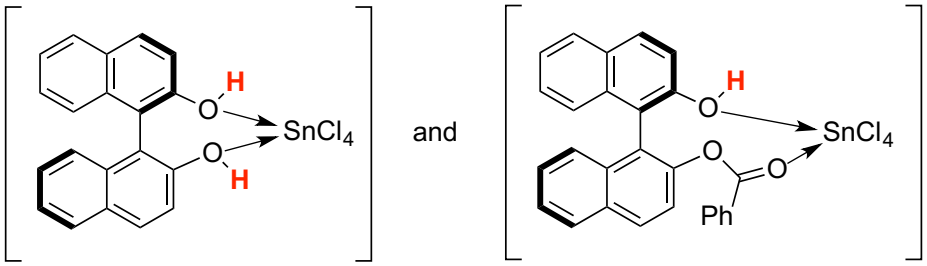

Figure 1.1. ***Lewis acid-assisted chiral Brønsted acid systems reported by Ishihara and Yamamoto.***

The LBA strategy has also been applied towards the activation of a chiral phosphoric acid catalyst. Such catalysts are commonly used to activate aldimines, but the LBA approach allows for the activation of less-basic aldehydes. Specifically, Ishihara and co-workers reported that a chiral BINOL-derived phosphoric acid and BBr_3 catalyst system could promote a highly enantioselective Diels-Alder reaction (Figure 1.2).[5]

---

[3] For reviews on Lewis-acid-assisted Brønsted acids, see: (a) Ishibashi, H.; Ishihara, K.; Yamamoto, H. *Chem. Rec.* **2002**, *2*, 177–188. (b) Yamamoto, H.; Futatsugi, K. *Angew. Chem. Int. Ed.* **2005**, *44*, 1924–1942.

[4] (a) Ishibashi, H.; Kaneeda, M.; Yamamoto, H. *J. Am. Chem. Soc.* **1994**, *116*, 11179–11180. (b) Nakamura, S.; Ishibashi, H.; Yamamoto, H. *J. Am. Chem. Soc.* **2000**, *122*, 8131–8140.

[5] Hatano, M.; Gato, Y.; Izumiseki, A.; Akakura, M.; Ishihara, K. *J. Am. Chem. Soc.* **2015**, *137*, 13472–13475.

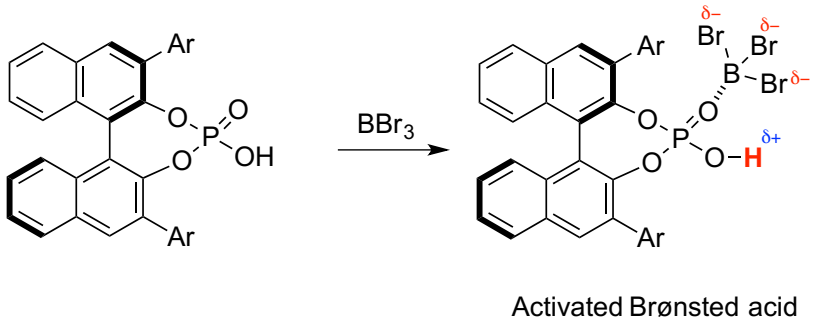

Figure 1.2. ***Enhanced acidity of chiral phosphoric acid via coordination to Lewis acid.***

The Maruoka group in 2013 reported a Lewis acid-activated chiral Brønsted acid catalyst that can be assembled in situ from the two components with distinct functions: a chiral diol ligand for enantioinduction and an achiral 2-boronobenzoic acid for tunable protonation (Figure 1.3).[6] Upon complex formation, coordination of the boronate ester to the carboxylic acid serves two purposes: (1) to activate the Brønsted acid and (2) to rigidify the structure of the chiral catalyst. The ingenuity of this combinatorial approach lies in its facile access to a library of chiral carboxylic acids. This catalyst system was successfully applied to enantioselective trans-aziridination of protected imines.

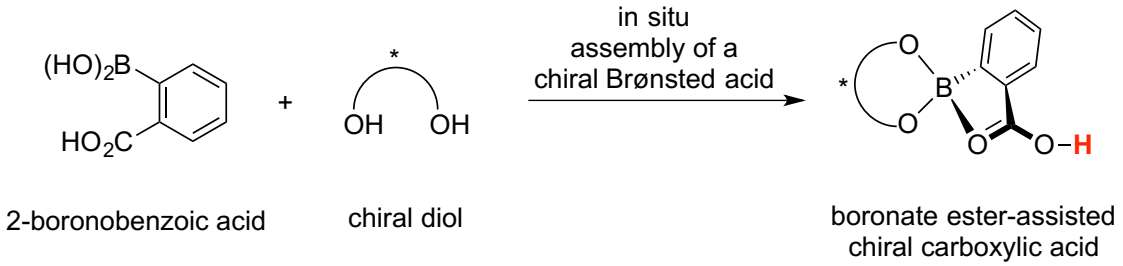

Figure 1.3. ***In situ assembled boronate ester-assisted chiral Brønsted acid.***

As demonstrated by the examples above, the LBA approach is a powerful method for acid catalyst activation in asymmetric transformations. This strategy allows for a decoupling of chiral information from acidity tuning on the Brønsted acid catalyst.

[6] Hashimoto, T.; Gálvez, A. O.; Maruoka, K. *J. Am. Chem. Soc.* **2013**, *135*, 17667–17670.

1.2.2. Brønsted Acid Activation via Coordination to Hydrogen-Bond Donors

Brønsted acids can be activated through coordination of hydrogen-bond donors to their conjugate-bases (Figure 1.4a). Schreiner and co-workers first reported this concept in a regioselective, but not enantioselective, alcoholysis of styrene oxides.[7] Achiral *N,N*'-bis-[3,5-bis-(trifluoromethyl)phenyl]-thiourea catalyst was used in combination with mandelic acid to afford β-alkoxy alcohols in excellent yield. Soon after this initial report, the Jacobsen group developed a protocol for enantioselective Pictet–Spengler reaction that takes advantage of the same catalytic principle (Figure 1.4b).[8] In this case, a chiral thiourea catalyst is thought to bind to benzoic acid through hydrogen-bonding, thereby increasing its acidity. The thiourea-acid complex can then protonate the imine substrate, forming a tight ion pair between the resulting cationic iminium intermediate and catalyst-bound benzoate anion. The chiral catalyst imparts enantioselectivity in a subsequent nucleophilic addition step.

Five years later, the Seidel group extended this catalytic concept to a catalyst system with covalently-linked hydrogen-bond donor and acid portions (Figure 1.4c).[9] Analogous to the Jacobsen report, the acidity of the carboxylic acid is enhanced through carboxylate-binding by the thiourea upon substrate protonation. However, the advantage of this system lies in the fact that positioning the carboxylic acid in close proximity to the H-bond donor results in a more efficient catalyst. In fact, in a head-to-head comparison on the same challenging substrate,[10] acid catalyst with an internal anion-binding capability catalyzes Pictet–Spengler reaction in better

[7] Weil, T.; Kotke, M.; Kleiner, C. M.; Schreiner, P. R. *Org. Lett*. **2008**, *10*, 1513–1516.

[8] Klausen, R. S.; Jacobsen, E. N. *Org. Lett*. **2009**, *11*, 887–890.

[9] Mittal, N.; Sun, D. X.; Seidel, D. *Org. Lett*. **2014**, *16*, 1012–1015.

[10] Unsubstituted triptamine and *o*-bromo benzaldehyde.

yield (87% vs. 45%), faster (reaction time of 2 vs. 10 days) and at lower temperature (r.t. vs. 35 °C) than the intermolecular system, albeit with lower enantioselectivity (79% vs. 95%).

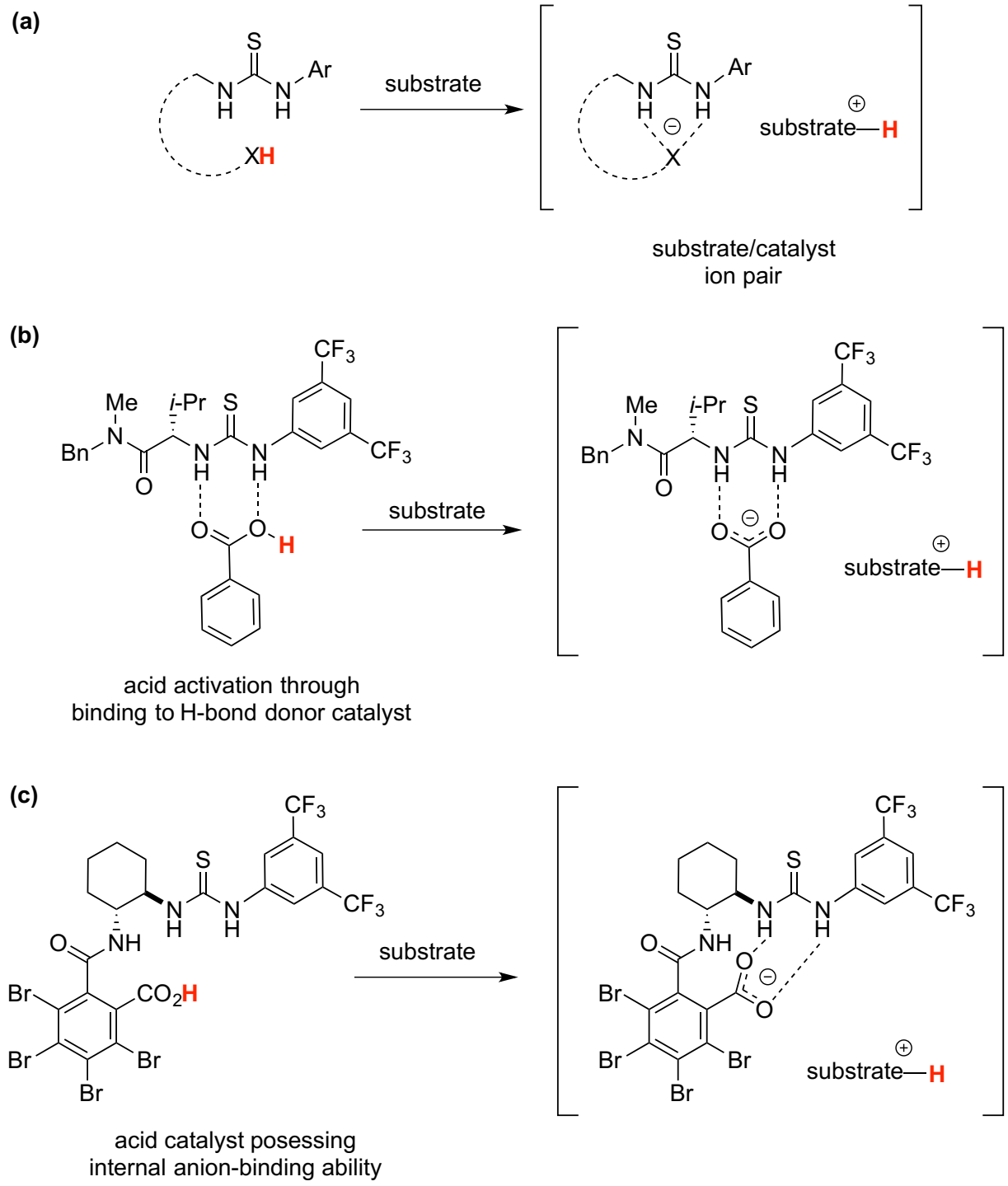

Figure 1.4. ***Brønsted acid activation via stabilization of the conjugate base through anion-binding.*** **(a)** General scheme for this mode of activation. **(b)** Intermolecular catalytic system reported by the Jacobsen group. **(c)** Catalytic system possessing covalently bound anion-binding and acid components reported by the Seidel group.

1.2.3. Enhancing Acidity of Hydrogen-Bond Donors via Coordination to Lewis and Brønsted Acids

Over the past 20 years asymmetric hydrogen-bond donor catalysis has become an important part of modern organic chemistry research. As a result a variety of methods to increase the potency of hydrogen-bond donors have been developed.[11] Many of these methods involve installation of electron-withdrawing groups on established catalysts or a search for new, stronger hydrogen-bonding motifs. In this Chapter we will focus on strategies to enhance hydrogen-bonding ability of ureas and thioureas via coordination of Lewis or Brønsted acids (Figure 1.5). Catalyst activation is achieved through polarization of urea/thiourea upon acid binding. Since this field is relatively underdeveloped, some of the approaches discussed below have not yet been applied to asymmetric catalysis, but we anticipate that they will find use in enantioselective transformations in the future.

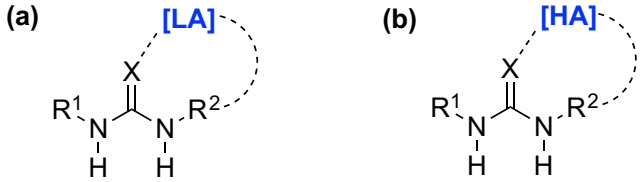

Figure 1.5. ***General scheme for enhancing hydrogen-bonding ability with Lewis (a) and Brønsted (b) acid promoters.***

Internal acid activation strategies for H-bond donors have been studied more than their intermolecular variants. In 2008, the Seidel group reported that a chiral thiourea containing an internal Brønsted acid, a protonated pyridine (Figure 1.6a), provided products of conjugate addition of indoles to trans-β-nitrostyrene in moderate enantioselectivity (46% ee).[12] This

[11] For a review on strategies to enhance H-bond donor catalysts, see: Auvil, T. J.; Schafer, A. G.; Mattson, A. E. *Eur. J. Org. Chem.* **2014**, 2633–2646.

[12] Ganesh, M.; Seidel, D. *J. Am. Chem. Soc.* **2008**, *130*, 16464–16465.

catalyst decreased reaction time from 192 to 3 hours as compared to a catalyst of similar structure, but possessing a 3,5-bis-trifluoromethylphenyl group.

The Smith group developed a catalyst scaffold that purportedly mimics the cooperative non-covalent interactions found in nature. Smith's thiourea catalyst is activated via hydrogen-bonding from the internal urea (Figure 1.6b).[13] This interaction is thought to strengthen when thiourea engages in hydrogen bonding, leading to rate acceleration and excellent enantioselectivities in Mukaiyama-Mannich reaction. Three years later, the Pihko group revisited this catalyst design and enhanced its performance through installation of a more-rigid linker and a more acidic urea unit.[14] This catalyst system was employed in asymmetric Mannich reaction between malonates and imines.

An external Brønsted acid promoter was studied by Herrera and co-workers in the asymmetric thiourea catalyzed Friedel-Crafts alkylation of indoles.[15] Complexation of mandelic acid to thiourea catalyst resulted in rate acceleration and enantioselectivity improvement beyond what either of those species achieve separately (Figure 1.6c).

The Mattson group developed the concept of hydrogen-bond donor activation through internal coordination of Lewis acids (Figure 1.6d).[16] Strategic placement of BF_2-group on the

[13] Jones, C. R.; Pantoş, G. D.; Morrison, A. J.; Smith, M. D. *Angew. Chem. Int. Ed.* **2009**, *48*, 7391–7394.

[14] Probst, N.; Madarász, Á.; Valkonen, A.; Pápai, I.; Rissanen, K.; Neuvonen, A.; Pihko, P. M. *Angew. Chem. Int. Ed.* **2012**, *51*, 8495–8499.

[15] Marquéz-López, E.; Alcaine, A.; Tejero, T.; Herrera, R. P. *Eur. J. Org. Chem*. **2011**, 3700–3705.

[16] For selected examples of internal Lewis acid assisted hydrogen-bond donor catalysis, see: (a) Huges, M. P.; Smith, B. D. *J. Org. Chem*. **1997**, *62*, 4492–4499. (b) Huges, M. P.; Shang, M.; Smith, B. D. *J. Org. Chem*. **1996**, *61*, 4510–4511. (c) Auvil, T. J.; Schafer, A. G.; Mattson, A. E. *Eur. J. Org. Chem.* **2014**, 2633–2646. (d) Nickerson, D. M.; Angeles, V. V.; Auvil, T. J.; So, S. S.; Mattson, A. E. *Chem. Commun*. **2013**, *49*, 4289–4291. (e) So, S. S.; Burkett, J. A.; Mattson, A. E. *Org. Lett*. **2011**, *13*, 716–719.

urea allowed for internal coordination between urea carbonyl and boron and resulted in over six orders of magnitude in acidity increase as compared to Schreiner's urea.

The use of external Lewis acids for H-bond donor activation was reported earlier this year by the Scheidt group.[17] A metal-organic framework (MOF) containing urea functionality can be activated by a TMSCl additive to provide significant rate accelerations in a Friedel-Crafts reaction. Prior to the work discussed in the remainder of this thesis, this methodology represents (to the best of our knowledge) the only example of hydrogen-bond donor activation with an external Lewis acid.

[17] Hall, E. A.; Redfern, L. R.; Wang, M. H.; Scheidt, K. A. *ACS Catal*. **2016**, *6*, 3248–3252.

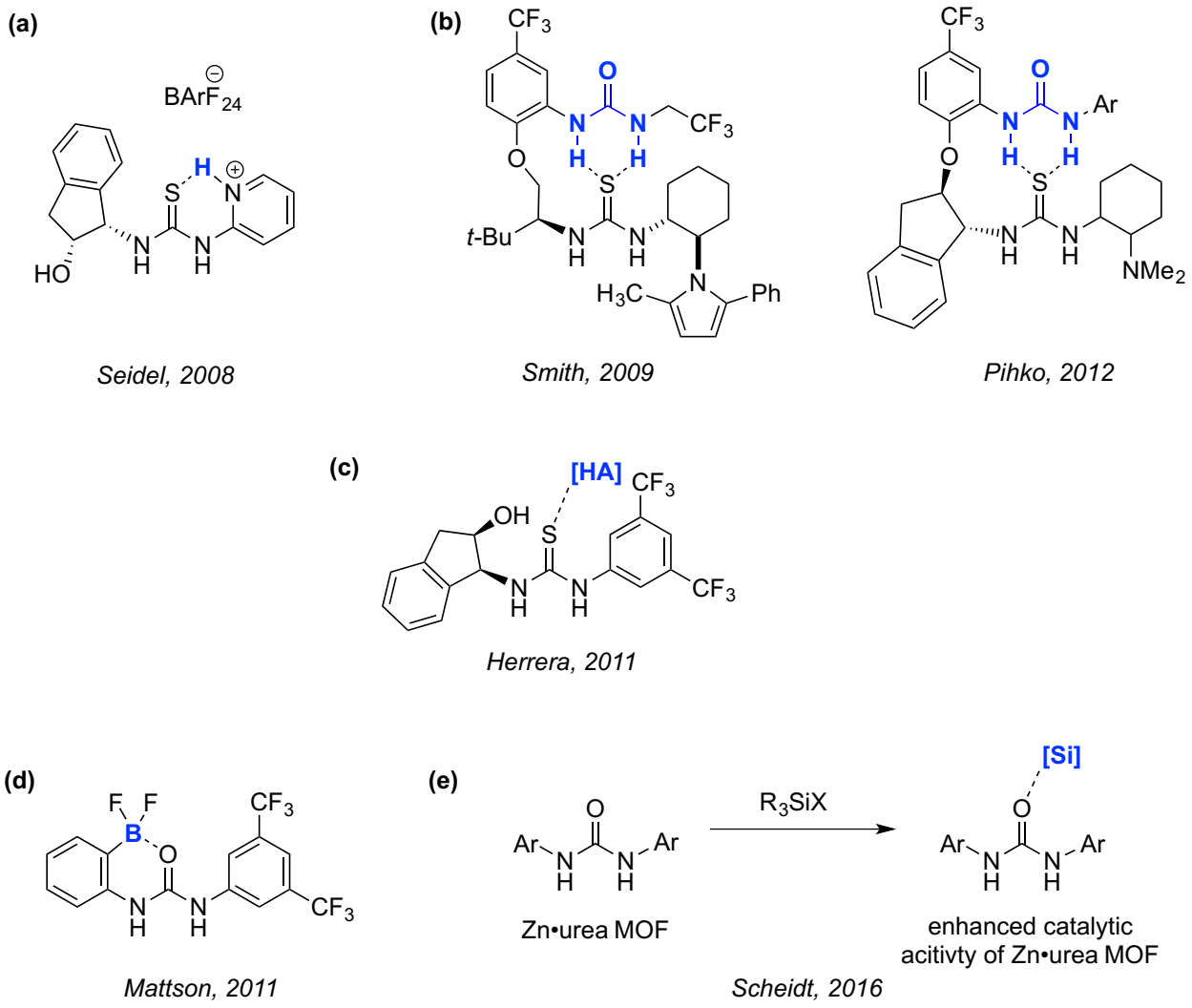

Figure 1.6. ***Strategies for activating H-bond donors with Lewis and Brønsted acids.*** **(a), (b)** Internal Brønsted acid activation strategies for chiral hydrogen-bond donors. **(c)** Activation of a chiral thiourea with an external Brønsted acid. **(d)** Internal Lewis acid activation of a urea hydrogen-bond donor. **(e)** External Lewis acid activation of a urea-containing MOF.

1.3. Lewis Acid Activation Strategies

1.3.1. Lewis Base Activation of Lewis Acids

Chiral Lewis acids are widely used catalysts for a variety of asymmetric transformations.[18] One of the major obstacles in asymmetric Lewis acid catalysis is that chiral Lewis basic ligands used to communicate enantioselectivity often reduce Lewis acidity, and hence reactivity, of the catalyst. However, over the past fifteen years, the Denmark group has reported a series of findings demonstrating that, under certain conditions, the coordination of Lewis basic ligands actually enhances the Lewis acidity of the central atom rather than diminishes it.[19] Denmark and co-workers were guided by Gutmann's rules, which describe bond-length and charge-variation in donor-acceptor interactions based on empirical observations.[20] In particular, coordination of a Lewis basic donor to a polyatomic Lewis acidic acceptor can result in a net increase of negative charge on the donor atom and a net increase of positive charge on the acceptor atom. At the extreme of this approach, one of the peripheral ligands on the Lewis acid may be ionized, resulting in a formal positive charge residing on the central atom of the Lewis acid (Figure 1.7).[19a-f] Consequently, the Lewis acid possesses a more electrophilic central atom and thus enhanced Lewis acidity.

---

[18] *Lewis Acids in Organic Synthesis*; Yamamoto, H., Ed.; Wiley-VCH: Weinheim, 2001.

[19] For a discussion of Lewis base activation of Lewis acids, see: (a) Denmark, S. E.; Wynn, T. *J. Am. Chem. Soc.* **2001**, *123*, 6199–6200. (b) Denmark, S. E.; Beutner, G. L. *J. Am. Chem. Soc.* **2003**, *125*, 7800–7801. (c) Denmark, S. E.; Beutner, G. L.; Wynn, T.; Eastgate, M. D. *J. Am. Chem. Soc.* **2005**, *127*, 3774–3789. (d) Denmark, S. E.; Heemstra, J. R. *J. Org. Chem.* **2007**, *72*, 5668–5688. (e) Denmark, S. E.; Chung, W. *Angew. Chem. Int. Ed.* **2008**, *47*, 1890–1892. (f) Denmark, S. E.; Chung, W.-j. *J. Org. Chem.* **2008**, *73*, 4582–4595. (g) Denmark, S. E.; Ueki, Y. *Organometallics* **2013**, *32*, 6631–6634.

[20] Gutmann, V. *The Donor-Acceptor Approach to Molecular Interactions*; Plenum Press: New York, 1978.

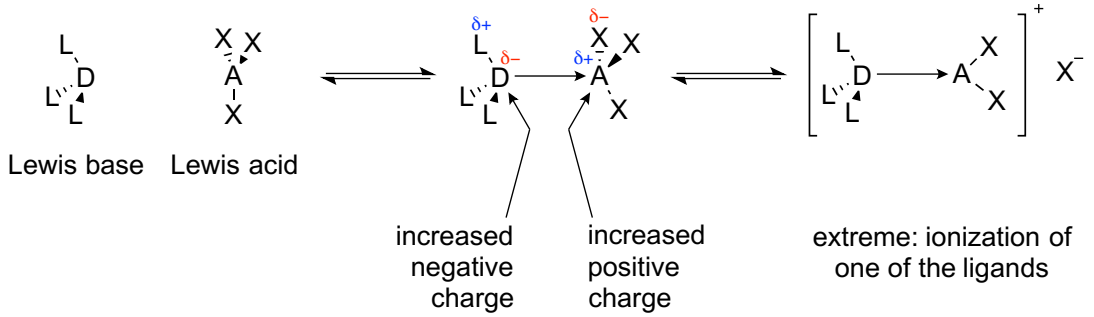

Figure 1.7. ***Coordination of Lewis base can result in enhanced electrophilicity of the central atom of Lewis acid.***

The Denmark group has successfully applied this concept of Lewis base activation of Lewis acids to a variety of asymmetric transformations using a combination of chiral phosphoramide Lewis base catalysts and $SiCl_4$. As described above, coordination of the chiral Lewis basic phosphoramide to weakly Lewis acidic $SiCl_4$ results in the formation of a chiral complex, with enhanced Lewis acidity (Figure 1.8).[19]

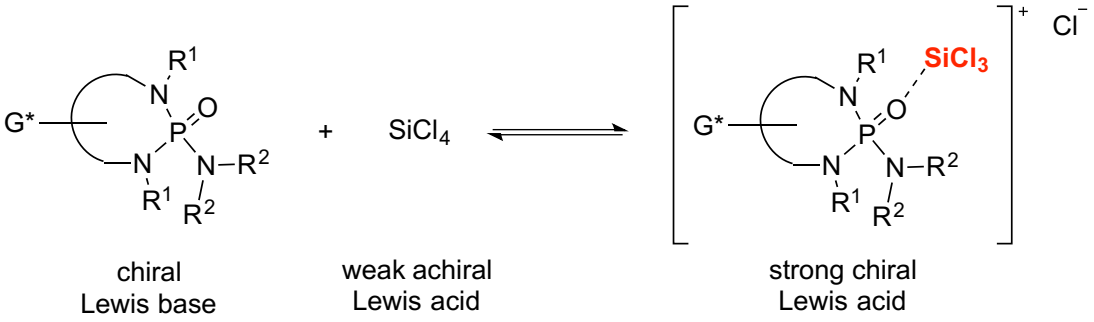

Figure 1.8. ***Denmark's strategy for generation of strong chiral Lewis acid catalysts: activation of weak Lewis acid with chiral Lewis base.***

1.3.2. Brønsted Acid Activation of Lewis Acids

Yamamoto and Ishihara pioneered the concept of Brønsted acid-assisted Lewis acids (BLA) in asymmetric catalysis using boron-based catalysts (Figure 1.9a).[21] They hypothesized that, upon substrate binding, hydrogen bonding from the Brønsted acid to the oxygen of phenol ligand on the boron center causes the Lewis acidity at boron to increase. This catalytic concept was successfully applied by both Yamamoto (Figure 1.9b) and, later, Corey in a highly enantioselective Diels-Alder reaction. In Corey's work, the cationic Lewis acid was generated via protonation of chiral oxazoborolidines at nitrogen by strong Brønsted acids, such as triflic acid or triflimide (Figure 1.9c).[22] They demonstrated that protonated oxazoborolidine is an extremely effective catalyst, leading to similar reaction rates as those promoted by triflic acid.[22a]

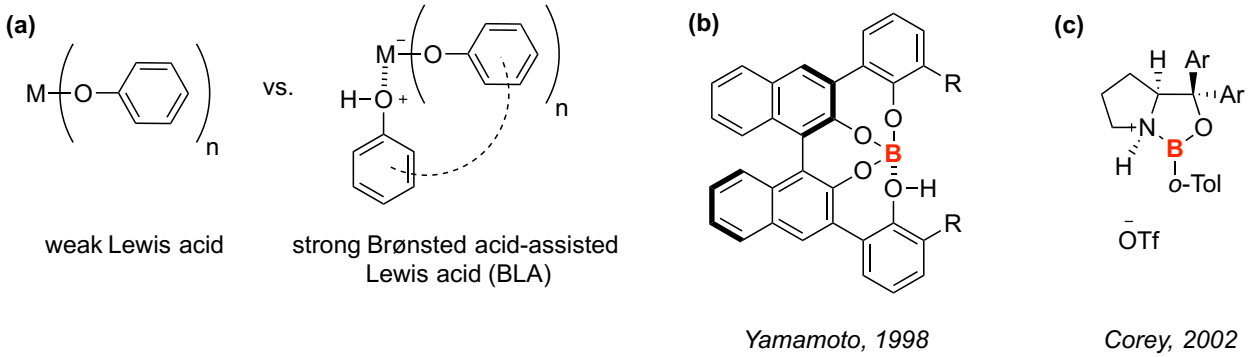

Figure 1.9. ***Examples of Brønsted acid activated Lewis acid catalysts.*** **(a)** A general scheme for BLA concept. **(b)** BLA catalytic system developed by Yamamoto. **(c)** Chiral protonated oxazoborolidine developed by Corey.

[21] (a) Ishihara, K.; Yamamoto, H. *J. Am. Chem. Soc.* **1994**, *116,* 1561–1562. (b) Ishihara, K.; Kurihara, H.; Matsumoto, M.; Yamamoto, H. *J. Am. Chem. Soc.* **1998**, *120,* 6920–6930.

[22] (a) Corey, E. J.; Shibata, T.; Lee, T. W. *J. Am. Chem. Soc.* **2002**, *124,* 3808–3809. (b) Ryu, D. H.; Lee, T. W.; Corey, E. J. *J. Am. Chem. Soc.* **2002**, *124,* 9992–9993. (c) Ryu, D. H.; Zhou, G.; Corey, E. J. *J. Am. Chem. Soc.* **2004**, *126,* 4800–4802.

1.4. Conclusions and Outlook

The development of strong chiral acid catalysts is becoming increasingly important.[23,24] In this Chapter, we present a number of strategies for the formation of more active acid catalysts with minimal perturbation to effective chiral catalyst structures. Given the plethora of Brønsted and Lewis acid-catalyzed reactions, these methods will no doubt find broad applications in asymmetric catalysis. In Chapters 2 – 4 of this thesis, we describe the development and applications of a novel catalyst system that incorporates elements of two activation modes described above: (1) Lewis base activation of Lewis acid and (2) enhanced acidity of hydrogen-bond donors via coordination to Lewis acids. This methodology is an important addition to the body of work described in this Chapter.

[23] Gatzenmeier, T.; Gemmeren, M.; Xie. Y.; Höfler, D.; Leutzsch, M.; List, B. *Science* **2016**, *351*, 949–952.

[24] Cheewala, C. D.; Collins, B. E.; Lambert, T. H. *Science* **2016**, *351*, 961–965.

Chapter 2

Development and Mechanistic Elucidation of an Squaramide-Catalyzed and Silyl Trifluoromethanesulfonate-Promoted Enantioselective (4+3) Cycloaddition[25]

2.1. Introduction

Dual hydrogen-bond (H-bond) donors have emerged as a useful class of catalysts for a variety of transformations. One source of the catalytic power of dual H-bond donors is their ability to abstract and bind anions.[26] Therefore, many enantioselective reactions with such catalysts rely on formation of a chiral ion pair between H-bond donor and the reactive cationic intermediate through tight binding of its counteranion. Anion-abstraction by the H-bond donor is the most direct route to the reactive intermediate, but it necessitates the use of substrates with excellent leaving groups, such as α-chloro ethers[27] (Figure 2.1a). Substrates lacking appropriately labile leaving groups are not susceptible to ionization by H-bond donor catalysts alone, and require alternative strategies for electrophile generation. One such strategy is the use of Brønsted acid promoters to obtain reactive electrophiles through activation of the acid (Figure 2.1b).[8] However, an analogous, and complementary approach with Lewis acids has not been

[25] This work was performed in collaboration with Steven M. Banik and Dr. Alan M. Hyde.

[26] For reviews, see: (a) Zhang, Z.; Schreiner, P. R. *Chem. Soc. Rev.* **2009**, *38*, 1187–1198. (b) Brak, K.; Jacobsen, E. N.; *Angew. Chem. Int. Ed.* **2013**, *52*, 534–561.

[27] Reisman, S. E.; Doyle, A. G.; Jacobsen, E. N. *J. Am. Chem. Soc.* **2008**, *130*, 7198–7199.

demonstrated. Combining a strongly ionizing promoter for electrophile generation with well-developed enantioinduction principles, such as anion-binding, could allow access to a rich array of highly selective, Lewis acid-promoted chemistry.

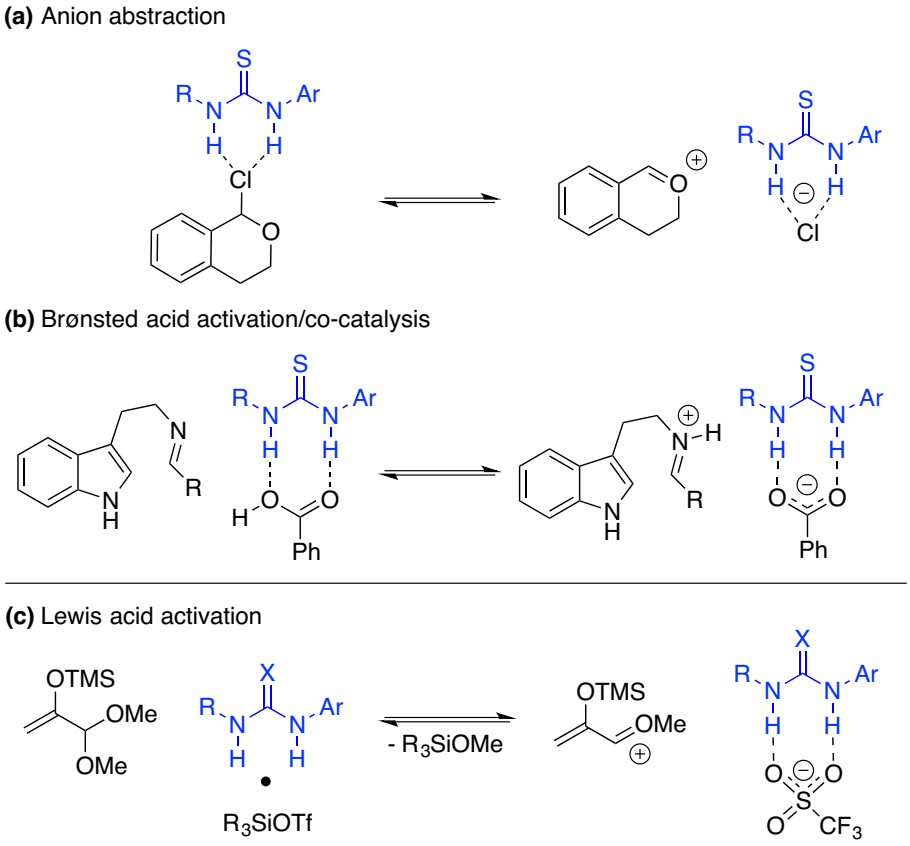

Figure 2.1. ***Methods used to access reactive ion-pairs in asymmetric catalysis with H-bond donors.*** **(a)** Substrates containing labile leaving groups are susceptible to direct ionization by H-bond donors. **(b)** Activation of Brønsted acid co-catalyst with an H-bond donor. **(c)** The use of Lewis acid promoters could allow access to reactive cationic intermediates directly from acetal substrates.

We considered that a Lewis acid promoter might be used in conjunction with a H-bond donor catalyst to access high-energy cationic intermediates, oxocarbenium ions, directly from acetal precursors. Acetals are attractive substrates for oxocarbenium chemistry due to their ease of synthesis and stability, but are generally unreactive towards weakly acidic hydrogen-bond donors due to the poor leaving group ability of alkoxides. We hypothesized that, trialkyl silyl

triflates, efficient promoters of acetal ionization, could facilitate the formation of the oxocarbenium-triflate ion pair associated with a chiral squaramide H-bond donor (Figure 2.1c).

The (4+3) cycloaddition between pyruvic aldehyde dimethyl acetal and furan was chosen as a model reaction to examine this proposed mode of activation and enantioinduction (Scheme 2.1).[28]

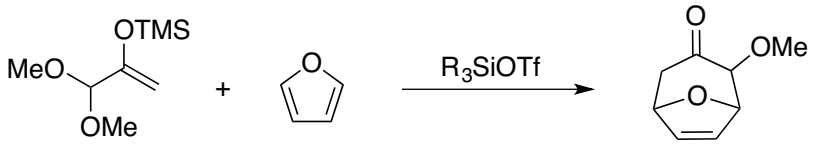

Scheme 2.1. ***Model (4+3) cycloaddition reaction.***

This transformation was chosen because it is promoted by silyl triflate and it has proven to be challenging for asymmetric catalysis.[29] Moreover, development of the asymmetric hydrogen-bond donor-catalyzed (4+3) cycloaddition would allow us to engage oxyallyl cations,[30] an unexplored class of reactive oxocarbenium intermediates in the context of ion-pairing catalysis. Herein we report a highly enantioselective squaramide-catalyzed (4+3) cycloaddition reaction, which results in the formation of complex enantioenriched seven-membered ring products.[31] We also provide evidence for a squaramide-silyl triflate interaction, which enhances the Lewis acidity of silicon and enables asymmetric catalysis with oxyallyl cationic intermediates.

---

[28] Murray, D. H.; Albizati, K. F. *Tetrahedron Lett*. **1990**, *31*, 4109–4112.

[29] Examples of asymmetric (4+3) cycloadditions: (a) Harmata, M. *Adv. Synth. Catal*. **2006**, *348*, 2297–2306. (b) Harmata, M.; Ghosh, S. K.; Hong, X., Wacharasindhu, S.; Kirchhoefer, P. *J. Am. Chem. Soc.* **2003**, *125*, 2058–2059. (c) Xiong, H.; Hsung, R. P.; Berry, C. R.; Rameshkumar, C. *J. Am. Chem. Soc.* **2001**, *123*, 7174–7175.

[30] (a) Harmata, M. *Chem. Commun*. **2010**, *46*, 8886–8903. (b) Harmata, M. *Chem. Commun*. **2010**, *46*, 8904–8922. (c) Lohse, A. G.; Hsung, R. P. *Chem. Eur. J.* **2011**, *17*, 3812-3822. (d) Niess, B.; Hoffmann, M. R. *Angew. Chem. Int. Ed.* **2005**, *44*, 26–29. (e) Harmata, M.; Rashatasakhon, P. *Tetrahedron* **2003**, *59*, 2371–2395.

[31] For a review of applications of chiral 8-Oxabicyclo[3.2.1]oct-6-en-3-ones to total synthesis, see: Hartung, I. V.; Hoffmann, M. R. *Angew. Chem. Int. Ed.* **2004**, *43*, 1934–1949.

2.2. Results and Discussion

2.2.1. Initial Findings

We carried out preliminary experiments to evaluate whether chiral hydrogen-bond donors could be viable catalysts for silyl triflate-promoted (4+3) cycloaddition between pyruvic aldehyde dimethyl acetal (**1a**) and furan. This screen included urea and thiourea catalysts, and squaramides, a less commonly used type of H-bonding catalysts. Squaramides have been demonstrated to be competent catalysts for a number of asymmetric reactions[32] and have been shown to bind a variety of anions with stronger association constants than the corresponding urea- and thiourea-based scaffolds.[33] An investigation of structurally similar catalysts, which varied only in the hydrogen-bond donor motif, revealed that squaramide catalyst **3c** was both significantly more selective and reactive than its urea (**3a**) and thiourea (**3b**) analogs in this transformation (Table 2.1). The increase in enantioselectivity with **3c** may be attributed to the tighter triflate binding to the squaramide as compared to the ureas and thioureas, resulting in enhanced stereochemical communication. However, the origin of the significant rate enhancement provided by **3c** over both the background reaction and the reactions with **3a** and **3b** could not be similarly attributed to the differential anion affinities (entries 1 – 4, Table 2.1). This

[32] (a) Malerich, J. P.; Hagihara, K.; Rawal, V. H. *J. Am. Chem. Soc.* **2008**, *130*, 14416–14417. (b) Zhu, Y.; Malerich, J. P.; Rawal, V. H. *Angew. Chem. Int. Ed*. **2010**, *49*, 153–156. (c) Konishi, H.; Lam, T. Y.; Malerich, J. P.; Rawal, V. H. *Org. Lett*. **2010**, *12*, 2028–2031. (d) Dai, L.; Wang, S.; Chen, F. *Adv. Synth. Catal*. **2010**, *352*, 2137–2141. (e) Alemán, J.; Parra, A.; Jiang, H.; Jørgensen, K. A. *Chem. Eur. J.* **2011**, *17*, 6890–6899. (f) Yang, K. S.; Nibbs, A. E.; Türkmen, Y. E.; Rawal, V. H. *J. Am. Chem. Soc.* **2013**, *135*, 16050–16053. (g) Zhang, H.; Lin, S.; Jacobsen, E. N. *J. Am. Chem. Soc.* **2014**, *136*, 16485–16488.

[33] (a) Quiñonero, D.; Prohens, R.; Garau, C.; Frontera, A.; Ballester, P.; Costa, A.; Deyá P. M. *Chem. Phys. Lett*. **2002**, *351*, 115–120. (b) Amendola, V.; Bergamaschi, G.; Boiocchi, M.; Fabrbrizzi, L.; Milani, M. *Chem. Eur. J.* **2010**, *16*, 4368–4380. (c) Rostami, A.; Colin, A.; Li, X. Y.; Chudzinski, M. G.; Lough, A. J.; Taylor, M. S. *J. Org. Chem*. **2010**, *75*, 3983–3992. (d) Amendola, V.; Fabbrizzi, L.; Mosca, L.; Schmidtchen, F. *Chem. Eur. J.* **2011**, *11*, 5972–5981. (e) Busschaert, N.; Kirby, I. L.; Young, S.; Coles, S. J.; Horton, P. N.; Light, M. E.; Gale, P. A. *Angew. Chem. Int. Ed.* **2012**, *51*, 4426–4430. (f) Lu, T.; Wheeler, S. E. *Chem. Eur. J.* **2013**, *19*, 15141–15147. (g) Edwards, S. J.; Valkenier, H.; Busschaert, N.; Gale, P.A.; Davis, A.P. *Angew. Chem. Int. Ed.* **2015**, *54*, 4592–4596. (h) Ni, X.; Li, X.; Wang, Z.; Cheng, J. *Org. Lett*. **2014**, *16*, 1786–1789.

result prompted a mechanistic study to gain insight into the unique efficacy of squaramide-derived catalysts under these reaction conditions.

Table 2.1. ***Initial catalytic reaction investigation.***

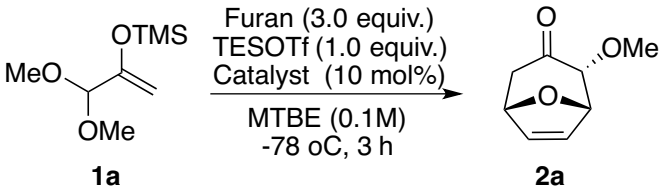

1a **2a**

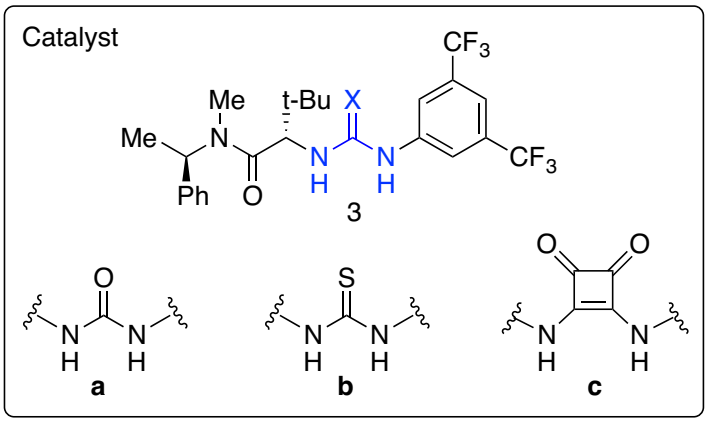

Entry	Catalyst	Yield (%)[a]	ee (%)[b]
1	-	9	n/a
2	**3a**	9	0
3	**3b**	19	5
4	**3c**	77	46

a. Reactions were performed on a 0.05 mmol scale. Yields were determined by GC.
b. ee values determined by gas chromatography analysis.

2.2.2. Elucidation of Squaramide-TESOTf Interactions

We began our mechanistic study by interrogating the nature of the interaction between squaramide catalysts and silyl triflate promoters. Squaramides have been previously shown to serve as both excellent cation and anion acceptors due to their ability to acquire partial aromatic character upon binding ligands through either accepting or donating H-bonds.[34] Therefore,

[34] (a) Tomàs, S.; Prohens, R.; Vega, M.; Rotger, M. C.; Deyà, P. M.; Ballester, P.; Costa, A. *J. Org. Chem*. **1996**, *61*, 9394–9401. (b) Prohens, R.; Tomàs, A.; Morey, J.; Deyà, P. M.; Ballester, P.; Costa, A. *Tetrahedron Lett.* **1998**, *39*,

catalyst **3c** is capable of complexing with TESOTf in two distinct fashions: a Lewis base-Lewis acid interaction between the squaramide carbonyls and the silicon of TESOTf,[35] and a hydrogen-bonding interaction with the triflate anion.

Table 2.2. ***Binding constants.***

Entry	Squaramide	Binding Partner	*Ka* (M^{-1})
1	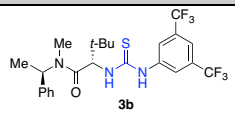 **3b**	$N(^{n}Bu)_4OTf$	$2 \cdot 10^1$
2	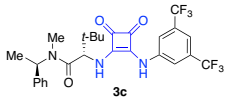 **3c**	$N(^{n}Bu)_4OTf$	$2 \cdot 10^2$
3	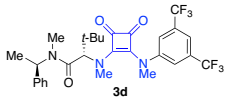 **3d**	TESOTf	$2 \cdot 10^3$
4	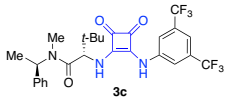 **3c**	TESOTf	$8 \cdot 10^5$

Binding constants (M^{-1}) were determined in [D_2]-dichloromethane by means of ^{1}H NMR spectroscopic titration.

The binding ability of thiourea- and squaramide-derived catalysts to tetrabutylammonium triflate ($N(^{n}Bu)_4OTf$) was evaluated (Table 2.2) and stronger binding of triflate with **3c** was observed as compared to **3b** (entries 1 vs. 2, Table 2.2). However, the magnitude of the binding constant between **3c** and $N(^{n}Bu)_4OTf$ was relatively low ($2 \cdot 10^2\ M^{-1}$), suggesting that hydrogen-bonding ability alone does not account for the differences in reactivity between **3b** and **3c**. We then evaluated the binding strength of the Lewis basic carbonyls of squaramide with silyl triflate. Catalyst **3d**, which is structurally similar to **3c** but lacks the hydrogen-bonding component, was synthesized and its binding constant to TESOTf was determined to be $2 \cdot 10^3\ M^{-1}$ (entry 3, Table

1063–1066. (c) Quiñonero, D.; Frontera, A.; Suñer, G. A.; Morey, J.; Costa, A.; Ballester, P.; Deyà, P. M. *Chem. Phys. Lett*. **2000**, *326*, 247–254. (d) Quiñonero, D.; Frontera, A.; Ballester, P.; Deyà, P. M. *Tetrahedron Lett.* **2000**, *41*, 2001–2005. (e) Storer, R. I.; Aciro, C.; Jones, L. H. *Chem. Soc. Rev*. **2011**, *40*, 2330–2346.

[35] Rotger, C.; Soberats, B.; Quiñonero, D.; Frontera, A.; Ballester, P.; Benet-Buchholz, J.; Deyá P. M.; Costa, A. *Eur. J. Org. Chem.* **2008**, *200*8, 1864–1868.

2.2), only slightly stronger than the binding of **3c** to the triflate anion (entry 2, Table 2.2). However, when both independent binding modes are allowed to operate cooperatively, strong binding between **3c** and TESOTf is observed (entry 4, Table 2.2). In fact, the magnitude of binding is the same as the product of the association constants of the independent binding modes. The molecularity of binding between squaramide **3c** and TESOTf was 1:1, as determined by the method of continuous variation.[36] These data suggest that the ability of **3c** to present both a moderately Lewis basic site and a strong hydrogen-bond donor is important for the overall strength of interaction between the squaramide catalyst and silyl triflate promoter.

Given the observed strong binding constant between TESOTf and squaramide catalyst, we investigated the possibility of catalyst-promoted acetal ionization by ^{1}H NMR spectroscopy. In the presence of silyl triflate promoter alone, substrate **1a** was unreactive and no evidence of ionization was observed (Figure 2.2a). Upon introduction of squaramide catalyst **3e** into the reaction mixture, ^{1}H resonances corresponding to compound **1a** diminished (Figure 2.2b), suggesting that catalyst **3e** induces decomposition of acetal **1a** in the presence of a silyl triflate promoter.

[36] Details on the method of continuous variation provided in the Experimental Section.

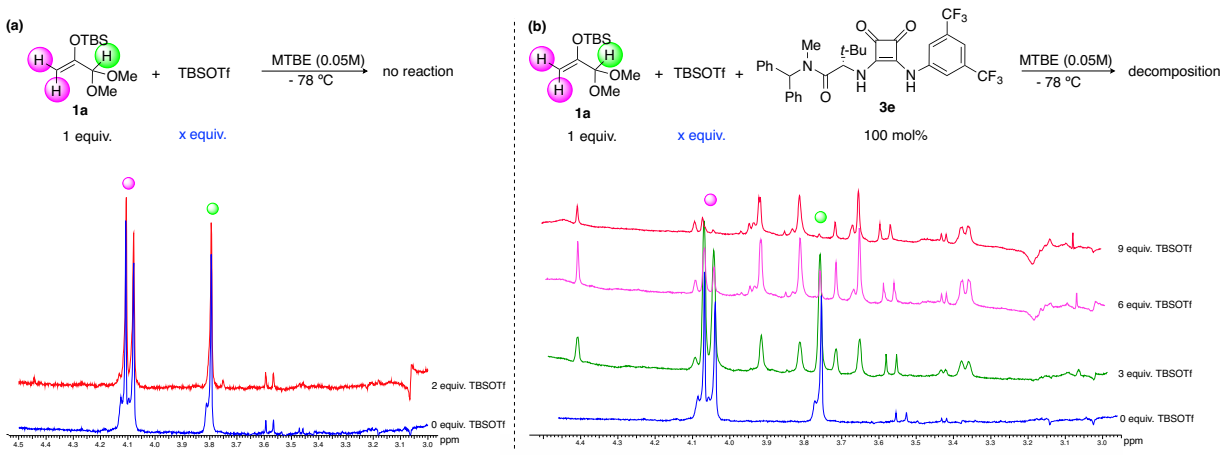

Figure 2.2. ***Assessment of squaramide involvement in acetal ionization by ^{1}H NMR.*** **(a)** Ionization of acetal was not observed in presence of silyl triflate at catalytically relevant conditions. **(b)** When squaramide was present in solution, NMR signals corresponding to acetal diminished upon addition of silyl triflate.

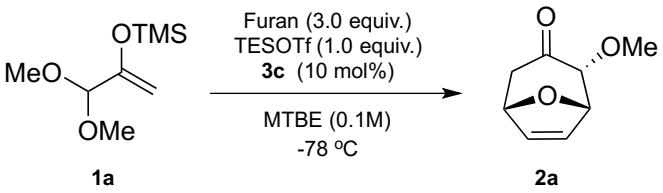

Scheme 2.2. ***Model reaction used for kinetic studies.***

Next, reaction-progress kinetic analysis of the reaction in Scheme 2.2 was undertaken. While the rate of the reaction was found to be independent of the concentrations of furan or silyl triflate promoter, an observed first-order dependence in both catalyst **3c** and substrate **1a**[37] led to the following rate equation (equation (2.1)):

$$r = \mathrm{d}[\mathbf{2a}]/\mathrm{d}t = k[\mathbf{1a}][\mathbf{3c}]_\mathrm{T} \quad (2.1)$$

This rate law, in combination with the aforementioned ^{1}H NMR studies, suggests a resting state complex between the squaramide and silyl triflate promoter and implicates ionization as the rate-determining step. This observation corroborates the previously established large binding constant between **3c** and TESOTf to further supports a catalyst resting state complex.

[37] This rate-law was confirmed for a reaction with the optimal catalyst **4h** on substrate **1a**; details are provided in the Experimental Section.

Spectroscopic evidence for the formation of a squaramide•TESOTf complex was obtained from the infrared signature of the squaramide carbonyls (Figure 2.3).[38] When TESOTf was titrated into a solution of catalyst **3c** and monitored by *in situ* infrared spectroscopy, carbonyl peaks attributed to the squaramide moiety decreased in intensity, consistent with the formation of the proposed complex. One equivalent of TESOTf relative to squaramide **3c** resulted in complete suppression of the carbonyl peaks, further supporting the proposed 1:1 stoichiometry of complexation.

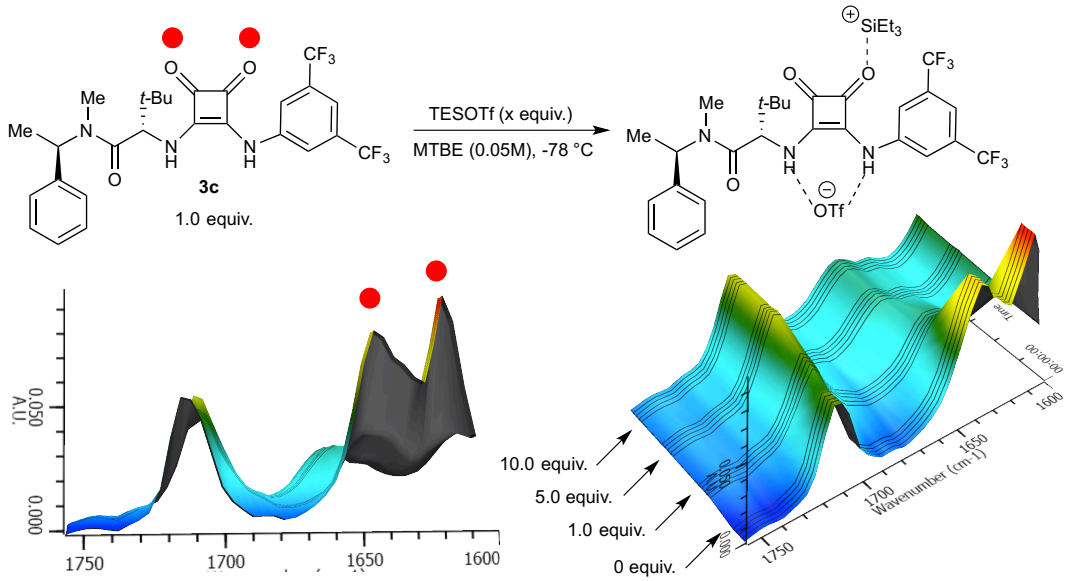

Figure 2.3. ***Titration of 3c with TESOTf***. Formation of the proposed complex between squaramide catalyst **3c** and silyl triflate promoter observed by *in situ* IR spectroscopy; two perspectives shown.

Though precise ^{1}H NMR characterization of the bound complex **3c•**TESOTf was elusive, computational modeling provided further insight into the precise nature of the interaction (Figure 2.4).[39] These calculations demonstrate that **3c•TMSOTf–III**, representing chelation between the two squaramide carbonyls and silicon, is a transition state between the two limiting singly bound complexes, **3c•TMSOTf–I** and **3c•TMSOTf–II**. The lowest energy complex, **3c•TMSOTf–I**,

[38] López, K. A.; Piña, M. N.; Quiñonero, D.; Ballester, P.; Morey, J. *J. Mater. Chem. A* **2014**, *2*, 8796–8803.

[39] Steven M. Banik performed calculations discussed here.

depicts the more electron-rich squaramide carbonyl engaging the cationic silicon, while the squaramide N-H protons are simultaneously hydrogen-bonding with the triflate ion. Though the relative free energies of different bound species varied with the nature of the carbonyl-silicon interaction, the hydrogen-bond lengths between the N-H protons and triflate remained relatively constant and short. We attribute this phenomenon to an enhanced acidity of the N-H protons as the developing positive charge, arising from the Si-carbonyl interaction, is delocalized throughout the squaramide moiety, maximizing binding to the relatively non-coordinating triflate anion.

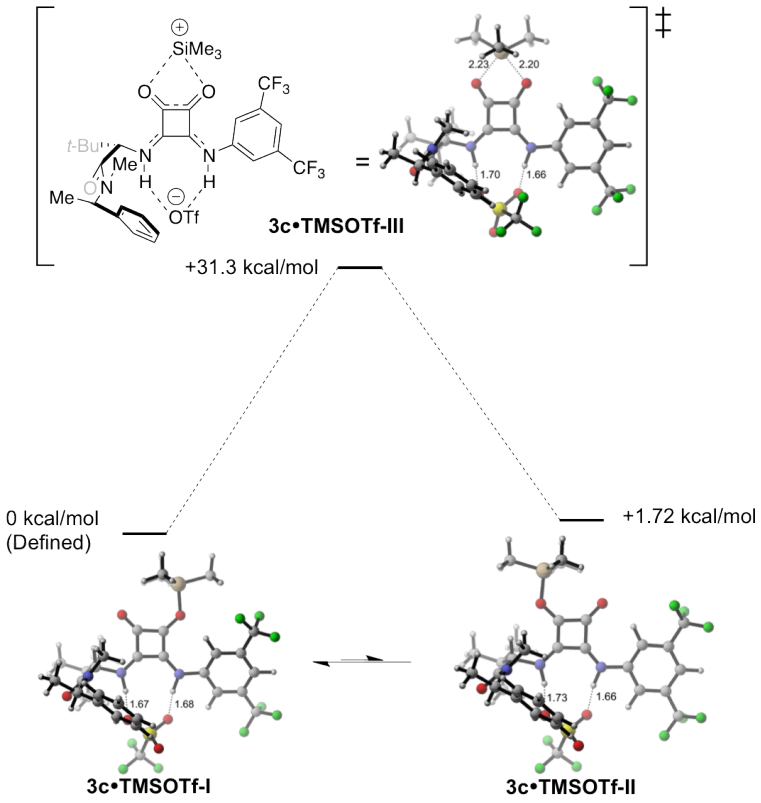

Figure 2.4. ***Calculated bound structures of 3c•TMSOTf.***[40]

[40] Structures calculated at B3LYP/6-31G(d), energies at B3LYP/6-31+G(d,p)).

Coordination of the Lewis basic carbonyls of the squaramide to Lewis acid (TESOTf) can enhance the hydrogen-bonding capability of the squaramide to the triflate anion.[41] Moreover, this interaction can also enhance the Lewis acidity of silicon, relative to free TESOTf. The ability of carbonyl compounds to activate silicon-based Lewis acids has been previously demonstrated in a number of enantioselective transformations.[19a-g]

Taken together, these findings lead to the proposed catalytic cycle in Figure 2.5 for the (4+3) cycloaddition reaction. Experimental evidence points to the formation of resting state **B**, wherein squaramide catalyst **A** and TESOTf form an activated complex. Complex **B** reacts with an acetal substrate to generate the corresponding oxyallyl cation. The squaramide catalyst remains associated with the anionic triflate, creating a pre-organized chiral environment for the associated oxyallyl cation (Complex **C**) and enabling subsequent enantioselective (4+3) cycloaddition. We propose that under our reaction conditions the enhanced Lewis acidity of complex **B** enables ionization to proceed more rapidly than with silyl triflate alone.

[41] For examples of hydrogen-bond donor activation through acid binding, see: references in Chapter 1, Section 1.2.3 of this thesis.

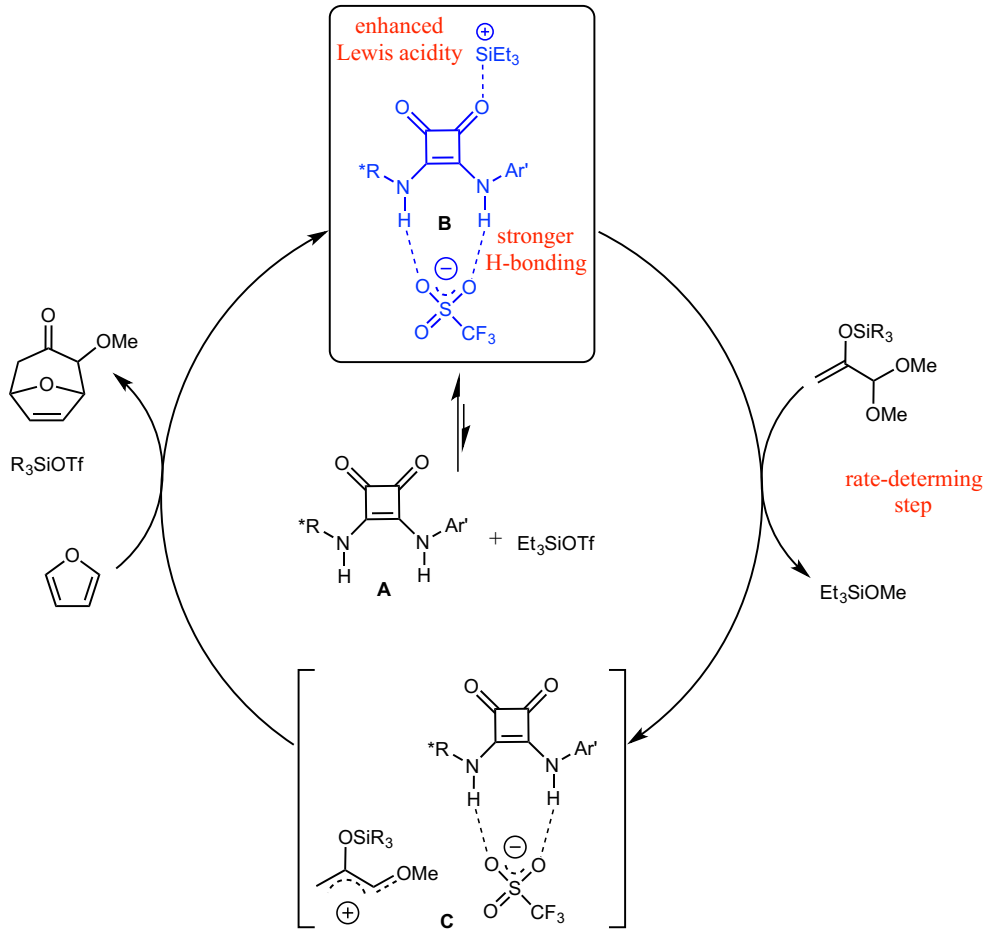

Figure 2.5. ***Proposed catalytic cycle.***[42]

2.2.3. Catalyst Optimization

With an understanding that the unique catalytic efficiency of **3c** is derived from squaramide unit itself, we sought to enhance the enantioselectivity of the (4+3) cycloaddition via modifications of the amide-portion of the catalyst. While our mechanistic studies employed substrate **1a**, substrate **1b** was later found to provide higher levels of enantioselectivity and proved a more appropriate model for selectivity optimization. The enantioselectivity of (4+3) reactions was found to be particularly sensitive to the amide-portion of the catalyst. Arylpyrrolidine catalysts (**4**) have been identified as particularly selective catalysts for reactions

[42] Strong binding between TESOTf and squaramides suggests that under conditions where TESOTf is used in excess to squaramide catalyst, another molecule of silyl triflate will bind squaramide carbonyl in complex **C**.

with cationic intermediates and variation of the aryl substituent[43] provided a valuable parameter for catalyst optimization. Catalyst **4a**, which lacks an aryl group, afforded only trace reactivity and selectivity (entry 3, Table 2.3). Expanding the aromatic group from phenyl (**4b**) to 1-napthyl (**4c**) provided an increase in enantioselectivity (entries 4-5). In contrast to the beneficial effect of the 1-napthyl substituent relative to phenyl, a 2-napthyl substituent (**4d**) diminished the enantioselectivity (entry 6). These results suggest that not only the size, but also the connectivity of the aromatic group, has a profound effect on its ability to induce secondary interactions in the enantiodetermining transition state and afford high levels of enantioselectivity. A number of different isomeric phenanthryl-derived arylpyrrolidine catalysts were thus examined. Catalyst **4g** afforded the highest yield and enantioselectivity as compared to **4e** and **4f** (entries 7-9). Merging the optimal connectivity with the apparent trend in size of the aryl group, 1-pyrenyl catalyst **4h** resulted in the highest enantioselectivity (89%) for the (4+3) cycloaddition reaction of **1b** and furan (entry 10). In order to assess the importance of the hydrogen-bonding component and anion-binding ability of the catalyst for enantioselectivity, it was necessary to exclude the possibility that catalyst **4h** acts exclusively as a chiral Lewis base to activate the silyl triflate promoter. Therefore, catalyst **5h**, wherein the acidic N–H bonds have been replaced with N–Me substituents, was synthesized. Lacking the ability to engage with triflate anion, catalyst **5h** was only moderately reactive and selective in the reaction (entry 11), confirming that cooperative agency of an H-bond donor is indispensable for attaining both good yield and high enantioselectivity in (4+3) reactions through this catalytic pathway.

[43] Lin, S.; Jacobsen, E. N. *Nature Chem.* **2012**, *4*, 817–824.

Table 2.3. ***Catalyst optimization.***

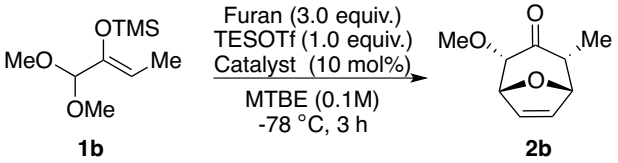

1b **2b**

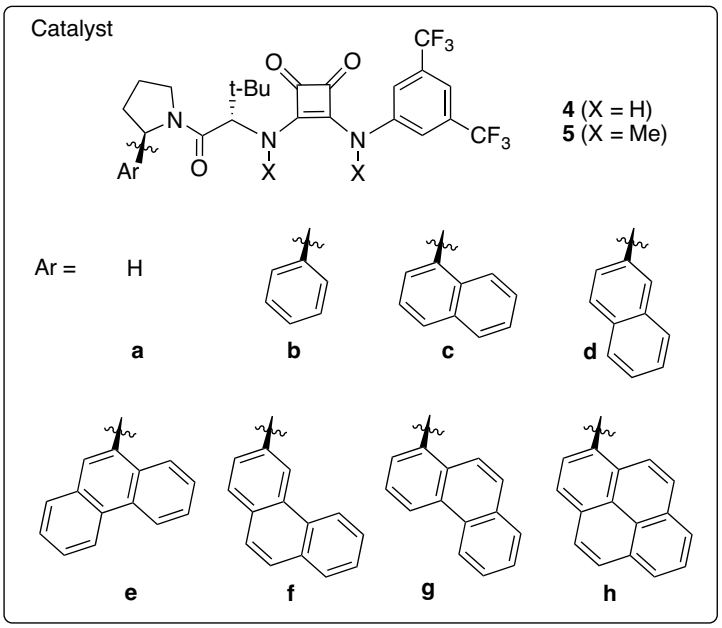

Entry	Catalyst	Yield (%)[a]	ee (%)[b]
1	-	10	n/a
2	**3c**	36	-16
3	**4a**	17	6
4	**4b**	49	40
5	**4c**	56	54
6	**4d**	32	5
7	**4e**	76	79
8	**4f**	69	71
9	**4g**	74	88
10	**4h**	82	89
11	**5h**	31	16

a. Reactions were performed on a 0.05 mmol scale. Yields were determined by GC.
b. ee values determined by gas chromatography analysis.

2.2.4. Investigation of Substrate Scope

A variety of oxyallyl cation precursors and furan derivatives were evaluated to define the scope of the (4+3) cycloadditions (Table 2.4). Substrates bearing a methyl substituent at the R^2 position afforded the highest enantioselectivities (entry 5 vs. entries 1-3, Table 2.4) and both dimethoxy and dibenzyloxy acetals (entry 4) provided high levels of enantioselectivity under the reaction conditions. A number of 3-substituted furans reacted in high yields with good to excellent enantioselectivities. High regioselectivity was observed in products **2f** and **2g**, which could find use in further elaborations via cross-coupling (entries 6-7). A 3,4-disubstituted furan proved to be a suitable nucleophilic component despite the steric bulk of the substituents, although only moderate enantioselectivities resulted (entry 12). Strongly electron-withdrawing groups and substitutions at the 2-position of furan nucleophiles were not well tolerated under these conditions, providing only trace amounts of products.

Table 2.4. ***Substrate scope of (4+3) cycloaddition.***

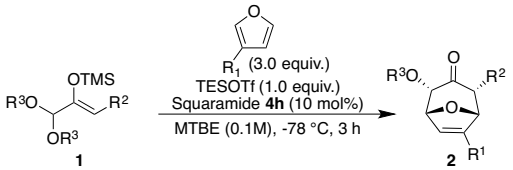

Entry	Starting Material	Furan	Product	r.r.	Yield (%)[a]	ee (%)
1	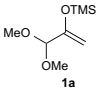 1a		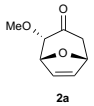 2a	n/a	69	71
2		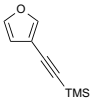	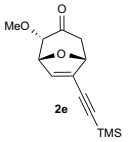 2e	>20:1	70	86
3	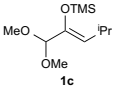 1c		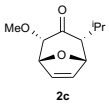 2c	n/a	55	77
4	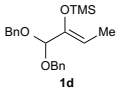 1d		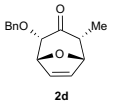 2d	n/a	74	92
5	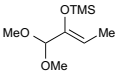 1b		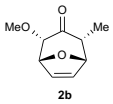 2b	n/a	82	89
6			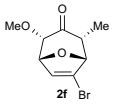 2f	>20:1	68	94
7		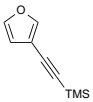	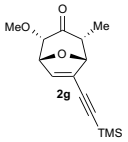 2g	>20:1	98	96
8			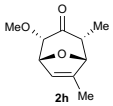 2h	2.8:1	77	90
9			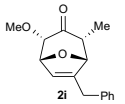 2i	1.5:1	97	88
10			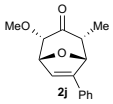 2j	11:1	95	87
11		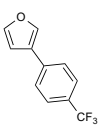	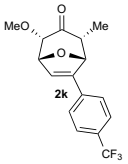 2k	13:1	96	95
12			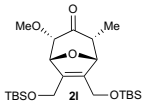 2l	n/a	82	66

a. Isolated combined yields of regioisomers are reported (purified chromatographically).

2.3. Conclusions

We propose a novel mode of catalysis by hydrogen-bond donors, wherein the squaramide catalyst performs a dual function of activating a silicon-based Lewis acid while simultaneously engaging in hydrogen-bonding to the corresponding anion. This method has been successfully applied to the synthesis of enantioenriched seven-membered rings via a (4+3) cycloaddition, with enantioselectivity derived from an anion-binding interaction. We envision that this new protocol for ionization of acetals could be applied to the rich carbonyl chemistry enabled by silicon Lewis acids. Further studies on applications of this methodology are discussed in Chapters 3 and 4 of this thesis and more work is currently ongoing in our laboratory.

2.4. Experimental Section

2.4.1. General Information

All reactions were performed in flame-dried 10 mL round-bottom flasks unless otherwise noted. The flasks were fitted with rubber septa and reactions were conducted under nitrogen. Stainless steel syringes were used to transfer air- and moisture-sensitive liquids. Flash chromatography was performed using silica gel 60 (230-400 mesh) from EM Science. Commercial reagents were purchased from Aldrich, Alfa Aesar, Strem or TCI, and used as received with the following exceptions: dichloromethane, tetrahydrofuran, toluene, ethyl ether, *t*-butyl methyl ether were dried by passing through columns of activated molecular sieves. Triethylamine was distilled from CaH_2 at 760 torr. *s*-Butyllithium was titrated using diphenylacetic acid as an indicator. Proton nuclear magnetic resonance (^{1}H NMR) spectra and carbon nuclear magnetic resonance (^{13}C NMR) spectra were recorded on Inova-600 (600 MHz) and Inova-500 (500 MHz) spectrometers. Chemical shifts for protons are reported in parts per million downfield from tetramethylsilane and are referenced to residual protium in NMR solvent ($CHCl_3$ = δ 7.27, CH_2Cl_2 = δ 5.32, DMSO = δ 2.50). Chemical shifts for carbon are reported in parts per million downfield from tetramethylsilane and are referenced to the carbon resonance of the solvent ($CDCl_3$ = δ 77.0, CD_2Cl_2 = δ 54.0, DMSO = δ 39.5). Data are represented as follows: chemical shift, multiplicity (br. = broad, s = singlet, d = doublet, t = triplet, q = quartet, m = multiplet), coupling constants in Hertz (Hz), integration. Infrared (IR) spectra were obtained using Bruker Optics Tensor 27 FTIR spectrometer. In situ infrared (IR) data was collected using ReactIR^{TM} iC10 (Mettler Toledo). Optical rotations were measured using a 1mL cell with 0.5 dm path length on a Jasco DIP 370 digital polarimeter. The mass spectra were obtained on a Bruker micrOTOF-Q II time-of-flight LC/MS spectrometer. Chiral GC analysis was performed suing

Agilent Technologies 7890A GC system with commercial β-Cyclosil (30 m x 0.25 mm x 0.25 μm) columns. Chiral HPLC analysis was performed using an Agilent Technologies 1200 series instrument with commercial Chiralpak columns.

2.4.2. Preparation and Characterization of Squaramide Catalysts[44]

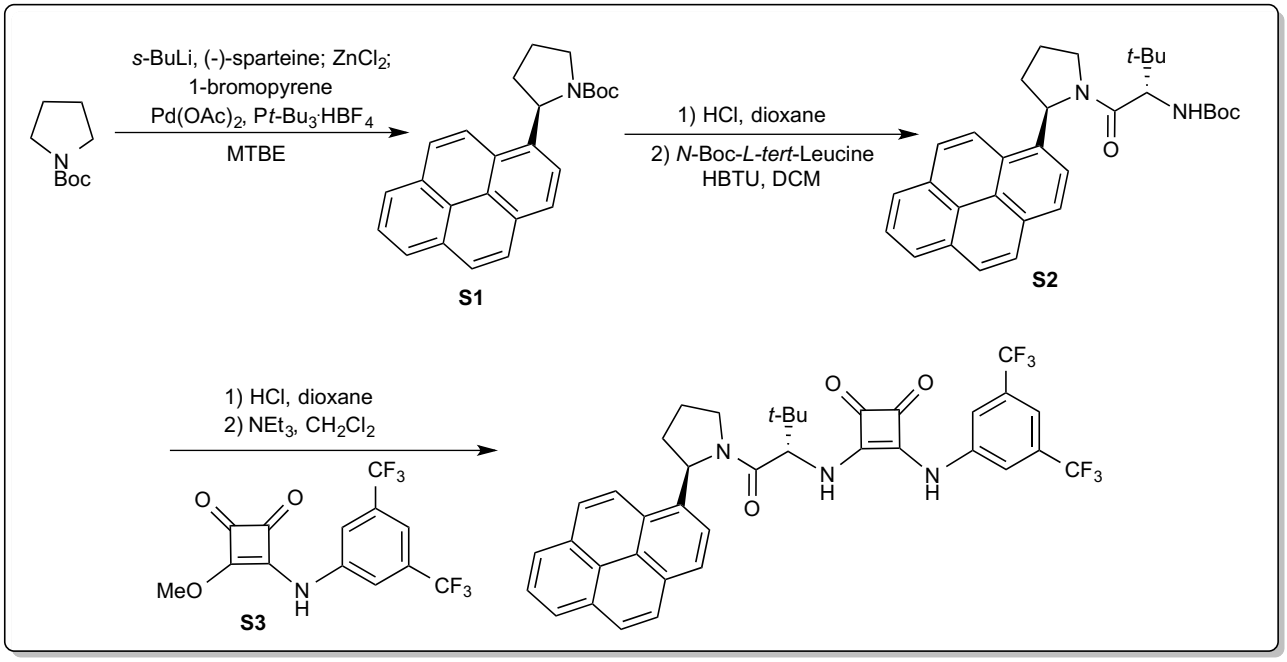

Scheme 2.3. ***Synthesis of squaramide catalyst 4h*.**

[44] For synthesis and characterization of catalysts **4a**, **4b** and **4e**, see: Zhang, H.; Lin, S.; Jacobsen, E. N. *J. Am. Chem. Soc.* **2014**, *136*, 16485–16488.

tert-butyl (*R*)-2-(pyren-1-yl)pyrrolidine-1-carboxylate (**S1**):

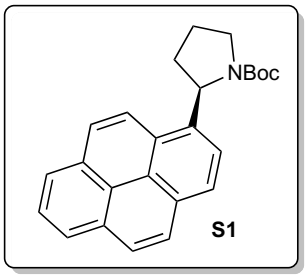

To *N*-Boc pyrrolidine (426 μL, 2.43 mmol, 1.2 equiv.) was added (–)-sparteine (558 μL, 2.43 mmol, 1.2 equiv.) and MTBE (5.70 mL) under N_2. The reaction vessel was cooled to –78 °C, and a solution of *sec*-butyl lithium (1.1 M in cyclohexane, 2.2 mL, 2.4 mmol, 1.2 equiv.) was added dropwise over 40 minutes and the reaction mixture was stirred at –78 °C. After 3 hours, a solution of $ZnCl_2$ (1.0 M in diethyl ether, 2.4 mL, 2.4 mmol, 1.2 equiv.) was added dropwise over 30 minutes at –78 °C, and the reaction mixture was stirred at –78 °C. After 30 minutes, the reaction mixture was warmed to room temperature and stirred. After 30 minutes, 1-bromopyrene (570 mg, 2.03 mmol, 1 equiv.) was added, followed by $Pd(OAc)_2$ (36 mg, 0.16 mmol, 8 mol%) and $P(t\text{-Bu})_3 \bullet HBF_4$ (53 mg, 0.18 mmol, 9 mol%) at room temperature and stirred. After 36 hours, 150 μL aqueous NH_4OH (28%) was added and the mixture was stirred. After 1 hour, the mixture was filtered through celite and the filter cake was washed with 100 mL MTBE. The resulting organic solution was washed with aqueous 1 M HCl (50 mL), and H_2O (2×50 mL). The organic layer was dried over anhydrous Na_2SO_4 and concentrated under reduced pressure. The resulting residue was purified by flash chromatography on silica gel (0% to 40% ethyl acetate in hexanes) to yield **S1** as a pale yellow solid (400 mg, 53%).

^{1}H NMR (600 MHz, $CDCl_3$) δ 8.28 (d, J = 9.4 Hz, 1H), 8.22–8.10 (m, 4H), 8.05–7.95 (m, 3H), 7.85 (d, J = 8.2 Hz, 1H), 5.90 (m, 1H), 3.91–3.75 (m, 2 H), 2.05–1.85 (m, 4H), 1.02 (s, 9H);

select minor rotamer resonances: δ 7.80 (d, J = 7.6 Hz, 1H), 6.06 (d, J = 7.0 Hz, 1 H), 3.72–3.62 (m, 1H), 2.63 (m, 4H), 1.51 (br. s, 9H); (rotamer ratio in $CDCl_3$ = 1.6:1);

^{13}C NMR (125 MHz, $CDCl_3$) major and minor rotamer resonances δ 154.8, 138.6, 137.4, 131.6, 130.9, 130.5, 130.2, 127.7, 127.5, 127.2, 126.9, 126.0, 125.1, 124.9, 122.9, 122.6, 122.1, 79.6, 79.9, 58.7, 47.8, 47.4, 35.7, 34.6, 28.8, 28.2, 23.8, 23.5;

FTIR (neat, cm^{-1}) ν_{max} 2977, 1693, 1395, 1366, 1155, 1121, 847, 758 cm^{-1};

LRMS (ESI-TOF) calculated for $C_{25}H_{25}NO_2$ $[M+Na]^+$ 394.2, found 394.2;

$[\alpha]_D^{23}$ = +53.2° (c = 1.0, $CHCl_3$).

tert-butyl ((*S*)-3,3-dimethyl-1-oxo-1-((*R*)-2-(pyren-1-yl)pyrrolidin-1-yl)butan-2-yl)carbamate (**S2**):

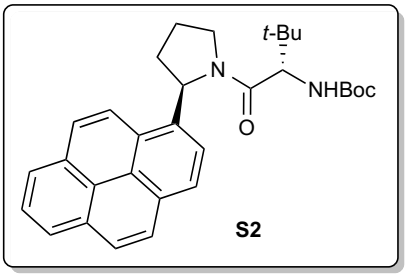

S2

To **S1** (390 mg, 1.08 mmol, 1 equiv.) was added HCl (4.0 M in dioxane, 2.6 mL, 10.5 equiv.). The mixture was stirred for 2 hours at room temperature and concentrated under reduced pressure to yield a beige solid. To this solid was added Boc-L-*tert*-leucine (316 mg, 1.37 mmol, 1.3 equiv.), HBTU (518 mg, 1.37 mmol, 1.3 equiv.), DCM (10.0 mL), and DIPEA (549 μL, 3.15 mmol, 3.0 equiv.). The reaction was stirred at room temperature. After 48 hours, the reaction mixture was diluted with DCM (10 mL) and extracted with H_2O (10 mL), saturated aqueous $NaHCO_3$ (10 mL), and H_2O (10 mL). The organic layer was dried over anhydrous $MgSO_4$ and

concentrated under reduced pressure. The crude residue was purified by column chromatography (0 to 40% ethyl acetate in hexanes) to yield **S2** as a white foamy solid (515 mg, 98%).

^{1}H NMR (600 MHz, $CDCl_3$) δ 8.28 (d, *J* = 8.8 Hz, 1H), 8.24–8.10 (m, 3H), 8.05–7.96 (m, 4H), 7.67 (d, *J* = 8.2 Hz, 1H), 6.27 (d, *J* = 7.6 Hz, 1H), 5.27 (d, *J* = 10.0 Hz, 1H), 4.53 (d, *J* = 10.0 Hz, 1H), 3.95–3.85 (m, 2H), 2.10–2.00 (m, 4H), 1.61 (s, 9H), 1.10 (s, 9H); select minor rotamer resonances: δ 8.47 (d, *J* = 9.4 Hz, 1H), 7.79 (d, *J* = 7.6 Hz, 1H), 6.72 (d, *J* = 8.2 Hz, 1H), 5.11 (d, *J* = 10.6 Hz, 1H), 4.51–4.47 (m, 1H), 3.96–3.90 (m, 2H), 2.60–2.51 (m, 4H), 1.51 (s, 9H), 0.62 (s, 9H); (rotamer ratio in $CDCl_3$ = 2.1:1);

^{13}C NMR (125 MHz, $CDCl_3$) major rotamer resonances δ 171.1, 156.7, 136.0, 131.5, 130.8, 130.5, 127.6, 127.5, 127.2, 127.0, 126.0, 125.4, 125.2, 125.1, 125.1, 124.8, 122.9, 122.1, 79.8, 59.0, 58.7, 48.8, 34.6, 33.7, 28.6, 26.7, 23.8;

FTIR (neat, cm^{-1}) ν_{max} 2973, 2360, 2341, 1778, 1707, 1644, 1497, 1428, 1169, 757 cm^{-1};

LRMS (ESI-TOF) calculated for $C_{31}H_{36}N_2O_3$ $[M+Na]^+$ 507.2624, found 507.2687;

$[\alpha]_D^{23}$ = +25.8° (c = 1.0, $CHCl_3$).

3-((3,5-bis(trifluoromethyl)phenyl)amino)-4-(((*S*)-3,3-dimethyl-1-oxo-1-((*R*)-2-(pyren-1-yl)pyrrolidin-1-yl)butan-2-yl)amino)cyclobut-3-ene-1,2-dione (**4h**):

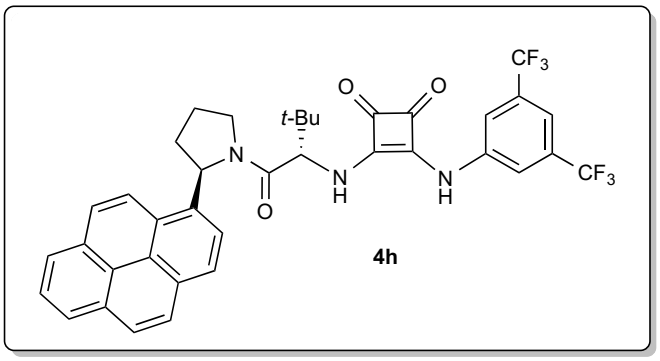

To Boc-protected amine **S2** (533 mg, 1.1 mmol, 1 equiv.) was added HCl (2.8 mL, 4M in dioxane, 11 mmol, 10.0 equiv.) dropwise at room temperature. The reaction mixture was stirred for another 2 hours at room temperature and then concentrated under vacuum to give a yellow foamy solid, which was used directly in the next step. DCM (5.5 mL) and NEt_3 (0.3 mL, 2.2 mmol, 2.0 equiv.) and **S3**[45] (373 mg, 1.1 mmol, 1.0 equiv.) were added and the reaction mixture was stirred at room temperature for 24 h. Then aqueous 1N NaOH (10 ml) solution was added and the biphasic mixture was stirred for 2 hours (this step allows for decomposition of any remaining **S3** and its subsequent purification from the desired product). The mixture was then diluted with DCM (20 ml) and water (20 ml) and layers were separated. Organic layer was washed with brine (20 ml), dried over anhydrous $MgSO_4$ and concentrated. The crude product was purified by flash chromatography on silica gel column (10% to 50% EtOAc in hexanes) to give **4h** as a foamy yellow solid (556 mg, 73% over two steps).

^{1}H NMR (600 MHz, DMSO) major rotamer resonances: δ 10. 38 (s, 1H), 8.44 (d, J = 9.4 Hz, 1H), 8.26 – 8.22(m, 4H), 8.13 – 8.02 (m, 5H), 7.71 (d, J = 8.2, 1H), 7.66 (s, 1H), 6.17 (dd, J = 2.4, 8.2 Hz, 1H), 5.19 (d, J = 10.6 Hz, 1H), 4.29 – 4.26 (m, 1H), 3.98 – 3.93 (m, 1H), 2.64 – 2.56 (m, 1H), 2.06 – 1.88 (m, 4H), 1.08 (s, 9H); select minor rotamer resonances: δ 10.22 (s, 1H), 4.72 (d, J = 10.6 Hz, 1H), 0.62 (s, 9H); (rotamer ratio in DMSO = 3.1:1);

^{13}C NMR (125 MHz, DMSO) major and minor rotamer resonances δ 185.0, 181.1, 169.6, 168.5, 163.1, 141.5, 137.2, 132.0, 131.7, 131.3, 130.6, 130.0, 127.8, 127.1, 127.0, 126.9, 126.6, 125.6, 125.5, 125.1, 124.7, 124.5, 123.5, 122.8, 122.5, 118.4, 61.8, 58.7, 48.8, 36.2, 35.8, 34.1, 26.5, 26.3, 23.9;

FTIR (neat, cm^{-1}) ν_{max} 1601, 1427, 1379, 1277, 1181, 1132, 846 cm^{-1};

[45] **S3** was synthesized via previously reported procedure: Yang, W.; Du, D. M. *Org. Lett*. **2010**, *12*, 5450-5453.

HRMS (ESI-TOF) calculated for $C_{38}H_{31}F_6N_3O_3$ $[M+H]^+$ 692.2348, found 692.2378;

$[\alpha]_D^{25}$ = –19.4° (c = 1.0, $CHCl_3$).

(*S*)-2-((2-((3,5-bis(trifluoromethyl)phenyl)amino)-3,4-dioxocyclobut-1-en-1-yl)amino)-*N*,3,3-trimethyl-*N*-((*R*)-1-phenylethyl)butanamide (**3c**):

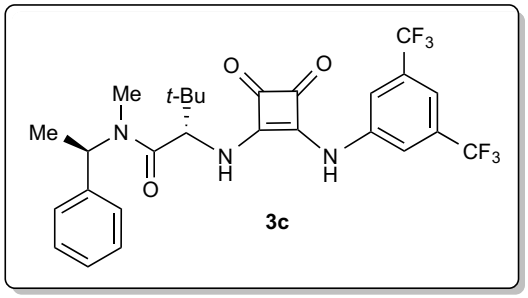

3c

^{1}H NMR (600 MHz, DMSO) major rotamer resonances: δ 10.50 (s, 1H), 8.38 (d, J = 10.0 Hz, 1H), 8.09 (s, 2H), 7.68 (S, 1H), 7.21 – 7.37(m, 5H), 5.92 (q, J=7.0 Hz, 1H), 5.16 (d, J=10.0 Hz, 1H), 2.81 (s, 3H), 1.48 (d, J=7.0 Hz, 3H), 1.04 (s, 9H); select minor rotamer resonances: δ 10.44 (s, 1H), 5.29 (d, J=10.0 Hz, 1H), 0.99 (s, 9H); (rotamer ratio in DMSO = 4.9:1);

^{13}C NMR (125 MHz, DMSO) major and minor rotamer resonances δ 184.9, 184.7, 180.8, 170.6, 170.2, 169.3, 163.0, 141.6, 140.5, 131.9, 131.7, 128.9, 127.4, 124.7, 122.5, 118.6, 115.2, 59.6, 50.8, 36.8, 36.3, 30.7, 26.4, 26.3, 16.4;

FTIR (neat, cm^{-1}) ν_{max} 1579, 1531, 1371, 1275, 1193, 1121, 699, 681 cm^{-1};

HRMS (ESI-TOF) calculated for $C_{27}H_{27}F_6N_3O_3$ $[M+Na]^+$: 578.1854, found: 578.1810;

$[\alpha]_D^{25}$ = +100.4° (c = 1.0, $CHCl_3$).

3-((3,5-bis(trifluoromethyl)phenyl)amino)-4-(((*S*)-3,3-dimethyl-1-((*R*)-2-(naphthalen-1-yl)pyrrolidin-1-yl)-1-oxobutan-2-yl)amino)cyclobut-3-ene-1,2-dione (**4c**):

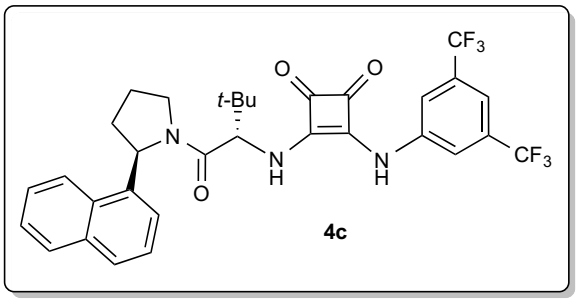

^{1}H NMR (600 MHz, DMSO) major rotamer resonances: δ 10.36 (s, 1H), 8.21 (d, J=10.0 Hz, 1H), 8.09 (s, 2H), 7.81 (dd, J=8.2, 4.1 Hz, 2H), 7.69 (s, 1H), 7.50 (m, 1H), 7.39 (t, J=7.6 Hz, 1H), 7.35 (dd, J=8.2, 1.8 Hz, 1H), 7.28 (t, J=7.6 Hz, 1H), 5.25 (dd, J=8.2, 2.9 Hz, 1H), 5.05 (d, J=10.0 Hz, 1H), 4.04 - 4.14 (m, 1H), 3.78 - 3.86 (m, 1H), 3.66 - 3.77 (m, 1H), 2.24 – 2.46 (m, 1H), 1.87 - 2.01 (m, 2H), 1.77 - 1.88 (m, 1H), 1.04 (s, 9H); select minor rotamer resonances: δ 10.35 (s, 1H), 8.29 (d, J=10.6 Hz, 1 H), 5.31 (dd, J=8.2, 2.3 Hz, 1H), 4.77 (d, J=10.6 Hz), 0.52 (s, 9H); (rotamer ratio in DMSO = 2.4:1);

^{13}C NMR (125 MHz, CD_2Cl_2) major and minor rotamer resonances δ 169.1, 133.2, 132.9, 132.7, 132.1, 128.8, 127.9, 127.6, 127.3, 126.5, 126.2, 125.8, 124.3, 123.6, 123.0, 118.4, 116.3, 62.3, 61.3, 48.9, 47.7, 36.4, 35.9, 35.5, 35.2, 33.8, 29.7, 25.8, 25.6, 23.4;

FTIR (neat, cm^{-1}) ν_{max} 1602, 1554, 1426, 1377, 1276, 1178, 680 cm^{-1};

HRMS (ESI-TOF) calculated for $C_{32}H_{29}F_6N_3O_3$ $[M+Na]^+$: 640.2011, found: 640.1992;

$[\alpha]_D^{25}$ = +107.1° (c = 0.7, $CHCl_3$).

3-((3,5-bis(trifluoromethyl)phenyl)amino)-4-(((*S*)-3,3-dimethyl-1-((*R*)-2-(naphthalen-2-yl)pyrrolidin-1-yl)-1-oxobutan-2-yl)amino)cyclobut-3-ene-1,2-dione (**4d**):

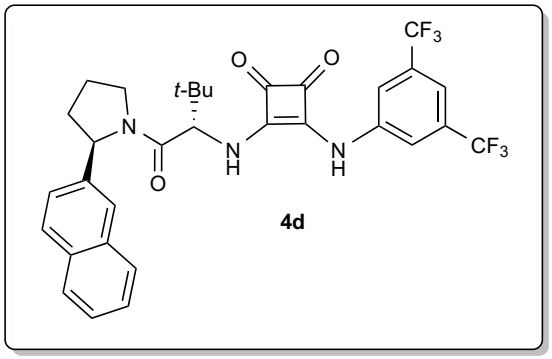

^{1}H NMR (500 MHz, DMSO) major rotamer resonances: δ 10.41 (s, 1H), 8.25 (d, J = 10.0 Hz, 1H), 8.06 (s, 2H), 7.88 (d, J = 7.7 Hz, 1H), 7.80 (d, J = 7.8 Hz, 1H), 7.71 (s, 1H), 7.51 – 7.46 (m, 2H), 7.41 (d, J = 10.2 Hz, 1H), 7.02 (t, J = 7.0 Hz, 1H), 5.22 (dd, J = 8.0, 4.0 Hz, 1H), 5.04 (d, J = 10.0 Hz, 1H), 3.90 – 3.80 (m, 1H), 3.56 – 3.51 (m, 1H), 2.48 – 2.42 (m, 1H), 2.06 – 1.93 (m, 2H), 1.92 – 1.79 (m, 2H), 1.00 (s, 9H); select minor rotamer resonances: δ 4.47 (d, J = 9.6 Hz, 1H), 4.01 – 3.94 (m, 1H), 2.37 – 2.27 (m, 1H); (rotamer ratio in DMSO = 2.0:1);

^{13}C NMR (125 MHz, DMSO) major and minor rotamer resonances δ 185.0, 169.6, 168.4, 131.9, 141.3, 133.2, 132.4, 132.0, 131.7, 128.8, 128.2, 127.9, 127.8, 126.9, 126.2, 125.8, 125.0, 124.7, 123.7, 122.5, 118.5, 115.3, 61.9, 61.7, 60.9, 55.4, 48.4, 40.5, 40.4, 40.3, 40.2, 40.0, 39.8, 39.7, 39.5, 35.9, 35.7, 34.1, 26.3, 26.1, 23.6, 22.0, 16.8;

FTIR (neat, cm^{-1}) ν_{max} 1770, 1600, 1512, 1377, 1251, 1168, 1020, 698 cm^{-1};

HRMS (ESI-TOF) calculated for $C_{32}H_{29}F_6N_3O_3$ $[M+H]^+$: 618.2191, found: 618.3002;

$[\alpha]_D^{25}$ = –206.7° (c = 0.5, $CHCl_3$).

3-((3,5-bis(trifluoromethyl)phenyl)amino)-4-(((*S*)-3,3-dimethyl-1-oxo-1-((*R*)-2-(phenanthren-3-yl)pyrrolidin-1-yl)butan-2-yl)amino)cyclobut-3-ene-1,2-dione (**4f**):

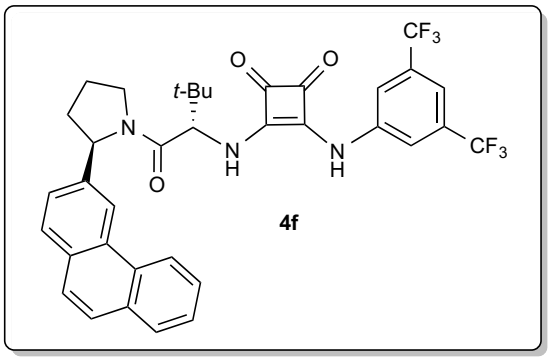

4f

^{1}H NMR (600 MHz, DMSO) major rotamer resonances: δ 10.24 (s, 1H), 8.98 (s, 1H), 8.52 (d, J = 10.0 Hz, 1H), 8.31 (s, 1H), 8.23 (d, J = 10 Hz, 1H), 7.92 (s, 1H), 7.88 (d, J = 8.2 Hz, 1H), 7.83 (d, J = 8.8 Hz, 1H), 7.73 (dd, J = 12.3, 8.8 Hz, 2H), 7.47 (dd, J= 8.2, 1.2 Hz, 1H), 7.21 – 7.37 (m, 2H), 5.34 (dd, J = 8.2, 2.9 Hz, 1H), 5.11 (d, J = 10.0 Hz), 4.24 (qd, J = 5.9, 4.7 Hz, 1H), 3.84 (dd, J = 10.0, 7.6 Hz, 1H), 2.39 (dq, J = 12.3, 8.4 Hz, 1H), 1.99 – 1.85 (m, 1H), 1.04 (s. 9H); select minor rotamer resonances: δ 10.41 (s, 1H), 8.97 (s, 1H), 4.89 (d, J = 10.0 Hz, 1H), 0.42 (s, 9H); (rotamer ratio in DMSO = 2.1:1);

^{13}C NMR (125 MHz, DMSO) major and minor rotamer resonances δ 189.7, 189.6, 185.8, 185.6, 174.4, 174.3, 174.2, 173.2, 168.1, 168.0, 147.8, 147.0, 146.3, 146.1, 137.0, 136.9, 136.8, 136.7, 136.4, 135.4, 134.7, 134.6, 133.6, 131.6, 130.5, 129.4, 127.2, 125.1, 123.4, 120.0, 66.8, 65.8, 53.4, 52.3, 40.8, 40.5, 40.4, 39.1, 31.0, 30.7, 30.0, 28.4, 27.3, 16.4;

FTIR (neat, cm^{-1}) ν_{max} 1557, 1430, 1378, 1277, 1179, 1132, 701 cm^{-1};

HRMS (ESI-TOF) calculated for $C_{36}H_{31}F_6N_3O_3$ $[M+Na]^+$: 690.2167, found: 690.2175;

$[\alpha]_D^{25}$ = +210.4° (c = 1.0, $CHCl_3$).

3-((3,5-bis(trifluoromethyl)phenyl)amino)-4-(((*S*)-3,3-dimethyl-1-oxo-1-((*R*)-2-(phenanthren-1-yl)pyrrolidin-1-yl)butan-2-yl)amino)cyclobut-3-ene-1,2-dione (**4g**):

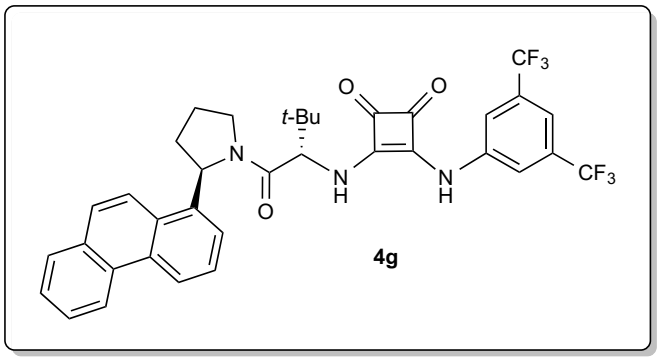

^{1}H NMR (600 MHz, CD_2Cl_2) major rotamer resonances: δ 10.97 (s, 1H), 9.36 (d, J = 8.7 Hz, 1H), 9.24 (d, J = 8.5 Hz, 1H), 8.81 (m, 1H), 8.66 (d, J = 9.0 Hz, 1H), 8.67 – 8.59 (br s, 2H), 8.54 (d, J = 8.2 Hz, 1H), 8.46 (d, J = 8.9 Hz, 1H), 8.28 – 8.19 (br s, 2H), 8.17 (m, 1H), 8.07 (m, 1H), 7.75 (d, J = 6.7 Hz, 1H), 6.49 (d, J = 8.3 Hz, 1H), 5.67 (m, 1H), 4.70 (m, 1H), 2.56 (m, 1H), 2.44 (m, 1H), 2.34 (m, 1H), 1.77 (m, 2H), 1.19 (s, 9H); (rotamer ratio in CD_2Cl_2 = 7.0:1);

^{13}C NMR (125 MHz, CD_2Cl_2) major and minor rotamer resonances δ 169.5, 169.2, 162.6, 140.3, 137.1, 132.6, 132.4, 131.7, 131.2, 130.7, 130.4, 130.2, 128.6, 128.5, 128.0, 127.6, 127.3, 127.0, 126.9, 125.5, 125.2, 124.1, 122.9, 122.7, 121.9, 121.7, 121.0, 119.8, 118.2, 116.1, 62.2, 59.1, 56.5, 49.1, 48.0, 36.2, 35.8, 35.3, 34.3, 33.2, 31.9, 29.7, 29.3, 26.1, 25.9, 25.7, 23.3, 22.7, 21.1, 18.2, 13.9, 11.4;

FTIR (neat, cm^{-1}) ν_{max} 1599, 1554, 1424, 1276, 1179, 1130 cm^{-1};

HRMS (ESI-TOF) calculated for $C_{36}H_{31}F_6N_3O_3$ $[M+Na]^+$: 690.2167, found: 690.2159;

$[\alpha]_D^{25}$ = –99.2° (c = 0.5, $CHCl_3$).

(*S*)-2-((2-((3,5-bis(trifluoromethyl)phenyl)(methyl)amino)-3,4-dioxocyclobut-1-en-1-yl)(methyl)amino)-*N*,3,3-trimethyl-*N*-((*R*)-1-phenylethyl)butanamide (**3d**):

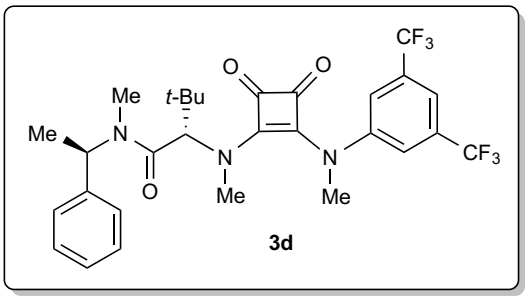

3d

To **3c** (100 mg, 0.18 mmol, 1 equiv.) was added $CsCO_3$ (180 mg, 0.54 mmol, 3.0 equiv.) and DMF (2.66 mL). The reaction mixture was cooled to 0 °C and methyl iodide (40 μL, 0.65 mmol, 3.6 equiv.) was added. The reaction mixture was warmed to room temperature and stirred vigorously. After 3 days, the reaction mixture was diluted with ethyl acetate (10 mL) and washed with H_2O (4×10 mL). The organic layer was dried with anhydrous $MgSO_4$ and concentrated under reduced pressure. The crude residue was purified by flash column chromatography on silica gel (0 to 60% ethyl acetate in hexanes) to yield **3d** as a yellow powder (84.0 mg, 80%).

^{1}H NMR (600 MHz, $CDCl_3$) major rotamer resonances: δ 7.61 (s, 1 H), 7.39 - 7.41 (m, 1 H), 7.17 - 7.37 (m, 6 H), 6.04 (q, *J*=7.0 Hz, 1 H), 5.55 (s, 1 H), 3.70 (s, 3 H), 2.78 (s, 3 H), 2.74 (s, 3 H), 1.47 (d, *J*=7.0 Hz, 3 H), 1.11 (s, 9 H); (rotamer ratio in $CDCl_3$ = 3.3:1);

^{13}C NMR (125 MHz, $CDCl_3$) major and minor rotamer resonances δ 188.1, 187.8, 184.8, 184.7, 175.1, 174.7, 167.7, 167.4, 165.0, 164.9, 146.4, 146.3, 140.1, 139.6, 133.8, 133.6, 133.5, 133.3, 133.2, 133.0, 128.7, 128.6, 127.7, 127.6, 127.3, 127.2, 126.7, 126.1, 123.9, 121.7, 119.0, 118.8, 117.4, 117.3, 63.8, 62.7, 55.0, 50.8, 39.3, 39.2, 37.6, 37.5, 37.4, 37.3, 30.1, 28.9, 27.3, 27.1, 26.8, 18.6, 15.7;

FTIR (neat, cm^{-1}) ν_{max} 1572, 1491, 1392, 1379, 1275, 1175, 1004, 699, 682 cm^{-1};

HRMS (ESI-TOF) calculated for $C_{29}H_{31}F_6N_3O_3$ $[M+Na]^+$: 606.2167, found: 606.2137;

$[\alpha]_D^{25}$ = –69.2° (c = 0.5, $CHCl_3$).

3-((3,5-bis(trifluoromethyl)phenyl)(methyl)amino)-4-(((*S*)-3,3-dimethyl-1-oxo-1-((*R*)-2-(pyren-1-yl)pyrrolidin-1-yl)butan-2-yl)(methyl)amino)cyclobut-3-ene-1,2-dione (**5h**):

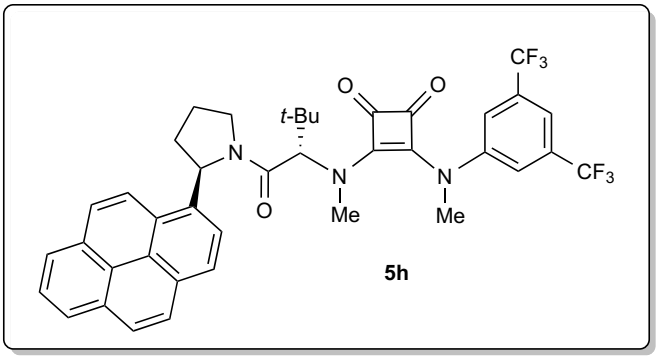

5h

To **4h** (200 mg, 0.28 mmol, 1 equiv.) was added $CsCO_3$ (282 mg, 0.87 mmol, 3.0 equiv.) and DMF (4.26 mL). The reaction mixture was cooled to 0 °C and methyl iodide (65 μL, 1.04 mmol, 3.6 equiv.) was added. The reaction mixture was warmed to room temperature and stirred vigorously. After 3 days, the reaction mixture was diluted with ethyl acetate (20 mL) and washed with H_2O (4×20 mL). The organic layer was dried with anhydrous $MgSO_4$ and concentrated under reduced pressure. The crude residue was purified by flash column chromatography on silica gel (0 to 60% ethyl acetate in hexanes) to yield **5h** as a yellow powder (120.0 mg, 58%).

^{1}H NMR (600 MHz, $CDCl_3$) major rotamer resonances: δ 8.28 (d, *J*=8.8 Hz, 1 H), 8.15 - 8.20 (m, 2 H), 8.12 (d, *J*=9.4 Hz, 1 H), 7.96 - 8.07 (m, 4 H), 7.60 (s, 1 H), 7.52 (d, *J*=7.6 Hz, 1 H), 7.43 (s, 2 H), 6.23 - 6.28 (m, 1 H), 5.70 (s, 1 H), 4.09 - 4.19 (m, 1 H), 4.02 (dt, *J*=10.6, 8.2 Hz, 1 H), 3.80 (s, 3 H), 2.62 (s, 3 H), 2.49 - 2.59 (m, 1 H), 2.01 - 2.16 (m, 3 H), 1.12 (s, 9 H); select minor rotamer resonances: δ 7.26 (s, 2 H), 3.77 (s, 1 H), 2.82 (s, 1 H), 0.81 (s, 9 H); (rotamer ratio in $CDCl_3$ = 3.6:1);

^{13}C NMR (125 MHz, $CDCl_3$) major and minor rotamer resonances δ 188.2, 187.2, 185.0, 175.5, 175.2, 167.2, 166.2, 165.1, 164.5, 146.5, 146.3, 136.1, 134.6, 133.8, 133.6, 133.3, 133.0, 131.3, 131.1, 130.7, 130.5, 127.9, 127.8, 127.5, 127.3, 127.2, 126.0, 125.7, 125.3, 125.2, 124.9, 124.3, 123.8, 123.2, 123.0, 122.4, 121.7, 121.3, 118.8, 118.5, 117.5, 65.4, 59.4, 59.0, 49.0, 47.6, 39.4, 39.3, 37.6, 37.2, 35.5, 33.5, 27.1, 26.8, 24.3, 20.9;

FTIR (neat, cm^{-1}) ν_{max} 1574, 1379, 1274, 1179, 1128, 884, 682 cm^{-1};

HRMS (ESI-TOF) calculated for $C_{40}H_{35}F_6N_3O_3$ $[M+Na]^+$: 742.2480, found: 742.2457;

$[\alpha]_D^{25}$ = –112.4° (c = 0.5, $CHCl_3$).

2.4.3. Preparation and Characterization of Substrates

((3,3-dimethoxyprop-1-en-2-yl)oxy)trimethylsilane (**1a**):

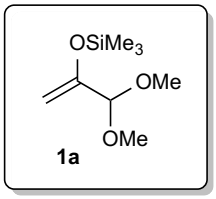

1a

Procedure for synthesis of **1a** was previously reported[46].

^{1}H NMR (600 MHz, $CDCl_3$) δ 4.53 (d, J=12.9 Hz, 2 H), 4.35 (s, 1 H), 3.33 (s, 6 H), 0.23 (s, 9 H);

^{13}C NMR (125 MHz, $CDCl_3$) δ 153.2, 102.2, 92.8, 53.3, 0.1;

FTIR (neat, cm^{-1}) ν_{max} 1251, 1114, 1059, 1028, 839, 753 cm^{-1};

HRMS (ESI-TOF) calculated for $C_8H_{18}O_3Si$ $[M+Na]^+$: 213.0923, found: 213.0902.

[46] Murray, D. H.; Albizati, K. F. *Tetrahedron Lett.* **1990**, *31*, 4109–4112.

(*Z*)-((1,1-dimethoxybut-2-en-2-yl)oxy)trimethylsilane (**1b**):

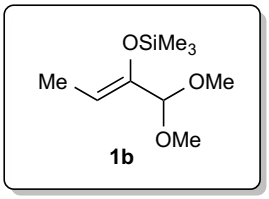

Synthesis of 1,1-dimethoxybutan-2-one has been reported[47]. **1b** was then synthesized on 12.9 mmol scale via a modified procedure for synthesis of **1a**: LiHMDS (1M in THF, 1.0 equiv.) was used instead of LDA to ensure formation of Z-isomer of **1b** exclusively. Compound **1b** was then purified via vacuum distillation (70 ^{o}C at 10 torr) to yield clear oil.

^{1}H NMR (600 MHz, $CDCl_3$) δ 4.99 (q, J=6.5 Hz, 1H), 4.45 (s, 1H), 3.33 (s, 6H), 1.58 (d, J=7.0 Hz, 3H), 0.20 (s, 9H);

^{13}C NMR (125 MHz, $CDCl_3$) δ 146.1, 105.8, 103.5, 53.8, 10.3, 0.64;

FTIR (neat, cm^{-1}) ν_{max} 1250, 1114, 1091, 1046, 842, 755 cm^{-1};

HRMS (ESI-TOF) calculated for $C_9H_{20}O_3Si$ $[M+Na]^+$: 227.1079, found: 227.1080.

[47] For synthesis of 1,1-dimethoxybutan-2-one, see: Ayla-Mata, F.; Barrera-Mendoza, C.; Jumenez-Vazquez, H. A.; Vargas-Diaz, E.; Zepeda, L. G. *Molecules* **2012**, *17*, 13864–13878.

(*Z*)-((1,1-dimethoxy-4-methylpent-2-en-2-yl)oxy)trimethylsilane (**1c**):

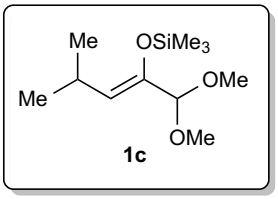

1c

1,1-dimethoxy-4-methylpentan-2-one was prepared via previously reported procedure for synthesis of 1,1-dimethoxybutan-2-one. **1c** was prepared via the same procedure as **1b** and purified via vacuum distillation (90 ^{o}C at 10 torr) to yield clear oil.

^{1}H NMR (600 MHz, $CDCl_3$) δ 4.76 (d, J=9.4 Hz, 1H), 4.43 (s, 1H), 3.32 (s, 6H), 2.58 - 2.70 (m, 1H), 0.96 (d, J=5.9 Hz, 6H), 0.20 (s, 1H);

^{13}C NMR (125 MHz, $CDCl_3$) δ 143.0, 119.2, 103.4, 53.6, 24.5, 23.0, 0.5;

FTIR (neat, cm^{-1}) ν_{max} 1249, 1102, 1080, 1058, 999, 838, 754 cm^{-1};

HRMS (ESI-TOF) calculated for $C_{11}H_{24}O_3Si$ $[M+Na]^+$: 255.1392, found: 255.1390.

(*Z*)-((1,1-bis(benzyloxy)but-2-en-2-yl)oxy)trimethylsilane (**1d**):

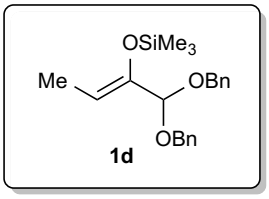

1d [48] was prepared via the same procedure as compound **1b** and purified via column chromatography using davisil grade silica gel (10% to 30% diethyl ether in hexanes).

^{1}H NMR (600 MHz, $CDCl_3$) δ 7.15 - 7.49 (m, 10 H), 5.13 (d, J=6.5 Hz, 1 H), 4.83 (s, 1 H), 4.64 (d, J=1.0 Hz, 2H), 4.51 (d, J=1.0 Hz, 2H), 1.62 (d, J=6.5 Hz, 3 H), 0.18 (s, 9 H);

^{13}C NMR (125 MHz, $CDCl_3$) δ 146.4, 138.1, 128.6 – 127.4 (m), 106.4, 100.0, 67.9, 10.4, 0.7;

FTIR (neat, cm^{-1}) ν_{max} 1249, 1040, 1025, 840, 732, 695 cm^{-1};

HRMS (ESI-TOF) calculated for $C_{21}H_{28}O_3Si$ $[M+Na]^+$: 379.1705, found: 379.1725.

[48] 1,1-bis(benzyloxy)butan-2-one was prepared from 1,1-dimethoxybutan-2-one via transacetalization (Benzyl alcohol (5.0 equiv.), PTSA•H_2O (10 mol%), cyclohexane (0.5 M), reflux with Dean-Stark apparatus).

2.4.4. General Procedure for Squaramide-Catalyzed (4+3) Cycloaddition

Method A (reaction optimization): A 1-dram vial was equipped with a magnetic stir bar, closed with a cap containing a rubber septum, flame-dried and subsequently cooled under vacuum. The vial was placed under N_2 and charged with substrate **1b** (0.05 mmol, 1 equiv.), furan (11 μL, 0.15 mmol, 3.0 equiv.), **4h** (3.5 mg, 0.005 mmol, 10 mol%) and *t*-butyl methyl ether (0.5 mL). The mixture was then cooled to -78 ºC on the dry ice-acetone bath. TESOTf (11.0 μL, 0.05 mmol, 1.0 equiv.) was added via syringe. The reaction was stirred for 3 h at -78 ºC, and then quenched via addition of 100 μL of a 6:1 MeOH:Et_3N solution via syringe.

Method B (preparative scale reactions): A 10 mL round-bottom flask was equipped with a magnetic stir bar, flame-dried and subsequently cooled under vacuum. The flask was placed under N_2 and charged with substrate **1b** (0.25 mmol, 1 equiv.), furan (55 μL, 0.75 mmol, 3.0 equiv.), **4h** (17.3 mg, 0.025 mmol, 10 mol%) and *t*-butyl methyl ether (2.5 mL). The mixture was then cooled to -78 ºC on the dry ice-acetone bath. TESOTf (57.0 μL, 0.25 mmol, 1.0 equiv.) was added via syringe. The reaction was stirred for 3 h at -78 ºC, and then quenched via addition of 500 μL of a 6:1 MeOH:Et_3N solution via syringe. The crude reaction mixture was concentrated and purified by column chromatography with hexane/ethyl ether as eluent (10:1 to 2:1) to yield pure **2b**. When applicable, regioselectivity was determined via ^1H NMR on crude reaction mixture prior to column chromatography. Reported yields are averages of two runs.

2.4.5. Characterization of Products 2a-2l

(1*R*,2*S*,5*R*)-2-methoxy-8-oxabicyclo[3.2.1]oct-6-en-3-one (**2a**):

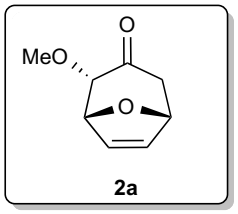

2a

Followed procedure B for (4+3) cycloaddition from **1a** (47.6 mg, 0.25 mmol) and purified using silica gel chromatography to give 26.3 mg (69% yield) of **2a** as yellow oil.

^{1}H NMR (600 MHz, $CDCl_3$) δ 6.29 (s, 2H), 5.02 (dd, *J*=11.2, 5.3 Hz, 2H), 3.96 (d, *J*=5.3 Hz, 1H), 3.58 (s, 3H), 2.77 (dd, *J*=15.3, 4.7 Hz, 1H), 2.36 (d, *J*=15.3 Hz, 1H);

^{13}C NMR (125 MHz, $CDCl_3$) δ 204.5, 134.7, 131.5, 87.0, 79.3, 78.4, 59.8, 45.9;

FTIR (neat, cm^{-1}) ν_{max} 1724, 1116, 1045, 962, 727 cm^{-1};

HRMS (ESI-TOF) calculated for $C_8H_{10}O_3$ $[M+Na]^+$: 177.0528, found: 177.0501;

$[\alpha]_D^{25}$ = –3.6° (c = 1.0, $CHCl_3$).

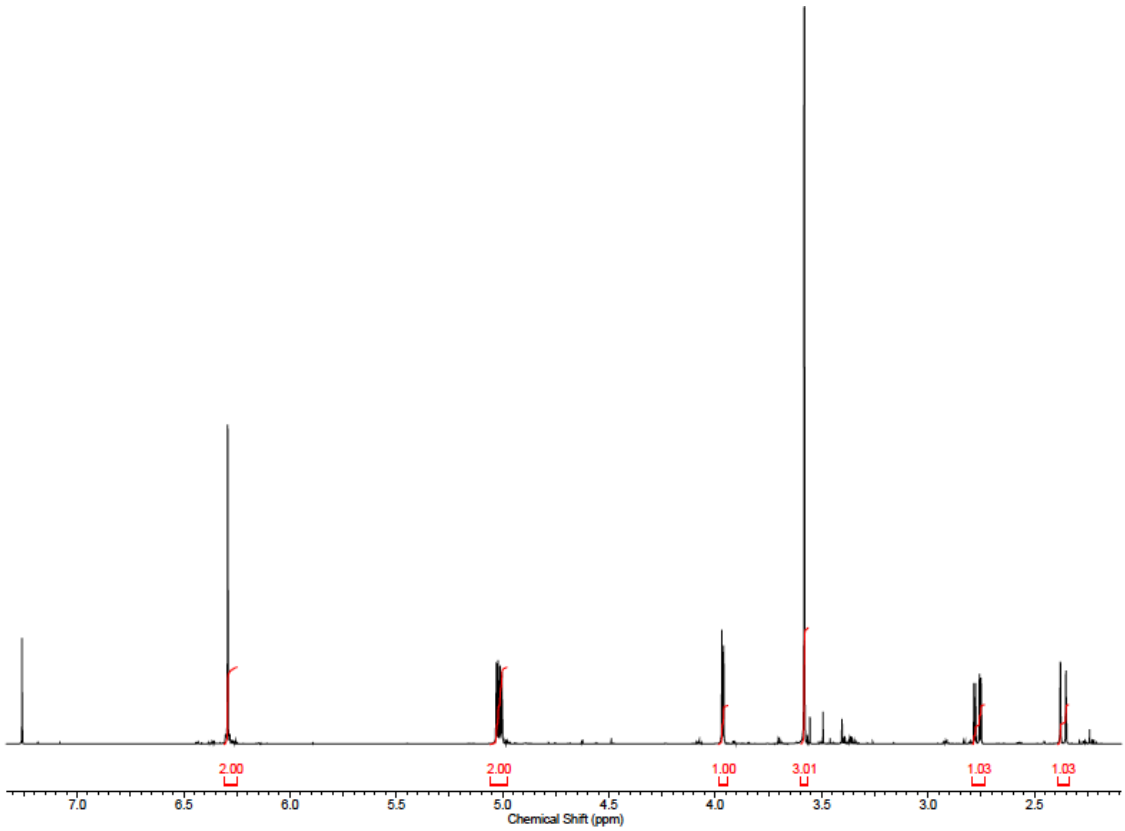
2.00
2.00
1.00
3.01
1.03
1.03
7.0
6.5
6.0
5.5
5.0
4.5
4.0
3.5
3.0
2.5
Chemical Shift (ppm)

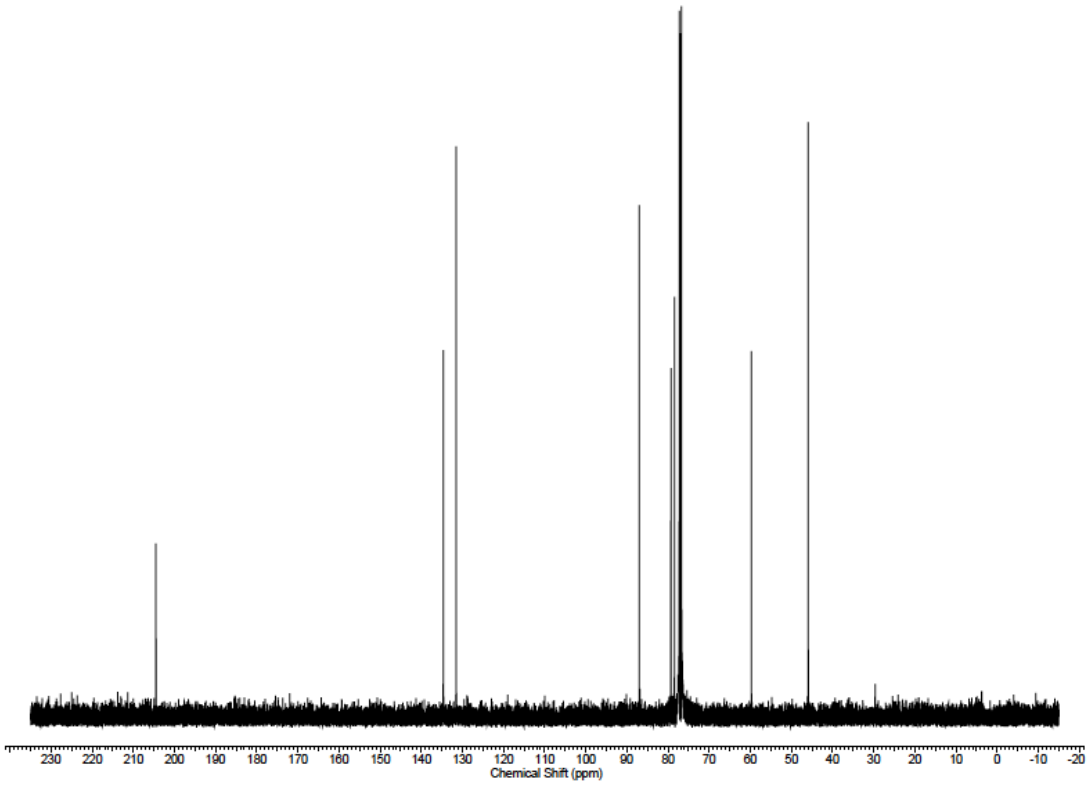
230
220
210
200
190
180
170
160
150
140
130
120
110
100
90
80
70
60
50
40
30
20
10
0
-10
-20
Chemical Shift (ppm)

Racemic sample: GC (β-Cyclosil, 30 m x 0.25 mm x 0.25 µm, 60 to 160 °C, 2 °C/min)

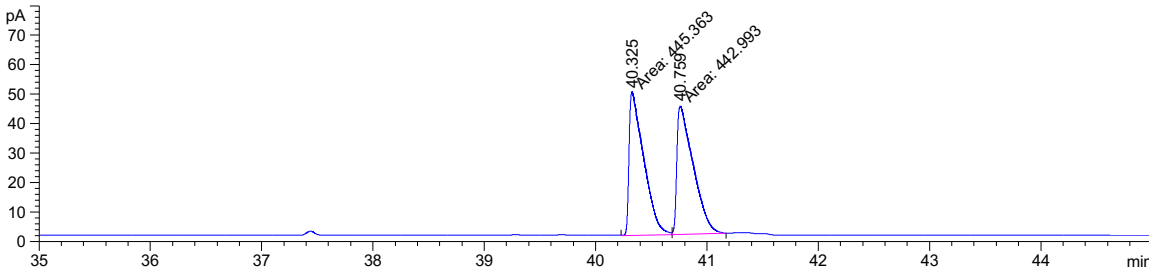

Peak #	RetTime [min]	Type	Width [min]	Area [pA*s]	Height [pA]	Area %
1	40.325	MF	0.1524	445.36328	48.69243	50.13340
2	40.759	FM	0.1694	442.99323	43.59036	49.86660

Enantioenriched Sample: GC (β-Cyclosil, 30 m x 0.25 mm x 0.25 µm, 60 to 160 °C, 2 °C/min), 71% e.e.

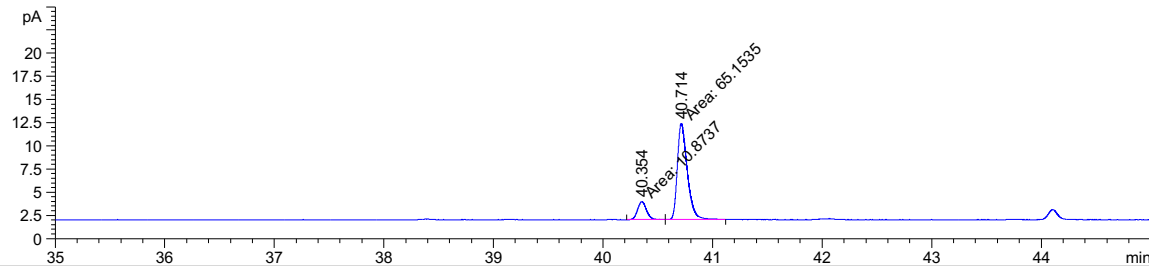

Peak #	RetTime [min]	Type	Width [min]	Area [pA*s]	Height [pA]	Area %
1	40.354	MF	0.0931	10.87366	1.94629	14.30234
2	40.714	FM	0.1050	65.15348	10.33869	85.69766

(1*R*,2*S*,4*R*,5*S*)-2-methoxy-4-methyl-8-oxabicyclo[3.2.1]oct-6-en-3-one (**2b**):

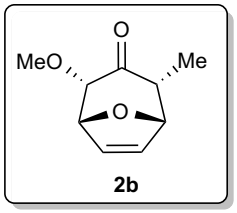

2b

Followed procedure B for (4+3) cycloaddition from **1b** (102.2 mg, 0.50 mmol) and purified using silica gel chromatography to give 68.9 mg (82% yield) of **2b** as off-white solid.

^{1}H NMR (600 MHz, $CDCl_3$) δ 6.35 (ddd, J = 1.8, 6.5, 12.3 Hz, 2H), 5.01 (dd, J = 1.5, 4.4 Hz, 1H),

4.83 (dd, J = 1.2, 3.5 Hz, 1H), 3.98 (d, J = 5.3 Hz, 1H), 3.59 (s, 3H), 2.84 (dq, J = 2.4, 4.7 Hz, 1H), 0.98 (d, J = 7.0 Hz, 3H);

^{13}C NMR (125 MHz, $CDCl_3$) δ 206.3, 133.4, 133.1, 86.1, 82.9, 80.0, 59.7, 50.2, 9.5;

FTIR (neat, cm^{-1}) ν_{max} 1715, 1125, 1068, 936, 741 cm^{-1};

HRMS (ESI-TOF) calculated for $C_9H_{12}O_3$ $[M+Na]^+$: 191.0684, found: 191.0677;

$[\alpha]_D^{25}$ = –51.6° (c = 1.0, $CHCl_3$).

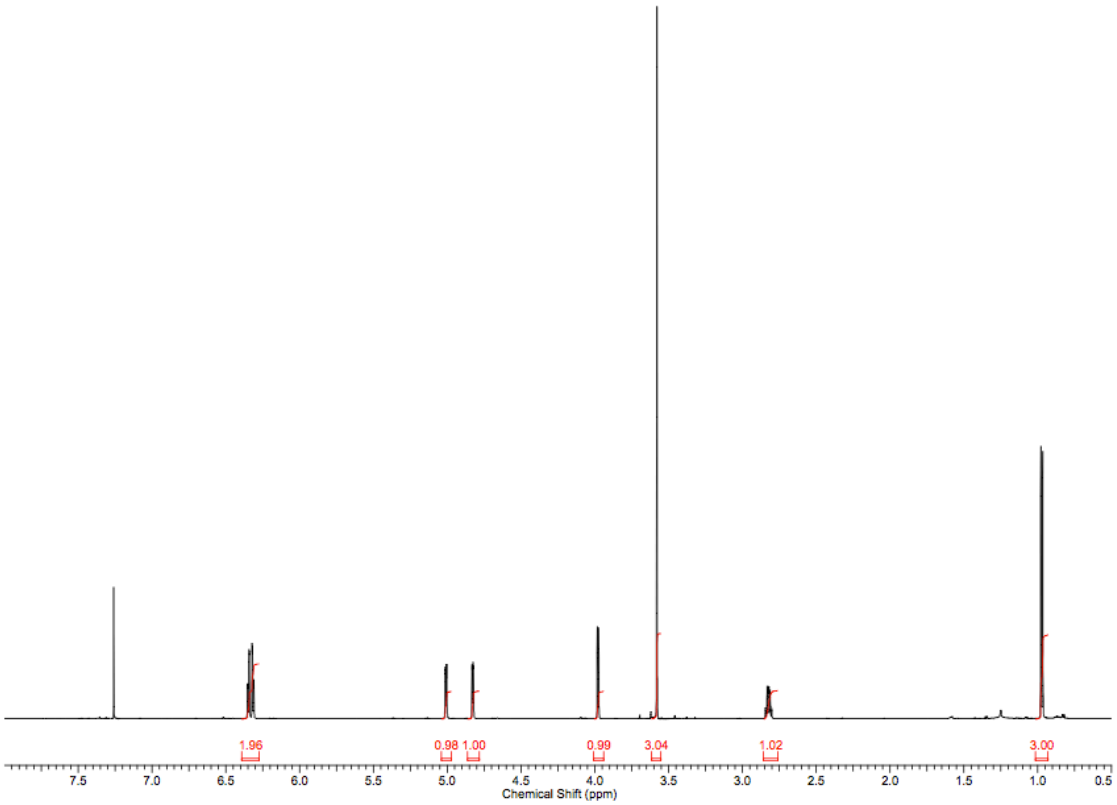
1.96
0.98
1.00
0.99
3.04
1.02
3.00
7.5
7.0
6.5
6.0
5.5
5.0
4.5
4.0
3.5
3.0
2.5
2.0
1.5
1.0
0.5
Chemical Shift (ppm)

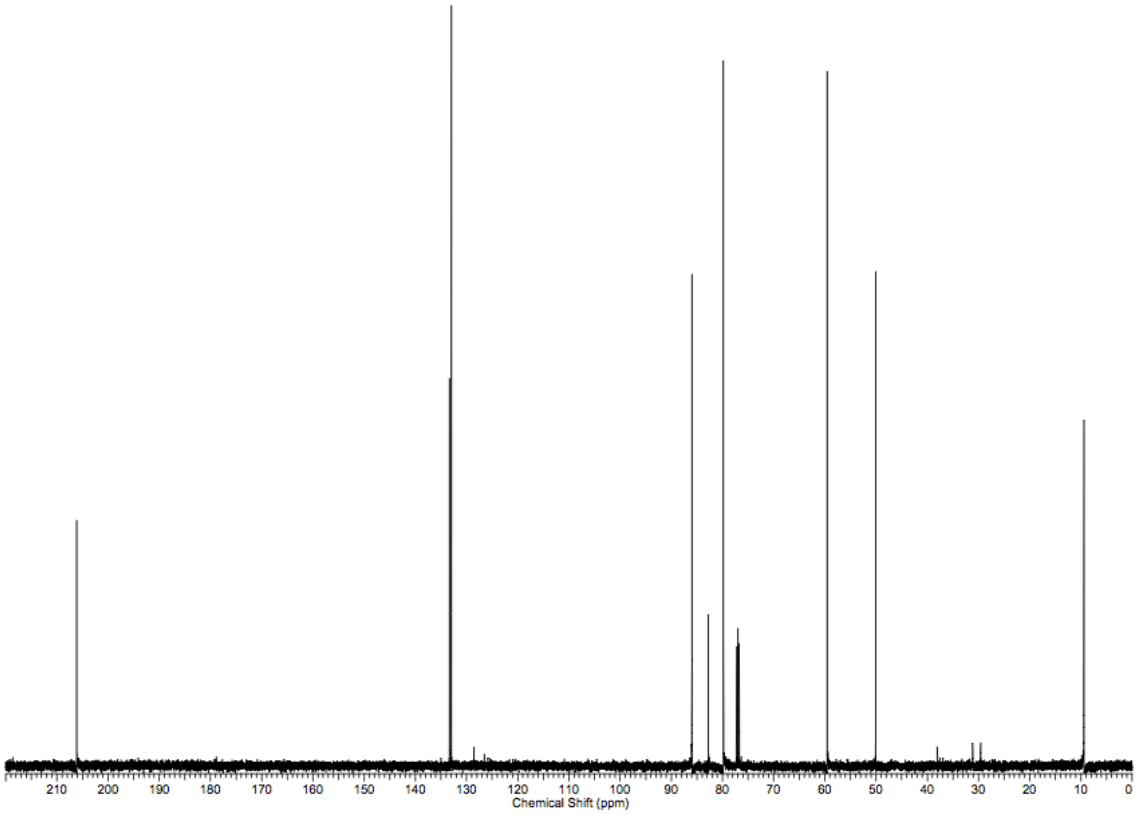
210
200
190
180
170
160
150
140
130
120
110
100
90
80
70
60
50
40
30
20
10
0
Chemical Shift (ppm)

Racemic sample: GC (β-Cyclosil, 30 m x 0.25 mm x 0.25 µm, 60 to 160 °C, 2 °C/min)

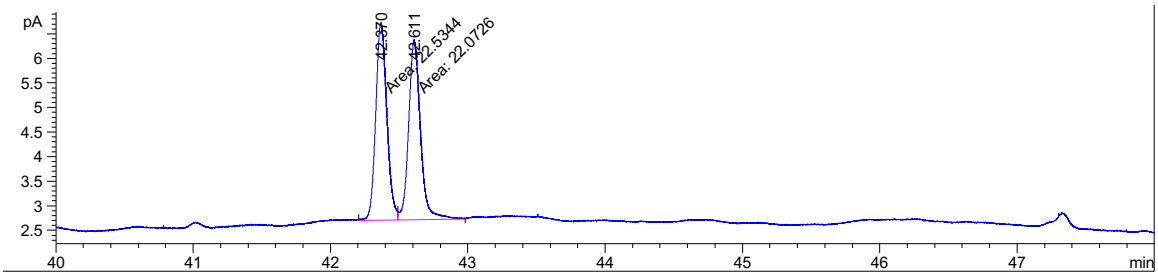

Peak #	RetTime [min]	Type	Width [min]	Area [pA*s]	Height [pA]	Area %
1	42.370	MF	0.0934	22.53436	4.01915	50.51760
2	42.611	FM	0.1003	22.07259	3.66933	49.48240

Enantioenriched Sample: GC (β-Cyclosil, 30 m x 0.25 mm x 0.25 µm, 60 to 160 °C, 2 °C/min), 89% e.e.

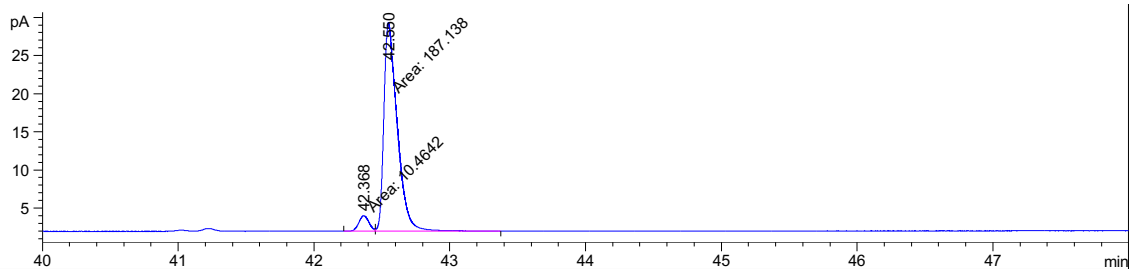

Peak #	RetTime [min]	Type	Width [min]	Area [pA*s]	Height [pA]	Area %
1	42.368	MF	0.0864	10.46417	2.01807	5.29556
2	42.550	FM	0.1140	187.13840	27.35389	94.70444

(1*S*,2*R*,4*S*,5*R*)-2-isopropyl-4-methoxy-8-oxabicyclo[3.2.1]oct-6-en-3-one (**2c**):

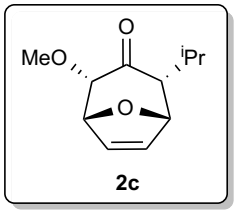

2c

Followed procedure B for (4+3) cycloaddition from **1c** (58.1 mg, 0.25 mmol) and purified using silica gel chromatography to give 26.8 mg (55% yield) of **2c** as yellow oil.

^{1}H NMR (600 MHz, $CDCl_3$) δ 6.20 - 6.30 (m, 2H), 4.99 (ddd, *J*=11.7, 4.7, 1.8 Hz, 2H), 3.91 (d, *J*=5.3 Hz, 2H), 3.56 (s, 3H), 2.57 (dd, *J*=7.6, 4.7 Hz, 1H), 1.91 - 2.07 (m, 1H), 1.04 (d, *J*=7.0 Hz, 3H), 0.91 (d, *J*=7.0 Hz, 3H);

^{13}C NMR (125 MHz, $CDCl_3$) δ 205.2, 133.7, 132.1, 86.0, 80.9, 80.1, 62.4, 59.6, 24.2, 22.7, 20.0;

FTIR (neat, cm^{-1}) ν_{max} 1720, 1129, 1080, 928, 838, 734 cm^{-1};

HRMS (ESI-TOF) calculated for $C_{11}H_{16}O_3$ $[M+Na]^+$: 219.0997, found: 219.0935;

$[\alpha]_D^{25}$ = –27.6° (c = 1.0, $CHCl_3$).

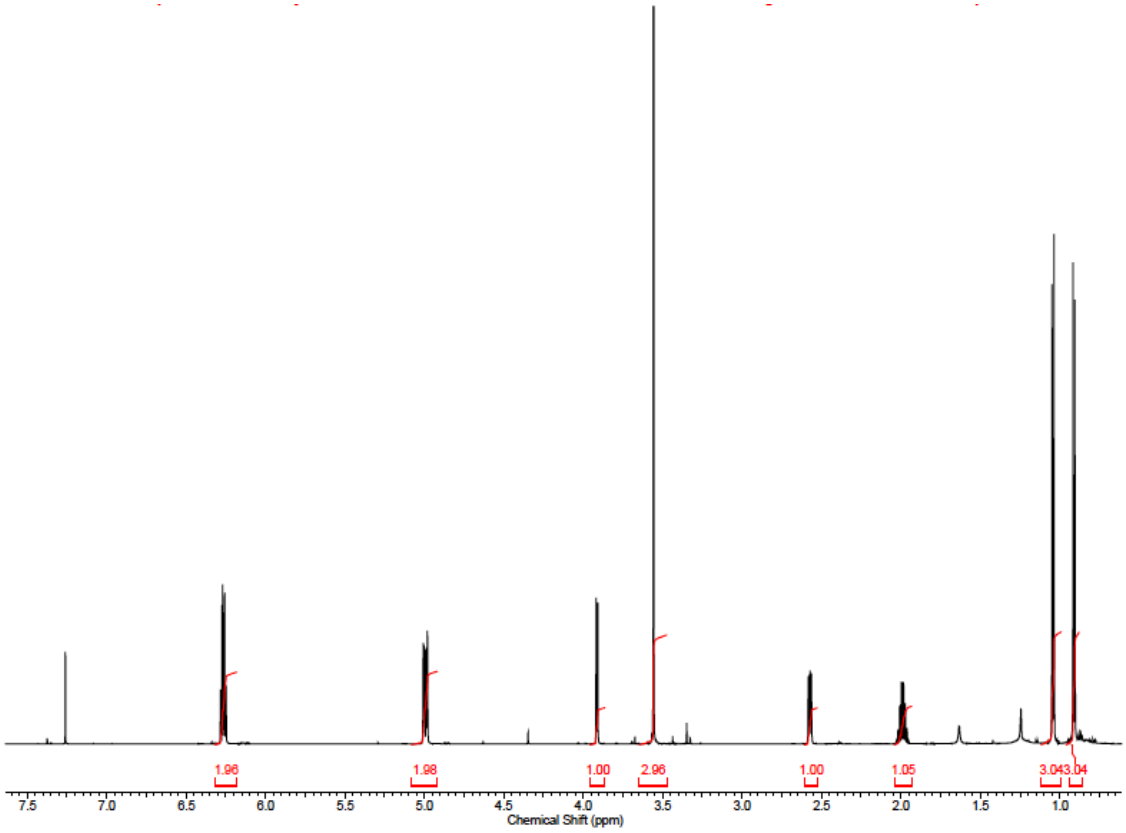
1.96
1.98
1.00
2.96
1.00
1.05
3.04
3.04
7.5
7.0
6.5
6.0
5.5
5.0
4.5
4.0
3.5
3.0
2.5
2.0
1.5
1.0
Chemical Shift (ppm)

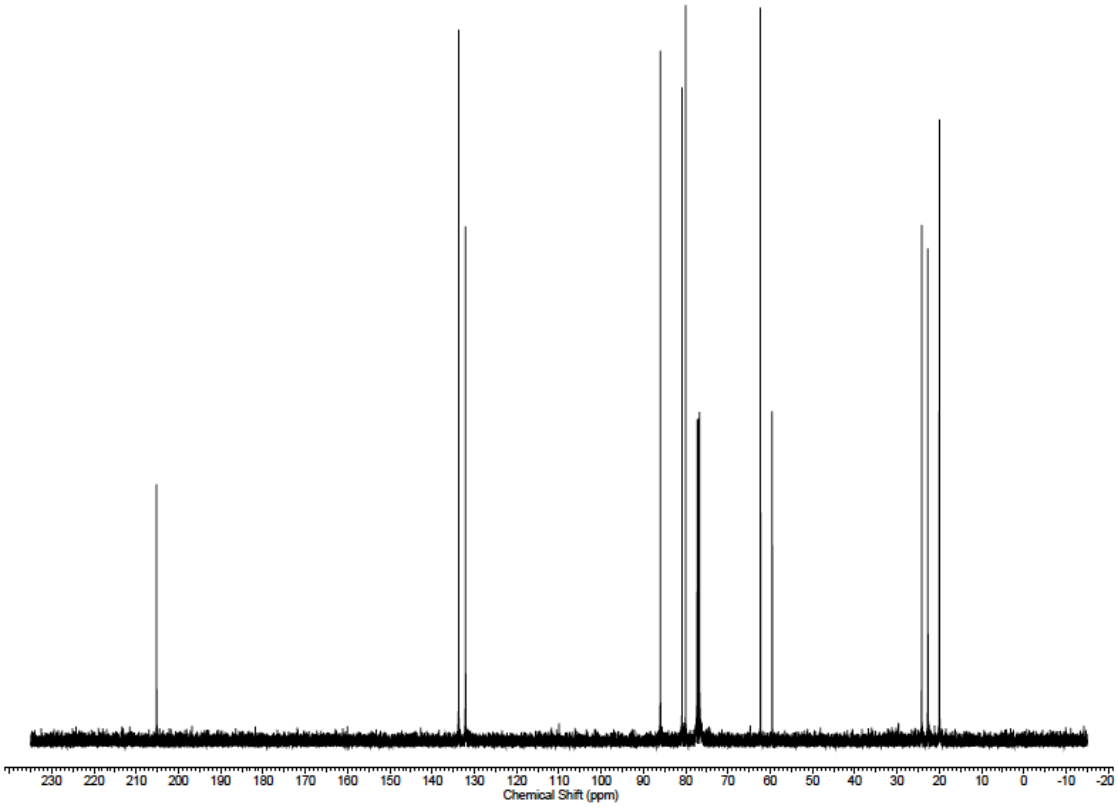
230
220
210
200
190
180
170
160
150
140
130
120
110
100
90
80
70
60
50
40
30
20
10
0
-10
-20
Chemical Shift (ppm)

Racemic sample: GC (β-Cyclosil, 30 m x 0.25 mm x 0.25 µm, 60 to 160 °C, 2 °C/min)

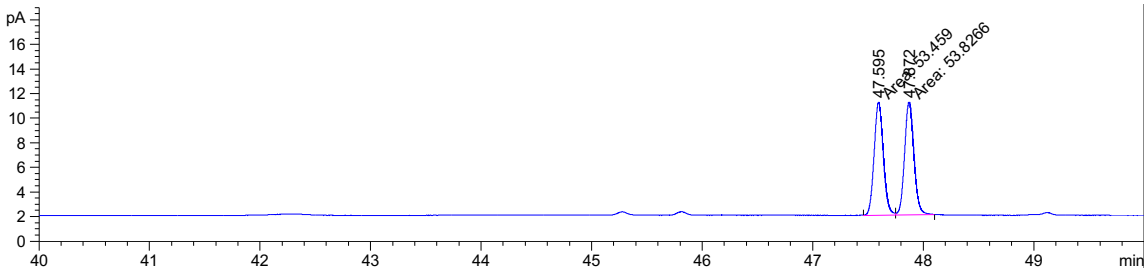

Peak #	RetTime [min]	Type	Width [min]	Area [pA*s]	Height [pA]	Area %
1	47.595	MF	0.0973	53.45900	9.15904	49.82869
2	47.872	FM	0.0980	53.82658	9.15051	50.17131

Enantioenriched Sample: GC (β-Cyclosil, 30 m x 0.25 mm x 0.25 µm, 60 to 160 °C, 2 °C/min), 77% e.e.

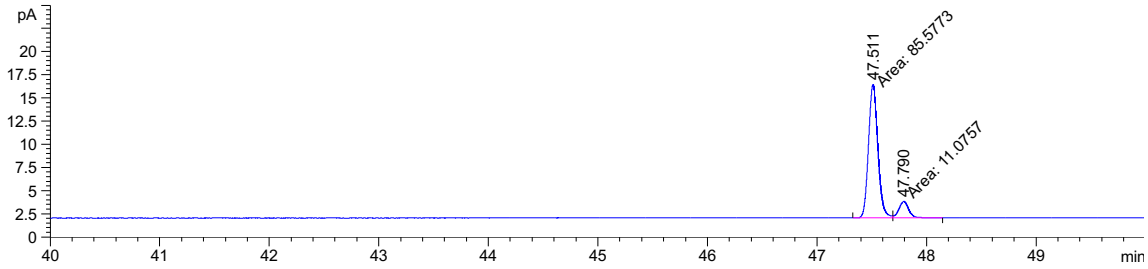

Peak #	RetTime [min]	Type	Width [min]	Area [pA*s]	Height [pA]	Area %
1	47.511	MF	0.0990	85.57735	14.39996	88.54079
2	47.790	FM	0.1042	11.07568	1.77097	11.45921

(1*R*,2*S*,4*R*,5*S*)-2-(benzyloxy)-4-methyl-8-oxabicyclo[3.2.1]oct-6-en-3-one (**2d**):

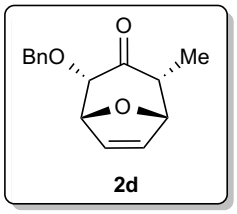

2d

Followed procedure B for (4+3) cycloaddition from **1d** (89.1 mg, 0.25 mmol) and purified using silica gel chromatography to give 45.4 mg (74% yield) of **2d** as dark yellow oil.

^{1}H NMR (600 MHz, $CDCl_3$) δ 7.27 - 7.40 (m, 5H), 6.39 (dd, J=5.9, 1.8 Hz, 1H), 6.32 (dd, J=5.9, 1.8 Hz, 1H), 4.97 (d, J=11.7 Hz, 1H), 4.91 (dd, J=5.3, 1.8 Hz, 1H), 4.82 (dd, J=4.7, 1.8 Hz, 1H), 4.62 (d, J=11.7 Hz, 1H), 4.15 (d, J=5.9 Hz, 1H), 2.80 (qd, J=6.8, 4.7 Hz, 1H), 0.98 (d, J=7.0 Hz, 3H);

^{13}C NMR (125 MHz, $CDCl_3$) δ 206.7, 137.7, 133.4, 128.5, 128.0, 83.3, 82.9, 80.5, 73.5, 50.2, 9.6;

FTIR (neat, cm^{-1}) ν_{max} 1721, 1126, 1067, 935, 733, 699 cm^{-1};

HRMS (ESI-TOF) calculated for $C_{15}H_{16}O_3$ $[M+Na]^+$: 267.0997, found: 267.0943;

$[\alpha]_D^{25}$ = –46.0° (c = 1.0, $CHCl_3$).

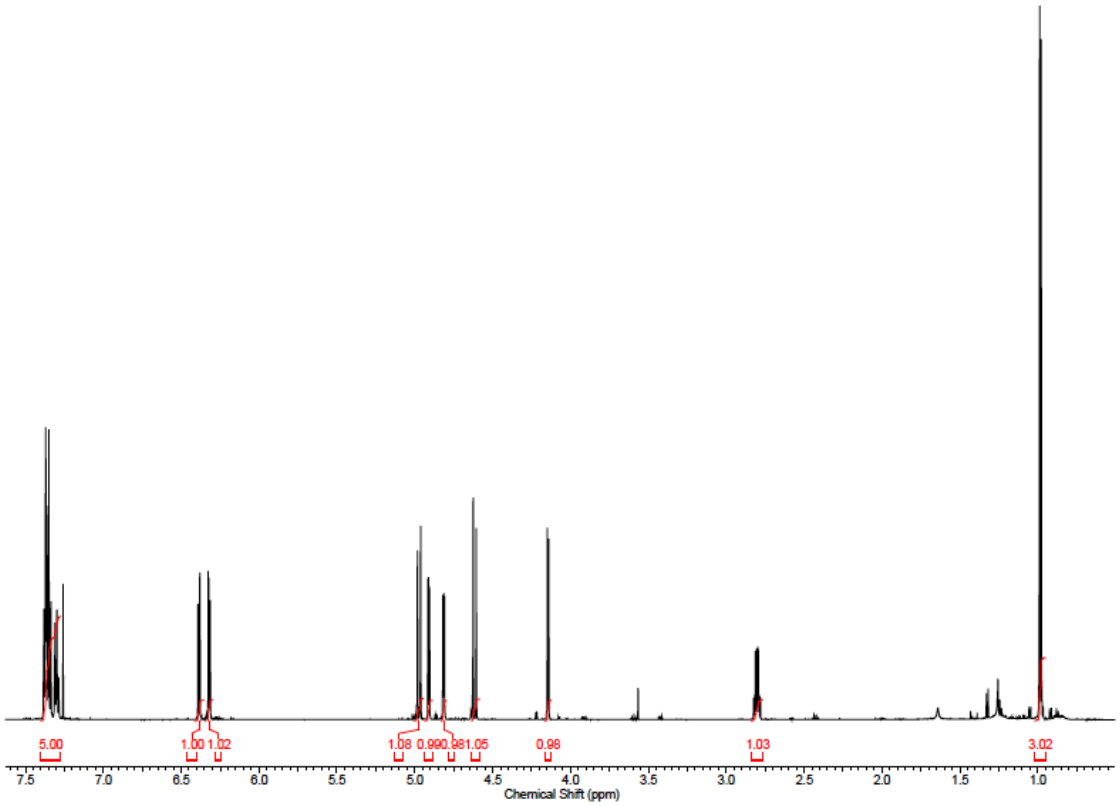
5.00
1.00
1.02
1.08
0.99
0.98
1.05
0.98
1.03
3.02
Chemical Shift (ppm)

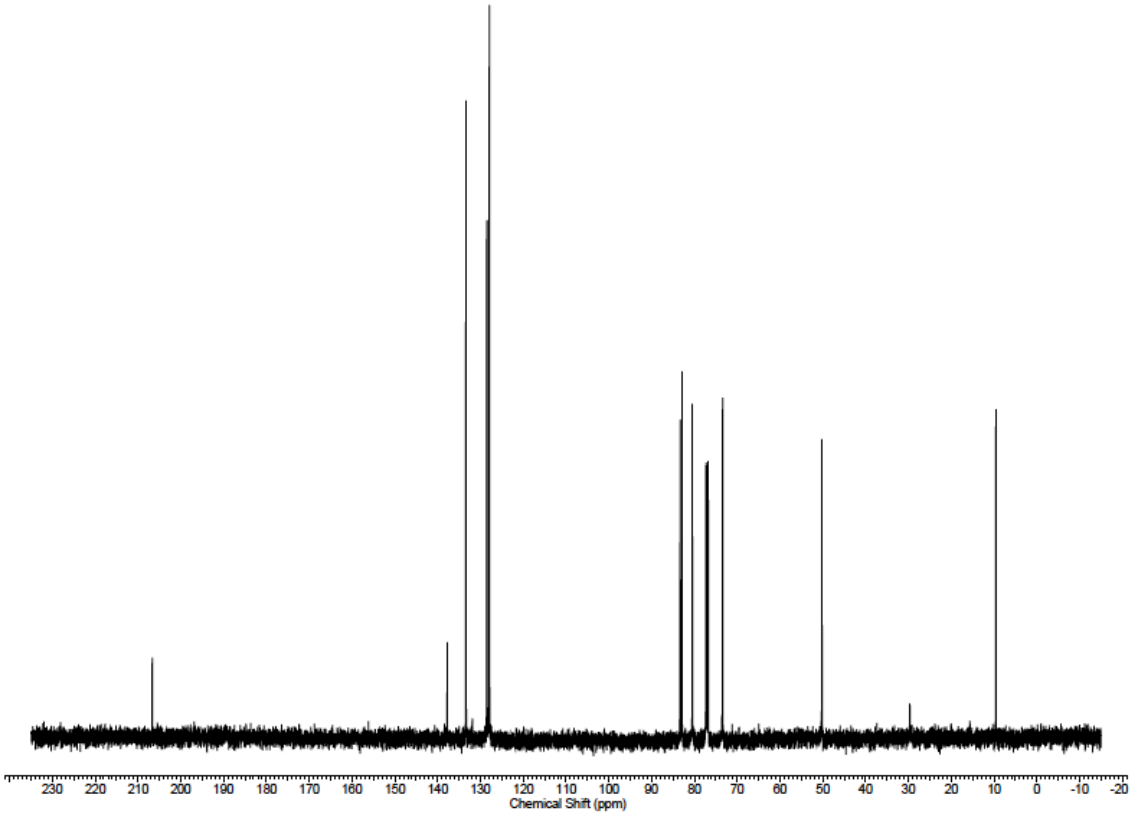
Chemical Shift (ppm)

Racemic sample: HPLC (ChiralPak AD-H, 5% IPA/hexanes, 1 mL/min, 210 nm)

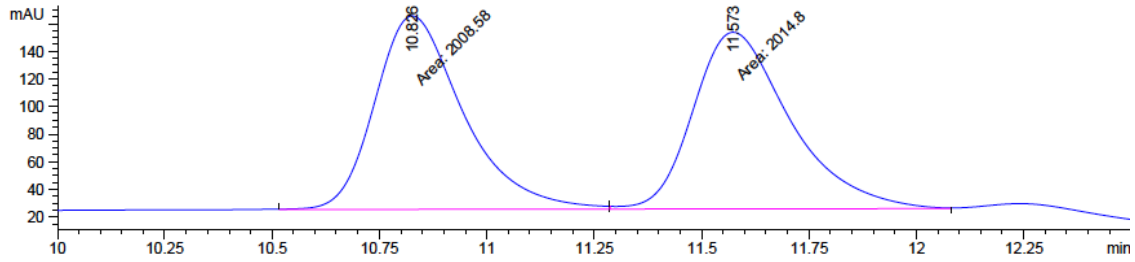

Peak #	RetTime [min]	Type	Width [min]	Area [mAU*s]	Height [mAU]	Area %
1	10.826	MF	0.2388	2008.58252	140.20815	49.9227
2	11.573	FM	0.2623	2014.80029	128.01041	50.0773

Enantioenriched Sample: HPLC (ChiralPak AD-H, 5% IPA/hexanes, 1 mL/min, 210 nm), 92% e.e.

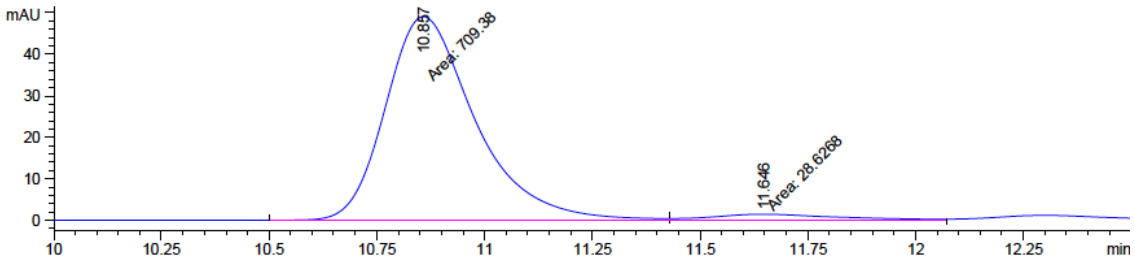

Peak #	RetTime [min]	Type	Width [min]	Area [mAU*s]	Height [mAU]	Area %
1	10.857	MF	0.2411	709.38013	49.04121	96.1211
2	11.646	MF	0.3369	28.62678	1.41602	3.8789

(1*R*,2*S*,5*R*)-2-methoxy-6-((trimethylsilyl)ethynyl)-8-oxabicyclo[3.2.1]oct-6-en-3-one (**2e**):

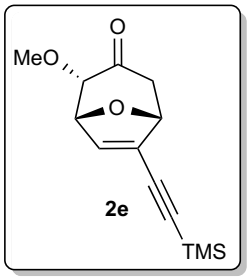

Followed procedure B for (4+3) cycloaddition from **1a** (47.6 mg, 0.25 mmol) and purified using silica gel chromatography to give 44.0 mg (70% yield) of two regioisomers of **2e** (>20:1 r.r.) as off-white crystalline solid.

^{1}H NMR (600 MHz, $CDCl_3$) δ 6.42 (d, J=1.8 Hz, 1H), 5.05 (dd, J=5.3, 2.3 Hz, 1H), 4.89 (d, J=4.7 Hz, 1H), 3.94 (d, J=5.3 Hz, 1H), 3.59 (s, 3H), 2.74 (dd, J=15.6, 5.0 Hz, 1H), 2.57 (d, J=15.3 Hz , 1H), 0.17 (s, 9H);

^{13}C NMR (125 MHz, $CDCl_3$) δ 204.3, 135.6, 130.8, 103.9, 95.8, 86.0, 81.0, 80.4, 60.1, 45.4, -0.1;

FTIR (neat, cm^{-1}) ν_{max} 1725, 1250, 1113, 965, 839, 760, 738 cm^{-1};

HRMS (ESI-TOF) calculated for $C_{13}H_{18}O_3Si$ $[M+Na]^+$: 273.0923, found: 273.0939;

$[\alpha]_D^{25}$ = +73.4° (c = 1.0, $CHCl_3$).

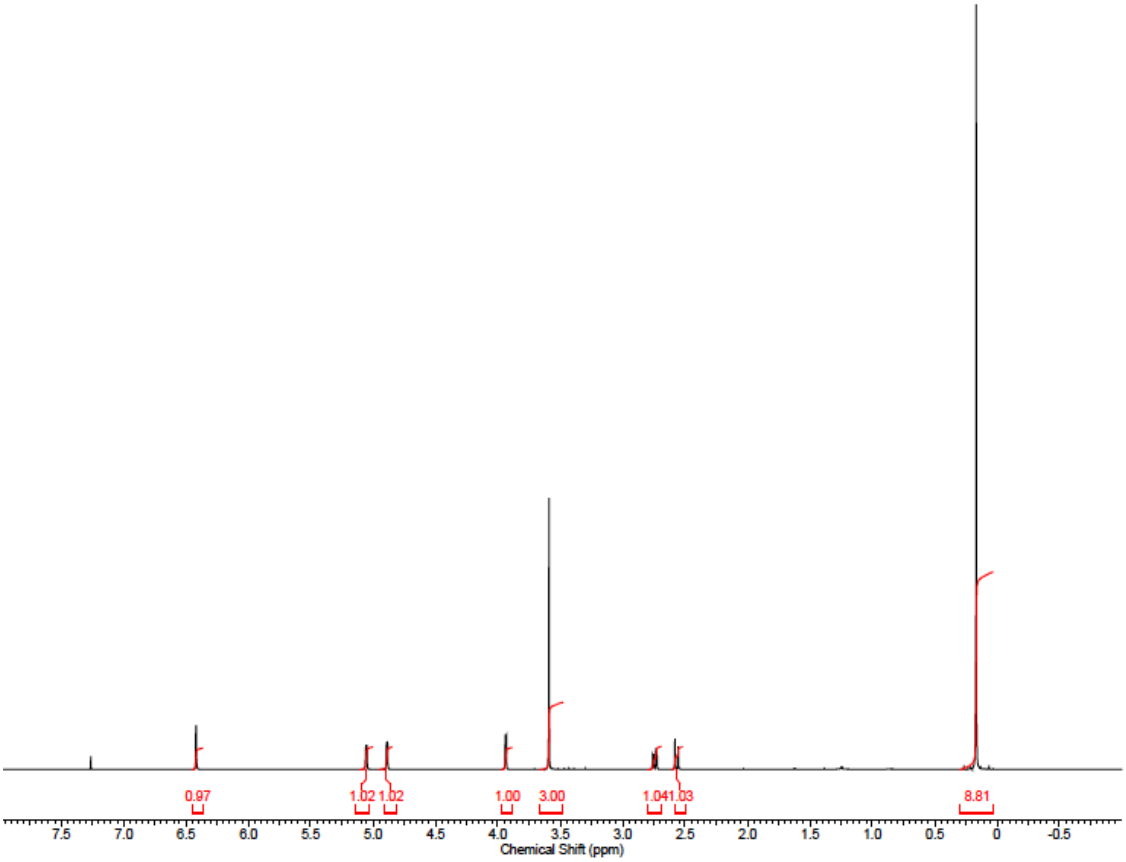
0.97
1.02
1.02
1.00
3.00
1.04
1.03
8.81
7.5 7.0 6.5 6.0 5.5 5.0 4.5 4.0 3.5 3.0 2.5 2.0 1.5 1.0 0.5 0 -0.5
Chemical Shift (ppm)

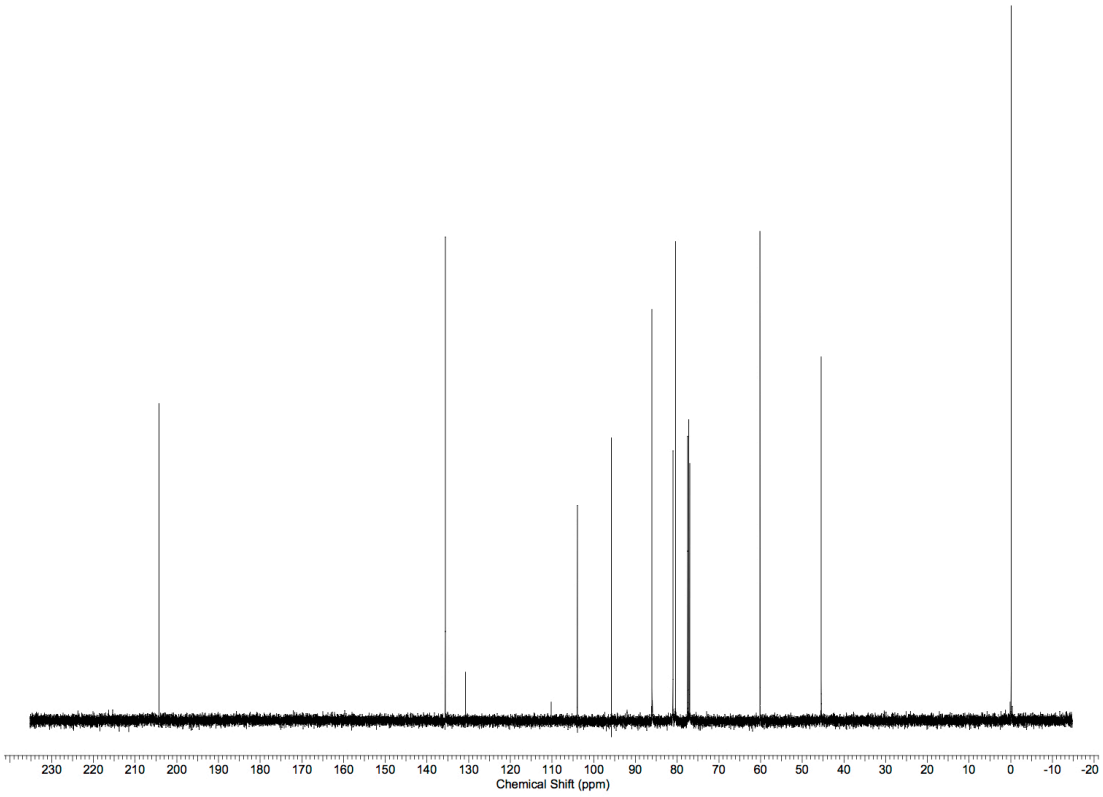
230 220 210 200 190 180 170 160 150 140 130 120 110 100 90 80 70 60 50 40 30 20 10 0 -10 -20
Chemical Shift (ppm)

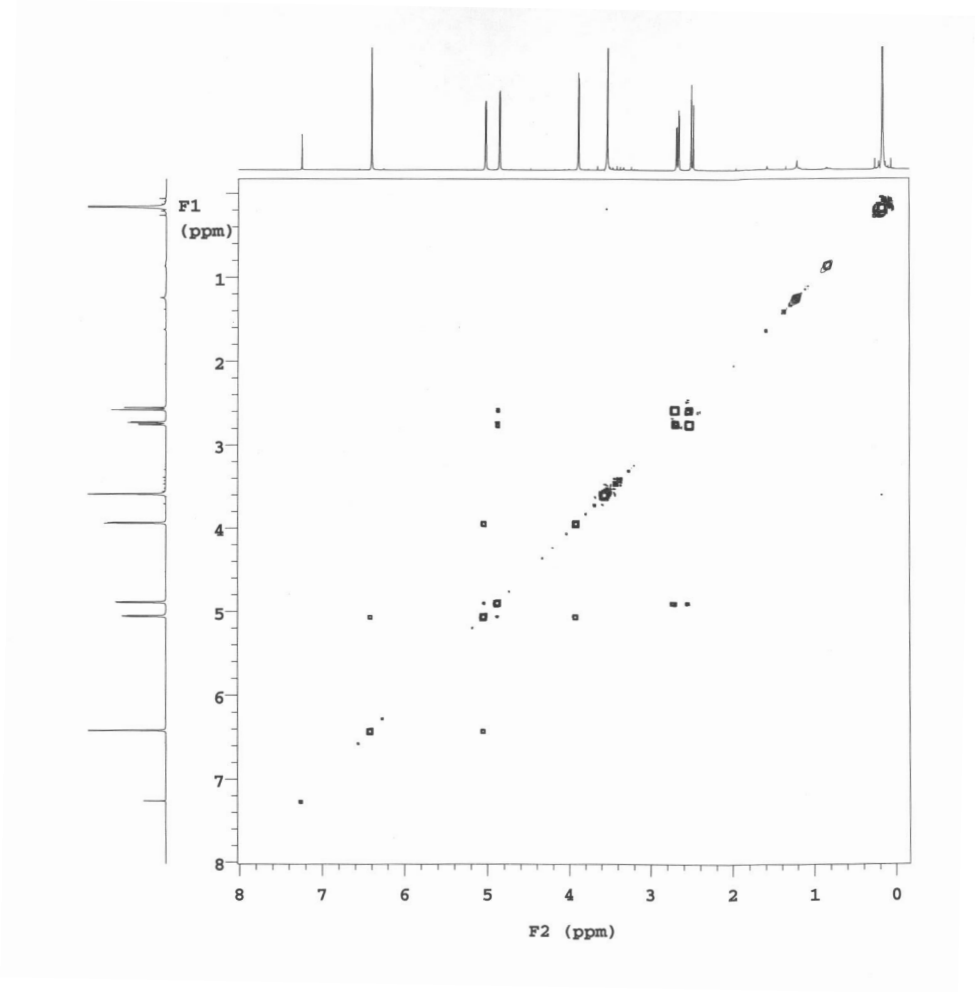

Racemic sample: GC (β-Cyclosil, 30 m x 0.25 mm x 0.25 µm, 150 °C for 55 min)

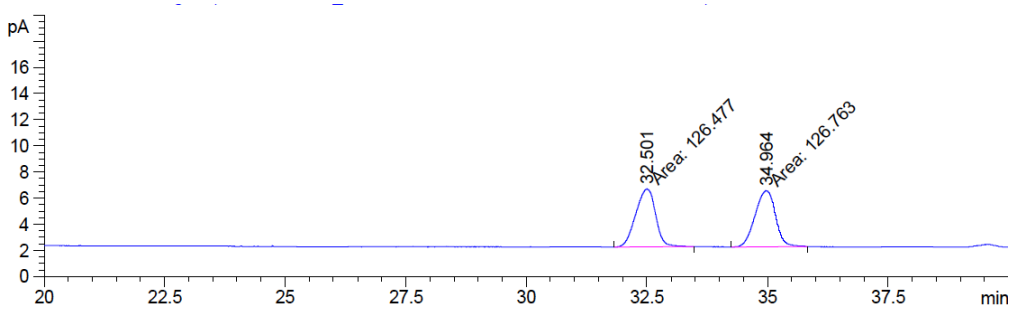

Peak #	RetTime [min]	Type	Width [min]	Area [pA*s]	Height [pA]	Area %
1	32.501	MM	0.4728	126.47708	4.45846	49.94349
2	34.964	MM	0.4894	126.76331	4.31724	50.05651

Enantioenriched Sample: GC (β-Cyclosil, 30 m x 0.25 mm x 0.25 μm, 150 °C for 55 min), 86% e.e.

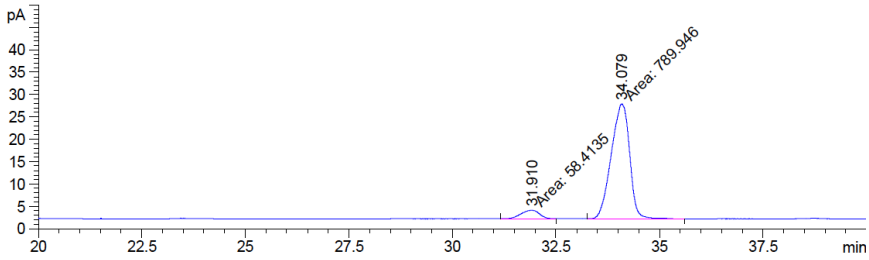

Peak #	RetTime [min]	Type	Width [min]	Area [pA*s]	Height [pA]	Area %
1	31.910	MM	0.5113	58.41353	1.90416	6.88547
2	34.079	MM	0.5126	789.94629	25.68418	93.11453

(1*R*,2*S*,4*R*,5*R*)-6-bromo-2-methoxy-4-methyl-8-oxabicyclo[3.2.1]oct-6-en-3-one (**2f**):

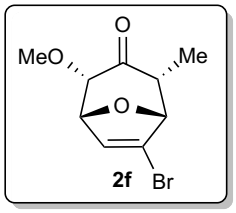

Followed procedure B for (4+3) cycloaddition from **1b** (100 mg, 0.49 mmol) and purified using silica gel chromatography to give 82 mg (68% yield) of two regioisomers of **2f** (>20:1 r.r.) as clear oil.

^{1}H NMR (600 MHz, $CDCl_3$) δ 6.42 (d, J = 2.4 Hz, 1H), 4.95 (dd, J = 2.4, 4.7 Hz, 1H), 4.70 (d, J = 4.7 Hz, 1H), 3.98 (d, J = 4.7 Hz, 1H), 3.59 (s, 3H), 2.98 (dq, J = 2.9, 4.7 Hz, 1H), 1.21 (d, J = 7.0 Hz, 3H);

^{13}C NMR (125 MHz, $CDCl_3$) δ 205.3, 131.7, 123.7, 85.8, 85.1, 81.2, 59.8, 50.6, 9.5;

FTIR (neat) ν_{max} 1722, 1125, 1057, 999, 941, 871 cm^{-1};

HRMS (ESI-TOF) calculated for $C_9H_{11}BrO_3$ [M+Na^+]: 268.9798, found: 268.9780.

$[\alpha]_D^{25}$ = –7.0° (c = 1.0, $CHCl_3$).

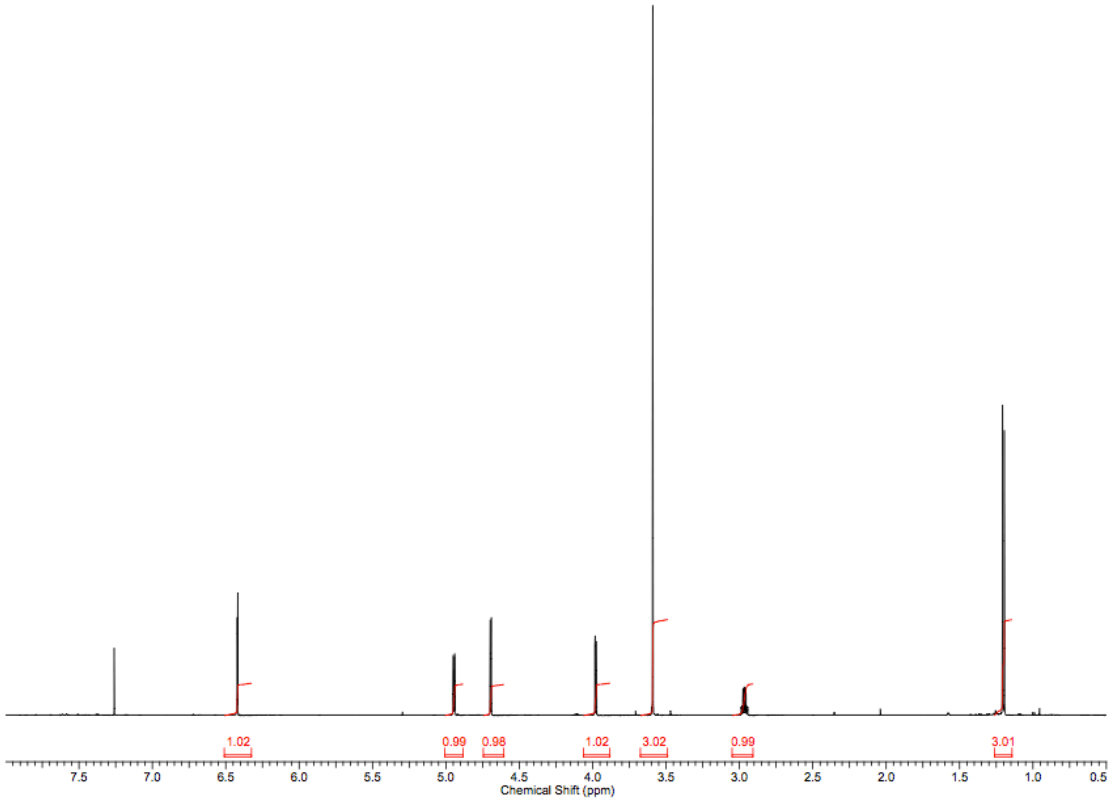
1.02
0.99
0.98
1.02
3.02
0.99
3.01
7.5
7.0
6.5
6.0
5.5
5.0
4.5
4.0
3.5
3.0
2.5
2.0
1.5
1.0
0.5
Chemical Shift (ppm)

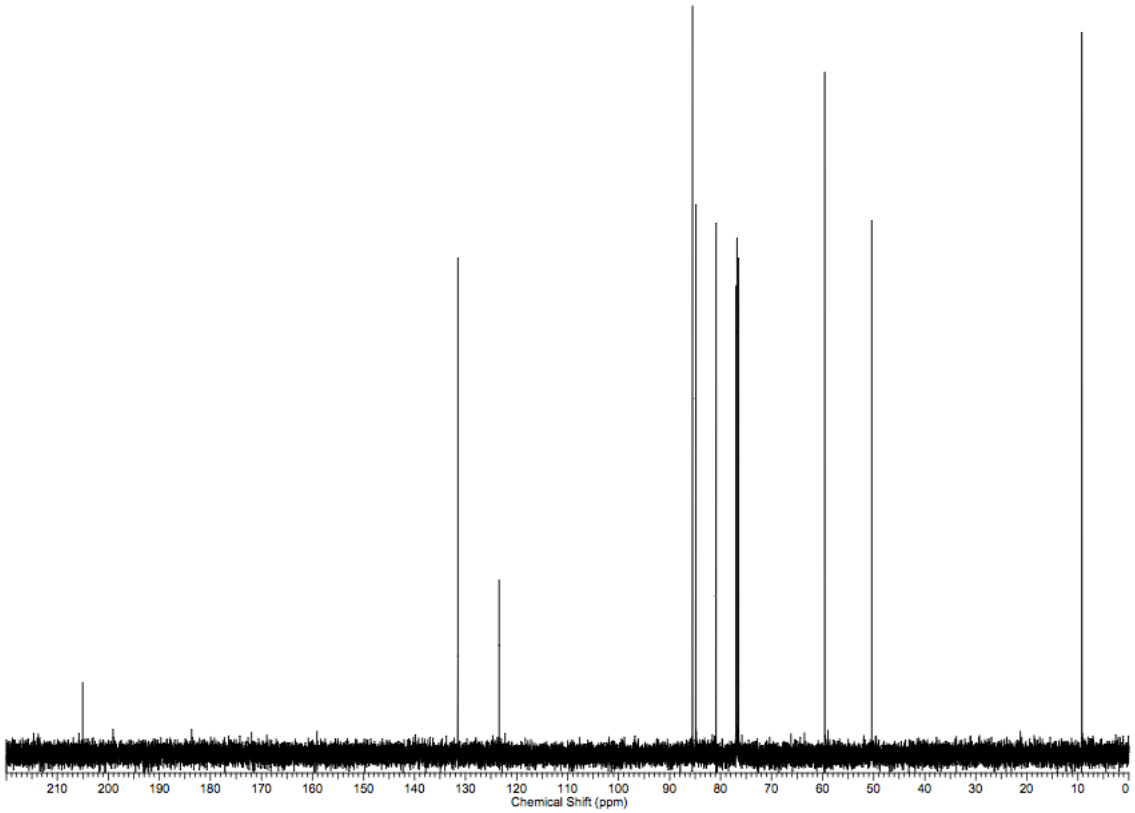
210
200
190
180
170
160
150
140
130
120
110
100
90
80
70
60
50
40
30
20
10
0
Chemical Shift (ppm)

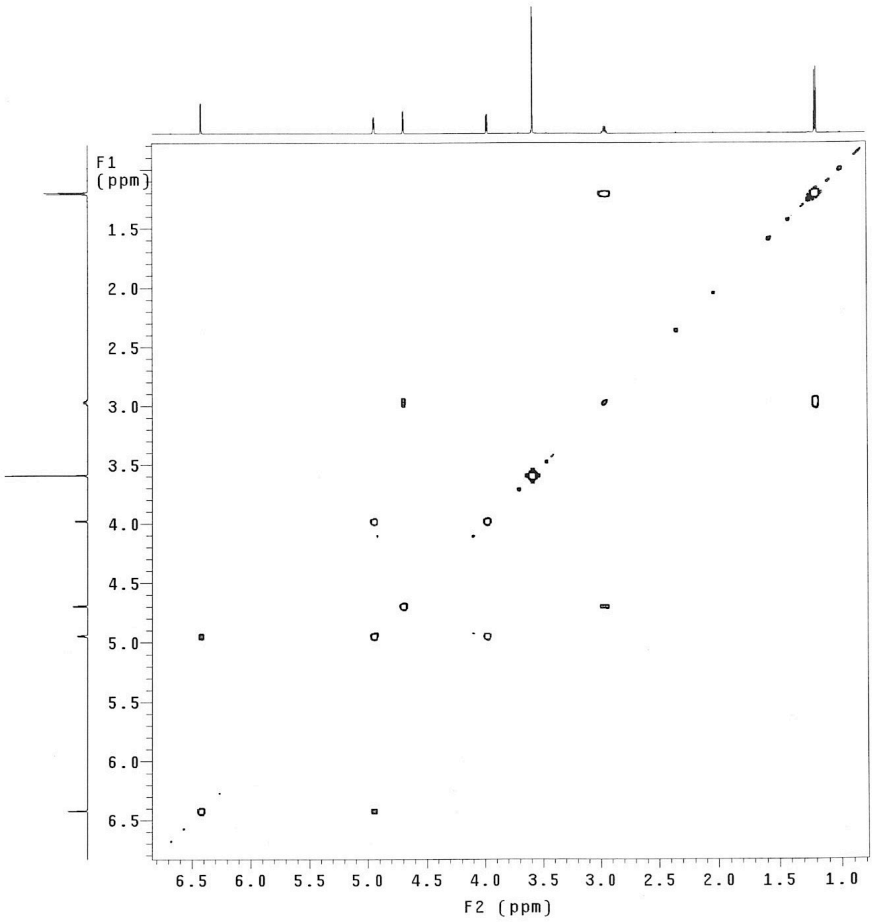

Racemic Sample: GC (β-Cyclosil, 30 m x 0.25 mm x 0.25 µm, 60 to 160 °C, 0.5 °C/min)

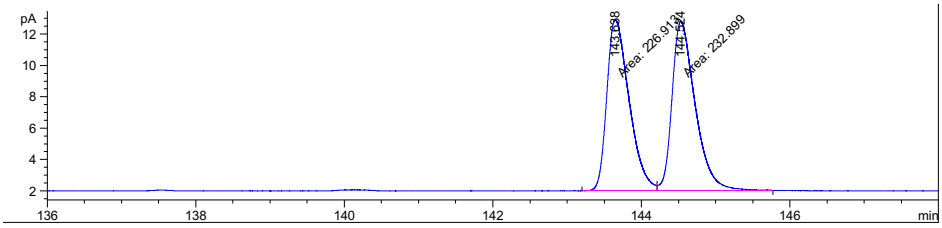

Peak #	RetTime [min]	Type	Width [min]	Area [pA*s]	Height [pA]	Area %
1	143.638	MF	0.3467	226.91266	10.90739	49.34907
2	144.524	FM	0.3589	232.89876	10.81404	50.65093

Enantioenriched Sample: GC (β-Cyclosil, 30 m x 0.25 mm x 0.25 µm, 60 to 160 °C, 0.5 °C/min), 94% e.e.

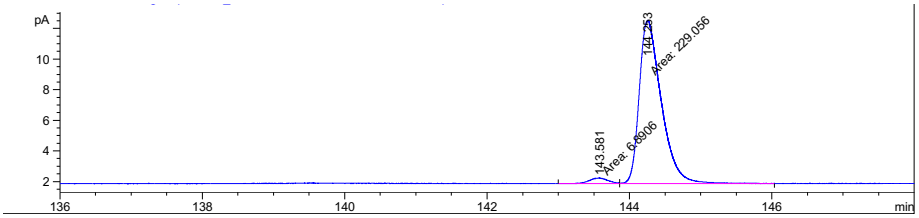

Peak #	RetTime [min]	Type	Width [min]	Area [pA*s]	Height [pA]	Area %
1	143.581	MF	0.3008	6.89060	3.81851e-1	2.92041
2	144.253	FM	0.3575	229.05551	10.67932	97.07959

(1*R*,2*S*,4*R*,5*R*)-2-methoxy-4-methyl-6-((trimethylsilyl)ethynyl)-8-oxabicyclo[3.2.1]oct-6-en-3-one (**2g**):

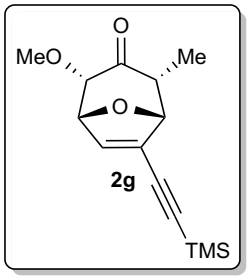

Followed procedure for (4+3) cycloaddition from **1b** (51.1 mg, 0.25 mmol) and purified using silica gel chromatography to give 65.5 mg (98% yield) of two regioisomers of **2g** (>20:1 r.r.) as pale yellow oil.

^{1}H NMR (600 MHz, $CDCl_3$) δ 6.44 (d, J = 2.4 Hz, 1H), 5.02 (dd, J = 1.8, 2.9 Hz, 1H), 4.75 (d, J = 4.7 Hz, 1H), 3.98 (d, J = 5.3 Hz, 1H), 3.57 (s, 3H), 1.12 (dq, J = 1.8, 5.3 Hz, 1H), 1.13 (d, J = 7.0 Hz, 3H), 0.15 (s, 9H);

^{13}C NMR (125 MHz, $CDCl_3$) δ 205.7, 136.6, 129.5, 103.9, 97.1, 85.6, 84.9, 80.7, 59.7, 50.7, 8.9, -0.4;

FTIR (neat, cm^{-1}) ν_{max} 1724, 1126, 899, 842, 760 cm^{-1};

HRMS (ESI-TOF) calculated for $C_{14}H_{20}O_3Si$ $[M+Na]^+$: 287.1079, found: 287.1057.

$[\alpha]_D^{25}$ = +43.0° (c = 1.0, $CHCl_3$).

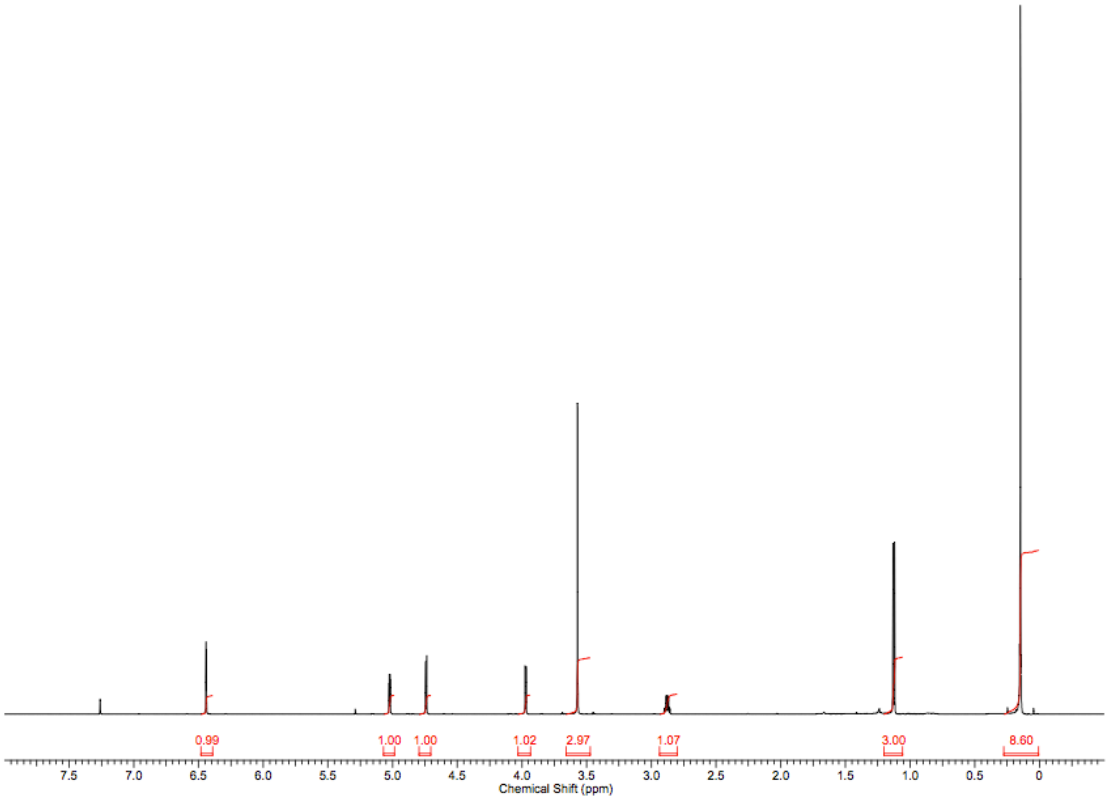
0.99
1.00
1.00
1.02
2.97
1.07
3.00
8.60
Chemical Shift (ppm)

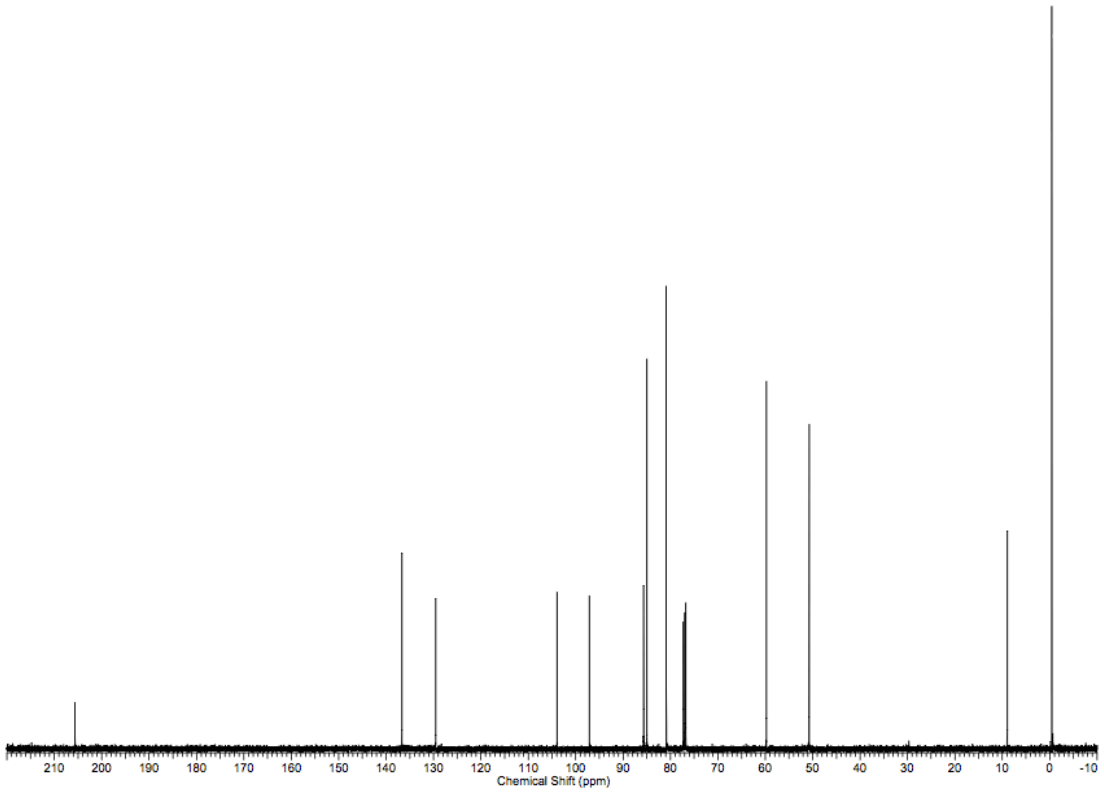
Chemical Shift (ppm)

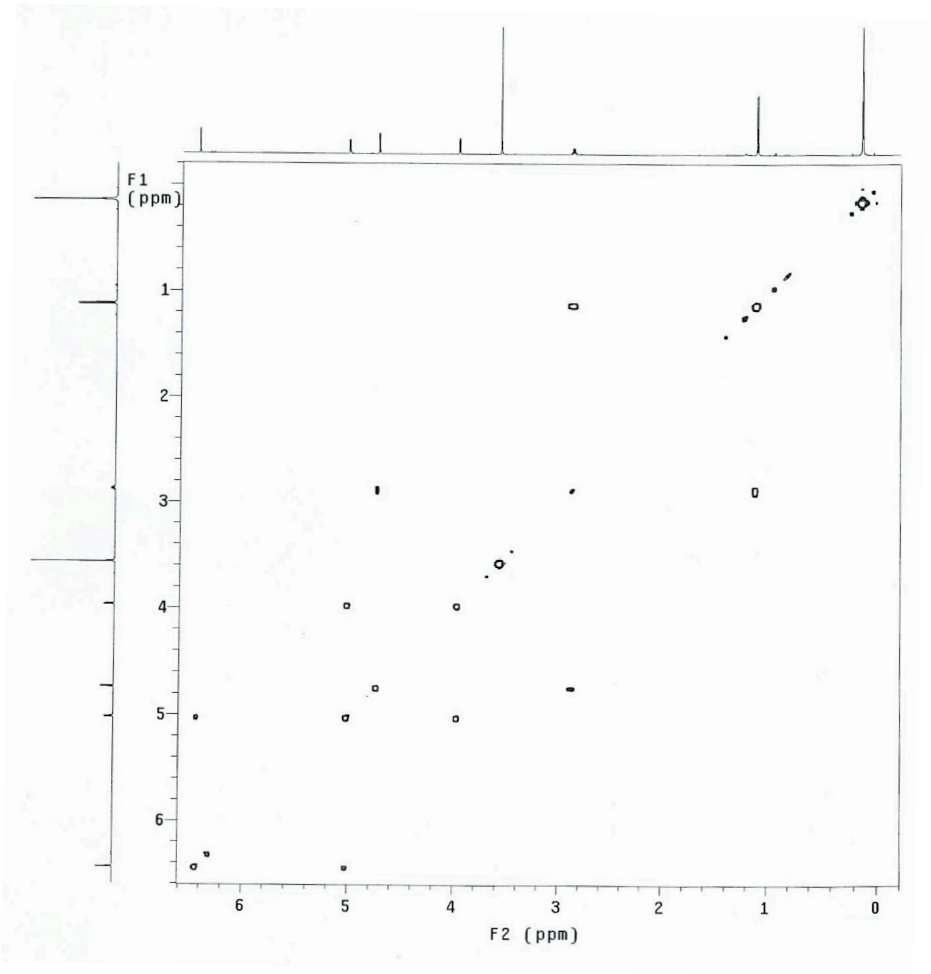

Racemic Sample: GC (β-Cyclosil, 30 m x 0.25 mm x 0.25 µm, 150 °C, 55 min)

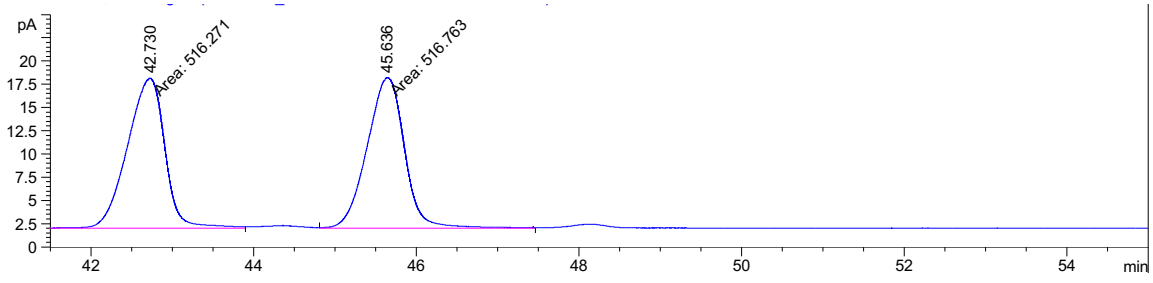

Peak #	RetTime [min]	Type	Width [min]	Area [pA*s]	Height [pA]	Area %
1	42.730	MF	0.5326	516.27130	16.15439	49.97622
2	45.636	FM	0.5311	516.76263	16.21782	50.02378

Enantioenriched Sample: GC (β-Cyclosil, 30 m x 0.25 mm x 0.25 µm, 150 °C, 55 min), 96% e.e.

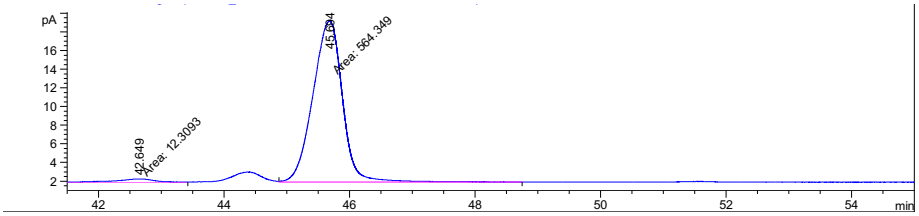

Peak #	RetTime [min]	Type	Width [min]	Area [pA*s]	Height [pA]	Area %
1	42.649	MF	0.6074	12.30931	3.37763e-1	2.13460
2	45.694	FM	0.5420	564.34857	17.35349	97.86540

(1*R*,2*S*,4*R*,5*R*)-2-methoxy-4,6-dimethyl-8-oxabicyclo[3.2.1]oct-6-en-3-one (**2h**):

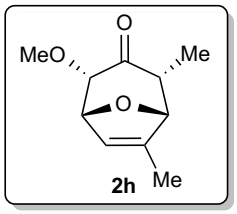

Followed procedure for (4+3) cycloaddition from **1b** (51.1 mg, 0.25 mmol) and purified using silica gel chromatography to give 35.1 mg (77% yield) of two regioisomers of **2h** (1:2.8 r.r.) as a yellow oil.

^{1}H NMR (600 MHz, $CDCl_3$) δ 5.88 - 5.93 (m, 1H), 4.90 (dt, *J*=4.3, 1.4 Hz, 1H), 4.57 (d, *J*=4.1 Hz, 1H), 3.98 (d, *J*=4.7 Hz, 1H), 3.58 (s, 3H), 2.93 (dd, *J*=7.0, 4.7 Hz, 1H), 1.85 (s, 3H), 1.06 (d, *J*=7.0 Hz, 3H);

^{13}C NMR (125 MHz, $CDCl_3$) δ 206.6, 145.0, 126.0, 86.0, 85.8, 80.4, 59.6, 50.6, 29.7, 14.9, 9.2;

FTIR (neat, cm^{-1}) ν_{max} 1720, 1200, 1124, 1069, 1010, 931 cm^{-1};

HRMS (ESI-TOF) calculated for $C_{10}H_{14}O_3$ $[M+Na]^+$: 205.0841, found: 205.0851.

$[\alpha]_D^{25}$ = – 3.2° (c = 1.0, $CHCl_3$).

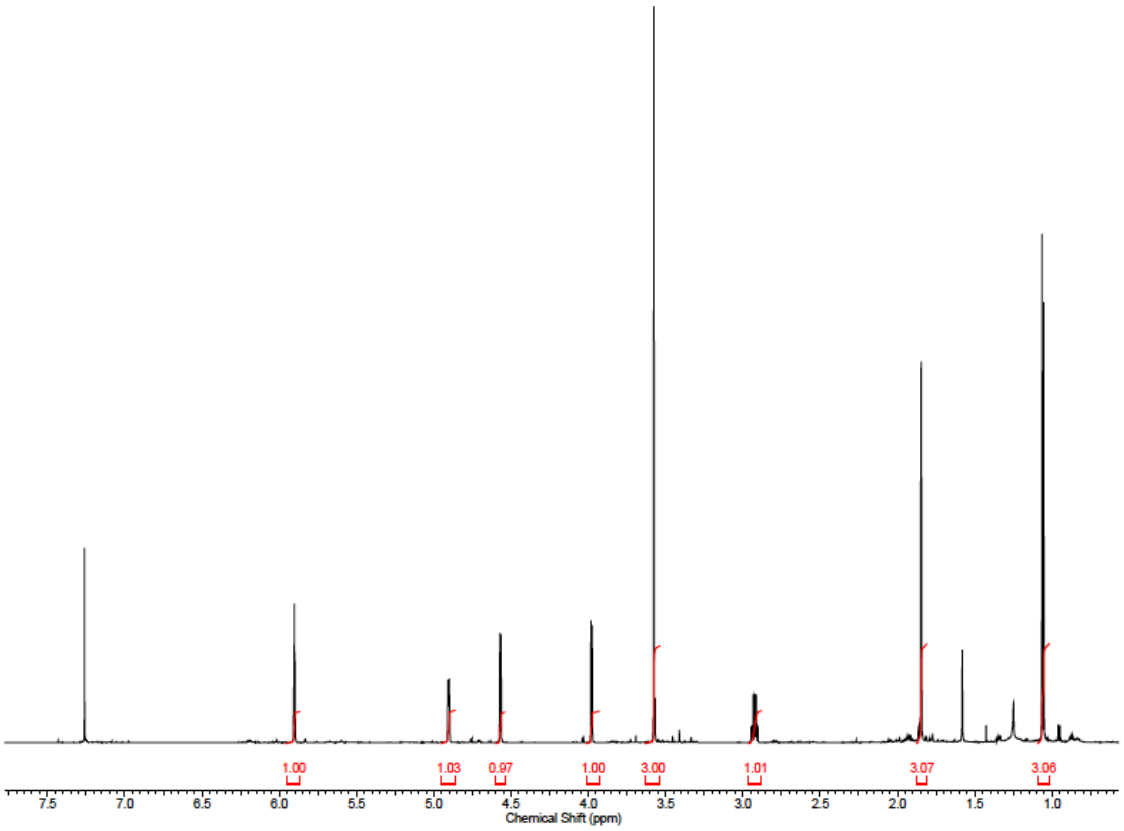
1.00
1.03
0.97
1.00
3.00
1.01
3.07
3.06
7.5
7.0
6.5
6.0
5.5
5.0
4.5
4.0
3.5
3.0
2.5
2.0
1.5
1.0
Chemical Shift (ppm)

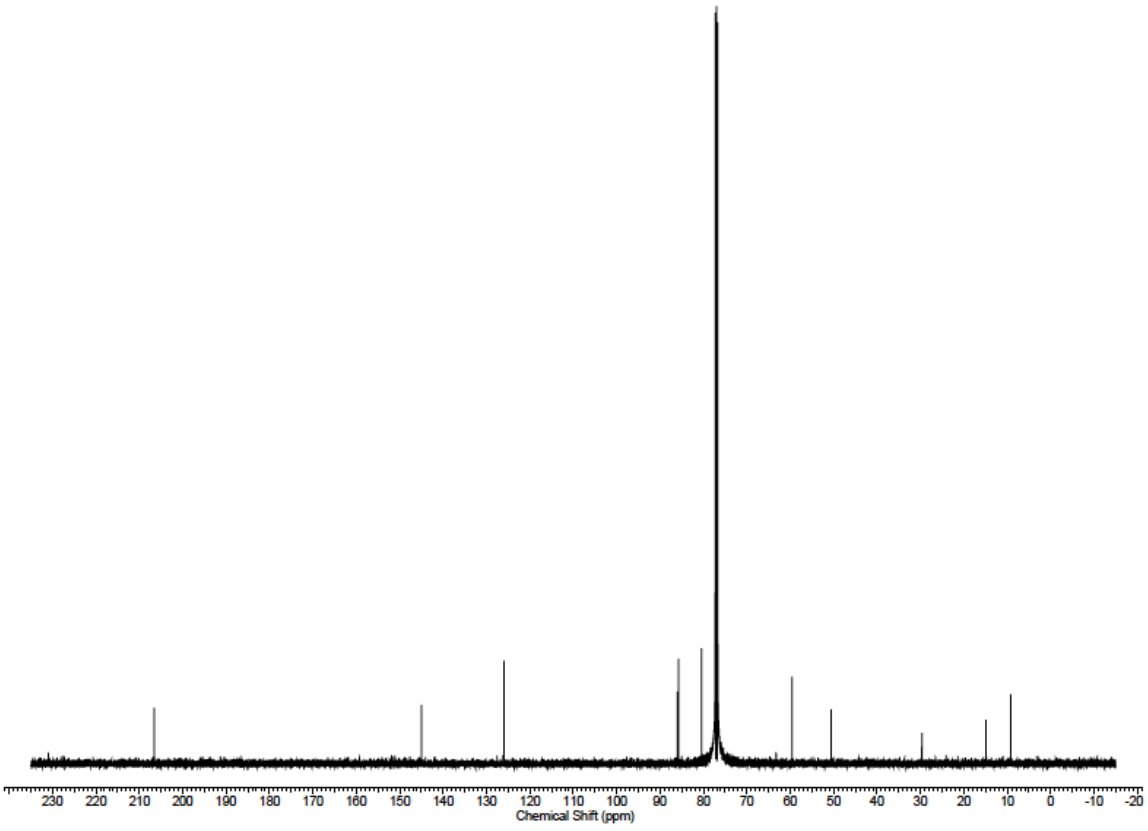
230
220
210
200
190
180
170
160
150
140
130
120
110
100
90
80
70
60
50
40
30
20
10
0
-10
-20
Chemical Shift (ppm)

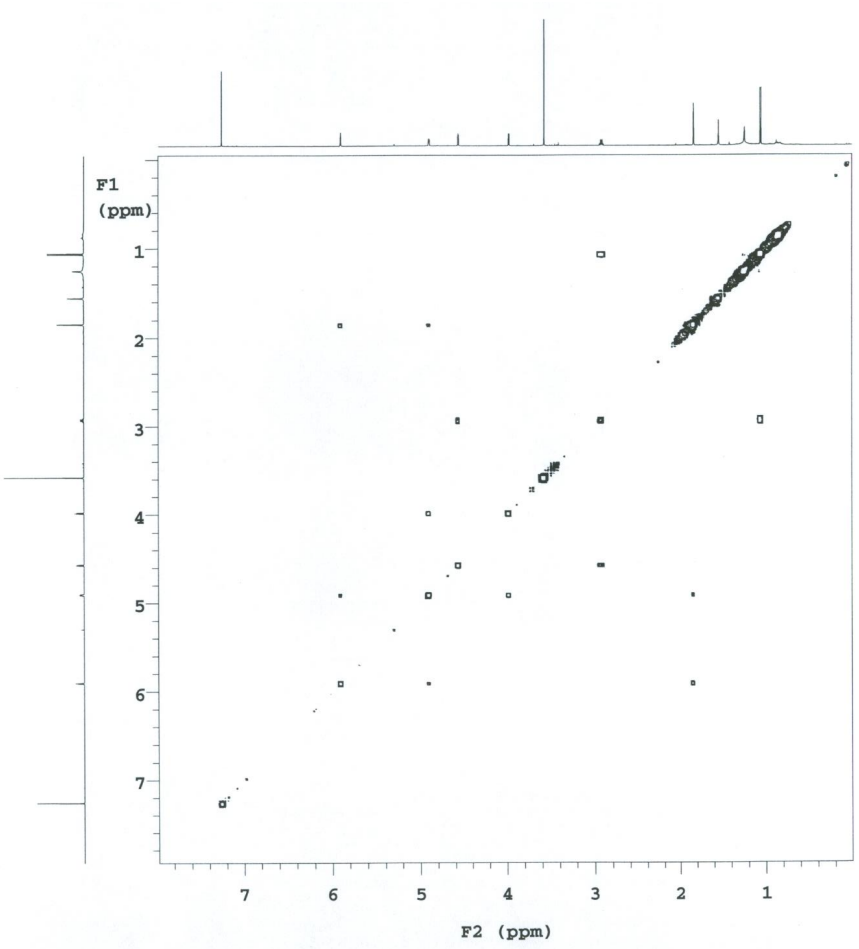

Racemic Sample: GC (β-Cyclosil, 30 m x 0.25 mm x 0.25 µm, 60 to 160 °C, 2 °C/min)

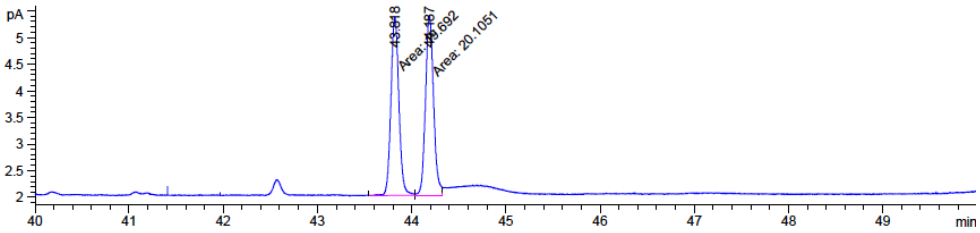

Peak #	RetTime [min]	Type	Width [min]	Area [pA*s]	Height [pA]	Area %
1	43.818	MF	0.0983	19.69196	3.34006	49.48095
2	44.187	FM	0.0995	20.10509	3.36899	50.51905

Enantioenriched Sample: GC (β-Cyclosil, 30 m x 0.25 mm x 0.25 µm, 60 to 160 °C, 2 °C/min), 90 % e.e.

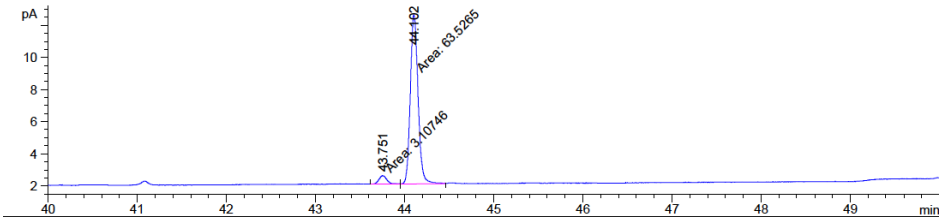

Peak #	RetTime [min]	Type	Width [min]	Area [pA*s]	Height [pA]	Area %
1	43.751	MF	0.0971	3.10746	5.33402e-1	4.66347
2	44.102	MF	0.1003	63.52652	10.55622	95.33653

(1*R*,2*S*,4*R*,5*R*)-6-benzyl-2-methoxy-4-methyl-8-oxabicyclo[3.2.1]oct-6-en-3-one (**2i**):

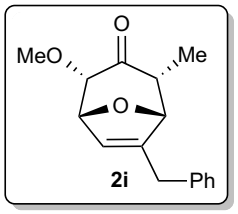

Followed procedure for (4+3) cycloaddition from **1b** (51.1 mg, 0.25 mmol) and purified using silica gel chromatography to give 62.6 mg (97% yield) of two regioisomers of **2i** (1:1.5 r.r.) as a pale yellow oil.

^{1}H NMR (600 MHz, $CDCl_3$) δ 7.26 - 7.33 (m, 2H), 7.20 - 7.24 (m, 1H), 7.14 (d, *J*=7.6 Hz, 2H), 5.81 - 5.87 (m, 1H), 4.87 - 4.96 (m, 1H), 4.58 (d, *J*=4.7 Hz, 1H), 4.01 (d, *J*=4.7 Hz, 1H), 3.58 - 3.63 (m, 1H), 3.57 (s, 3H), 3.35 (d, *J*=17.0 Hz, 1H), 2.88 - 2.97 (m, 1H), 1.13 (d, *J*=7.0 Hz, 3H);

^{13}C NMR (125 MHz, $CDCl_3$) δ 206.4, 148.9, 137.5, 128.8, 128.7, 127.0, 126.7, 86.0, 84.1, 80.4, 59.6, 50.7, 35.9, 9.4;

FTIR (neat, cm^{-1}) ν_{max} 1720, 1124, 1068, 944, 901, 699 cm^{-1};

HRMS (ESI-TOF) calculated for $C_{16}H_{18}O_3$ $[M+Na]^+$: 281.1154, found: 281.1178.

$[\alpha]_D^{25}$ = –31.2° (c = 1.0, $CHCl_3$).

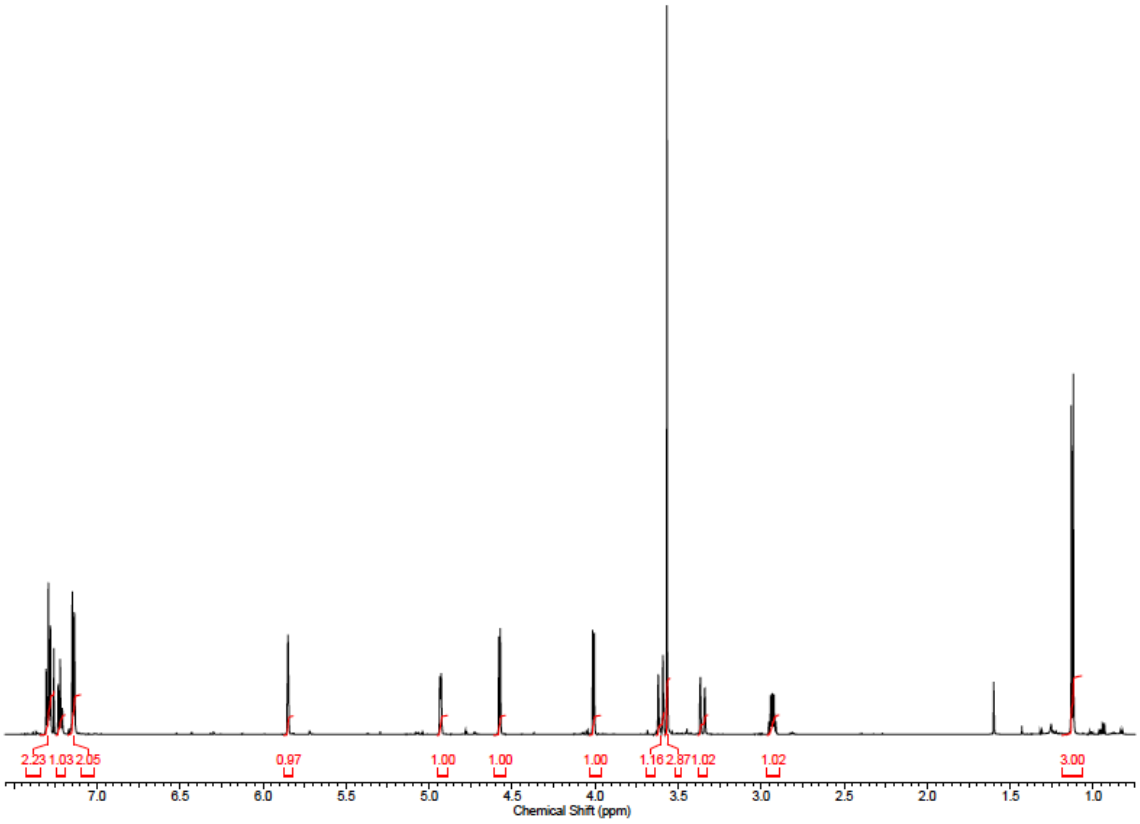
2.23
1.03
2.05
0.97
1.00
1.00
1.00
1.16
2.87
1.02
1.02
3.00
7.0
6.5
6.0
5.5
5.0
4.5
4.0
3.5
3.0
2.5
2.0
1.5
1.0
Chemical Shift (ppm)

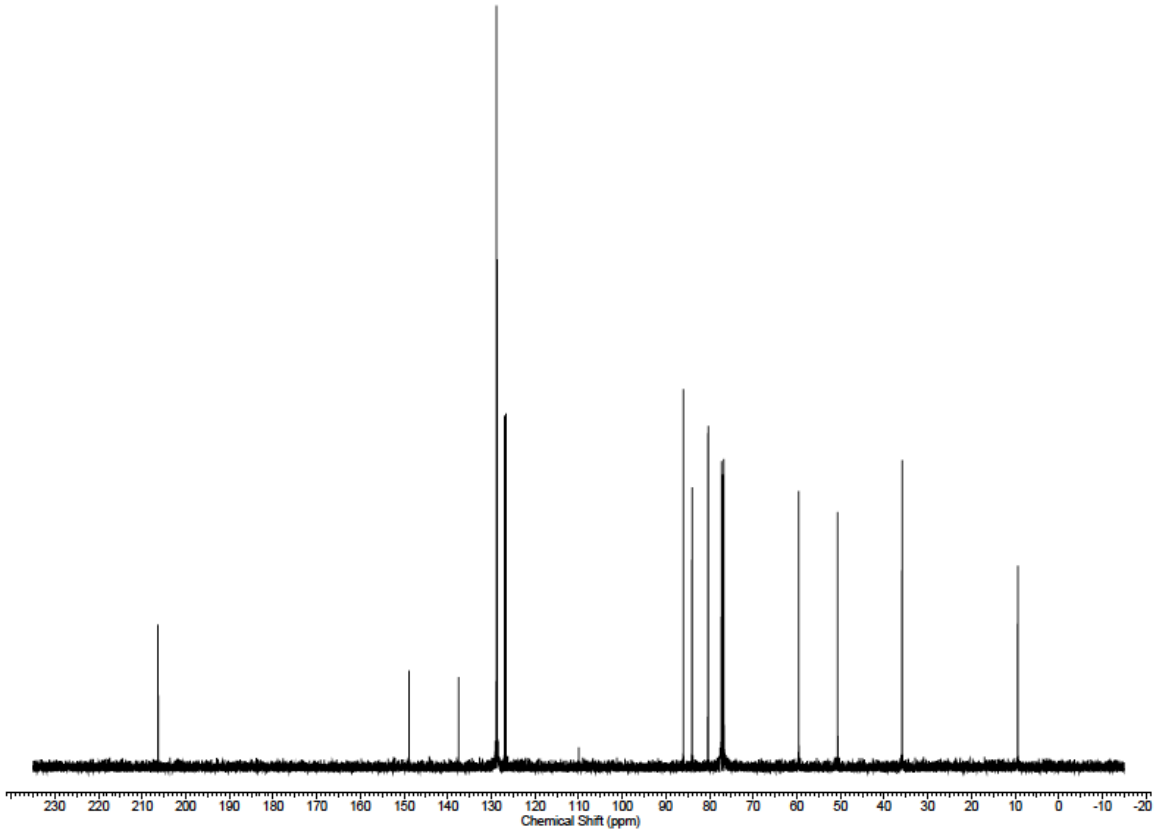
230
220
210
200
190
180
170
160
150
140
130
120
110
100
90
80
70
60
50
40
30
20
10
0
-10
-20
Chemical Shift (ppm)

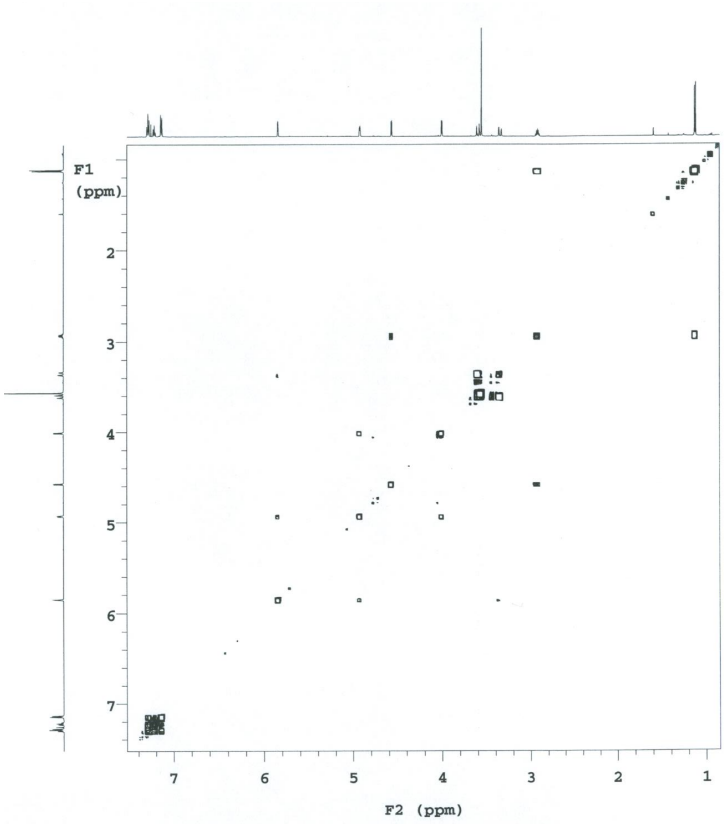

Racemic Sample: GC (β-Cyclosil, 30 m x 0.25 mm x 0.25 µm, 170 °C for 90 min)

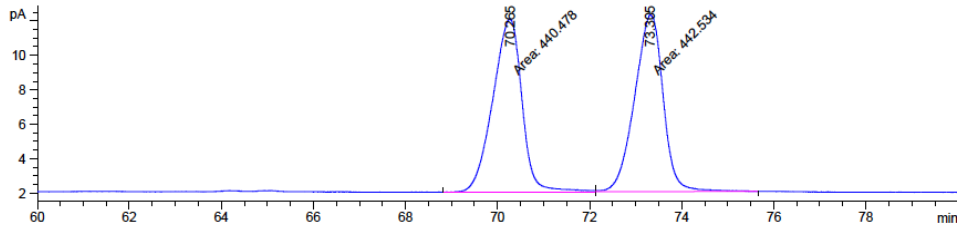

Peak #	RetTime [min]	Type	Width [min]	Area [pA*s]	Height [pA]	Area %
1	70.265	MF	0.7294	440.47791	10.06553	49.88356
2	73.305	FM	0.7166	442.53430	10.29295	50.11644

Enantioenriched Sample: GC (β-Cyclosil, 30 m x 0.25 mm x 0.25 μm, 170 °C for 90 min), 88% e.e.

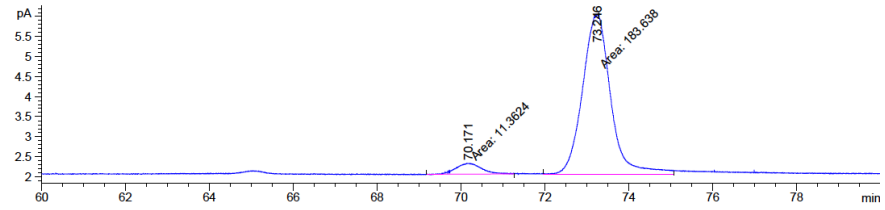

Peak #	RetTime [min]	Type	Width [min]	Area [pA*s]	Height [pA]	Area %
1	70.171	MM	0.6968	11.36240	2.71762e-1	5.82687
2	73.246	MF	0.7670	183.63754	3.99047	94.17313

(1*R*,2*S*,4*R*,5*R*)-2-methoxy-4-methyl-6-phenyl-8-oxabicyclo[3.2.1]oct-6-en-3-one (**2j**):

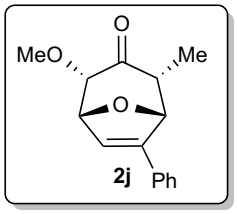

Followed procedure for (4+3) cycloaddition from **1b** (51.1 mg, 0.25 mmol) and purified using silica gel chromatography to give 57.9 mg (95% yield) of two regioisomers of **2j** (1:11 r.r.) as a viscous pale yellow oil.

^{1}H NMR (600 MHz, $CDCl_3$) δ 7.34 - 7.37 (m, 2H), 7.25 - 7.33 (m, 3H), 6.52 (d, *J*=2.3 Hz, 1H), 5.36 (d, *J*=4.7 Hz, 1H), 5.13 (dd, *J*=5.0, 2.1 Hz, 1H), 4.09 (d, *J*=5.3 Hz, 1H), 3.62 (s, 3H), 3.02 (dd, *J*=7.0, 4.7 Hz, 1H), 0.82 (d, *J*=7.0 Hz, 3H);

^{13}C NMR (125 MHz, $CDCl_3$) δ 206.0, 147.6, 132.4, 128.7, 128.6, 126.7, 124.7, 86.2, 83.1, 81.0, 59.7, 51.1, 9.9;

FTIR (neat, cm^{-1}) ν_{max} 1720, 1125, 1072, 934, 757, 693 cm^{-1};

HRMS (ESI-TOF) calculated for $C_{15}H_{16}O_3$ $[M+Na]^+$: 267.0997, found: 267.1041.

$[\alpha]_D^{25}$ = –53.8° (c = 1.0, $CHCl_3$).

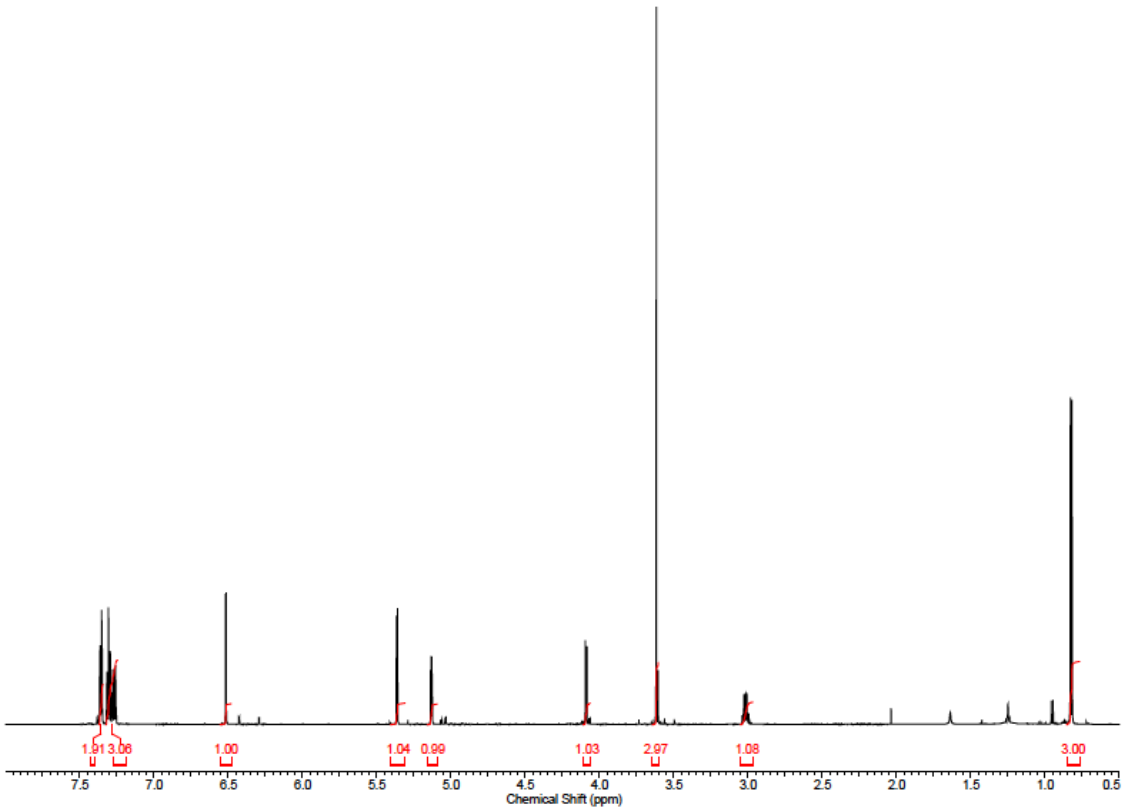
1.91
3.06
1.00
1.04
0.99
1.03
2.97
1.08
3.00
7.5
7.0
6.5
6.0
5.5
5.0
4.5
4.0
3.5
3.0
2.5
2.0
1.5
1.0
0.5
Chemical Shift (ppm)

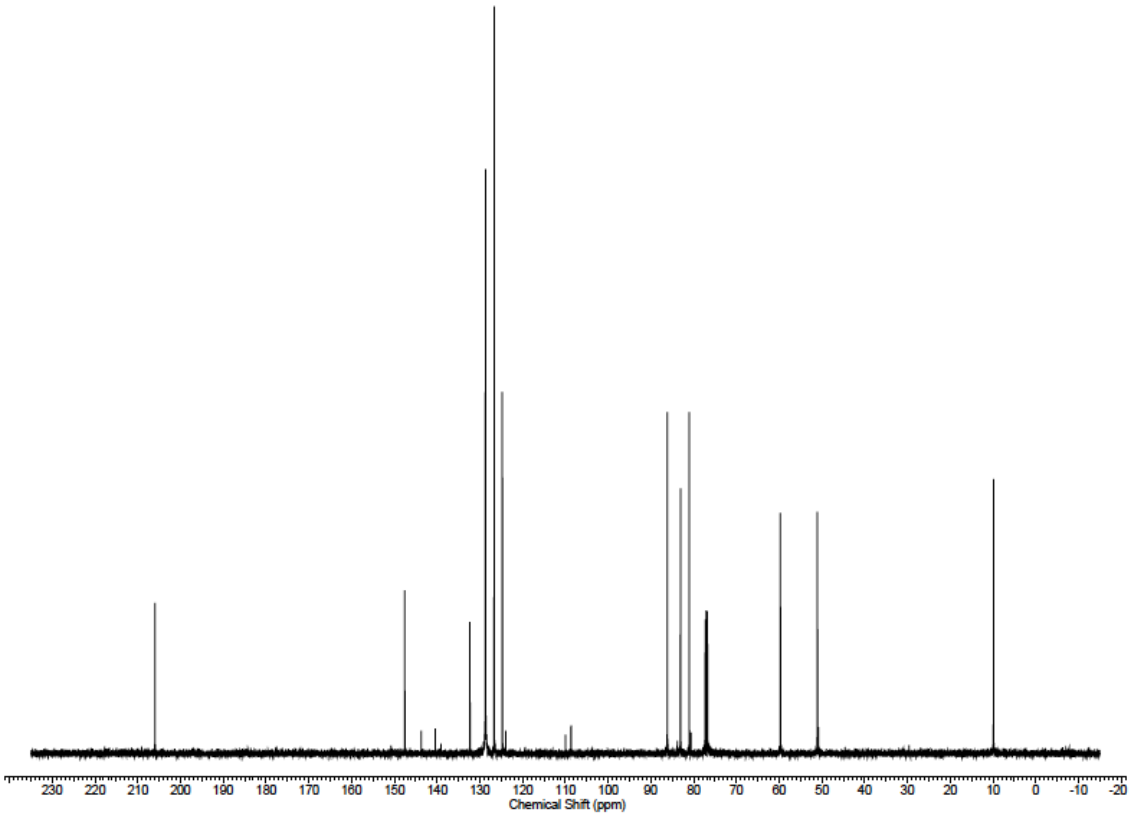
230
220
210
200
190
180
170
160
150
140
130
120
110
100
90
80
70
60
50
40
30
20
10
0
-10
-20
Chemical Shift (ppm)

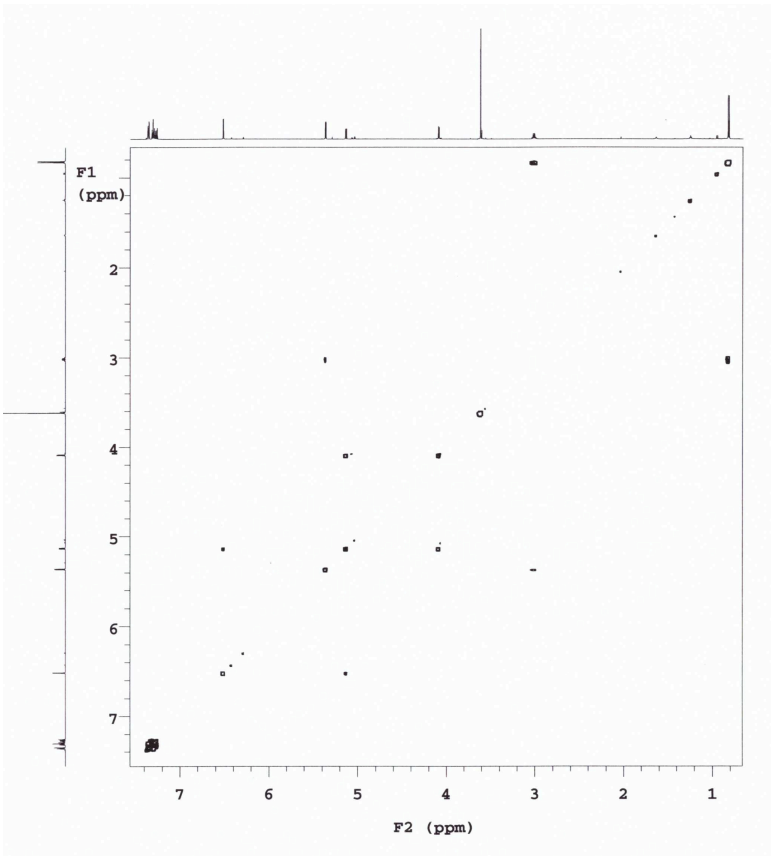

Racemic Sample: GC (β-Cyclosil, 30 m x 0.25 mm x 0.25 µm, 170 °C for 90 min)

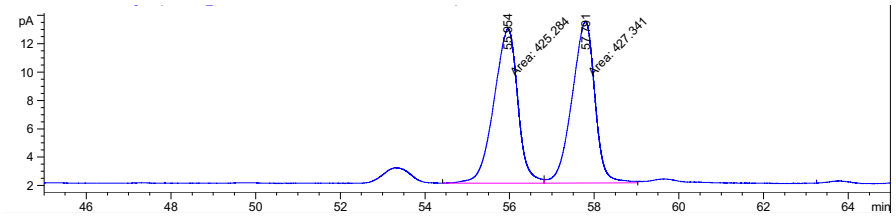

Peak #	RetTime [min]	Type	Width [min]	Area [pA*s]	Height [pA]	Area %
1	55.954	MF	0.6504	425.28375	10.89777	49.87935
2	57.791	MF	0.6229	427.34109	11.43466	50.12065

Enantioenriched Sample: GC (β-Cyclosil, 30 m x 0.25 mm x 0.25 μm, 170 °C for 90 min), 87% e.e.

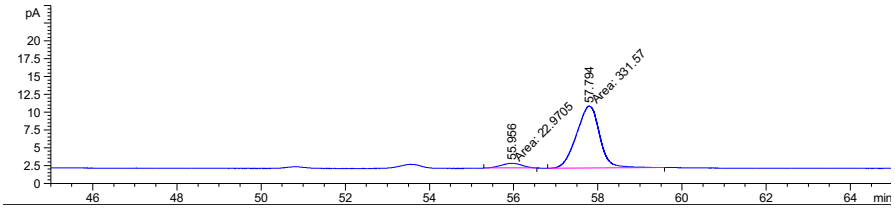

Peak #	RetTime [min]	Type	Width [min]	Area [pA*s]	Height [pA]	Area %
1	55.956	MM	0.5677	22.97053	6.74382e-1	6.47895
2	57.794	MM	0.6351	331.57037	8.70059	93.52105

(1*R*,2*S*,4*R*,5*R*)-2-methoxy-4-methyl-6-(4-(trifluoromethyl)phenyl)-8-oxabicyclo[3.2.1]oct-6-en-3-one (**2k**):

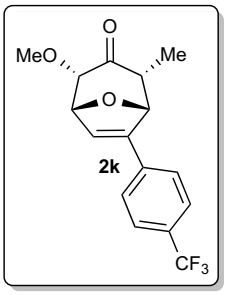

Followed procedure for (4+3) cycloaddition from **1b** (51.1 mg, 0.25 mmol) and purified using silica gel chromatography to give 75.0 mg (96% yield) of two regioisomers of **2k** (1:13 r.r.) as pale yellow oil.

^{1}H NMR (600 MHz, $CDCl_3$) δ 7.56 (d, *J*=8.2 Hz, 2H), 7.46 (d, *J*=8.2 Hz, 2H), 6.64 (d, *J*=2.3 Hz, 1H), 5.37 (d, *J*=4.7 Hz, 1H), 5.15 (dd, *J*=5.3, 2.3 Hz, 1H), 4.10 (d, *J*=4.7 Hz, 1H), 3.61 (s, 3H), 2.95 - 3.11 (m, 1H), 0.81 (d, *J*=7.0 Hz, 3H);

^{13}C NMR (125 MHz, $CDCl_3$) δ 205.6, 146.4, 135.7, 127.8, 126.9, 125.8, 125.7, 125.6, 86.1, 83.0, 81.1, 59.8, 51.0, 9.9;

FTIR (neat, cm^{-1}) ν_{max} 1720, 1323, 1112, 1068, 942, 812 cm^{-1};

HRMS (ESI-TOF) calculated for $C_{16}H_{15}F_3O_3$ $[M+Na]^+$: 335.0871, found: 335.0866.

$[\alpha]_D^{25}$ = –40.8° (c = 1.0, $CHCl_3$).

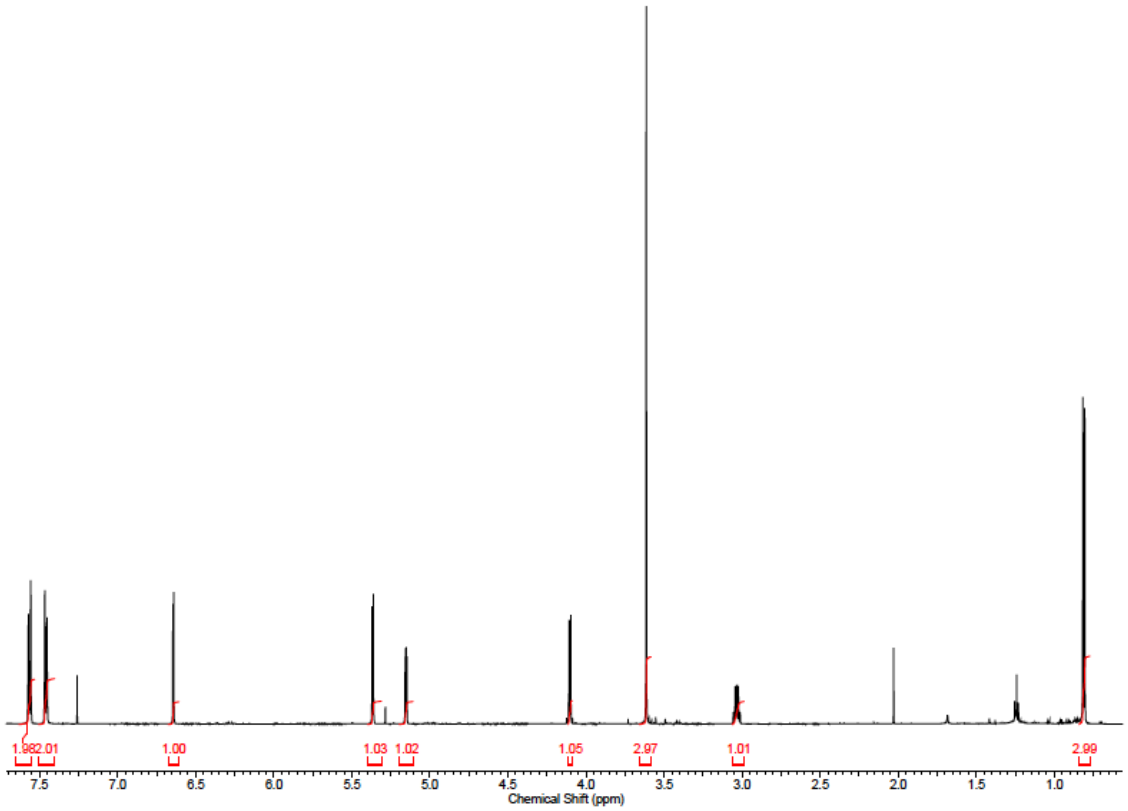
1.98
2.01
1.00
1.03
1.02
1.05
2.97
1.01
2.99
7.5
7.0
6.5
6.0
5.5
5.0
4.5
4.0
3.5
3.0
2.5
2.0
1.5
1.0
Chemical Shift (ppm)

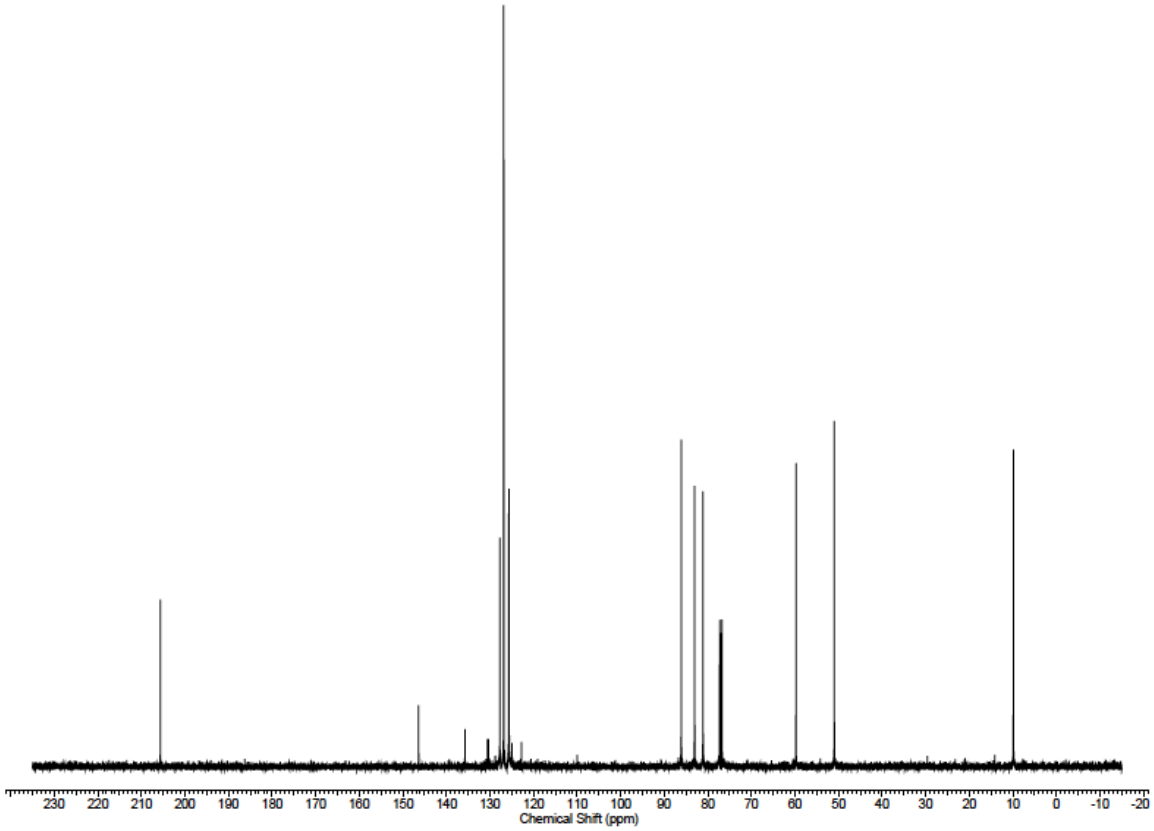
230
220
210
200
190
180
170
160
150
140
130
120
110
100
90
80
70
60
50
40
30
20
10
0
-10
-20
Chemical Shift (ppm)

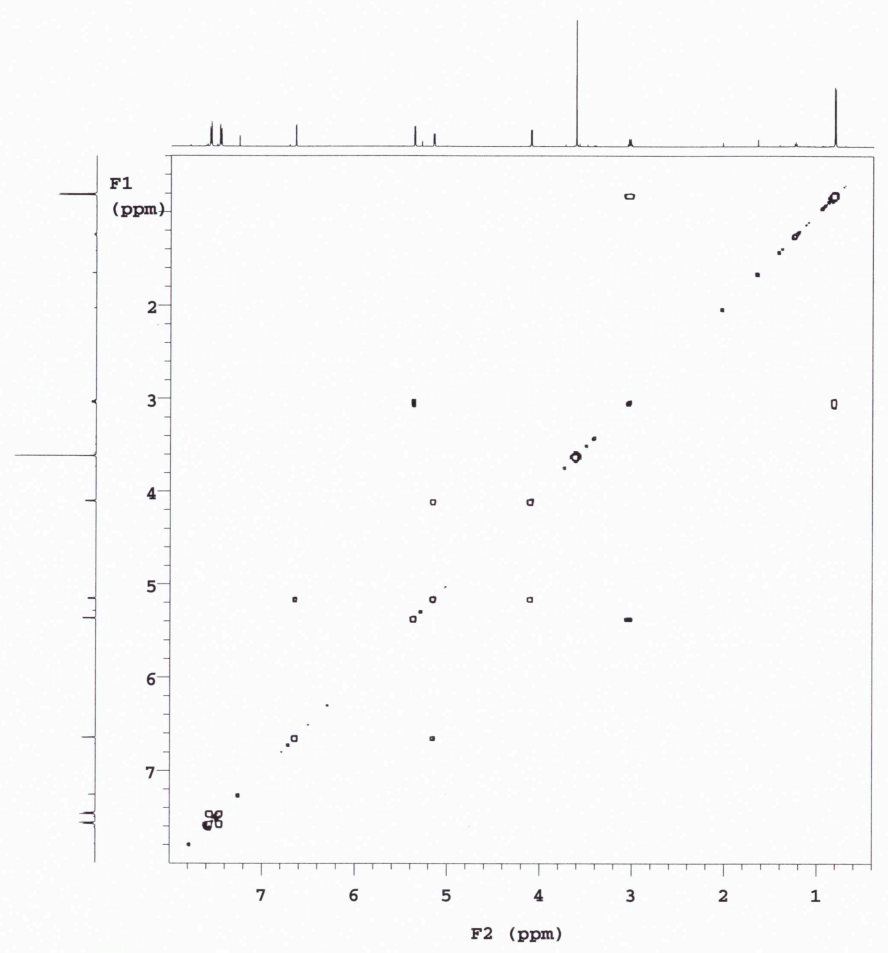

Racemic Sample: GC (β-Cyclosil, 30 m x 0.25 mm x 0.25 µm, 170 °C for 90 min)

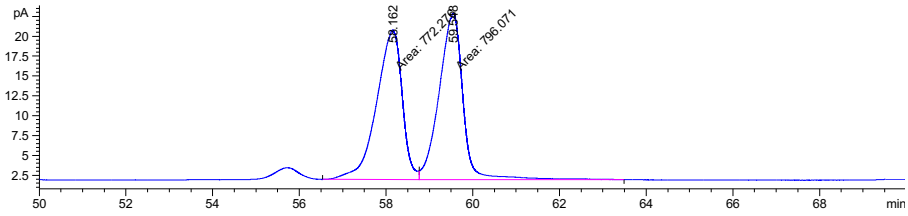

Peak #	RetTime [min]	Type	Width [min]	Area [pA*s]	Height [pA]	Area %
1	58.162	MF	0.6838	772.27582	18.82324	49.24138
2	59.548	FM	0.6349	796.07147	20.89743	50.75862

Enantioenriched Sample: GC (β-Cyclosil, 30 m x 0.25 mm x 0.25 µm, 170 °C for 90 min), 95 % e.e.

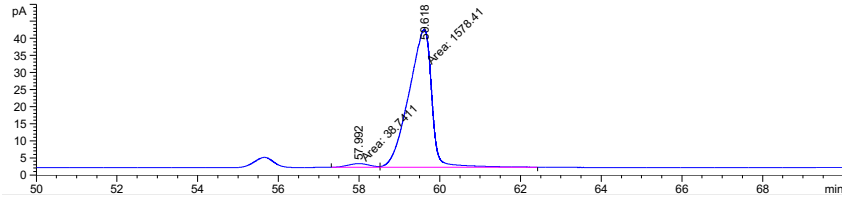

Peak #	RetTime [min]	Type	Width [min]	Area [pA*s]	Height [pA]	Area %
1	57.992	MF	0.6057	38.74109	1.06604	2.39564
2	59.618	FM	0.6512	1578.40894	40.39838	97.60436

(1*R*,2*S*,4*R*,5*R*)-6,7-bis(((*tert*-butyldimethylsilyl)oxy)methyl)-2-methoxy-4-methyl-8-oxabicyclo[3.2.1]oct-6-en-3-one (**2l**):

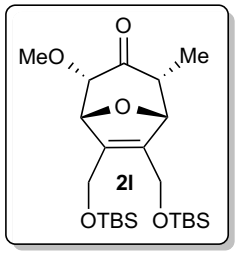

Followed procedure for (4+3) cycloaddition from **1b** (51.1 mg, 0.25 mmol) and purified using silica gel chromatography to give 93.7 mg (82% yield) of **2l** as a white crystalline solid.

^{1}H NMR (600 MHz, $CDCl_3$) δ 5.07 (d, *J*=4.7 Hz, 1H), 4.95 (d, *J*=4.1 Hz, 1H), 4.51 (d, *J*=14.1 Hz, 1H), 4.36 (d, *J*=14.1 Hz, 1H), 4.18 (d, *J*=14.1 Hz, 1H), 4.11 (d, *J*=14.1 Hz, 1H), 4.03 (d, *J*=5.3 Hz, 1H), 3.54 (s, 3H), 2.90 (dd, *J*=7.0, 4.7 Hz, 1H), 1.03 (d, *J*=7.0 Hz, 3H), 0.80 - 0.90 (m, 18H), 0.00 - 0.07 (m, 12H);

^{13}C NMR (125 MHz, $CDCl_3$) δ 206.2, 139.8, 138.9, 86.2, 84.1, 80.5, 59.3, 58.6, 58.2, 50.6, 25.8, 18.3, 9.0, -5.5;

FTIR (neat, cm^{-1}) ν_{max} 1727, 1252, 1120, 1057, 833, 775, 725 cm^{-1};

HRMS (ESI-TOF) calculated for $C_{23}H_{44}SiO_5$ $[M+Na]^+$: 479.2625, found: 479.2683.

$[\alpha]_D^{25}$ = –13.2° (c = 1.0, $CHCl_3$).

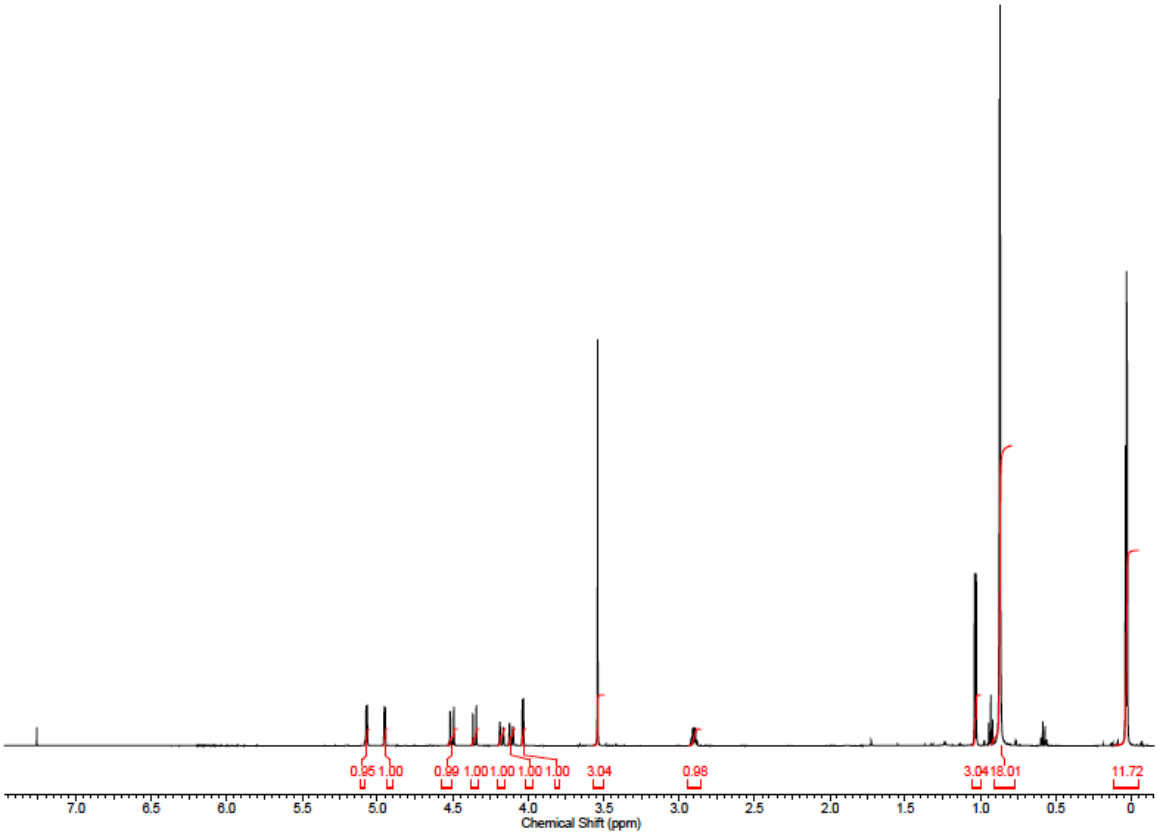
0.95 1.00 0.99 1.00 1.00 1.00 1.00 3.04 0.98 3.04 18.01 11.72
Chemical Shift (ppm)

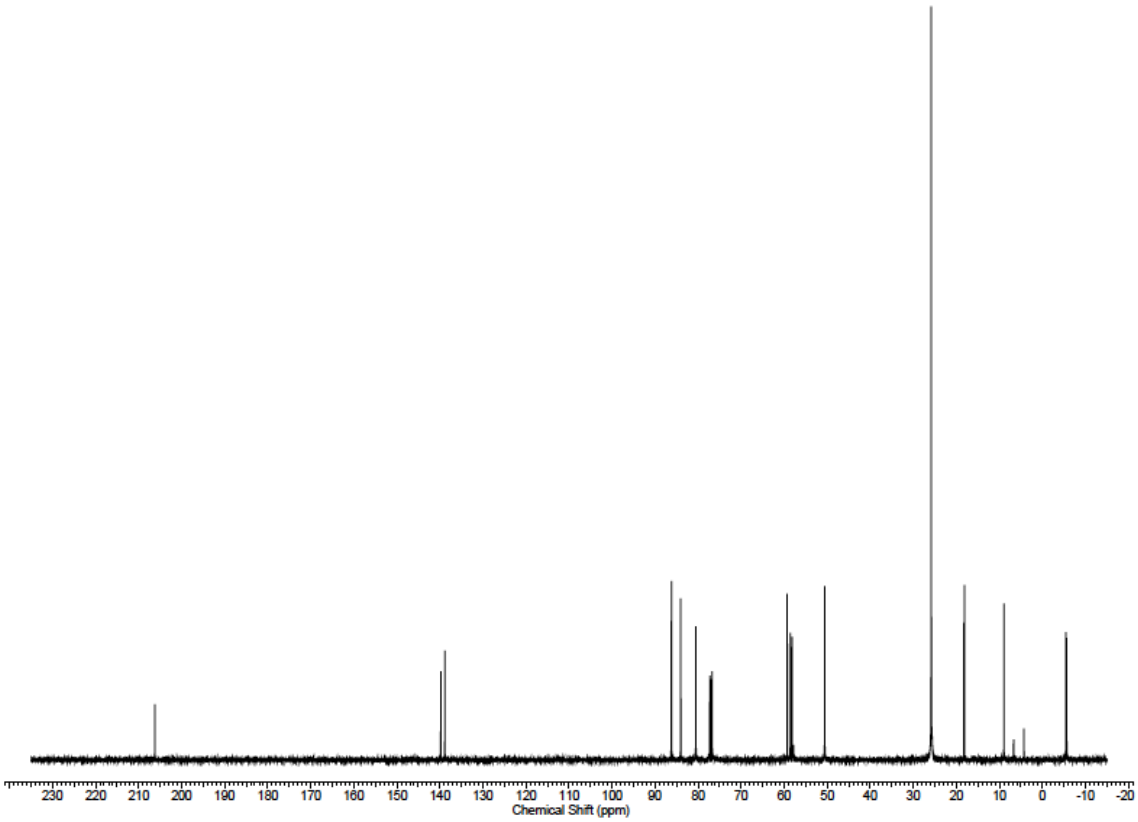
Chemical Shift (ppm)

Racemic Sample: HPLC (ChiralPak OB-H, 4% IPA/hexanes, 1 mL/min, 210 nm)

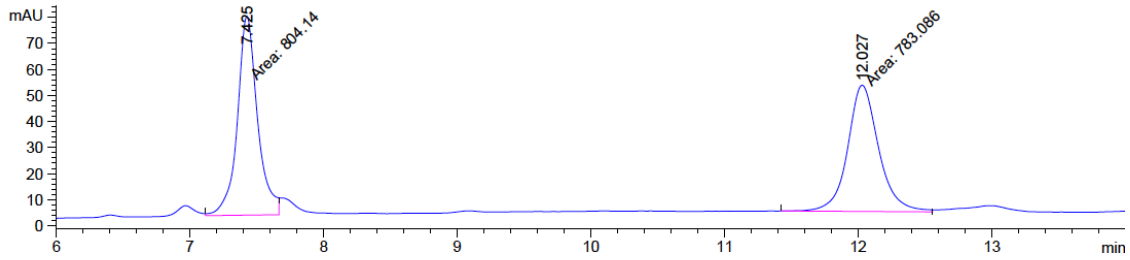

Peak #	RetTime [min]	Type	Width [min]	Area [mAU*s]	Height [mAU]	Area %
1	7.425	MF	0.1755	804.14014	76.34834	50.6632
2	12.027	MF	0.2696	783.08582	48.41183	49.3368

Enantioenriched Sample: HPLC (ChiralPak OB-H, 4% IPA/hexanes, 1 mL/min, 210 nm), 66% e.e.

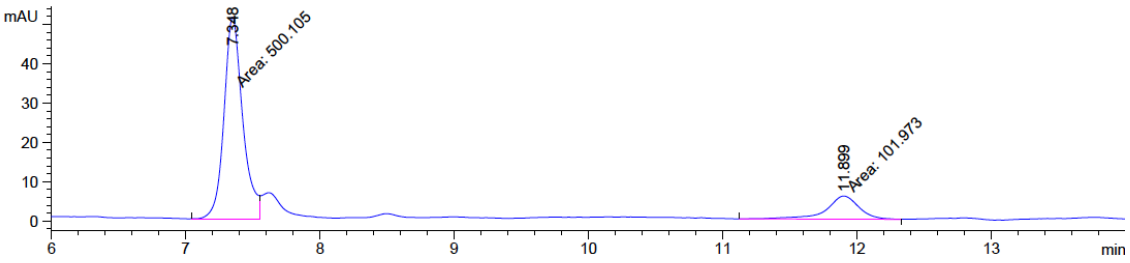

Peak #	RetTime [min]	Type	Width [min]	Area [mAU*s]	Height [mAU]	Area %
1	7.348	MF	0.1624	500.10501	51.32166	83.0632
2	11.899	MM	0.2870	101.97278	5.92163	16.9368

2.4.6. X-Ray Crystallographic Report[49]

2.4.6.1. X-Ray Crystallographic Report for Compound 2b

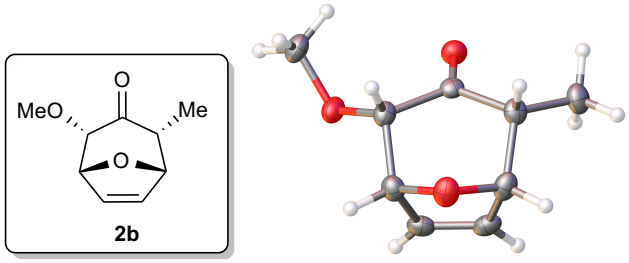

A crystal mounted on a diffractometer was collected data at 100 K. The intensities of the reflections were collected by means of a Bruker APEX II DUO CCD diffractometer (Cu_{K_α} radiation, λ=1.54178 Å), and equipped with an Oxford Cryosystems nitrogen flow apparatus. The collection method involved 1.0° scans in ω at 30°, 55°, 80° and 115° in 2θ. Data integration down to 0.84 Å resolution was carried out using SAINT V8.30 A (Bruker diffractometer, 2013) with reflection spot size optimization. Absorption corrections were made with the program SADABS (Bruker diffractometer, 2013). The structure was solved by the direct methods procedure and refined by least-squares methods again F^2 using SHELXS-2013 and SHELXL-2013[50] with OLEX 2 interface.[51] Non-hydrogen atoms were refined anisotropically, and hydrogen atoms were allowed to ride on the respective atoms. Crystal data as well as details of data collection and refinement are summarized in Table 2.5, and geometric parameters are shown

[49] X-ray data was collected by Shao-Liang Zheng

[50] Sheldrick, G. M., *Acta Cryst*. **2008**, *A64*, 112–122.

[51] Dolomanov, O. V.; Bourhis, L. J.; Gildea, R. J.; Howard, J. A. K.; Puschmann, H. *J. Appl. Cryst*. **2009**, *42*, 339–341.

in Table 2.6. The Ortep plots produced with SHELXL-2013 program, and the other drawings were produced with Accelrys DS Visualizer 2.0.[52]

Table 2.5. ***Experimental details.***

Crystal data	
Chemical formula	$C_9H_{12}O_3$
M_r	168.19
Crystal system, space group	Orthorhombic, $P2_12_12_1$
Temperature (K)	100
a, b, c (Å)	8.8623 (14), 9.0115 (14), 10.5284 (17)
V (Å^3)	840.8 (2)
Z	4
Radiation type	Cu Ka
m (mm^{-1})	0.82
Crystal size (mm)	0.20 × 0.18 × 0.12
Data collection	
Diffractometer	Bruker D8 goniometer with CCD area detector diffractometer
Absorption correction	Multi-scan *SADABS*
T_{min}, T_{max}	0.682, 0.753
No. of measured, independent and observed [I > 2s(I)] reflections	20060, 1491, 1482
R_{int}	0.056
(sin q/l)$_{max}$ (Å^{-1})	0.597
Refinement	
$R[F^2 > 2s(F^2)]$, $wR(F^2)$, S	0.024, 0.062, 1.07
No. of reflections	1491
No. of parameters	112
H-atom treatment	H-atom parameters constrained

[52] Accelrys DS Visualizer v2.0.1, Accelrys Software. Inc. **2007**.

$D\rho_{max}$, $D\rho_{min}$ (e Å^{-3})	0.14, -0.12
Absolute structure	Flack x determined using 597 quotients [(I+)-(I-)]/[(I+)+(I-)] (Parsons and Flack (2004), Acta Cryst. A60, s61).
Absolute structure parameter	0.07 (6)

Computer programs: *APEX2* v2013.4.1 (Bruker-AXS, 2013), *SAINT* 8.30A (Bruker-AXS, 2012), *SHELXS2013* (Sheldrick, 2013), *SHELXL2013* (Sheldrick, 2013), Bruker *SHELXTL* (Sheldrick, 2013).

Table 2.6. ***Geometric parameters (Å, º).***

C1—O1	1.213 (2)	C6—O3	1.438 (2)
C1—C7	1.527 (2)	C6—C7	1.545 (2)
C1—C2	1.538 (2)	C6—H6	1.0000
C2—O2	1.4110 (19)	C7—C8	1.517 (2)
C2—C3	1.539 (2)	C7—H7	1.0000
C2—H2	1.0000	C8—H8A	0.9800
C3—O3	1.434 (2)	C8—H8B	0.9800
C3—C4	1.506 (2)	C8—H8C	0.9800
C3—H3	1.0000	C9—O2	1.426 (2)
C4—C5	1.324 (3)	C9—H9A	0.9800
C4—H4	0.9500	C9—H9B	0.9800
C5—C6	1.506 (2)	C9—H9C	0.9800
C5—H5	0.9500		
O1—C1—C7	121.86 (15)	O3—C6—H6	111.8
O1—C1—C2	120.87 (14)	C5—C6—H6	111.8
C7—C1—C2	117.20 (13)	C7—C6—H6	111.8
O2—C2—C1	112.20 (13)	C8—C7—C1	112.45 (14)
O2—C2—C3	107.29 (13)	C8—C7—C6	112.97 (15)
C1—C2—C3	108.35 (13)	C1—C7—C6	107.18 (13)
O2—C2—H2	109.6	C8—C7—H7	108.0

C1—C2—H2	109.6	C1—C7—H7	108.0
C3—C2—H2	109.6	C6—C7—H7	108.0
O3—C3—C4	103.13 (13)	C7—C8—H8A	109.5
O3—C3—C2	106.80 (13)	C7—C8—H8B	109.5
C4—C3—C2	109.42 (13)	H8A—C8—H8B	109.5
O3—C3—H3	112.3	C7—C8—H8C	109.5
C4—C3—H3	112.3	H8A—C8—H8C	109.5
C2—C3—H3	112.3	H8B—C8—H8C	109.5
C5—C4—C3	108.05 (15)	O2—C9—H9A	109.5
C5—C4—H4	126.0	O2—C9—H9B	109.5
C3—C4—H4	126.0	H9A—C9—H9B	109.5
C4—C5—C6	107.70 (15)	O2—C9—H9C	109.5
C4—C5—H5	126.1	H9A—C9—H9C	109.5
C6—C5—H5	126.1	H9B—C9—H9C	109.5
O3—C6—C5	103.06 (14)	C2—O2—C9	114.12 (13)
O3—C6—C7	107.89 (13)	C3—O3—C6	103.03 (12)
C5—C6—C7	110.10 (13)		
O1—C1—C2—O2	18.3 (2)	C2—C1—C7—C8	164.59 (14)
C7—C1—C2—O2	-158.64 (14)	O1—C1—C7—C6	-137.04 (15)
O1—C1—C2—C3	136.56 (15)	C2—C1—C7—C6	39.86 (17)
C7—C1—C2—C3	-40.37 (17)	O3—C6—C7—C8	177.84 (13)
O2—C2—C3—O3	179.05 (12)	C5—C6—C7—C8	-70.38 (17)
C1—C2—C3—O3	57.70 (16)	O3—C6—C7—C1	-57.75 (16)
O2—C2—C3—C4	68.07 (16)	C5—C6—C7—C1	54.03 (17)
C1—C2—C3—C4	-53.28 (16)	C1—C2—O2—C9	-90.26 (16)
O3—C3—C4—C5	-22.68 (17)	C3—C2—O2—C9	150.85 (13)
C2—C3—C4—C5	90.70 (16)	C4—C3—O3—C6	36.77 (15)
C3—C4—C5—C6	-0.61 (18)	C2—C3—O3—C6	-78.51 (15)
C4—C5—C6—O3	23.62 (17)	C5—C6—O3—C3	-37.15 (15)
C4—C5—C6—C7	-91.26 (17)	C7—C6—O3—C3	79.31 (15)
O1—C1—C7—C8	-12.3 (2)		

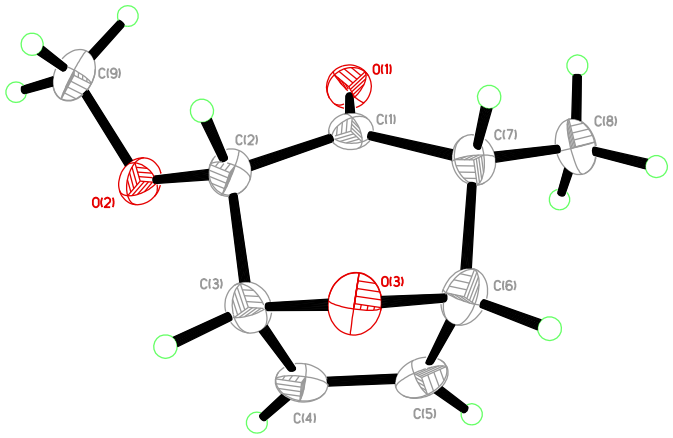

Figure 2.6. ***Perspective views showing 50% probability displacement.***

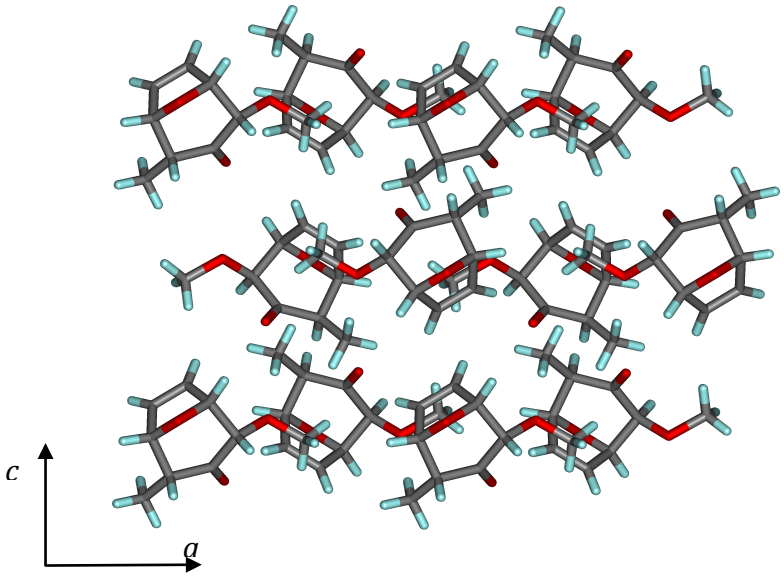

Figure 2.7. ***Three-dimensional supramolecular architecture viewed along the b-axis direction.***

2.4.6.2. X-Ray Crystallographic Report for Compound S4

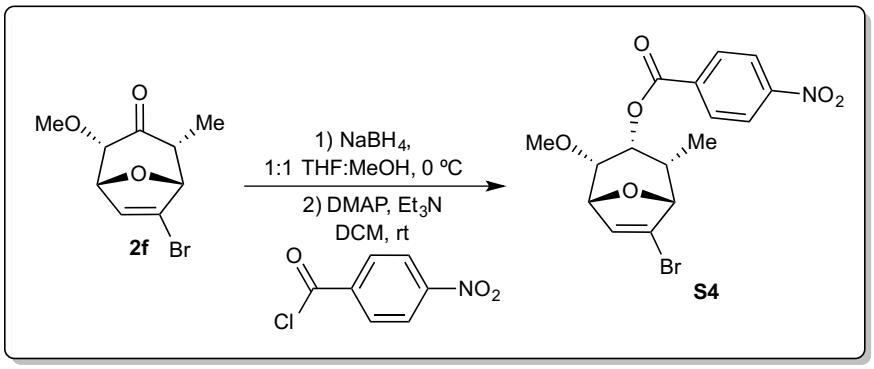

Scheme 2.4. ***Synthesis of compound S4, a crystalline derivative of 2f.***

(1*R*,2*S*,3*R*,4*S*,5*R*)-6-bromo-2-methoxy-4-methyl-8-oxabicyclo[3.2.1]oct-6-en-3-yl 4-nitrobenzoate (**S4**):

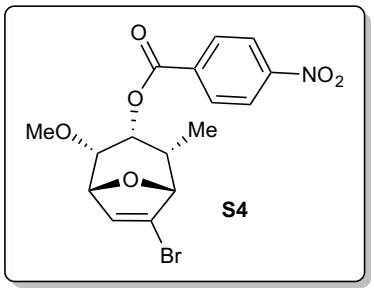

A 10 mL round bottom flask, equipped with a magnetic stir bar, was flame dried under vacuum and let cool to room temperature, and then filled with nitrogen. **4f** (40 mg, 0.16 mmol) and 0.4 mL THF and 0.4 mL of MeOH were added. Stirring was started and reaction was cooled to 0 °C on water/ice bath. The first batch of sodium borohydride (6.0 mg, 0.16 mmol, 1.0 equiv.) was added and the reaction mixture was stirred for 1 h at 0 °C. After 1 h, second bath of sodium borohydride (3.0 mg, 0.08 mmol, 0.5 equiv.) was added and stirred for an additional 1 h at 0 °C. Acetic acid was then added dropwise until gas evolution ceased. Reaction mixture was concentrated and 10 mL DCM and 5mL of sodium bicarbonate (aq. sat.) were added, the mixture was poured into extraction funnel and layers were separated. Aqueous layer was washed with

DCM (2 x 10 mL). Combined organic layers were dried over Na_2SO_4, filtered and concentrated. The resulting material was deemed clean enough to be used directly in the next step.

A 10 mL round bottom flask, equipped with a magnetic stir bar, was flame dried under vacuum and let cool to room temperature, and then filled with nitrogen. Crude product from previous reaction was added using DCM (3.4 mL). Then DMAP (21 mg, 0.17 mmol, 1.0 equiv.), 4-nitrobenzoyl chloride (39 mg, 0.21 mmol, 1.5 equiv.) and triethylamine (0.1 mL, 0.85 mmol, 5.0 equiv.) were added to the reaction flask. Reaction was allowed to stir at room temperature under N_2 for 24 h. 10 mL of NaOH (1 M, aq.) were added to the reaction mixture and stirred for 20 min. Reaction mixture was then poured into extraction funnel and extracted with DCM (3 x 10 mL). Combined organic layer was dried over Na_2SO_4, filtered and concentrated. Product was purified by column chromatography with hexane/ethyl ether as eluent (10:1 to 2:1) to yield pure **S4** as a single diastereomer in 35 mg (55 % yield over two steps) as white crystalline solid.

^{1}H NMR (600 MHz, $CDCl_3$) δ 8.30 (dd, J = 12.3, 8.2 Hz, 4H), 6.54 (d, J = 1.8 Hz, 1H), 5.86 (t, J = 4.7 Hz, 1H), 4.68 (d, J = 1.8 Hz, 1H), 4.37 (d, J = 4.0 Hz, 1H), 3.73 (t, J = 4.7 Hz, 1H), 3.35 (s, 3H), 2.54 (dt, J = 8.2, 4.1 Hz, 1H), 1.09 (d, J = 7.6 Hz, 3H);

^{13}C NMR (125 MHz, $CDCl_3$) δ 164.5, 150.6, 135.4, 132.3, 131.0, 123.5, 84.6, 79.5, 76.7, 70.8, 58.2, 36.8, 12.0;

FTIR (neat, cm^{-1}) ν_{max} 1716, 1529, 1275, 1103, 863, 719 cm^{-1};

HRMS (ESI-TOF) calculated for $C_{16}H_{16}BrNO_6$ $[M+Na]^+$: 420.0059, found: 420.0085;

$[\alpha]_D^{25}$ = +101.8° (c = 1.0, $CHCl_3$).

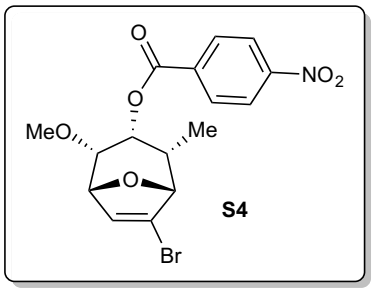

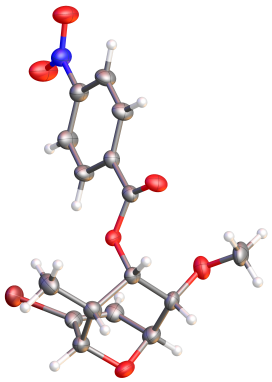

A crystal mounted on a diffractometer was collected data at 100 K. The intensities of the reflections were collected by means of a Bruker APEX II DUO CCD diffractometer (Cu_{K_α} radiation, λ=1.54178 Å), and equipped with an Oxford Cryosystems nitrogen flow apparatus. The collection method involved 1.0° scans in ω at 30°, 55°, 80° and 115° in 2θ. Data integration down to 0.84 Å resolution was carried out using SAINT V7.46 A[53] with reflection spot size optimisation. Absorption corrections were made with the program SADABS (Bruker diffractometer, 2009). The structure was solved by the direct methods procedure and refined by least-squares methods again F^2 using SHELXS-97 and SHELXL-97[50] with OLEX 2 interface.[51] Non-hydrogen atoms were refined anisotropically, and hydrogen atoms were allowed to ride on the respective atoms. Crystal data as well as details of data collection and refinement are summarized in Table S1, and geometric parameters are shown in Table S2. The Ortep plots produced with SHELXL-97 program, and the other drawings were produced with Accelrys DS Visualizer 2.0.[52]

[53] Bruker AXS APEX II, Bruker AXS, Madison, Wisconsin, **2009**.

Table 2.7. ***Experimental details.***

Crystal data	
Chemical formula	$C_{16}H_{16}BrNO_6$
M_r	398.21
Crystal system, space group	Hexagonal, $P6_5$
Temperature (K)	100
a, c (Å)	22.2019 (12), 7.7538 (4)
V (Å^3)	3310.0 (3)
Z	6
Radiation type	Cu Ka
m (mm^{-1})	2.76
Crystal size (mm)	0.24 × 0.10 × 0.08
Data collection	
Diffractometer	Bruker D8 goniometer with CCD area detector diffractometer
Absorption correction	Multi-scan *SADABS*
T_{min}, T_{max}	0.557, 0.809
No. of measured, independent and observed [I > 2s(I)] reflections	33377, 3738, 3503
R_{int}	0.095
(sin q/l)$_{max}$ (Å^{-1})	0.595
Refinement	
$R[F^2 > 2s(F^2)]$, $wR(F^2)$, S	0.032, 0.078, 1.04
No. of reflections	3738
No. of parameters	219
No. of restraints	1
H-atom treatment	H atoms treated by a mixture of independent and constrained refinement
Dρ$_{max}$, Dρ$_{min}$ (e Å^{-3})	0.41, -0.37
Absolute structure	Flack H D (1983), Acta Cryst. A39, 876-881
Absolute structure parameter	-0.072 (16)

Computer programs: *APEX2* v2009.3.0 (Bruker-AXS, 2009), *SAINT* 7.46A (Bruker-AXS, 2009), *SHELXS97* (Sheldrick, 2008), *SHELXL97* (Sheldrick, 2008), Bruker *SHELXTL* (Sheldrick, 2008).

Table 2.8. ***Geometric parameters (Å, º).***

C1—O3	1.447 (3)	C8—H8C	0.9800
C1—C7	1.535 (4)	C9—O2	1.429 (4)
C1—C2	1.551 (4)	C9—H9A	0.9800
C1—H1	1.0000	C9—H9B	0.9800
C2—O2	1.419 (3)	C9—H9C	0.9800
C2—C3	1.531 (4)	C10—O4	1.216 (3)
C2—H2	1.0000	C10—O3	1.346 (3)
C3—O1	1.452 (4)	C10—C11	1.487 (4)
C3—C4	1.509 (5)	C11—C12	1.393 (4)
C3—H3	1.0000	C11—C16	1.393 (4)
C4—C5	1.321 (4)	C12—C13	1.384 (5)
C4—H4	0.9500	C12—H12	0.9500
C5—C6	1.505 (5)	C13—C14	1.375 (5)
C5—Br1	1.886 (3)	C13—H13	0.9500
C6—O1	1.450 (3)	C14—C15	1.389 (4)
C6—C7	1.540 (5)	C14—N1	1.469 (4)
C6—H6	1.0000	C15—C16	1.385 (5)
C7—C8	1.532 (4)	C15—H15	0.9500
C7—H7	1.0000	C16—H16	0.9500
C8—H8A	0.9800	N1—O5	1.213 (4)
C8—H8B	0.9800	N1—O6	1.232 (3)
O3—C1—C7	109.5 (3)	H8A—C8—H8B	109.5
O3—C1—C2	108.5 (2)	C7—C8—H8C	109.5
C7—C1—C2	111.3 (2)	H8A—C8—H8C	109.5
O3—C1—H1	109.1	H8B—C8—H8C	109.5

C7—C1—H1	109.1	O2—C9—H9A	109.5
C2—C1—H1	109.1	O2—C9—H9B	109.5
O2—C2—C3	109.3 (2)	H9A—C9—H9B	109.5
O2—C2—C1	111.3 (2)	O2—C9—H9C	109.5
C3—C2—C1	111.4 (2)	H9A—C9—H9C	109.5
O2—C2—H2	108.2	H9B—C9—H9C	109.5
C3—C2—H2	108.2	O4—C10—O3	124.0 (3)
C1—C2—H2	108.2	O4—C10—C11	123.8 (3)
O1—C3—C4	103.0 (2)	O3—C10—C11	112.1 (2)
O1—C3—C2	104.6 (3)	C12—C11—C16	119.9 (3)
C4—C3—C2	113.6 (2)	C12—C11—C10	117.9 (3)
O1—C3—H3	111.7	C16—C11—C10	122.2 (3)
C4—C3—H3	111.7	C13—C12—C11	120.6 (3)
C2—C3—H3	111.7	C13—C12—H12	119.7
C5—C4—C3	105.9 (3)	C11—C12—H12	119.7
C5—C4—H4	127.1	C14—C13—C12	118.1 (3)
C3—C4—H4	127.1	C14—C13—H13	121.0
C4—C5—C6	110.7 (3)	C12—C13—H13	121.0
C4—C5—Br1	126.5 (3)	C13—C14—C15	123.1 (3)
C6—C5—Br1	122.4 (2)	C13—C14—N1	119.0 (3)
O1—C6—C5	100.1 (2)	C15—C14—N1	117.9 (3)
O1—C6—C7	105.6 (3)	C16—C15—C14	118.1 (3)
C5—C6—C7	113.9 (2)	C16—C15—H15	121.0
O1—C6—H6	112.1	C14—C15—H15	121.0
C5—C6—H6	112.1	C15—C16—C11	120.2 (3)
C7—C6—H6	112.1	C15—C16—H16	119.9
C8—C7—C1	112.0 (2)	C11—C16—H16	119.9
C8—C7—C6	112.7 (3)	O5—N1—O6	123.9 (3)
C1—C7—C6	111.3 (3)	O5—N1—C14	118.2 (3)
C8—C7—H7	106.8	O6—N1—C14	117.9 (3)
C1—C7—H7	106.8	C6—O1—C3	102.8 (2)
C6—C7—H7	106.8	C2—O2—C9	112.3 (3)
C7—C8—H8A	109.5	C10—O3—C1	117.3 (2)

C7—C8—H8B	109.5		
O3—C1—C2—O2	-44.0 (3)	O4—C10—C11—C16	-176.3 (3)
C7—C1—C2—O2	-164.6 (3)	O3—C10—C11—C16	6.4 (4)
O3—C1—C2—C3	78.4 (3)	C16—C11—C12—C13	-1.5 (5)
C7—C1—C2—C3	-42.2 (4)	C10—C11—C12—C13	178.5 (3)
O2—C2—C3—O1	-175.7 (2)	C11—C12—C13—C14	2.7 (5)
C1—C2—C3—O1	60.8 (3)	C12—C13—C14—C15	-2.1 (5)
O2—C2—C3—C4	72.8 (3)	C12—C13—C14—N1	178.7 (3)
C1—C2—C3—C4	-50.7 (3)	C13—C14—C15—C16	0.2 (5)
O1—C3—C4—C5	-23.1 (3)	N1—C14—C15—C16	179.5 (3)
C2—C3—C4—C5	89.5 (3)	C14—C15—C16—C11	1.1 (5)
C3—C4—C5—C6	-2.2 (3)	C12—C11—C16—C15	-0.4 (5)
C3—C4—C5—Br1	-175.4 (2)	C10—C11—C16—C15	179.6 (3)
C4—C5—C6—O1	26.5 (3)	C13—C14—N1—O5	-170.9 (3)
Br1—C5—C6—O1	-160.06 (19)	C15—C14—N1—O5	9.9 (5)
C4—C5—C6—C7	-85.7 (3)	C13—C14—N1—O6	9.2 (5)
Br1—C5—C6—C7	87.8 (3)	C15—C14—N1—O6	-170.1 (3)
O3—C1—C7—C8	48.4 (4)	C5—C6—O1—C3	-39.6 (3)
C2—C1—C7—C8	168.4 (3)	C7—C6—O1—C3	79.0 (3)
O3—C1—C7—C6	-78.8 (3)	C4—C3—O1—C6	39.5 (3)
C2—C1—C7—C6	41.2 (4)	C2—C3—O1—C6	-79.5 (3)
O1—C6—C7—C8	173.8 (3)	C3—C2—O2—C9	146.6 (2)
C5—C6—C7—C8	-77.3 (3)	C1—C2—O2—C9	-89.8 (3)
O1—C6—C7—C1	-59.4 (3)	O4—C10—O3—C1	8.7 (4)
C5—C6—C7—C1	49.5 (4)	C11—C10—O3—C1	-174.0 (2)
O4—C10—C11—C12	3.7 (4)	C7—C1—O3—C10	-141.5 (2)
O3—C10—C11—C12	-173.5 (2)	C2—C1—O3—C10	96.8 (3)

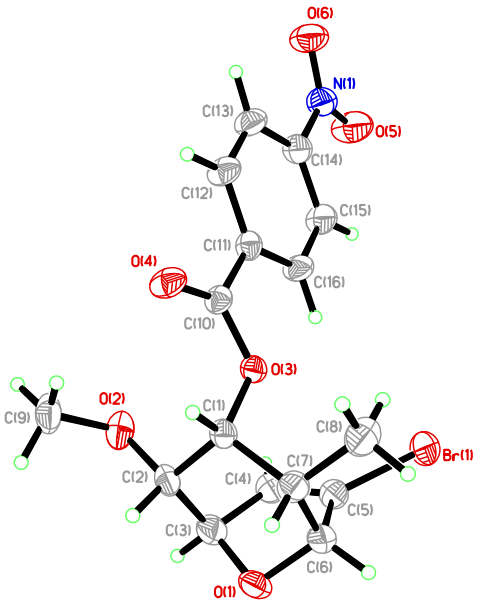

Figure 2.8. ***Perspective views showing 50% probability displacement.***

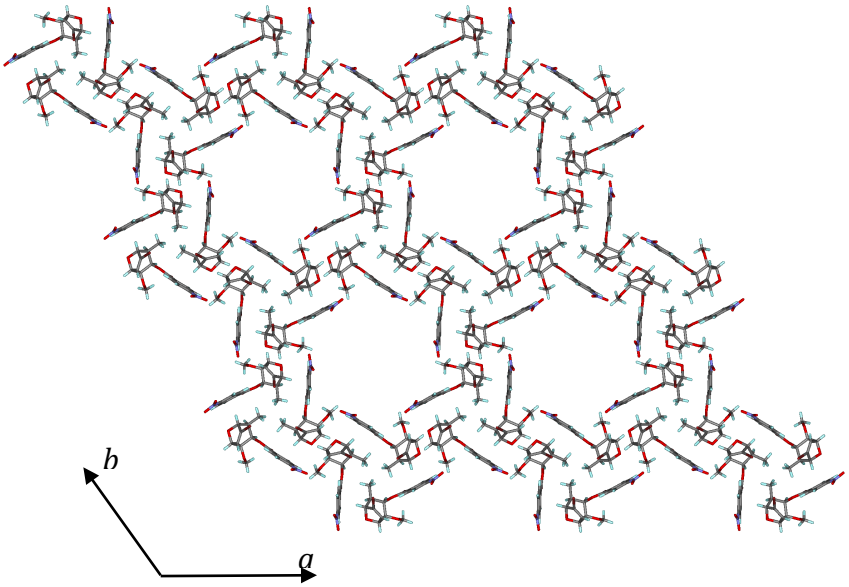

Figure 2.9. ***Three-dimensional supramolecular architecture viewed along the c-axis direction.***

2.4.7. Procedure for ^{1}H NMR Studies on Starting Material Ionization

An oven-dried screw cap NMR tube was cooled in a desiccator and then flushed with argon, closed with a cap and put under argon using a needle inlet. 0.7 mL of stock solution of **1a** in MTBE (0.05M, which corresponds to **1a** 8.1 mg, 0.035 mmol, 1 equiv.) was added via a syringe. An Inova-500 (500 MHz) spectrometer was used to conduct low-temperature NMR. The probe was cooled to -78 ºC, and a spectrum of **1a** in MTBE was obtained (spectrum of characteristic protons shown in blue, Figure S5). The NMR tube was then ejected from the probe and TBSOTf (17.0 µL, 0.07 mmol, 2.0 equiv.) was quickly added via syringe, the tube was shaken to ensure mixing and returned to NMR. Obtained spectrum showed no decomposition of **1a** upon addition of TBSOTf at -78 ºC (shown in red, Figure 2.10).

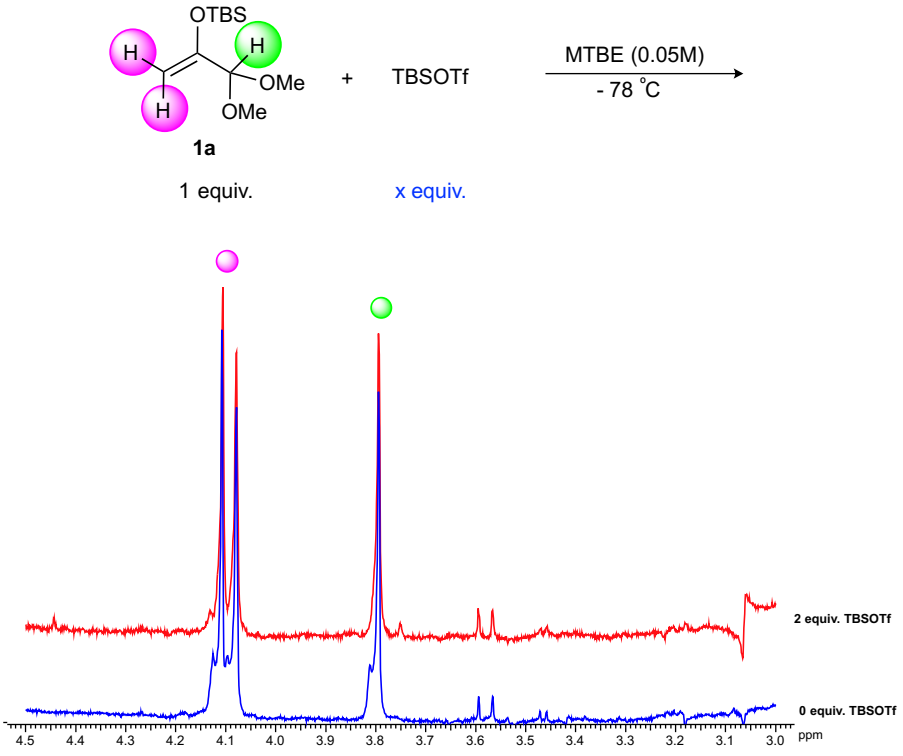

Figure 2.10. ***Ionization of 1a in absence of catalyst:*** **1a** in MTBE at -78 ºC (blue); **1a** and TBSOTf in MTBE at -78 ºC (red).

An oven-dried screw cap NMR tube was cooled in a desiccator and then flushed with argon. The tube was then charged with 21.6 mg of catalyst **S5** (0.035 mmol, 1.0 equiv.), closed and put under argon. 0.7 mL of stock solution of **1a** in MTBE (0.05M, which corresponds to **1a** 8.1 mg, 0.035 mmol, 1.0 equiv.) was added via a syringe. An Inova-500 (500 MHz) spectrometer was used to conduct low-temperature NMR. The probe was cooled to -78 ºC, and spectrum of **1a** in presence of **S5** in MTBE was obtained (spectrum of characteristic signals shown in blue, Figure 2.11). NMR tube was then ejected and TBSOTf (total equivalents as shown, Figure 2.11) was added via a syringe, the tube was quickly shaken to ensure mixing and returned to NMR. Obtained spectra showed decomposition of **1a** upon addition of TBSOTf at -78 ºC in presence of catalyst **S5** (shown in green, magenta and red, Figure 2.11).

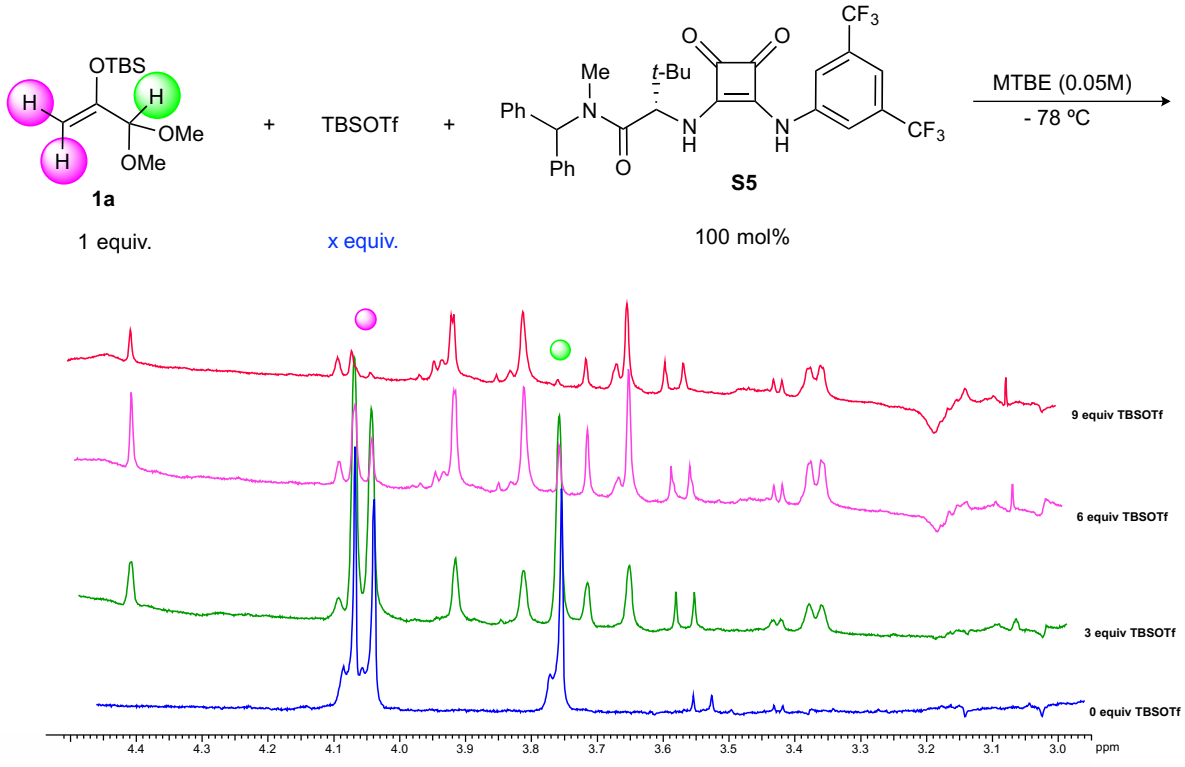

Figure 2.11. ***Decomposition of 1a upon addition of TBSOTf in presence of squaramide catalyst.***

2.4.8. Examination of Solvent and Promoter

All reactions in this section were set up according to Method A.

Investigation of solvent:

Table 2.9. ***Investigation of solvent effect.***

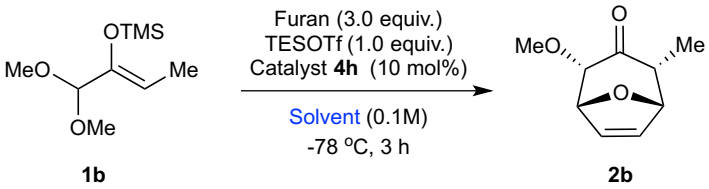

Entry	Solvent	Yield (%)	ee (%)
1	Toluene	65	23
2	DCM	36	33
3	THF	80	42
4	Et_2O	64	72
5	CPME	78	78
6	MTBE	82	89

Investigation of promoter:

Table 2.10. ***Investigation of Lewis acid effect on substrate 1b.***

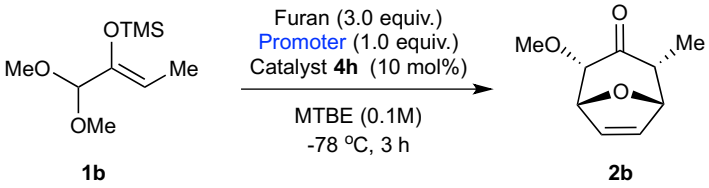

Entry	Promoter	Yield (%)	ee (%)
1	TMSOTf	76	86
2	TBSOTf	83	88
3	TESOTf	82	89
4	TIPSOTf	81	89
5	TfOH	75	84
6	TMSOMs	n.r.	-

Table 2.11. ***Early investigation of Lewis acid effect on substrate 1a.***[54]

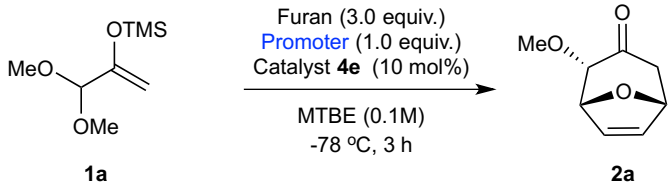

Entry	Promoter	Yield (%)	ee (%)
1	$TMSNTf_2$[a]	29	3
2	$HBF_4 \cdot OEt_2$	19	25
3	TMSCl	n.r.	-
4	HCl	n.r.	-
5	BCl_3	n.r.	-
6	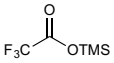	n.r.	-

a. catalyst **4c** was used in this reaction instead of **4e**.

2.4.9. Catalyst Structure Investigation

Investigation of arylpyrrolidino moiety of catalysts **4a-h** on substrate **2b** has been presented in the main text. All reactions in this section were set up according to Method A.

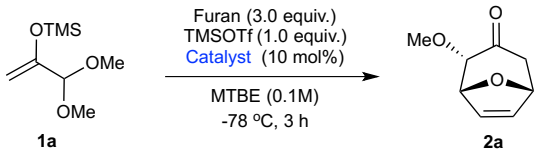

Scheme 1.5. ***Reaction used for early catalyst optimization.***

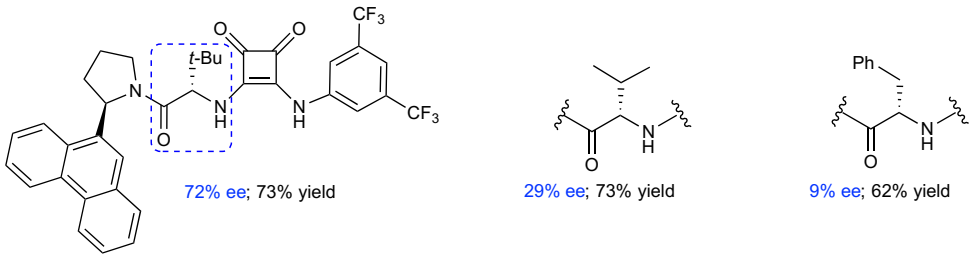

Figure 1.12. ***Investigation of amino acid linker (early studies on substrate 1a).***

[54] Results in this table were obtained by Dr. Alan M. Hyde

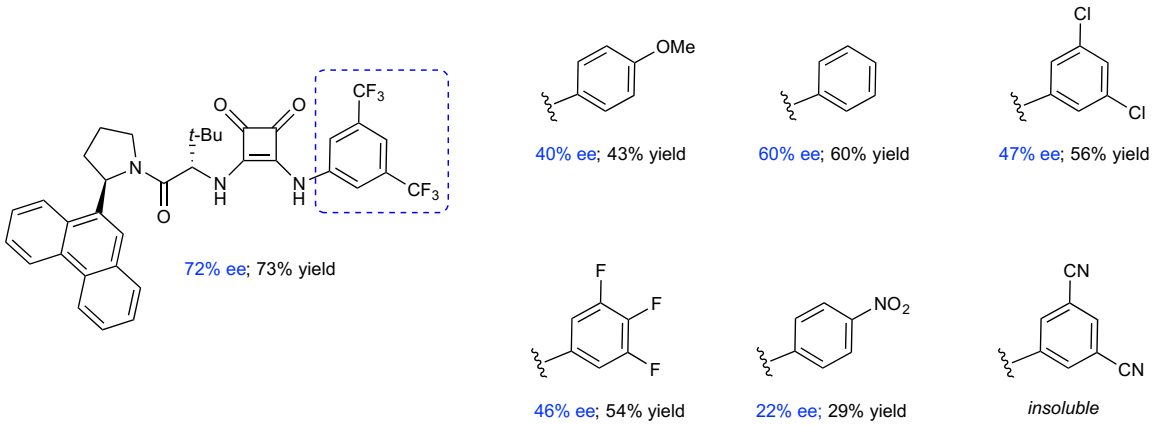

Figure 2.13. ***Investigation of electronics of the squaramide unit (early studies on substrate 1a).***

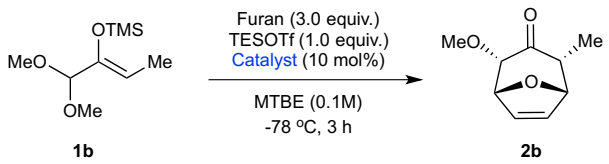

Scheme 2.6. ***Reaction used for further catalyst investigation.***

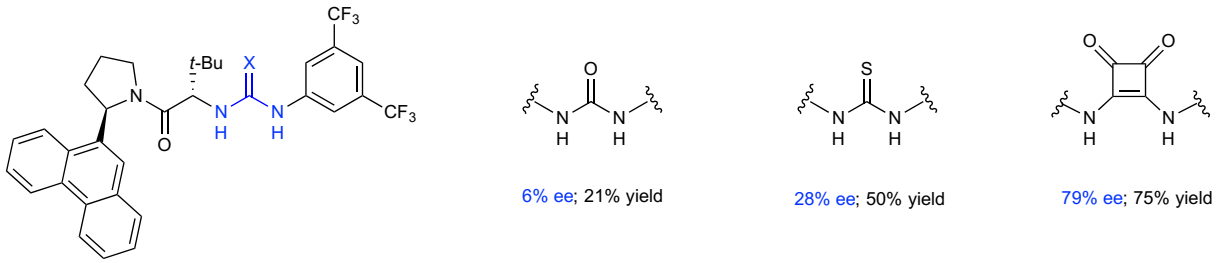

Figure 2.14. ***Investigation of hydrogen bond donor unit (using substrate 1b).***

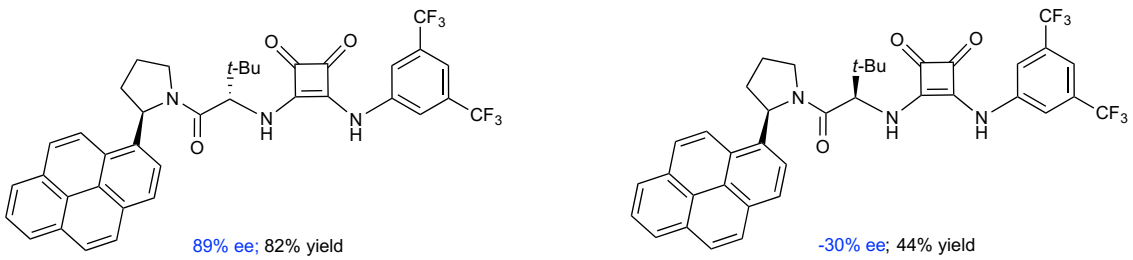

Figure 2.15. ***Investigation of diastereomers of catalyst 4h.***

2.4.10. Data for Kinetics Analysis with In Situ IR Spectroscopy and Derivation of Empirical Rate Laws

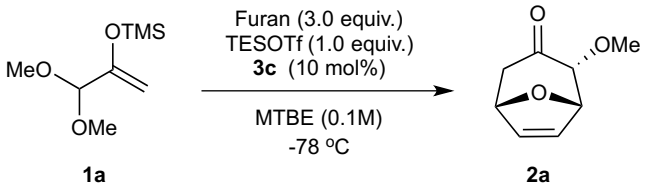

Scheme 2.7. ***Reaction used for kinetic analysis with catalyst 3c.***

Representative procedure:

An oven-dried 10 mL two-neck round bottom flask equipped with a 1/8" stir bar was allowed to cool in a desiccator. The flask was then charged with substrate **1a** (19mg, 0.1 mmol, 1 equiv.), furan (22 μL, 0.30 mmol, 3.0 equiv.), **3c** (5.6 mg, 0.01 mmol, 10 mol%) and MTBE (1.0 mL). The side arm was closed with a septum, and flask was attached to the in situ infrared spectroscopy probe (that was previously dried with a heat gun), secured with a small clamp and the reaction was put under nitrogen atmosphere through an inlet needle in the side arm septum. Reaction mixture was then cooled to -78 ºC on the dry ice-acetone bath and stirring started. Continuous data collection (4 scan/min, 50 scans/spectrum) was started to define baseline in absence of product **2a**. TESOTf (23.0 μL, 0.10 mmol, 1.0 equiv.) was added via syringe through the septum in flask's side arm. Reaction was run until IR absorbance of carbonyl functionality of product **2a** (height to two-point baseline, 1733 cm^{-1} to 1850/1690 cm^{-1}) became level, when it was quenched via addition of 200 μL of a 6:1 MeOH:Et_3N solution via syringe.

Intensity of the signal was converted to concentration of **2a** using dilution calibration curve (shown in Figure S7 below). Figure S8 shows a representative plot of concentration of **2a** versus time and a seventh-order polynomial fit to the data. Concentration versus time data were

converted to rate versus concentration data by analytical differentiation of a seventh-order polynomial fit using previously described methods.[55]

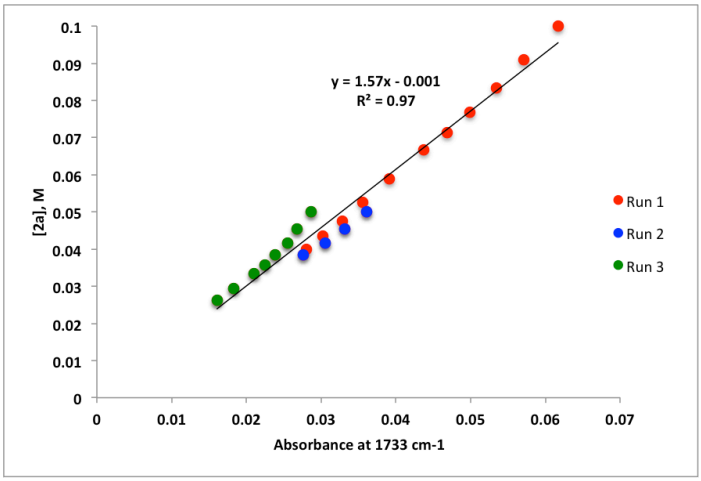

Figure 2.16. ***IR dilution calibration curve for product 2a.***

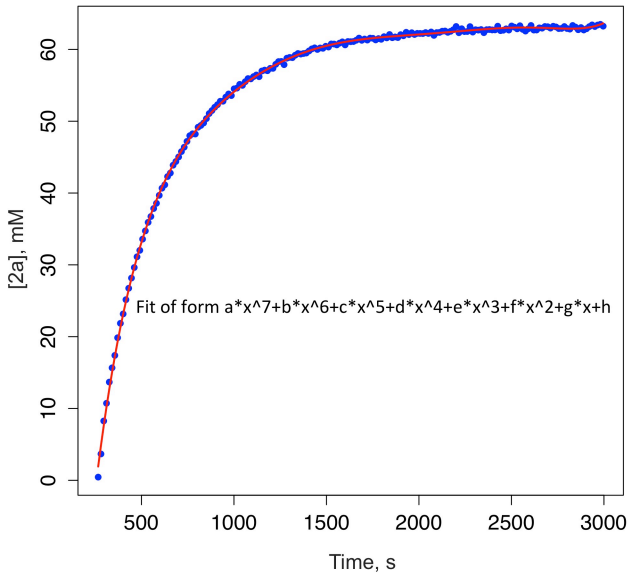

Figure 2.17. ***[2a] vs. time plot (blue dots) and a seventh-order polynomial fit (red line).***

[55] Zuend, S. J.; Jacobsen, E. N. *J. Am. Chem. Soc*. **2007**, *129*, 15872-15883.

Table 2.12. ***Investigation of order dependence on catalyst 3c.***

$[\mathbf{3c}]_0$ (M)	15% yield	30% yield	45% yield
0.005	0.048	0.032	0.017
0.0075	0.076	0.051	0.022
0.015	0.132	0.093	0.049
0.02	0.160	0.116	0.066

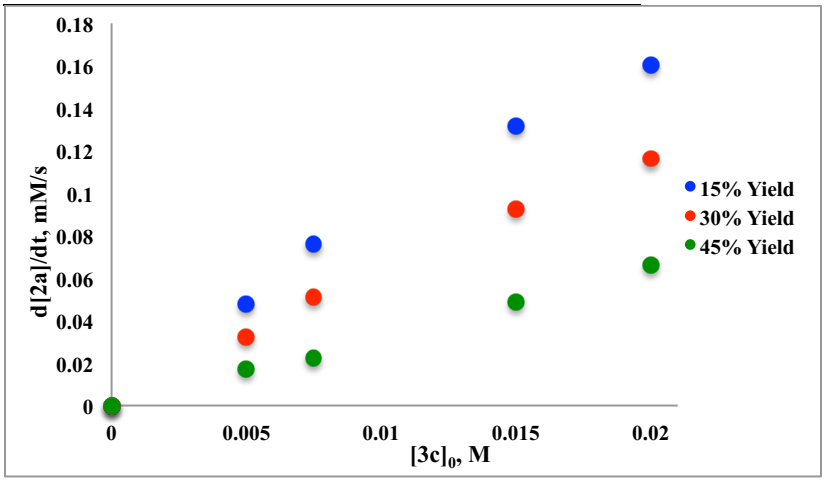

Figure 2.18. ***Investigation of order dependence on catalyst 3c.***

Table 2.13. ***Investigation of order dependence on silyl triflate promoter loading.***

$[\mathbf{TESOTf}]_0$ (M)	15% yield	30% yield	45% yield
0.05	0.082	0.055	0.024
0.1	0.094	0.062	0.032
0.15	0.076	0.047	0.020
0.2	0.087	0.056	0.025

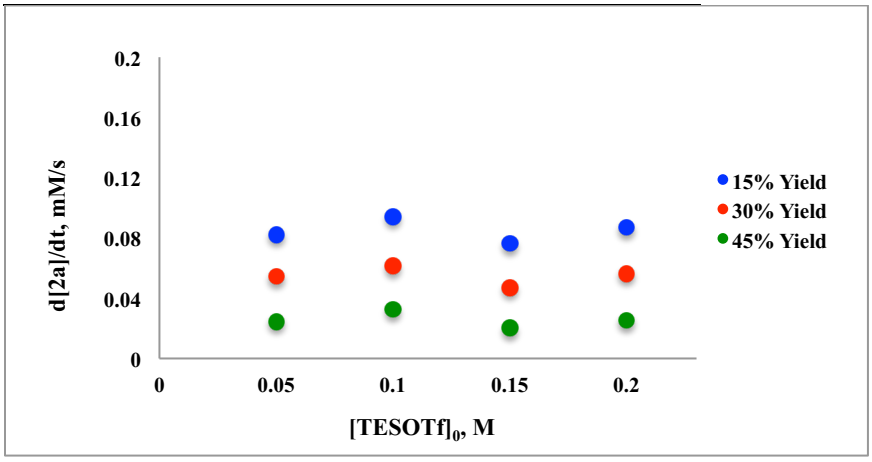

Figure 2.19. ***Investigation of order dependence on silyl triflate promoter loading.***

Table 2.14. ***Investigation of order dependence on furan loading.***

[**Furan**]$_0$ (M)*	15% yield	30% yield	45% yield
0.1	0.068	0.041	0.011
0.15	0.070	0.041	0.013
0.3	0.110	0.080	0.042
0.45	0.114	0.081	0.045
0.6	0.109	0.072	0.035

*At lower initial concentrations of furan, other side reactions take place, which results in overall lower yield of product **2a**. However, reaction still displays zero order in furan.

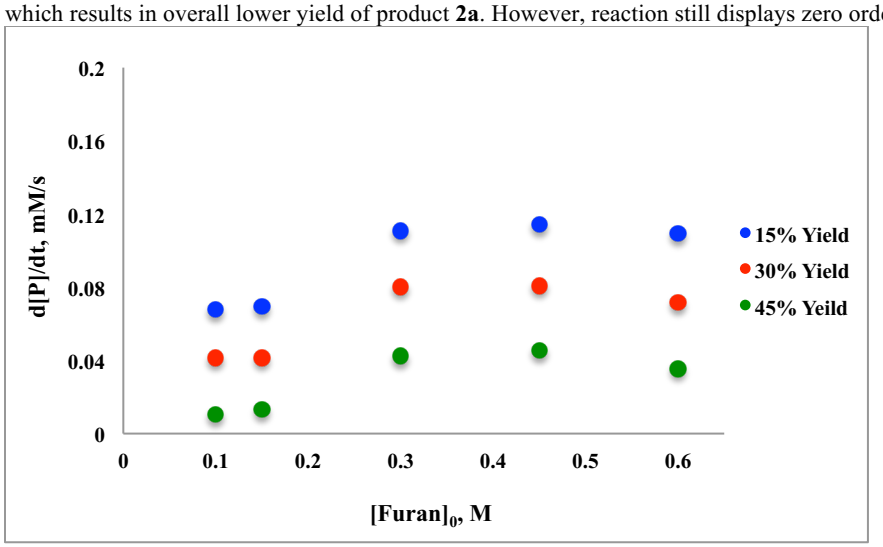

Figure 2.20. ***Investigation of order dependence on furan loading.***

Table 2.15. ***Investigation of order dependence on starting material 1a.***

0.05 M		0.1 M		0.15 M		0.2 M	
[**2a**] (mM)	d[**2a**]/dt (mM/s)	[**2a**] (mM)	d[**2a**]/dt (mM/s)	[**2a**] (mM)	d[**2a**]/dt (mM/s)	[**2a**] (mM)	d[**2a**]/dt (mM/s)
0.11	0.049	0.72	0.084	0.37	0.131	0.43	0.152
1.44	0.048	1.70	0.082	5.06	0.128	4.50	0.148
2.82	0.047	5.90	0.080	9.36	0.124	10.01	0.144
3.84	0.046	9.04	0.078	12.09	0.121	13.30	0.141
4.23	0.045	10.95	0.076	14.43	0.118	16.38	0.137
4.92	0.044	11.70	0.074	16.65	0.114	18.54	0.133
5.40	0.043	13.30	0.072	18.89	0.111	21.00	0.130
6.75	0.042	14.10	0.070	20.81	0.108	23.16	0.126
7.34	0.041	15.30	0.068	23.10	0.105	25.67	0.123
8.05	0.040	15.59	0.066	24.29	0.102	27.64	0.119
8.09	0.039	16.96	0.065	25.89	0.099	29.14	0.116
8.91	0.039	18.13	0.063	27.65	0.097	31.36	0.113
9.81	0.038	18.75	0.061	29.48	0.094	32.99	0.110
9.77	0.037	19.58	0.060	30.36	0.091	34.94	0.107

10.68	0.036	20.98	0.058	32.50	0.089	36.67	0.104
10.98	0.035	20.97	0.057	33.35	0.087	38.09	0.101
11.66	0.035	22.18	0.055	34.76	0.084	39.99	0.099
12.19	0.034	23.10	0.054	35.80	0.082	41.45	0.096
12.82	0.033	23.90	0.052	37.16	0.080	42.80	0.093
13.35	0.032	24.21	0.051	38.01	0.077	43.78	0.091
13.92	0.032	25.05	0.050	39.73	0.075	45.18	0.088
13.92	0.031	25.93	0.048	40.68	0.073	47.04	0.086
14.61	0.030	26.63	0.047	41.68	0.071	48.13	0.084
14.86	0.030	26.66	0.046	42.65	0.069	48.78	0.082
15.49	0.029	27.79	0.045	43.71	0.067	50.04	0.079
15.88	0.028	28.61	0.043	44.76	0.066	51.21	0.077
16.20	0.028	28.91	0.042	45.30	0.064	52.57	0.075
16.78	0.027	29.88	0.041	46.35	0.062	53.35	0.073
16.85	0.027	30.22	0.040	47.40	0.060	54.51	0.071
17.46	0.026	31.07	0.039	48.09	0.059	55.09	0.069
17.86	0.026	31.13	0.038	49.16	0.057	56.52	0.067
18.14	0.025	32.44	0.037	49.69	0.055	56.98	0.066
18.39	0.024	32.45	0.036	50.43	0.054	58.07	0.064
18.56	0.024	32.98	0.035	51.61	0.052	59.43	0.062
19.47	0.023	33.66	0.034	51.84	0.051	60.20	0.060
19.16	0.023	33.67	0.033	52.33	0.050	60.66	0.059
19.80	0.022	34.55	0.032	53.22	0.048	61.66	0.057
20.40	0.022	35.02	0.032	54.19	0.047	62.36	0.056
20.37	0.021	35.71	0.031	54.51	0.046	63.13	0.054
20.34	0.021	35.42	0.030	55.65	0.044	64.02	0.053
21.04	0.021	35.98	0.029	55.90	0.043	64.49	0.051
21.22	0.020	36.66	0.028	56.23	0.042	65.47	0.050
21.57	0.020	37.49	0.028	56.95	0.041	66.34	0.049
21.50	0.019	38.19	0.027	58.05	0.040	66.58	0.047
22.06	0.019	38.16	0.026	57.84	0.039	67.63	0.046
22.53	0.018	38.52	0.026	58.82	0.038	68.39	0.045
22.83	0.018	38.99	0.025	59.30	0.037	68.22	0.044
22.84	0.018	38.93	0.024	59.97	0.036	68.86	0.042
23.60	0.017	38.92	0.024	60.39	0.035	69.65	0.041
23.77	0.017	40.30	0.023	60.82	0.034	70.42	0.040
23.94	0.017	40.08	0.022	60.80	0.033	70.63	0.039
24.00	0.016	40.70	0.022	61.97	0.032	71.71	0.038
24.15	0.016	40.84	0.021	62.07	0.031	71.90	0.037
24.58	0.015	40.65	0.021	62.48	0.030	72.23	0.036
24.09	0.015	41.16	0.020	62.91	0.029	73.45	0.035
25.23	0.015	41.60	0.020	63.23	0.028	73.42	0.034
25.41	0.015	41.77	0.019	63.52	0.028	73.85	0.033

25.55	0.014	42.90	0.019	64.11	0.027	74.26	0.032
25.79	0.014	42.38	0.018	64.25	0.026	74.47	0.031
25.57	0.014	42.70	0.018	64.41	0.025	75.04	0.031
26.35	0.013	43.26	0.017	65.08	0.025	75.68	0.030
26.41	0.013	42.79	0.017	65.53	0.024	75.79	0.029
26.36	0.013	43.52	0.016	65.56	0.023	76.56	0.028
26.85	0.012	43.71	0.016	66.17	0.023	76.88	0.027
26.53	0.012	43.69	0.015	66.21	0.022	77.22	0.027
26.88	0.012	44.58	0.015	66.75	0.022	77.80	0.026
27.59	0.012	44.31	0.015	66.54	0.021	78.16	0.025
27.49	0.011	44.45	0.014	67.14	0.020	78.01	0.025
27.33	0.011	44.64	0.014	67.90	0.020	78.51	0.024
27.52	0.011	44.63	0.013	67.64	0.019	78.77	0.023
28.25	0.011	45.15	0.013	68.07	0.019	79.75	0.023
27.79	0.010	45.21	0.013	67.78	0.018	79.30	0.022
28.21	0.010	45.63	0.012	68.36	0.018	79.55	0.021
28.05	0.010	45.60	0.012	68.26	0.017	80.43	0.021
28.26	0.010	46.42	0.012	68.97	0.017	80.26	0.020
28.64	0.010	45.95	0.012	68.95	0.016	80.88	0.020
28.80	0.009	46.05	0.011	69.42	0.016	80.61	0.019
29.18	0.009	46.31	0.011	69.48	0.015	81.58	0.019
28.94	0.009	46.85	0.011	69.64	0.015	81.21	0.018
29.19	0.009	46.71	0.010	70.24	0.015	81.80	0.018
28.96	0.009	46.98	0.010	70.05	0.014	82.05	0.017
29.63	0.008	47.05	0.010	69.69	0.014	82.39	0.017
29.77	0.008	47.37	0.010	70.91	0.013	82.24	0.016
29.54	0.008	47.36	0.009	71.24	0.013	82.72	0.016
29.80	0.008	47.44	0.009	71.18	0.013	82.63	0.015
29.75	0.008	47.57	0.009	71.29	0.012	83.40	0.015
30.54	0.008	47.47	0.009	71.86	0.012	83.24	0.015
30.57	0.007	47.20	0.008	71.18	0.012	83.54	0.014
30.48	0.007	48.52	0.008	71.83	0.011	83.78	0.014
30.41	0.007	47.52	0.008	71.91	0.011	83.82	0.014
30.32	0.007	47.85	0.008	72.04	0.011	84.30	0.013
30.52	0.007	48.13	0.008	71.98	0.010	84.37	0.013
30.24	0.007	48.26	0.007	71.93	0.010	84.38	0.012
30.95	0.006	48.25	0.007	72.32	0.010	84.75	0.012
31.32	0.006	48.18	0.007	72.97	0.010	84.90	0.012
31.46	0.006	48.74	0.007	72.41	0.009	85.08	0.011
31.18	0.006	48.39	0.007	73.32	0.009	85.11	0.011
31.52	0.006	48.66	0.006	73.06	0.009	85.52	0.011
31.09	0.006	48.58	0.006	73.25	0.009	85.52	0.011
31.11	0.006	49.21	0.006	73.20	0.008	85.79	0.010

31.31	0.006	48.96	0.006	73.01	0.008	86.08	0.010
32.35	0.005	48.80	0.006	74.01	0.008	86.12	0.010
32.03	0.005	49.60	0.006	73.44	0.008	86.03	0.009
31.55	0.005	48.53	0.005	74.00	0.007	86.07	0.009
31.87	0.005	48.97	0.005	74.03	0.007	86.17	0.009
31.75	0.005	49.62	0.005	73.93	0.007	86.55	0.009
31.90	0.005	49.42	0.005	73.91	0.007	86.91	0.009
31.66	0.005	49.74	0.005	74.28	0.007	86.67	0.008
32.26	0.005	49.39	0.005	74.40	0.007	87.03	0.008
32.39	0.005	49.49	0.005	74.60	0.006	87.14	0.008
32.21	0.004	49.98	0.005	74.94	0.006	87.51	0.008
32.49	0.004	49.96	0.004	74.84	0.006	87.62	0.007
32.86	0.004	50.13	0.004	74.72	0.006	87.61	0.007
32.59	0.004	49.74	0.004	74.91	0.006	87.85	0.007
32.80	0.004	49.85	0.004	74.59	0.006	88.37	0.007
32.35	0.004	50.56	0.004	75.37	0.005	87.42	0.007
32.46	0.004	50.12	0.004	75.46	0.005	87.41	0.006
32.77	0.004	50.41	0.004	74.88	0.005	88.08	0.006
32.97	0.004	50.56	0.004	75.05	0.005	87.70	0.006
32.48	0.004	50.71	0.004	75.03	0.005	88.12	0.006
33.09	0.004	50.41	0.003	75.70	0.005	88.30	0.006
32.93	0.004	50.36	0.003	75.46	0.005	88.40	0.006
32.85	0.003	50.46	0.003	75.72	0.004	88.37	0.005
33.36	0.003	50.20	0.003	75.74	0.004	88.65	0.005
32.75	0.003	50.68	0.003	75.92	0.004	88.64	0.005
33.80	0.003	50.59	0.003	75.72	0.004	88.73	0.005
32.81	0.003	50.79	0.003	75.77	0.004	89.08	0.005
33.04	0.003	50.91	0.003	75.88	0.004	88.74	0.005
33.49	0.003	51.13	0.003	76.08	0.004	88.76	0.005
33.23	0.003	50.74	0.003	76.01	0.004	89.34	0.005
33.41	0.003	51.10	0.003	76.11	0.004	88.65	0.004
33.50	0.003	51.23	0.003	76.41	0.003	89.41	0.004
33.51	0.003	51.12	0.003	76.27	0.003	89.42	0.004
33.49	0.003	51.22	0.002	76.34	0.003	89.18	0.004
33.80	0.003	50.91	0.002	75.94	0.003	89.64	0.004
33.50	0.003	51.28	0.002	76.26	0.003	89.45	0.004
33.56	0.003	50.87	0.002	76.97	0.003	89.49	0.004
33.79	0.002	51.12	0.002	76.46	0.003	89.70	0.004
33.81	0.002	51.66	0.002	76.87	0.003	89.41	0.004
34.21	0.002	50.94	0.002	76.66	0.003	89.67	0.003
33.49	0.002	51.21	0.002	76.58	0.003	89.76	0.003
33.79	0.002	51.19	0.002	76.55	0.003	89.96	0.003
33.93	0.002	51.26	0.002	76.99	0.003	89.78	0.003

33.52	0.002	51.50	0.002	76.23	0.002	89.96	0.003
34.44	0.002	51.69	0.002	76.86	0.002	90.09	0.003
33.91	0.002	51.45	0.002	76.87	0.002	90.06	0.003
34.05	0.002	51.91	0.002	77.03	0.002	89.78	0.003
34.21	0.002	51.74	0.002	77.12	0.002	90.28	0.003
34.00	0.002	51.61	0.002	76.66	0.002	90.42	0.003
34.12	0.002	51.74	0.002	76.84	0.002	90.38	0.003
33.77	0.002	51.43	0.002	77.23	0.002	90.51	0.003
33.74	0.002	51.85	0.002	76.94	0.002	90.47	0.002
34.14	0.002	51.49	0.001	77.53	0.002	90.48	0.002
34.31	0.002	51.76	0.001	77.12	0.002	90.04	0.002
33.68	0.002	51.53	0.001	77.14	0.002	91.28	0.002
34.36	0.002	52.02	0.001	77.15	0.002	90.37	0.002
33.97	0.002	51.56	0.001	77.58	0.002	90.29	0.002
34.51	0.002	51.36	0.001	77.18	0.002	90.61	0.002
34.37	0.002	51.44	0.001	77.28	0.002	90.71	0.002

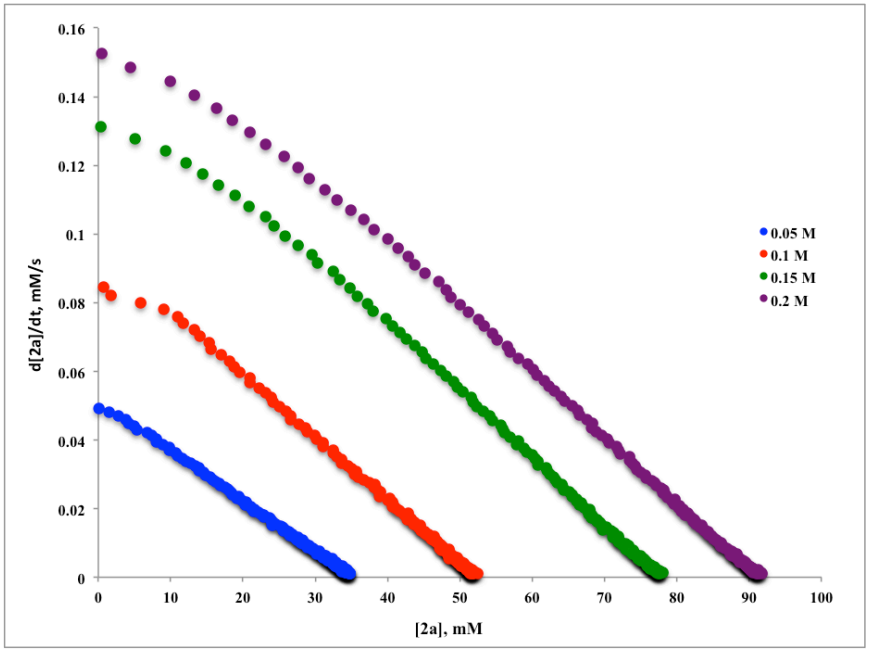

Figure 2.21. ***Investigation of order dependence on starting material 1a.***

Based on the observed orders in **1a**, **3c**, TESOTf and furan, empirical rate law was derived to be:

$$d[\mathbf{2a}]/dt = k_{obs}\,[\mathbf{1a}][\mathbf{3c}]$$

Representative procedure for kinetic studies with catalyst **4h** and furan-3-ylethynyltrimethylsilane:

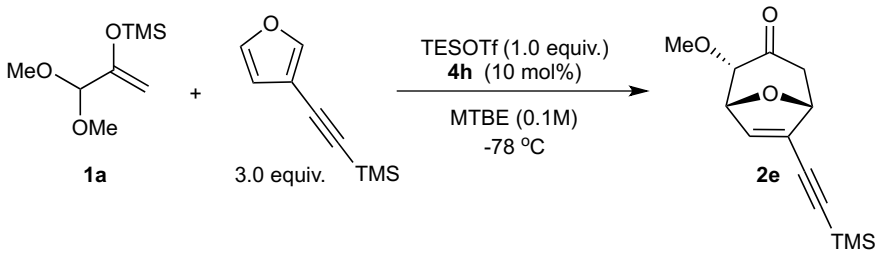

Scheme 2.8. ***Reaction used for kinetic analysis with catalyst 4h.***

An oven-dried 10 mL two-neck round bottom flask equipped with a 1/8" stir bar was allowed to cool in desiccator. The flask was then charged with substrate **1a** (19mg, 0.1 mmol, 1 equiv.), furan-3-ylethynyltrimethylsilane (54 μL, 0.30 mmol, 3.0 equiv.), **4h** (6.9 mg, 0.01 mmol, 10 mol%) and MTBE (1.0 mL). The side arm was closed with a septum, the flask was attached to the in situ infrared spectroscopy probe (that was previously dried with a heat gun), secured with a small clamp and the reaction was put under nitrogen atmosphere through an inlet needle at the side arm septum. The mixture was then cooled to -78 ºC on the dry ice-acetone bath and stirring started. Continuous data collection (4 scan/min, 50 scans/spectrum) was started to define baseline in absence of product. TESOTf (23.0 μL, 0.10 mmol, 1.0 equiv.) was added via syringe through the septum in the side arm via a syringe. Reaction was run until IR absorbance of carbonyl functionality of product **2e** (height to two-point baseline, 1733 cm^{-1} to 1850/1690 cm^{-1}) became level, when it was quenched via addition of 200 μL of a 6:1 MeOH:Et_3N solution via syringe.

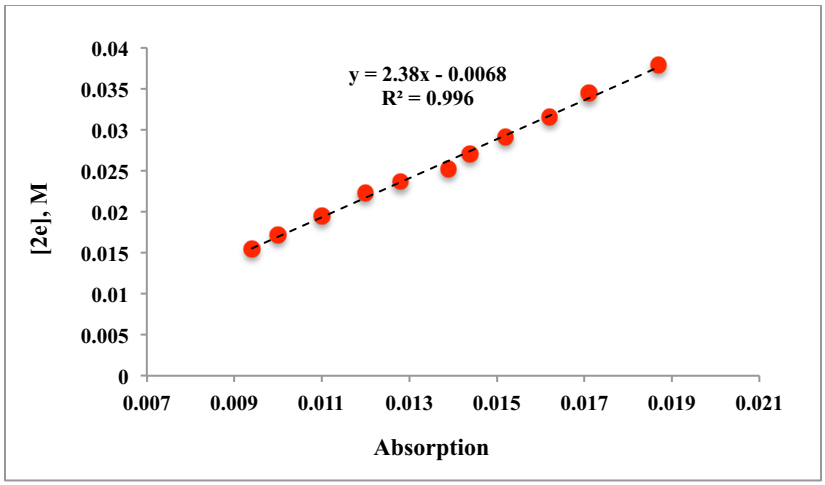

Figure 2.22. ***IR dilution calibration curve for product 2e.***

Table 2.16. ***IR dilution calibration for product 2e.***

[**2e**] (M)	Absorption
0.038	0.0187
0.034	0.0171
0.032	0.0162
0.029	0.0152
0.027	0.0144
0.025	0.0139
0.024	0.0128
0.022	0.012
0.019	0.011
0.017	0.01
0.015	0.0094

Table 2.17. ***Investigation of order dependence on silyl triflate promoter loading.***

[**TESOTf**]$_0$ (M)	30% yield	45% yield	60% yield
0.05	0.051	0.035	0.019
0.1	0.049	0.035	0.021
0.15	0.069	0.051	0.031
0.2	0.059	0.049	0.023

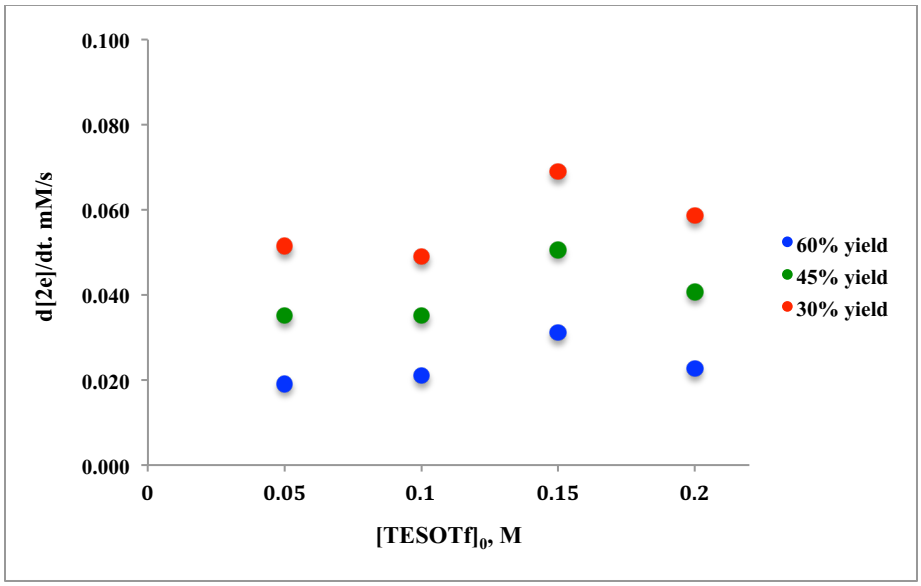

Figure 2.23. ***Investigation of order dependence on silyl triflate promoter loading.***

Table 2.18. ***Investigation of order dependence on furan-3-ylethynyltrimethylsilane.***

[**Furan-3-ylethynyltrimethylsilane**]$_0$ (M)	Rate (mM/s)		
	15% yield	30% yield	45% yield
0.15	0.082	0.055	0.024
0.3	0.094	0.062	0.032
0.45	0.076	0.047	0.020
0.6	0.087	0.056	0.025

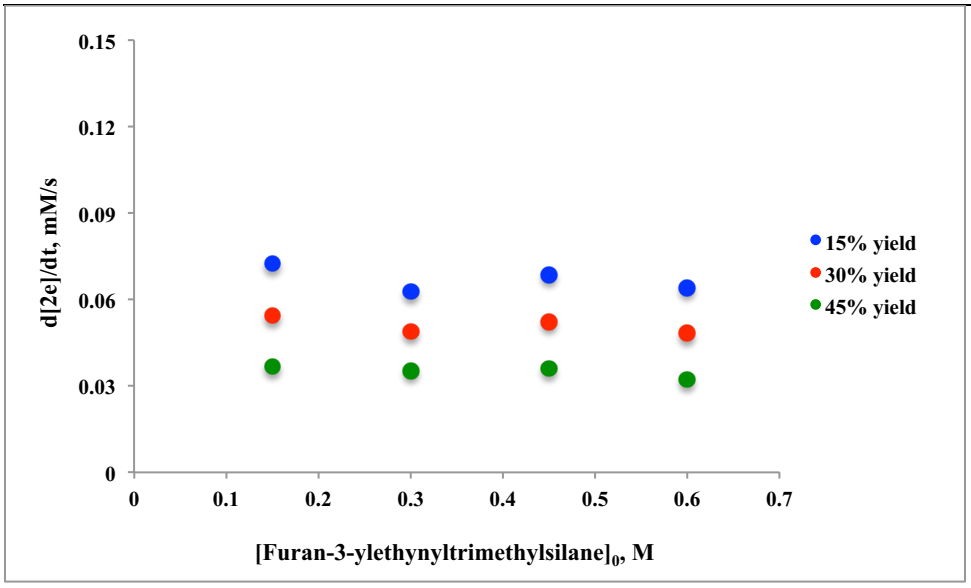

Figure 2.24. ***Investigation of order dependence on furan-3-ylethynyltrimethylsilane.***

Table 2.19. ***Investigation of order dependence on catalyst 4h.***

$[\mathbf{4h}]_0$ (M)	15% yield	30% yield	45% yield
0.005	0.041	0.032	0.023
0.0075	0.064	0.049	0.035
0.010	0.092	0.075	0.057
0.015	0.122	0.095	0.069

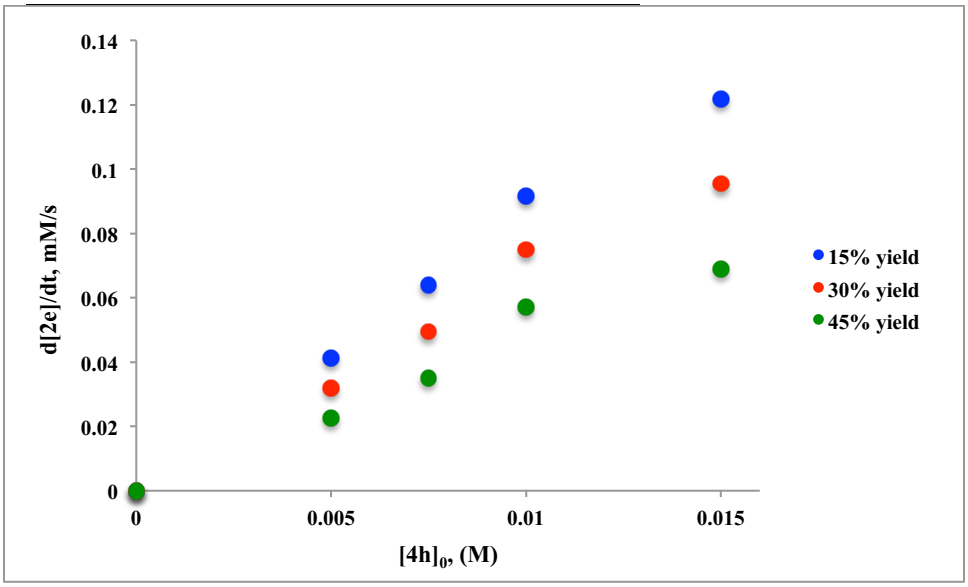

Figure 2.25. ***Investigation of order dependence on catalyst 4h.***

Table 2.20. ***Investigation of order dependence on starting material 1a.***

0.05 M		0.1 M		0.15 M		0.2 M	
[**2e**] (mM)	d[**2e**]/dt (mM/s)	[**2e**] (mM)	d[**2a**]/dt (mM/s)	[**2e**] (mM)	d[**2e**]/dt (mM/s)	[**2e**] (mM)	d[**2e**]/dt (mM/s)
3.56	0.044	3.98	0.072	14.60	0.097	1.23	0.115
5.27	0.043	4.78	0.071	16.31	0.095	6.95	0.112
5.72	0.042	6.72	0.070	18.02	0.094	10.48	0.111
6.77	0.042	8.28	0.069	19.67	0.093	12.53	0.109
8.03	0.041	9.18	0.068	21.09	0.091	14.53	0.108
8.71	0.040	10.05	0.067	21.78	0.090	16.03	0.106
9.02	0.040	11.50	0.066	23.83	0.088	18.25	0.105
9.02	0.039	12.28	0.065	24.79	0.087	19.45	0.104
10.48	0.039	13.18	0.065	26.63	0.086	22.01	0.102
10.38	0.038	13.73	0.064	28.22	0.084	23.22	0.101
10.20	0.038	14.72	0.063	29.32	0.083	24.19	0.100
11.09	0.037	15.58	0.062	30.30	0.082	26.28	0.099
12.02	0.036	16.55	0.061	31.58	0.081	28.35	0.097
12.22	0.036	17.38	0.060	33.23	0.079	29.49	0.096

13.03	0.035	18.39	0.060	33.27	0.078	31.29	0.095
13.50	0.035	19.19	0.059	35.75	0.077	32.76	0.094
13.52	0.034	20.13	0.058	36.44	0.076	33.40	0.092
14.08	0.034	21.28	0.057	37.94	0.075	35.02	0.091
14.94	0.033	22.15	0.057	38.78	0.074	36.34	0.090
15.23	0.033	21.75	0.056	40.60	0.073	38.42	0.089
15.95	0.032	22.92	0.054	42.15	0.070	40.93	0.087
16.25	0.031	24.81	0.054	43.36	0.069	41.60	0.086
16.69	0.031	25.51	0.053	44.12	0.068	42.50	0.084
17.93	0.030	26.38	0.052	45.30	0.067	44.22	0.083
18.70	0.030	27.93	0.051	47.29	0.065	46.84	0.081
18.77	0.029	28.75	0.050	48.31	0.064	47.88	0.080
18.58	0.029	28.95	0.049	49.78	0.063	48.76	0.079
20.03	0.028	31.04	0.048	51.65	0.061	50.36	0.077
20.54	0.027	31.61	0.047	52.18	0.060	52.13	0.076
20.12	0.027	31.89	0.047	52.97	0.059	52.88	0.075
21.25	0.026	33.30	0.046	54.54	0.058	55.19	0.073
21.40	0.026	34.43	0.045	55.21	0.057	56.21	0.072
23.11	0.025	35.97	0.044	57.44	0.055	58.73	0.070
23.34	0.025	36.73	0.043	58.54	0.054	59.95	0.070
23.28	0.024	36.97	0.043	59.21	0.053	60.39	0.069
23.96	0.024	38.43	0.041	60.54	0.052	62.25	0.067
23.72	0.023	39.43	0.041	61.56	0.051	63.60	0.066
24.26	0.023	39.61	0.040	61.99	0.050	64.56	0.065
25.32	0.022	40.73	0.039	63.03	0.049	66.38	0.064
25.89	0.022	40.74	0.039	63.51	0.048	68.11	0.063
26.93	0.021	41.79	0.038	65.20	0.047	69.04	0.061
26.64	0.021	43.33	0.037	67.02	0.046	70.34	0.060
27.35	0.020	44.00	0.036	67.81	0.045	72.15	0.059
27.50	0.020	44.93	0.036	68.78	0.044	72.27	0.058
28.10	0.019	46.05	0.035	69.88	0.043	74.95	0.057
28.01	0.019	46.78	0.034	70.09	0.042	75.50	0.056
29.26	0.019	46.64	0.033	71.15	0.041	76.92	0.054
29.47	0.018	48.19	0.033	72.40	0.040	77.90	0.054
29.88	0.018	48.27	0.032	72.43	0.039	78.74	0.053
29.93	0.018	48.52	0.032	73.07	0.039	79.50	0.052
30.40	0.017	49.15	0.031	73.71	0.038	81.30	0.051
31.02	0.017	50.02	0.031	75.13	0.037	81.99	0.050
30.48	0.017	50.84	0.030	75.88	0.037	82.59	0.050
31.08	0.016	50.52	0.030	75.54	0.036	82.64	0.049
31.50	0.016	51.42	0.029	76.29	0.035	84.51	0.048
31.75	0.016	51.97	0.029	76.40	0.035	84.16	0.048
32.30	0.015	52.72	0.028	77.63	0.034	86.59	0.047

32.34	0.015	52.77	0.028	78.79	0.033	86.81	0.046
32.33	0.015	54.02	0.027	79.44	0.032	87.51	0.045
33.01	0.015	54.69	0.027	79.78	0.032	88.45	0.044
33.43	0.014	54.95	0.026	80.36	0.031	89.72	0.043
33.19	0.014	56.11	0.025	81.90	0.030	91.36	0.042
33.78	0.014	56.08	0.025	82.73	0.029	92.47	0.042
34.23	0.013	56.62	0.024	83.81	0.029	93.12	0.040
34.77	0.013	57.44	0.024	83.23	0.028	94.19	0.040
34.91	0.013	58.43	0.023	84.36	0.027	94.68	0.039
36.15	0.012	58.07	0.023	84.74	0.027	94.92	0.038
35.53	0.012	59.68	0.022	85.51	0.026	96.91	0.037
35.23	0.012	59.98	0.021	86.68	0.025	97.14	0.036
36.18	0.011	60.51	0.021	87.17	0.025	98.05	0.036
36.58	0.011	61.17	0.020	87.75	0.024	99.41	0.035
37.28	0.011	61.67	0.020	87.61	0.023	100.68	0.034
38.52	0.010	62.94	0.018	89.94	0.021	103.31	0.031
38.55	0.010	63.89	0.018	90.66	0.021	103.71	0.031
39.57	0.009	64.53	0.017	91.93	0.020	104.59	0.030
39.63	0.009	64.45	0.017	92.19	0.020	106.16	0.029
39.34	0.009	64.70	0.016	92.05	0.019	105.69	0.029
38.79	0.009	64.74	0.016	92.20	0.019	106.18	0.029
39.12	0.009	65.18	0.016	93.14	0.019	107.02	0.028
40.11	0.008	67.57	0.014	95.18	0.017	110.23	0.025
40.90	0.007	68.87	0.012	96.91	0.014	113.66	0.023
42.09	0.007	69.30	0.012	96.56	0.014	113.13	0.022
41.77	0.006	69.19	0.012	96.86	0.014	114.52	0.022
41.83	0.006	69.31	0.012	96.75	0.014	114.89	0.022
42.14	0.006	70.64	0.010	98.85	0.012	116.74	0.020
42.43	0.006	70.66	0.010	98.68	0.012	116.70	0.020
42.89	0.006	70.83	0.010	99.40	0.012	117.16	0.019
42.58	0.005	70.59	0.010	99.28	0.012	117.29	0.019
42.81	0.005	72.03	0.009	99.74	0.011	118.54	0.018
43.37	0.005	71.84	0.009	100.14	0.011	119.14	0.018
43.30	0.005	71.89	0.009	99.92	0.011	118.61	0.018
43.35	0.005	72.49	0.009	100.72	0.011	119.45	0.017
43.20	0.005	72.12	0.009	100.76	0.010	119.16	0.017
43.08	0.005	72.44	0.009	100.27	0.010	119.43	0.017
43.65	0.005	72.68	0.008	101.43	0.010	120.39	0.017
43.11	0.005	72.35	0.008	101.44	0.010	120.73	0.016
43.82	0.005	73.11	0.008	100.95	0.010	121.46	0.016
43.86	0.004	73.06	0.007	102.95	0.009	121.76	0.015
43.70	0.004	73.78	0.007	101.81	0.009	122.20	0.015
43.47	0.004	74.24	0.007	101.96	0.009	122.89	0.015

43.78	0.004	73.76	0.007	102.93	0.008	122.71	0.014
43.83	0.004	74.09	0.007	102.71	0.008	123.56	0.014
44.41	0.003	74.54	0.006	103.61	0.007	124.71	0.013
44.26	0.003	74.77	0.006	103.78	0.007	125.21	0.012
43.94	0.003	74.79	0.006	103.74	0.007	125.00	0.012
45.25	0.003	75.26	0.006	104.45	0.007	125.72	0.012
44.86	0.003	74.82	0.005	103.83	0.007	125.03	0.012
44.73	0.003	75.48	0.005	103.94	0.006	126.49	0.011
44.69	0.003	75.63	0.005	105.70	0.006	126.70	0.011
45.21	0.003	75.68	0.005	105.17	0.006	126.83	0.011
45.20	0.003	75.25	0.005	104.76	0.006	127.43	0.011
45.60	0.003	75.91	0.005	104.81	0.006	127.39	0.011
45.30	0.003	75.53	0.005	105.54	0.006	128.32	0.010
44.73	0.003	76.25	0.004	106.06	0.006	126.98	0.010
44.36	0.003	76.14	0.004	105.36	0.006	128.12	0.010
44.96	0.003	76.04	0.004	105.69	0.005	127.84	0.010
45.34	0.002	76.38	0.004	106.33	0.005	129.18	0.009
45.21	0.002	77.00	0.004	106.74	0.005	129.32	0.009
45.09	0.002	77.16	0.004	106.77	0.005	130.20	0.009
45.64	0.002	76.14	0.004	106.69	0.005	129.75	0.009
45.87	0.002	76.97	0.003	107.03	0.004	129.78	0.008
45.81	0.002	77.00	0.003	107.63	0.004	130.60	0.007
46.09	0.002	77.43	0.003	107.21	0.004	131.61	0.007
45.37	0.002	77.34	0.003	107.54	0.004	132.01	0.007
45.57	0.002	77.71	0.003	108.23	0.003	132.11	0.006
45.86	0.002	77.74	0.003	108.66	0.003	132.81	0.006
46.09	0.002	77.06	0.002	108.14	0.003	134.61	0.004
46.25	0.002	78.10	0.002	108.41	0.003	135.02	0.004
46.17	0.001	77.81	0.002	109.32	0.003	135.30	0.004
46.00	0.001	78.91	0.002	108.98	0.003	137.03	0.003
46.07	0.001	77.79	0.002	109.64	0.003	137.12	0.003
46.07	0.001	79.05	0.002	109.39	0.003	136.10	0.003
45.64	0.001	77.90	0.002	108.73	0.003	136.88	0.003
46.49	0.001	78.22	0.002	109.64	0.002	137.20	0.003
46.68	0.001	78.58	0.002	109.56	0.002	136.72	0.003
45.84	0.001	78.85	0.002	109.55	0.002	137.63	0.003
46.21	0.001	78.89	0.002	109.54	0.002	137.25	0.002

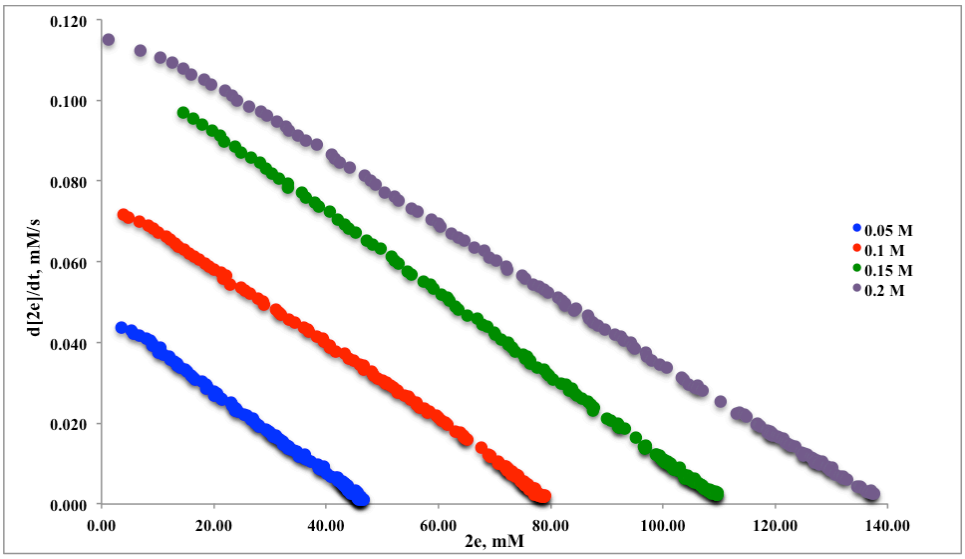

Figure 2.26. ***Investigation of order dependence on starting material 1a.***

2.4.11. Procedure for In Situ IR Spectroscopy for Resting State B Characterization

An oven-dried 10 mL two-neck round-bottomed flask equipped with a 1/8" stir bar was allowed to cool in desiccator. It was then charged with **3c** (27.8 mg, 0.05 mmol, 1 equiv.) and 1.0 mL of anhydrous MTBE. The side arm was closed with a septum, the flask was attached to the in situ infrared spectroscopy probe (that was previously dried with a heat gun), secured with a small clamp and the reaction was put under nitrogen atmosphere through an inlet needle at the side arm septum. Reaction was then cooled to -78 ºC on acetone/dry ice bath and stirring started. TESOTf was added as needed via a syringe through the side arm septum. Resulting 3-D spectrum (x-axis: wavelength (cm^{-1}), y-axis: intensity (A.U.), z-axis: time (s)) is shown below in two perspectives.

2.4.12. NMR Binding Studies

General procedure for quantitative binding studies in $CDCl_3$: The strength of binding between **3c** and TESOTf was determined via NMR titration experiments. Experiment was set up using stock solutions of catalyst **3c** and TESOTf in CD_2Cl_2. A 1 mL stock solution of **3c** (27.8 mg, 0.05 mmol, 50 mM) in CD_2Cl_2 and a 1 mL stock solution of TESOTf (11.8 µL, 0.05 mmol, 50 mM) in CD_2Cl_2 were prepared in dry 1 mL volumetric flasks. A series of solutions (10 mM in **3c)** with 0 – 10.0 equiv. of TESOTF were prepared in separate dry NMR tubes by combining certain volumes of stock solutions of **3c** and TESOTf and addition of CD_2Cl_2 to bring the total volume to 500 µL. 1H NMR spectrum of them was then recorded at 23°C. Chemical shift of the diagnostic ortho-protons (shown in blue) of squaramide **3c** was plotted against equivalents of TESOTf, and the data fit was made to the equation of the form:

$$\delta calc = \delta exp + \Delta\delta max * ((Ka*([\mathbf{3c}]+[TESOTf])+1) - (((\ Ka*([\mathbf{3c}]+[TESOTf])+1)^2)-$$

$$4*(Ka^2*([\mathbf{3c}]+[TESOTf])^{0.5})/(2*Ka*[\mathbf{3c}])$$

The "goal seek" function in excel was used to minimize $(\Delta\delta exp - \Delta\delta calc)^2$ and optimize Ka, where Ka is the association constant, δexp is the observed chemical shift of the squaramide proton at [TESOTf] in ppm, Δδmax is the difference between the chemical shift of squaramide proton when **3c** is completely bound to TESOTf and the chemical shift of free **3c**, and δcalc is chemical shift predicted by the function.

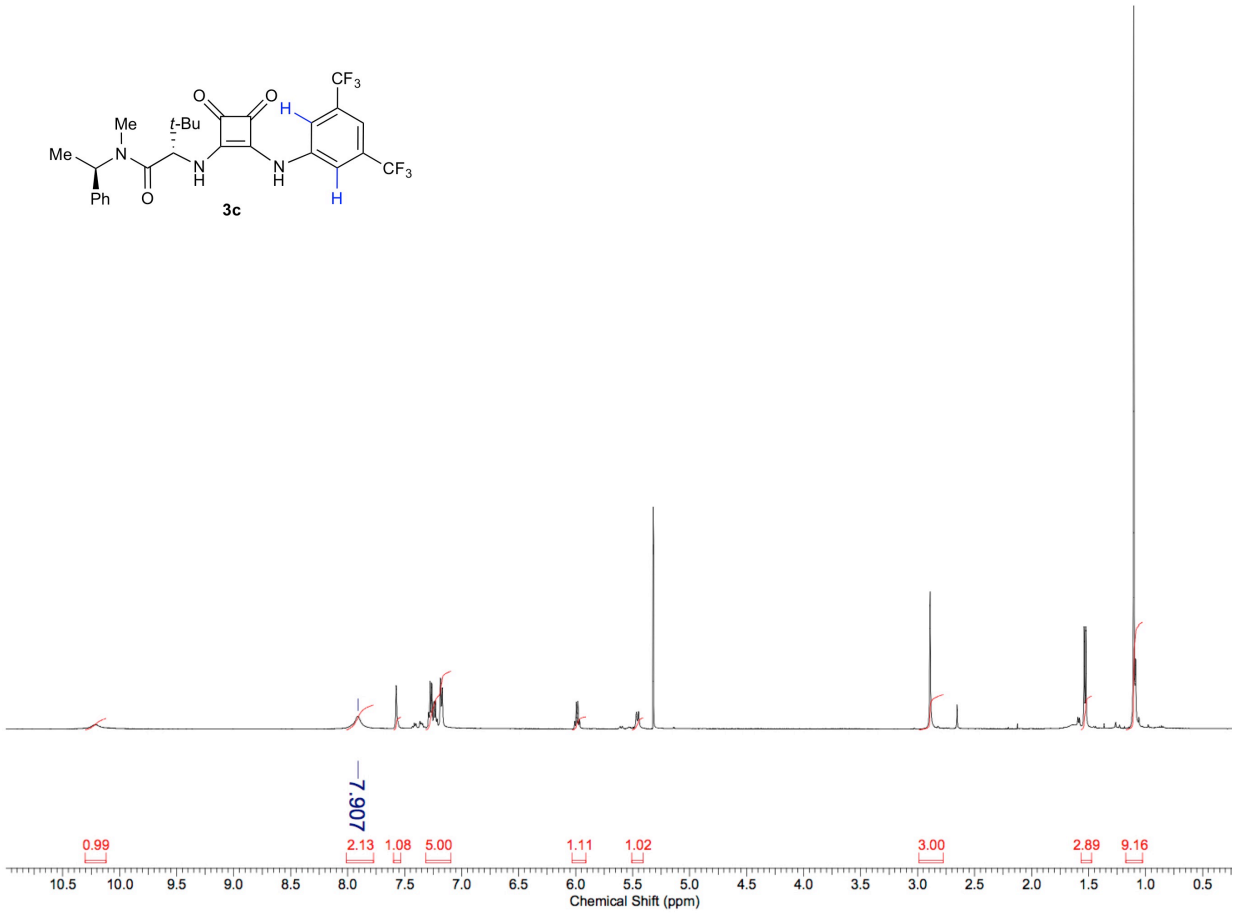

Figure 2.27. ***A representative ^{1}H NMR spectrum of 3c in CD_2Cl_2.***

Table 2.21. ***Investigation of binding strength between squaramide catalyst 3c and $N(nBu)_4OTf$.***

equiv. (OTf^-)	$[H]_0$/M	$[G]_0$/M	$[G]_0$/mM	δ_{exp} (ppm)	$\Delta\delta_{exp}$ (ppm)	δ_{calc} (ppm)	$\Delta\delta_{calc}$ (ppm)	$(\delta_{exp} - \delta_{calc})^2$
0	0.0100	0	0	7.907	0	7.907	0.000	0.0000000000
0.1	0.0100	0.0010	1	7.936	0.029	7.931	0.024	0.0000278046
0.2	0.0100	0.0020	2	7.958	0.051	7.953	0.046	0.0000225099
0.5	0.0100	0.0050	5	7.995	0.088	8.013	0.106	0.0003398671
1	0.0100	0.0100	10	8.082	0.175	8.090	0.183	0.0000608771
2	0.0100	0.0200	20	8.172	0.265	8.176	0.269	0.0000172555
3	0.0100	0.0300	30	8.219	0.312	8.217	0.310	0.0000036834
5	0.0100	0.0500	50	8.264	0.357	8.253	0.346	0.0001207128
10	0.0100	0.1000	100	8.291	0.384	8.280	0.373	0.0001117847
								Sum of Squared Errors = 0.0007

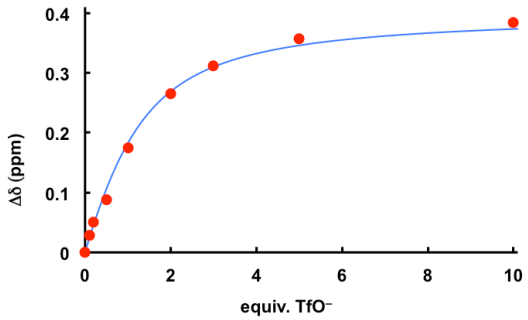

Figure 2.28. ***Binding curve for 3c and N(nBu)$_4$OTf:*** *Ka = 155 M^{-1}; $\Delta\delta_{max}$ = 0.4 ppm.*

Table 2.22. ***Investigation of binding strength between thiourea catalyst 3b and N(nBu)$_4$OTf.***

equiv. (OTf^-)	$[H]_0$/M	$[G]_0$/M	$[G]_0$/mM	δ_{exp} (ppm)	$\Delta\delta_{exp}$ (ppm)	δ_{calc} (ppm)	$\Delta\delta_{calc}$ (ppm)	$(\delta_{exp} - \delta_{calc})^2$
0	0.0100	0	0	7.814	0	7.814	0.000	0.0000000000
0.1	0.0100	0.0010	1	7.838	0.024	7.829	0.015	0.0000846604
0.2	0.0100	0.0020	2	7.845	0.031	7.843	0.029	0.0000034031
0.5	0.0100	0.0050	5	7.857	0.043	7.884	0.070	0.0007140089
1	0.0100	0.0100	10	7.959	0.145	7.944	0.130	0.0002302054
2	0.0100	0.0200	20	8.038	0.224	8.041	0.227	0.0000106630
3	0.0100	0.0300	30	8.113	0.299	8.116	0.302	0.0000090508
5	0.0100	0.0500	50	8.222	0.408	8.222	0.408	0.0000002074
10	0.0100	0.1000	100	8.375	0.561	8.360	0.546	0.0002131824
								Sum of Squared Errors = 0.00127

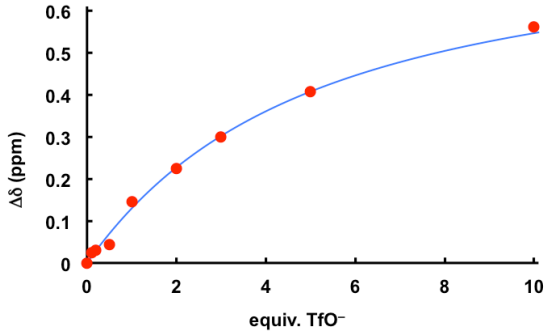

Figure 2.29. ***Binding curve for thiourea 3b and N(nBu)$_4$OT:*** *Ka = 23 M^{-1}; $\Delta\delta_{max}$ = 0.8 ppm.*

Table 2.23. ***Investigation of binding strength between squaramide catalyst 3c and TESOTf.***

equiv. TESOTf	$[H]_0$/M	$[G]_0$/M	$[G]_0$/mM	δ_{exp} (ppm)	$\Delta\delta_{exp}$ (ppm)	δ_{calc} (ppm)	$\Delta\delta_{calc}$ (ppm)	$(\delta_{exp} - \delta_{calc})^2$
0	0.0100	0	0	7.912	0	7.912	0.000	0.0000000000
0.1	0.0100	0.0010	1	7.931	0.019	7.927	0.015	0.0000176582
0.2	0.0100	0.0020	2	7.949	0.037	7.942	0.030	0.0000548323
0.5	0.0100	0.0050	5	8.000	0.088	7.986	0.074	0.0001965471
0.8	0.0100	0.0080	8	8.040	0.128	8.030	0.118	0.0000936616
1	0.0100	0.0100	10	8.057	0.145	8.058	0.146	0.0000017143
1.2	0.0100	0.0120	12	8.059	0.147	8.060	0.148	0.0000008149
1.5	0.0100	0.0150	15	8.058	0.146	8.060	0.148	0.0000038454
2	0.0100	0.0200	20	8.055	0.143	8.060	0.148	0.0000248051
								Sum of Squared Errors = 0.00036

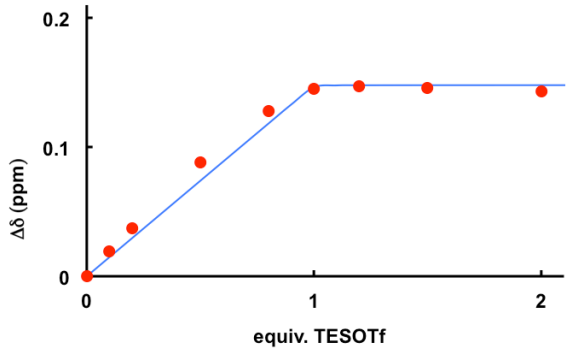

Figure 2.30. ***Binding curve for squaramide 3c and TESOTf:*** *Ka = 8•10^5 M^{-1}; $\Delta\delta_{max}$ = 0.15 ppm.*

Table 2.24. ***Investigation of binding strength between doubly methylated squaramide catalyst 3d and TESOTf.***

equiv. TESOTf	$[H]_0$/M	$[G]_0$/M	$[G]_0$/mM	δ_{exp} (ppm)	$\Delta\delta_{exp}$ (ppm)	δ_{calc} (ppm)	$\Delta\delta_{calc}$ (ppm)	$(\delta_{exp} - \delta_{calc})^2$
0	0.0100	0	0	7.645	0	7.645	0.000	0.0000000000
0.1	0.0100	0.0010	1	7.66	0.015	7.661	0.016	0.0000015234
0.2	0.0100	0.0020	2	7.68	0.035	7.677	0.032	0.0000072964
0.5	0.0100	0.0050	5	7.729	0.084	7.724	0.079	0.0000276468
0.8	0.0100	0.0080	8	7.767	0.122	7.764	0.119	0.0000086896
1	0.0100	0.0100	10	7.78	0.135	7.783	0.138	0.0000110623
1.2	0.0100	0.0120	12	7.798	0.153	7.795	0.150	0.0000095929
2	0.0100	0.0200	20	7.812	0.167	7.808	0.163	0.0000137087
								Sum of Squared Errors = 0.00006

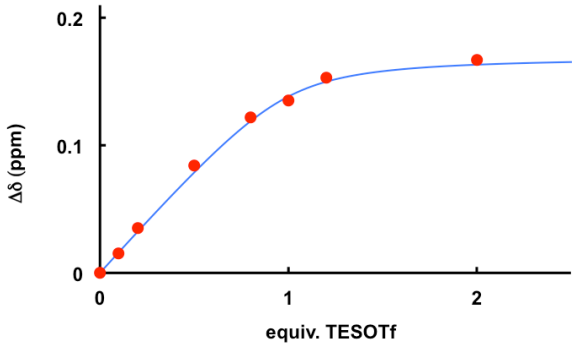

Figure 2.31. ***Binding curve for squaramide 3d and TESOTf:*** *Ka = 2•10^3 M^{-1}; $\Delta\delta_{max}$ = 0.17 ppm.*

The stoichiometry of **3c•TESOTf** complex was determined via method of continuous variation. Experiment was set up using stock solutions of catalyst **3c** and TESOTf in CD_2Cl_2. A 1 mL stock solution of **3c** (27.8 mg, 0.05 mmol, 50 mM) in CD_2Cl_2 and a 1 mL stock solution of TESOTf (11.8 µL, 0.05 mmol, 50 mM) in CD_2Cl_2 were prepared in 1 mL volumetric flasks. A series of solutions were prepared in separate dry NMR tubes by combining certain volumes of stock solutions of **3c** and TESOTf and addition of 300 µL of CD_2Cl_2 to bring the total volume to 500 µL. Total concentration of **3c** and TESOTf was kept constant ([**3c**]+[TESOTf] = 20 mM) and the relative concentration was varied. Changes in NMR shift of the ortho-protons (shown in blue) on the aryl side of squaramide **3c** were determined. The collected data was plotted as [cat]/(20 mM) vs (Δδ *[cat])/(20 mM). The stoichiometry of **3c•TESOTf** complex was determined using this method to be 1:1.

Table 2.25. ***Results of method of continuous variation between 3c and TESOTf.***

[**3c**] (mM)	[TESOTf] (mM)	δ (ppm)	Δδ (ppm)	[**3c**]/ ([**3c**]+[TESOTf])	(Δδ *[**3c**])/ ([**3c**]+[TESOTf)
20	0	7.912	0	1.000	0.000
15	5	7.972	0.060	0.750	0.045
12.5	7.5	8.021	0.109	0.625	0.068
10	10	8.071	0.159	0.500	0.079
7.5	12.5	8.069	0.157	0.375	0.059
5	15	8.074	0.162	0.250	0.041

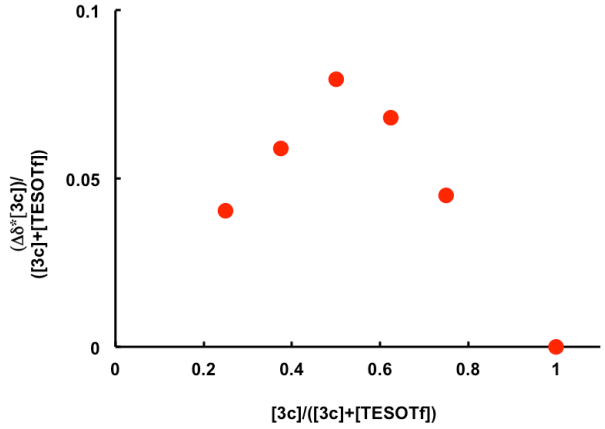

Figure 2.32. ***Job plot:*** *1:1 stoichiometry of binding between 3c and TESOTf .*

2.4.13. Non-Linear Effects Study

Reactions in this section were set up according to Method A.

Table 2.26. ***Non-linear effects study.***

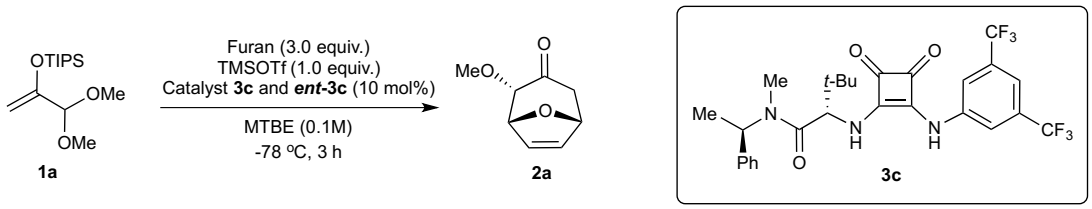

Entry	Catalyst ee (%)[a]	Product **2a** e.e. (%)
1	0	4[b]
2	20	22
3	40	41
4	80	69
5	100	81
6	-60	-43

a. Catalyst e.e. was calculated assuming both enantiomeric catalysts have perfect e.e. (100%). b. Small error in catalyst stock solution resulted in slight e.e. observation for racemic catalyst mixture.

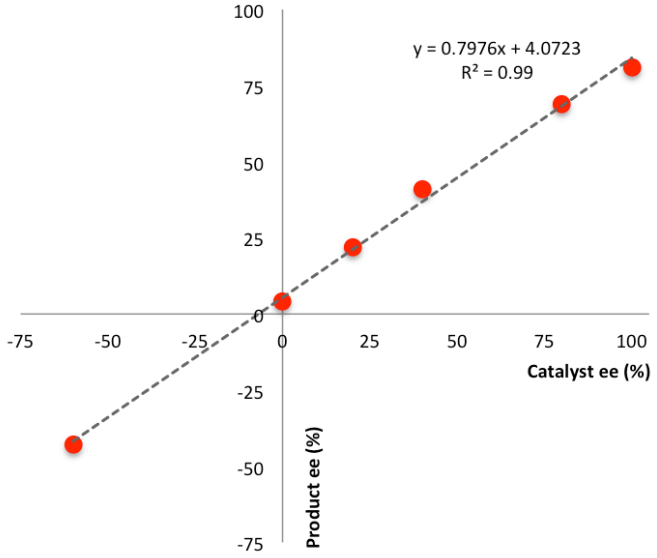

Figure 2.33. ***Plotted results of non-linear effects study.***

Conclusion: No non-linear effect was observed. This result is consistent with one molecule of squaramide catalyst being involved in the rate determining transition state.

2.4.14. Computational Studies

Computational Details: Calculations were executed using the Gaussian 09[56] program at the B3LYP level of theory and the 6-31+G(d) or 6-31G(d) basis set for all other atoms. Ground state optimizations were performed with the 6-31G(d) basis set, and single point energy calculations were performed with the 6-31+G(d) basis set. Default optimization convergence criteria, tight SCF convergence criteria, and default integration settings were used. Optimized structures correspond to gas-phase (298 K) structures unless noted. Solvation energies were evaluated by a self-consistent reaction field (SCRF) using the CPCM model with UFF radii. Stationary points were characterized by the presence of all positive eigenvalues of the Hessian for minima. All molecular structures were rendered in CYLView.[57]

[56] Gaussian 09, Revision A.02, Frisch, M. J.; Trucks, G. W.; Schlegel, H. B.; Scuseria, G. E.; Robb, M. A.; Cheeseman, J. R.; Scalmani, G.; Barone, V.; Mennucci, B.; Petersson, G. A.; Nakatsuji, H.; Caricato, M.; Li, X.; Hratchian, H. P.; Izmaylov, A. F.; Bloino, J.; Zheng, G.; Sonnenberg, J. L.; Hada, M.; Ehara, M.; Toyota, K.; Fukuda, R.; Hasegawa, J.; Ishida, M.; Nakajima, T.; Honda, Y.; Kitao, O.; Nakai, H.; Vreven, T.; Montgomery, J. A. Jr.; Peralta, J. E.; Ogliaro, F.; Bearpark, M.; Heyd, J. J.; Brothers, E.; Kudin, K. N.; Staroverov, V. N.; Kobayashi, R.; Normand, J.; Raghavachari, K.; Rendell, A.; Burant, J. C.; Iyengar, S. S.; Tomasi, J.; Cossi, M.; Rega, N.; Millam, J. M.; Klene, M.; Knox, J. E.; Cross, J. B.; Bakken, V.; Adamo, C. ; Jaramillo, J.; Gomperts, R.; Stratmann, R. E.; Yazyev, O.; Austin, A. J.; Cammi, R.; Pomelli, C.; Ochterski, J. W.; Martin, R. L.; Morokuma, K.; Zakrzewski, V. G.; Voth, G. A.; Salvador, P.; Dannenberg, J. J.; Dapprich, S.; Daniels, A. D.; Farkas, O.; Foresman, J. B.; Ortiz, J. V.; Cioslowski, J.; Fox, D. J. Gaussian, Inc., Wallingford CT **2009**.

[57] CYLview, 1.0b; Legault, C. Y., Université de Sherbrooke **2009**, (http://www.cylview.org).

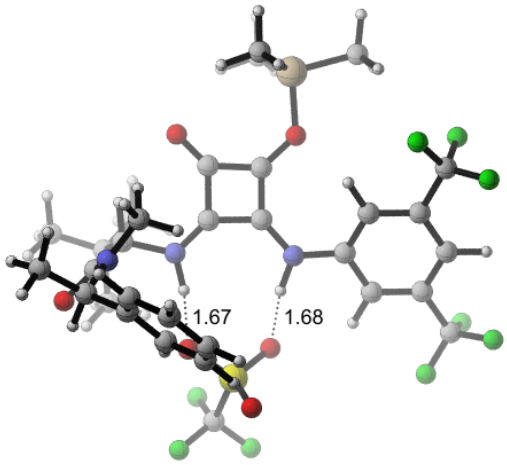

Charge = 0 Multiplicity = 1
Electronic Energy: (B3LYP/6-31G(d)) (AU) = –3404.86470237, (B3LYP/6-31+G(d)) (AU)= –3405.04353529
Solvent: gas phase
Imaginary Frequencies: 0

C	-2.00285	3.11052	2.92945
C	-1.24608	1.93642	2.76964
C	-2.20901	3.5912	4.22762
C	-0.70709	1.27368	3.87301
H	-1.05542	1.55289	1.7703
C	-1.68037	2.92171	5.33577
H	-2.78246	4.49808	4.38883
C	-0.92618	1.76263	5.16474
H	-0.09973	0.38434	3.72146
H	-1.85253	3.31816	6.33291
H	-0.50137	1.25159	6.0244
C	-0.73103	3.24079	-1.64787
H	-0.15408	4.16263	-1.59398
C	-1.23763	3.16339	-3.12747
C	-1.91462	1.82862	-3.4884
H	-2.83387	1.68014	-2.92099
H	-2.15942	1.82394	-4.55766
H	-1.25224	0.97666	-3.30438
C	-0.00902	3.35248	-4.04405
H	0.69661	2.52008	-3.9484
H	-0.32985	3.39254	-5.0914
H	0.53122	4.27878	-3.81808
C	-2.21527	4.3322	-3.3661
H	-3.1234	4.22554	-2.7659
H	-1.75008	5.29718	-3.12642
H	-2.50952	4.36487	-4.42148
N	-1.57951	3.90239	0.61573
C	-1.83846	3.2542	-0.56553
O	-2.90641	2.65473	-0.74289
C	1.51209	2.34982	-1.12436
C	2.62628	1.55181	-0.78416
C	2.34451	3.56548	-1.25447
C	3.56233	2.71329	-0.9204
O	4.75636	2.91559	-0.81238
O	2.11369	4.7418	-1.48854
N	2.7076	0.23523	-0.45614
H	1.83402	-0.2915	-0.41904
C	3.84281	-0.53442	-0.13591
C	3.63012	-1.88265	0.19976
C	5.14753	-0.02058	-0.13275
C	4.70912	-2.69658	0.53211
H	2.62406	-2.28612	0.21123
C	6.21135	-0.85917	0.20268
H	5.33381	1.02248	-0.37151
C	6.01182	-2.19738	0.53704
H	6.84684	-2.8306	0.80957
C	7.61517	-0.31114	0.1462
C	4.47046	-4.15147	0.83873
F	7.66831	0.98483	0.512
F	8.45382	-0.99747	0.95734
F	8.12721	-0.39257	-1.10401
F	5.37931	-4.63427	1.71611
F	4.55672	-4.91799	-0.27376
F	3.24531	-4.36484	1.36761
C	-2.59171	3.79307	1.69269
H	-3.34898	3.12723	1.27201
C	-3.2734	5.14365	1.94787
H	-2.60021	5.88409	2.3927
H	-3.64728	5.54351	1.00095

H	-4.12839	5.02207	2.62108
N	0.19509	2.15416	-1.28264
H	-0.22774	1.24652	-1.08188
C	-0.34301	4.60858	0.95958
H	0.22508	4.899	0.07928
H	0.29818	3.99203	1.59949
H	-0.59209	5.52146	1.5081
S	-0.99054	-1.53577	-0.34393
O	0.44804	-1.78655	-0.13059
O	-1.92635	-2.34403	0.48512
O	-1.35978	-0.09114	-0.37673
C	-1.31408	-2.12229	-2.08034
F	-0.49341	-1.49807	-2.93434
F	-1.12616	-3.43859	-2.17577
F	-2.58364	-1.84201	-2.43187
Si	5.77365	4.39298	-0.96216
C	6.4286	4.59784	0.78049
H	5.61838	4.71559	1.50934
H	5.61838	4.71559	1.50934
H	7.03559	3.73227	1.0646
H	7.06333	5.49072	0.8431
C	7.10445	4.00844	-2.22321
H	7.71531	3.15885	-1.90248
H	6.67806	3.78496	-3.20781
H	7.7689	4.87383	-2.34001
C	4.6738	5.81315	-1.49931
H	4.18862	5.60703	-2.45985
H	3.894	6.03081	-0.76149
H	5.27346	6.72361	-1.62108

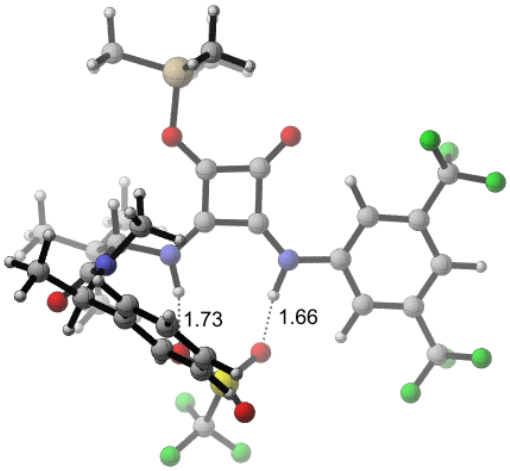

Charge = 0 Multiplicity = 1
Electronic Energy: (B3LYP/6-31G(d)) (AU) = –3404.86019784, (B3LYP/6-31+G(d)) (AU)= –3405.04079485
Solvent: gas phase
Imaginary Frequencies: 0

C	-2.00285	3.11052	2.92945
C	-1.24608	1.93642	2.76964
C	-2.20901	3.5912	4.22762
C	-0.70709	1.27368	3.87301
H	-1.05542	1.55289	1.7703
C	-1.68037	2.92171	5.33577
H	-2.78246	4.49808	4.38883
C	-0.92618	1.76263	5.16474
H	-0.09973	0.38434	3.72146
H	-1.85253	3.31816	6.33291
H	-0.50137	1.25159	6.0244
C	-0.73103	3.24079	-1.64787
H	-0.15408	4.16263	-1.59398
C	-1.23763	3.16339	-3.12747
C	-1.91462	1.82862	-3.4884
H	-2.83387	1.68014	-2.92099
H	-2.15942	1.82394	-4.55766
H	-1.25224	0.97666	-3.30438
C	-0.00902	3.35248	-4.04405
H	0.69661	2.52008	-3.9484
H	-0.32985	3.39254	-5.0914
H	0.53122	4.27878	-3.81808
C	-2.21527	4.3322	-3.3661
H	-3.1234	4.22554	-2.7659
H	-1.75008	5.29718	-3.12642
H	-2.50952	4.36487	-4.42148
N	-1.57951	3.90239	0.61573
C	-1.83846	3.2542	-0.56553
O	-2.90641	2.65473	-0.74289
C	1.51209	2.34982	-1.12436

C	2.62628	1.55181	-0.78416
C	2.34451	3.56548	-1.25447
C	3.56233	2.71329	-0.9204
O	4.75636	2.91559	-0.81238
O	2.11369	4.7418	-1.48854
N	2.7076	0.23523	-0.45614
H	1.83402	-0.2915	-0.41904
C	3.84281	-0.53442	-0.13591
C	3.63012	-1.88265	0.19976
C	5.14753	-0.02058	-0.13275
C	4.70912	-2.69658	0.53211
H	2.62406	-2.28612	0.21123
C	6.21135	-0.85917	0.20268
H	5.33381	1.02248	-0.37151
C	6.01182	-2.19738	0.53704
H	6.84684	-2.8306	0.80957
C	7.61517	-0.31114	0.1462
C	4.47046	-4.15147	0.83873
F	7.66831	0.98483	0.512
F	8.45382	-0.99747	0.95734
F	8.12721	-0.39257	-1.10401
F	5.37931	-4.63427	1.71611
F	4.55672	-4.91799	-0.27376
F	3.24531	-4.36484	1.36761
C	-2.59171	3.79307	1.69269
H	-3.34898	3.12723	1.27201
C	-3.2734	5.14365	1.94787
H	-2.60021	5.88409	2.3927
H	-3.64728	5.54351	1.00095
H	-4.12839	5.02207	2.62108
N	0.19509	2.15416	-1.28264
H	-0.22774	1.24652	-1.08188
C	-0.34301	4.60858	0.95958
H	0.22508	4.899	0.07928
H	0.29818	3.99203	1.59949
H	-0.59209	5.52146	1.5081
S	-0.99054	-1.53577	-0.34393
O	0.44804	-1.78655	-0.13059
O	-1.92635	-2.34403	0.48512
O	-1.35978	-0.09114	-0.37673
C	-1.31408	-2.12229	-2.08034
F	-0.49341	-1.49807	-2.93434
F	-1.12616	-3.43859	-2.17577
F	-2.58364	-1.84201	-2.43187
Si	3.18067	6.14344	-1.66135
C	3.83562	6.3483	0.08131
H	3.0254	6.46605	0.81016
H	4.44261	5.48273	0.36542
H	4.47036	7.24118	0.14392
C	4.51147	5.7589	-2.9224
H	5.12233	4.90931	-2.60167
H	4.08509	5.53543	-3.907
H	5.17593	6.62429	-3.03919
C	2.08082	7.56361	-2.1985
H	1.59564	7.35749	-3.15903
H	1.30102	7.78127	-1.46068
H	2.68048	8.47407	-2.32026

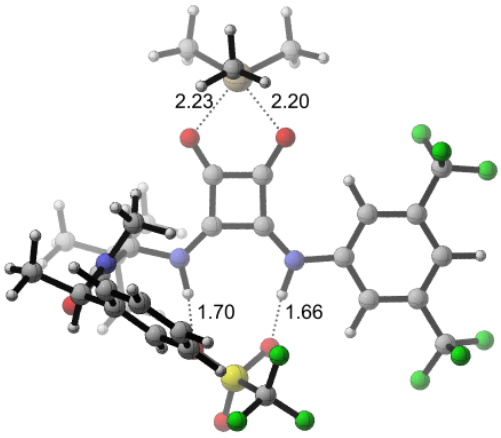

Charge = 0 Multiplicity = 1
Electronic Energy: (B3LYP/6-31G(d)) (AU) = –3404.81521651, (B3LYP/6-31+G(d)) (AU)= –3404.99360177
Solvent: gas phase
Imaginary Frequencies: 1

C	-0.88861	1.46864	-0.709
C	-0.53417	2.86562	-0.47556
C	0.8209	2.51271	-0.24955
C	0.53453	1.11322	-0.52069
C	2.54753	-0.28463	-0.31528
C	3.44231	0.7175	0.07202
H	3.13931	1.75477	0.15389
C	4.76902	0.37811	0.34171
C	4.30981	-1.92652	-0.15941
C	2.98219	-1.61385	-0.43233
H	2.28566	-2.38358	-0.74645
C	-3.7733	1.55258	-2.54939
C	-2.65718	2.25977	-3.34799
H	-2.3644	3.21387	-2.88934
H	-3.01753	2.47859	-4.35882
H	-1.76553	1.63303	-3.45334
C	-5.03761	2.43726	-2.59676
H	-5.85809	1.99159	-2.03063
H	-5.36421	2.55193	-3.63622
H	-4.83893	3.4425	-2.20175
C	-4.05825	0.1821	-3.19457
H	-3.18526	-0.47839	-3.17546
H	-4.32569	0.33256	-4.24713
H	-4.88304	-0.32977	-2.6984
N	-1.99081	0.80127	-0.92675
H	-1.95906	-0.24273	-0.88989
N	1.18121	-0.03877	-0.60172
H	0.68201	-0.86154	-1.01806
O	-0.94166	4.04996	-0.40062
O	1.68337	3.37742	0.05663
F	5.61559	1.64084	2.15084
F	5.44342	2.64555	0.23329
F	4.79647	-3.92759	0.99449
F	3.97971	-4.11277	-1.0124
C	5.21462	-0.93662	0.22948
H	6.25067	-1.18433	0.42675
C	4.77707	-3.36001	-0.23245
C	5.71264	1.45587	0.81496
F	6.99819	1.14967	0.54682
F	6.03324	-3.43969	-0.72309
S	-1.11873	-2.67337	-1.89931
O	0.2911	-2.17471	-2.01524
O	-1.86458	-1.92535	-0.83528
O	-1.82532	-2.87082	-3.16464
F	-0.29666	-5.18177	-1.97891
F	-0.19487	-4.26515	-0.00693
C	-0.9245	-4.3592	-1.13603
F	-2.11871	-4.87095	-0.82914
Si	0.77575	5.35702	0.17884
C	0.58237	5.28778	2.04446
H	-0.42718	4.9797	2.33557
H	1.30549	4.6097	2.50639
H	0.74943	6.29331	2.45198
C	2.48584	5.87233	-0.44198
H	3.29744	5.3413	0.06183
H	2.58246	5.68243	-1.51816
H	2.61243	6.95246	-0.29457
C	-0.36812	6.65165	-0.59686
H	-0.41465	6.54427	-1.68687
H	-1.38993	6.59334	-0.21251
H	0.03478	7.65099	-0.38583
C	-3.31518	1.44631	-1.05362
H	-3.24185	2.47804	-0.70133
C	-4.26379	0.66636	-0.09692
O	-5.31705	0.17772	-0.50323
C	-3.6781	-1.32755	2.88228
C	-2.76915	-2.18124	2.23474
C	-3.67229	-1.27932	4.28096
C	-1.8785	-2.96134	2.97037
H	-2.74257	-2.23948	1.14838
C	-2.7824	-2.0655	5.01899
H	-4.36889	-0.63481	4.8091
C	-1.88254	-2.90694	4.36693
H	-1.18701	-3.61233	2.44241
H	-2.79741	-2.01816	6.10493
H	-1.19189	-3.51895	4.94125
N	-3.86546	0.46846	1.19922
C	-4.6347	-0.49744	2.03056
H	-5.10175	-1.1641	1.30199
C	-5.7635	0.21028	2.7876
H	-5.39193	0.97636	3.47845
H	-6.43202	0.68984	2.06753
H	-6.34629	-0.51197	3.36876
C	-2.84925	1.26821	1.87437
H	-2.71772	2.23357	1.38205
H	-1.88419	0.75214	1.93372
H	-3.17877	1.46898	2.8977

Chapter 3

Squaramide and Silyl Trifluoromethanesulfonate co-Catalyzed Asymmetric Additions of π-Nucleophiles to Acetals

3.1. Introduction

Based on the findings discussed in Chapter 2 of this thesis, we hypothesized that the new mode of silyl triflate/chiral H-bond donor cooperative reactivity could be applied broadly in stereoselective substitution reactions of acetals (Figure 3.1).

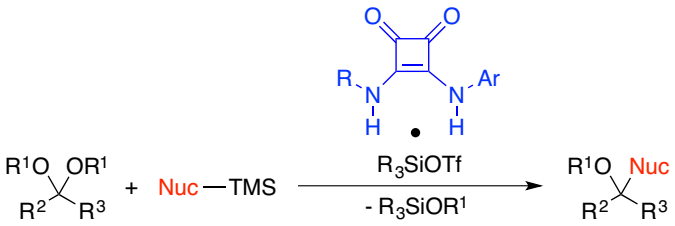

Figure 3.1. ***Proposed nucleophilic substitution of acetals using cooperative reactivity of squaramides and silyl triflates.***

Brønsted and Lewis acids have been previously shown to be efficient catalysts for substitution reactions of acetals.[58] A number of asymmetric intramolecular acetal substitution methods have been developed;[59] however, intermolecular examples remain scarce.[60,61] While

[58] (a) Kampen, D.; Ladepeche, A.; Claben, G.; List, B. *Adv. Synth. Catal*. **2008**, *350*, 962–966. (b) Kampen, D.; List, B. *Synlett* **2006**, *16*, 2589–2592. (c) Zerth, H. M.; Leonard, N. M.; Mohan, R. S. *Org. Lett*. **2003**, *5*, 55–57. (d) Oisaki, K.; Suto, Y.; Kanai, M.; Shibasaki, M. *J. Am. Chem. Soc*. **2003**, *125*, 5644–5645.

[59] (a) Covic, I.; Muller, S.; List, B. *J. Am. Chem. Soc*. **2010**, *132*, 17370–17373. (b) Covic, I.; Vellalath, S.; List, B. *J. Am. Chem. Soc*. **2010**, *132*, 8536–8539. (c) Sun, Z.; Winschel, G. A.; Zimmerman, P. M.; Nagorny, P. *Angew. Chem. Int. Ed*. **2014**, *53*, 1–6.

[60] (a) Umbayashi, N.; Hamashima, Y.; Sodeoka, M. *Angew. Chem. Int. Ed*. **2008**, *47*, 4196–4199. (b) Kobayashi, S.; Arai, K.; Yamakata, T.; Chen, Y.; Salter, M. M.; Yamashita, Y. *Adv. Synth. Catal*. **2011**, *353*, 1927–1932.

these methods demonstrate interest within the catalysis community for developing asymmetric acetal substitutions, all of the examples above are limited to one class of nucleophiles per method. Here we report methodology that allows for asymmetric addition of a variety of neutral π-nucleophiles (allylsilanes, silyl ketene acetals and silyl enol ethers) to a range of benzaldehyde-derived acetals with excellent yields and enantioselectivities.

3.2. Results and Discussion

3.2.1. Preliminary Experiments

In our initial studies, we surveyed a variety of acetals that, upon activation, would form oxocarbenium intermediates of wide-ranging stability as substrates for asymmetric nucleophilic substitution reactions. As shown in Figure 3.2, acetals possessing an α-carbonyl group would be expected to form highly destabilized oxocarbenium intermediates upon ionization. These substrates are thus likely to provide a reactivity challenge in the ionization step. On the other end of the spectrum, are ketone-derived acetals, which are known to generate highly stabilized oxocarbeniums. Such a propensity could present an alternative challenge for asymmetric catalysis, as facile ionization may lead to high levels of reactivity even in absence of the catalyst. We anticipated that in order to develop a highly selective asymmetric nucleophilic substitution of acetals, we would need to find a substrate class that allows access to the desired cationic intermediate while at the same time provides acceleration over background reactivity.

[61] For examples of asymmetric substitutions of ketone-derived acetals, see: (a) Oisaki, K.; Zhao, D.; Kanai, M.; Shibasaki, M. *J. Am. Chem. Soc*. **2006**, *128*, 7164–7165. (b) Denmark, S. E.; Fan, Y.; Eastgate, M. D. *J. Org. Chem*. **2005**, *70*, 5235–5248.

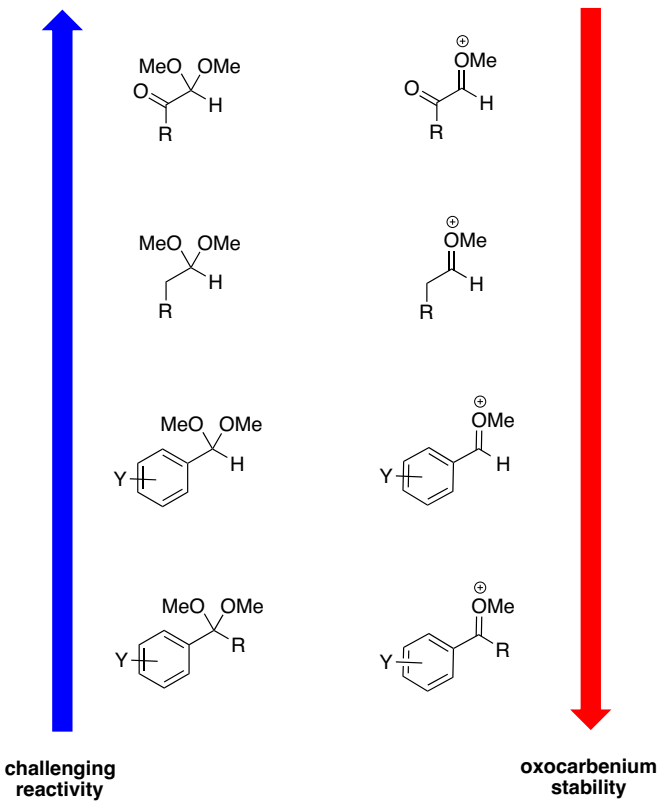

Figure 3.2. ***A survey of acetals to be explored for enantioselective nucleophilic substitution.*** As stability of the oxocarbenium intermediate increases so does the chance of a high level of the background reaction. However, acetals that would produce highly destabilized oxocarbenium ions might present a reactivity challenge in the ionization step.

In order to determine which acetal class is most suitable for asymmetric nucleophilic substitution, a screen of alkyl and arylaldehyde-derived as well as ketone-derived acetals was conducted under reaction conditions closely related to those of the (4+3) cycloaddition, discussed in Chapter 2. Neither aldehyde-derived (**1a**), nor ketone-derived (**1b**) acetals bearing an α-carbonyl group were reactive at a range of temperatures from -78 °C to 24 °C (Scheme 3.1).

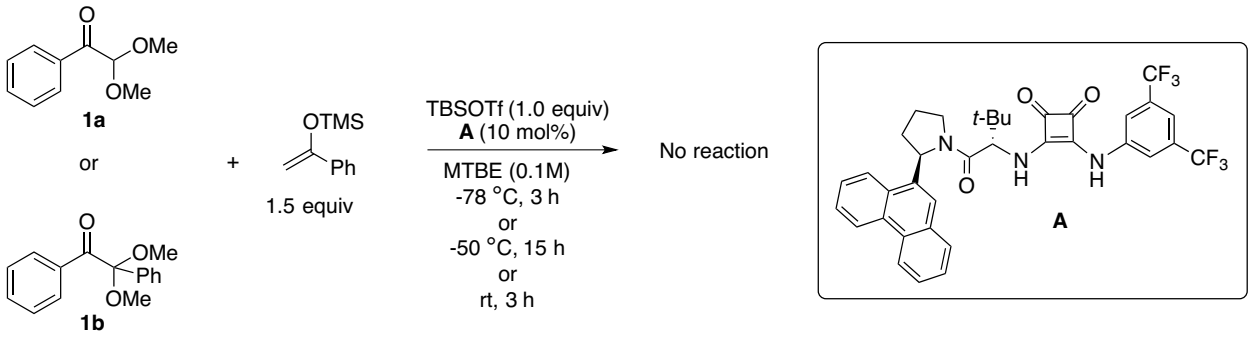

Scheme 3.1. ***Acetals bearing an α-carbonyl group were not reactive under a range of conditions.***

Alkyl acetal **1c** showed no conversion at -78 °C, but converted to product **2c** cleanly when the reaction mixture was warmed to -50 °C (Scheme 3.2a). Moreover, no reactivity was observed in the absence of the squaramide catalyst. Interestingly, when cyclic aliphatic acetal **1d** was used a substrate, no reactivity was observed even at room temperature (Scheme 3.2b). This finding highlights the potential challenge of developing glycosylation reactions with this catalytic system.[62]

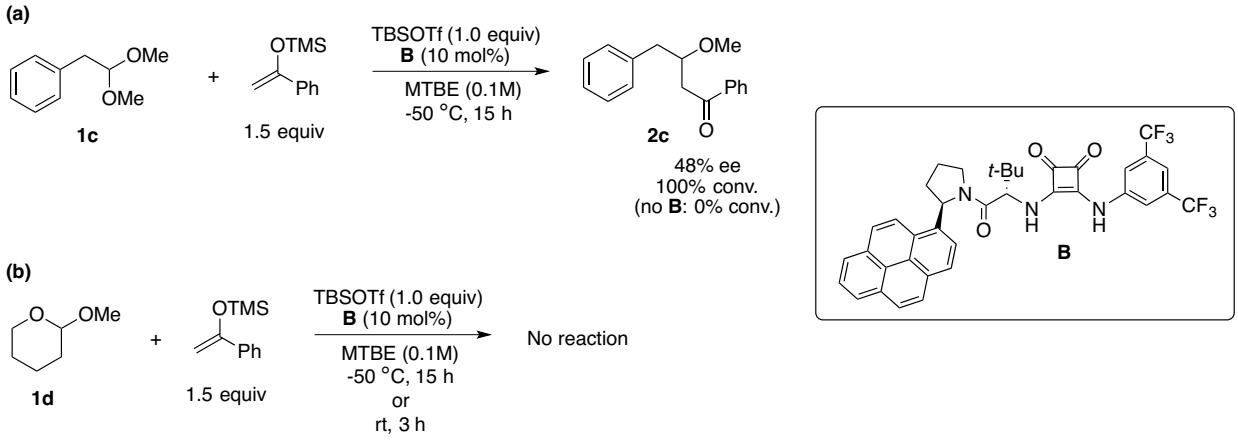

Scheme 3.2. ***Aliphatic acetals as substrates for squaramide-catalyzed nucleophilic substitution.*** **(a)** Acyclic alkyl acetals required higher reaction temperature for reactivity. **(b)** Cyclic aliphatic acetals, however, were not reactive under the above conditions, even at room temperature.

Benzaldehyde-derived dimethyl acetal **1e**, reacted cleanly with 1-phenyl-1-trimethylsiloxyethylene to provide desired addition product **2e** in a promising 70% ee with

[62] Dr. Elisabeth T. Hennessy was later able to overcome these reactivity challenges by employing glycosyl acetates instead of methyl glycosides as substrates for C-glycosylation reactions.

squaramide catalyst **A** (Scheme 3.3). Due to the fast reaction in absence of the catalyst, we anticipated that in order to obtain high enantioselectivity in this transformation, modification of the reaction conditions and substrate structure would be necessary to achieve the largest possible differentiation in the rate of catalyzed versus uncatalyzed reactions.

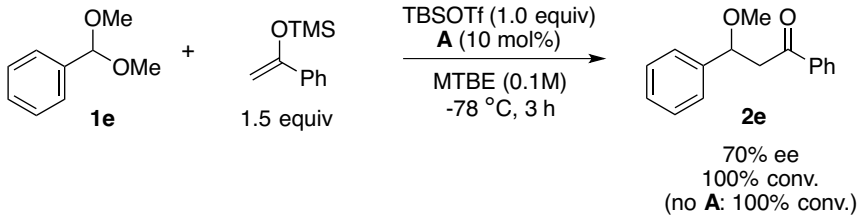

Scheme 3.3. ***Benzaldehyde-derived acetals as substrates for squaramide-catalyzed nucleophilic substitution.***

Acetophenone-derived methyl acetal **1f** provided substitution product **2f** cleanly and with 40% ee with catalyst **B** (Scheme 3.4). As anticipated, the background reactivity in absence of a catalyst was significant.

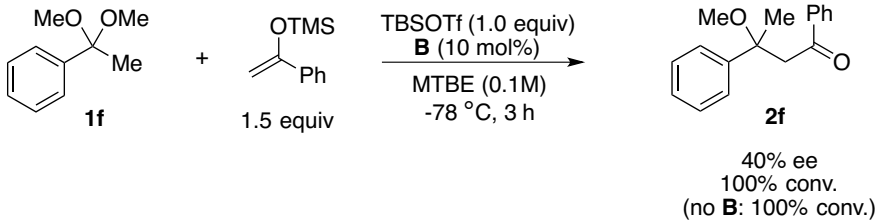

Scheme 3.4. ***Ketone-derived acetals as substrates for squaramide-catalyzed nucleophilic substitution.***

3.2.2. Investigation of Acetal Structure

Having examined the range of acetals shown in Figure 3.2 as substrates for asymmetric squaramide-catalyzed nucleophilic substitution, we decided to first focus our efforts on optimizing the reaction with benzaldehyde-derived acetals. This decision was guided by the promising enantioselectivity of 70% obtained with acetal **1e** and the modularity of this class of substrates with respect to the electronics on the aryl group as well as the size and electronics of the acetal substituents.

We first explored the effect of changing substrate structure on enantioselectivity of the reaction. Based on the observed high reactivity of **1e** in the absence of squaramide catalyst (Scheme 3.3), we hypothesized that destabilizing the oxocarbenium intermediate through electronic tuning would result in a slower reaction and allow for more catalyst control in the acetal ionization step.[63] Indeed, acetals **1h, 1i** and **3b** bearing electron-withdrawing 4-bromo substituents provided higher levels of enantioselectivity than benzaldehyde-derived acetals (entries 4-6 vs. 1-3, Table 3.1). Moreover, benzyl acetals resulted in higher enantioselectivity than their methyl and ethyl counterparts (entries 3 vs. 1-2, 6 vs. 4-5). Substrate **3b** thus resulted in the highest observed enantioselectivity of 88% with catalyst **B**.

[63] While kinetic studies were not performed on the reaction in Scheme 3.3, it would be reasonable to hypothesize that acetal ionization could be the rate-determining step here, given findings discussed in Chapter 2.

Table 3.1. ***Investigation of acetal structure.***[64]

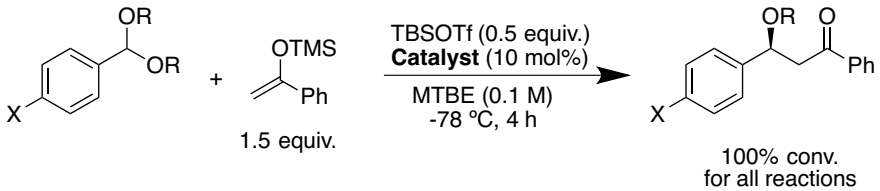

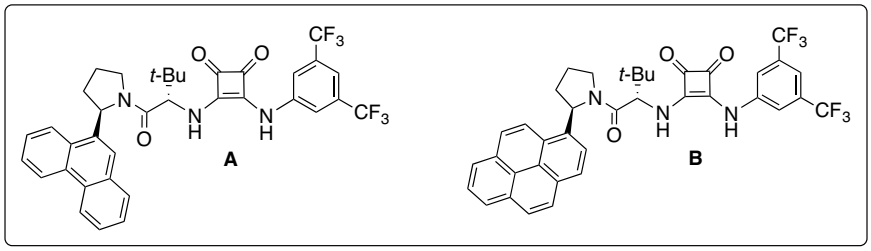

Entry	X	R (substrate)	ee[a] (%)	
			A	**B**
1		Me (**1e**)	70	13
2	H	Et (**1g**)	58	11
3		Bn (**3a**)	72	52
4		Me (**1h**)	82	51
5	Br	Et (**1i**)	69	29
6		Bn (**3b**)	85	88

a. ee values determined by chiral HPLC analysis.

[64] We discovered that we could use substoichiometric amounts of TBSOTf during reaction optimization. See Experimental Section for details.

3.2.3. Investigation of Catalyst Structure

With optimal substrate **3b** in hand, we examined the effect of the catalyst structure on the reaction outcome. No reactivity was observed with substrate **3b** in the absence of catalyst (entry 1, Table 3.2). Squaramide catalyst **5c** resulted in full conversion of **3b** to **4b** in 85% ee (entry 4). Consistent with our findings in Chapter 2, urea and thiourea analogs of catalyst **5c** provided no measurable acceleration of the reaction over background (entries 1-3). These results confirmed squaramides as optimal catalysts for this transformation.

Table 3.2. ***Investigation of the class of hydrogen-bond donor catalyst.***

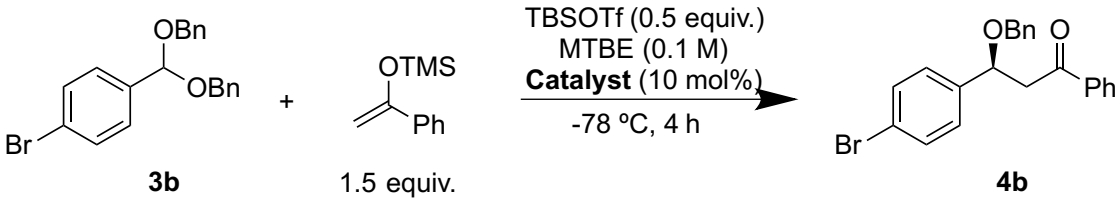

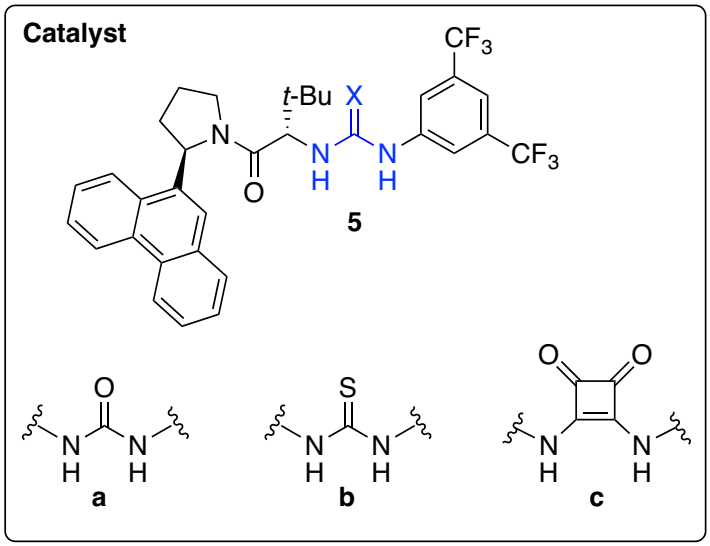

Entry	Catalyst	Conversion[a] (%)	ee[b] (%)
1	none	<5	n.d.
2	**5a**	<5	n.d.
3	**5b**	<5	n.d.
4	**5c**	100	85

a. Conversions determined by ^{1}H NMR analysis of the crude reaction mixture are reported.
b. ee values determined by chiral HPLC analysis.

Having established the squaramide structure as the optimal hydrogen-bonding motif for the catalyst, we investigated the effect of the amide portion of the catalyst on the enantioselectivity of the substitution reaction. Arylpyrrolidine catalyst **7b** was found to be more selective than analogous, but conformationally more labile catalysts **6a** and **6b** (entry 4 vs 1-2, Table 3.3). Following a trend that paralleled our findings in the (4+3) cycloaddition reaction, expanding the aromatic group from phenyl (**7b**) to 1-pyrenyl (**7h**) resulted in the highest enantioselectivity (88%) and conversion (100%) for the nucleophilic substitution of acetal **3b** (entry 10). A significant drop in enantioselectivity (from 88% to -5%) was observed when catalyst **6c**, a diastereomer of the optimal catalyst **7h,** was employed confirming that the relative orientation of stereogenic centers in the catalyst is crucially important for the enantioselectivity of the reaction (entry 12). Catalyst **8h**, which is structurally similar to **7h** but lacks the ability to engage with the triflate anion, was significantly less effective in this reaction (entry 11), confirming that the hydrogen-bonding component is indispensable for both good yield and enantioselectivity.

Table 3.3. ***Investigation of squaramide catalyst structure.***

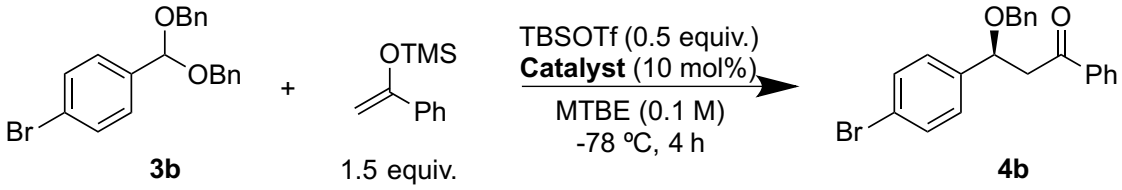

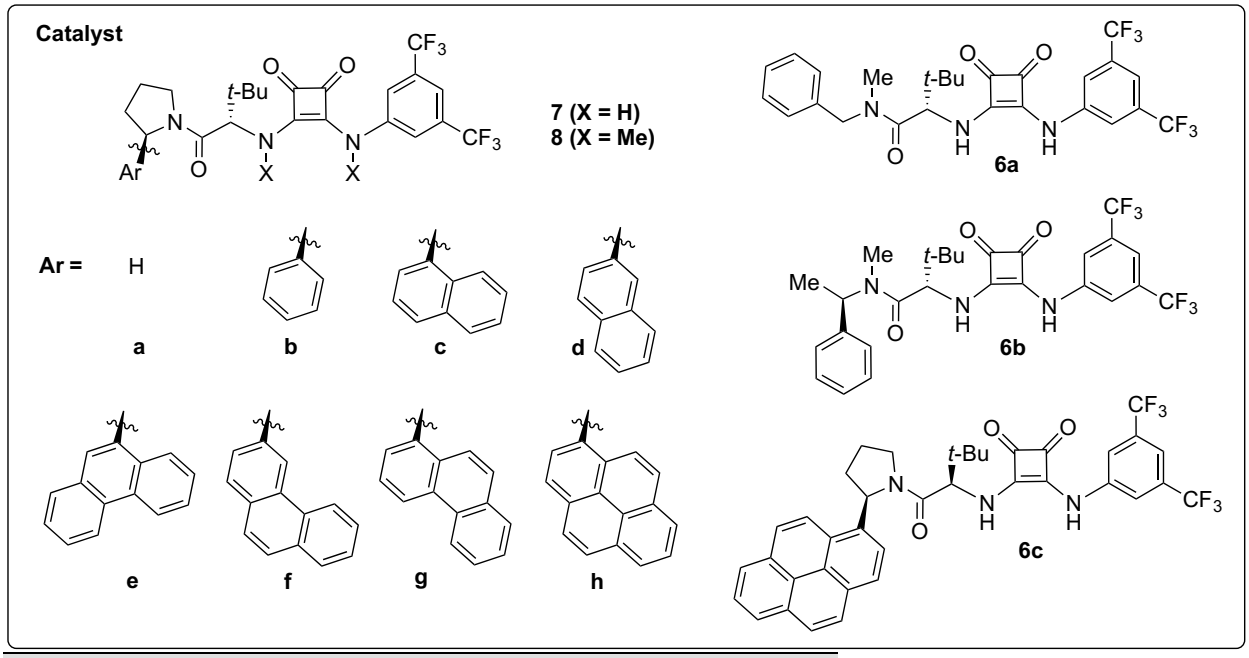

Entry	Catalyst	Conversion[a] (%)	ee[b] (%)
1	**6a**	38	26
2	**6b**	43	28
3	**7a**	10	10
4	**7b**	23	42
5	**7c**	31	72
6	**7d**	26	26
7	**7e**	100	85
8	**7f**	47	76
9	**7g**	100	87
10	**7h**	100	88
11	**8h**	43	2
12	**6c**	62	– 5

a. Conversions determined by ^{1}H NMR analysis of the crude reaction mixture are reported.
b. ee values determined by chiral HPLC analysis.

3.2.4. Optimization of Reaction Conditions

Having established the optimal substrate and catalyst structure for the nucleophilic substitution of acetals, we began our optimization of the reaction conditions. The effect of Lewis acid was first investigated. TMSOTf, TBSOTf and TESOTf provided identical reaction outcomes and can be used interchangeably (entries 1-3, Table 3.4). The use of TIPSOTf resulted in significantly lower conversion (55%) as compared with other silyl triflates (100%) (entry 4 vs 1-3), likely due to either poor accommodation of the sterically demanding triisopropyl silyl group in the congested transition state for this reaction or weakened binding of TIPSOTf to squaramide. Trifluoromethanesulfonic acid provided comparable reactivity and selectivity to silyl triflates (entry 5), suggesting that perhaps squaramides could activate Brønsted acids in a similar fashion to the activation of Lewis acids as discussed in Chapter 2.

Table 3.4. ***Investigation of Lewis acid promotor.***

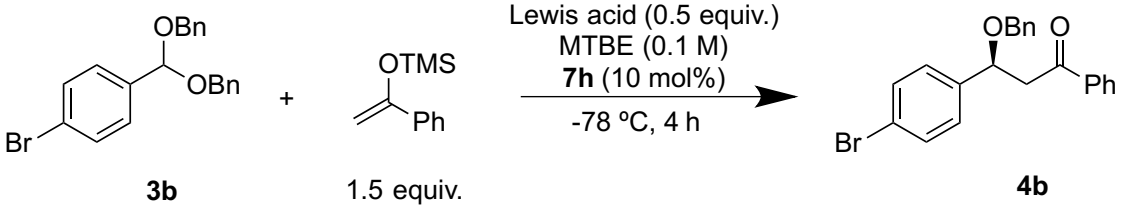

3b 1.5 equiv. **4b**

Entry	Lewis Acid	Conversion[a] (%)	ee[b] (%)
1	TMSOTf	100	88
2	TBSOTf	100	88
3	TESOTf	100	88
4	TIPSOTf	55	88
5	TfOH	100	87

a. Conversions determined by ^{1}H NMR analysis of the crude reaction mixture are reported.
b. ee values determined by chiral HPLC analysis.

Next, we investigated the effect of solvent on the reaction. Reactivity was observed only in ethereal solvents, with methyl *t*-butyl ether providing the highest levels of reactivity and enantioselectivity (entry 1, Table 3.5).

Table 3.5. ***Investigation of solvent effect.***

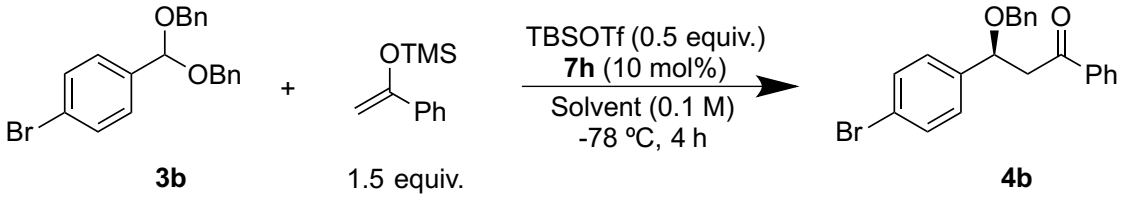

3b 1.5 equiv. **4b**

Entry	Solvent	Conversion[a] (%)	ee[b] (%)
1	MTBE	100	88
2	CPME	49	84
3	Et_2O	95	81
4	THF	43	2
5	Toluene	n.r.	n.d.
6	DCM	n.r.	n.d.
7	Benzene	n.r.	n.d.

a. Conversions determined by ^{1}H NMR analysis of the crude reaction mixture are reported.
b. ee values determined by chiral HPLC analysis.

Given the low rate of background reactivity we then evaluated the effect of lower catalyst loading on substrate **3b**. Upon lowering of catalyst loading from 10 mol% to 0.5 mol%, only marginal decrease in enantioselectivity (88% to 86%) was found; however, the reaction slowed down significantly (entry 5 vs. 1, Table 3.6). The catalyst loading could be decreased to 5 mol% without any loss of reactivity or enantioselectivity (entry 4).

Table 3.6. ***Catalyst loading investigation (part 1).***

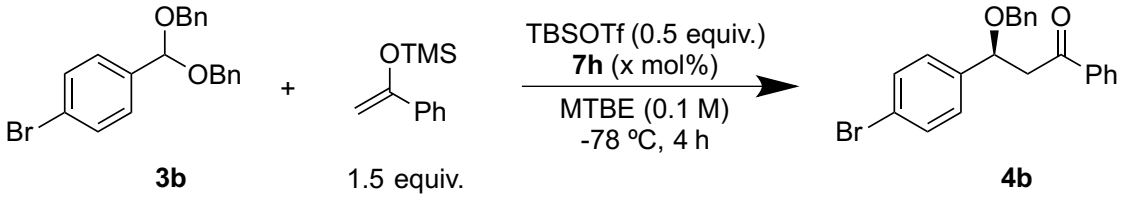

3b 1.5 equiv. **4b**

Entry	Catalyst Loading (mol%)	Conversion[a] (%)	ee[b] (%)
1	0.5	29	86
2	1.0	44	86
3	2.0	66	86
4	5.0	100	88
5	10	100	88

a. Conversions determined by ^{1}H NMR analysis of the crude reaction mixture are reported.
b. ee values determined by chiral HPLC analysis.

Despite the appeal of lower catalyst loading, it was still necessary to evaluate this parameter with a less reactive substrate **3c** (Table 3.7) to ensure high conversion across a range of electronically varied acetals. Lowering the catalyst loading from 10 mol% to 5 mol% resulted in a significant decrease in conversion from 70% to 39% in this case (entries 4-5). Therefore, a catalyst loading of 10 mol% was chosen for further investigation into the reaction scope.

Table 3.7. ***Catalyst loading investigation (part 2).***

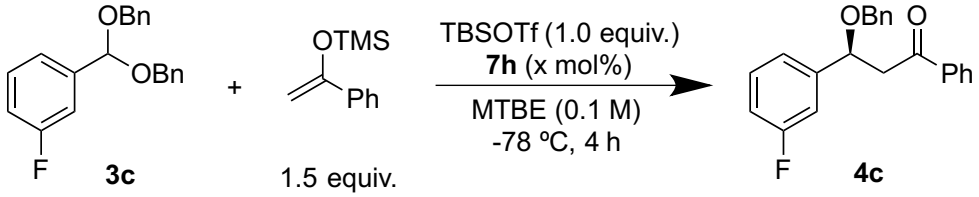

Entry	Catalyst Loading (mol%)	Conversion[a] (%)	ee[b] (%)
1	0.5	n.r.	n.d.
2	1.0	<5	n.d.
3	2.0	<5	n.d.
4	5.0	39	93
5	10	70	93

a. Conversions determined by ^{1}H NMR analysis of the crude reaction mixture are reported.
b. ee values determined by chiral HPLC analysis.

3.2.5. Acetal Scope and Limitations

A number of substituted dibenzyl arylaldehyde-derived acetals were evaluated under the optimized conditions for the squaramide-catalyzed nucleophilic substitution reaction (Table 3.8). Unsubstituted benzaldehyde-derived substrate **4a** resulted in enantioselectivity of only 51% (entry 1, Table 3.8). However, incorporation of electron-withdrawing groups in the substrate resulted in a significant boost in enantioselectivity of up to 97% with *m*-chloro-substituted acetal **3h** (entry 8). Lower conversions, and consequently yields, were observed for more electron-poor substrates **4g** – **4i** (entries 6, 8, 10). However, reactivity could be restored from 50% to 97% yield by running the reaction at higher temperature (-65° C instead of -78° C) for 24h with

minimal loss in enantioselectivity (94% vs. 96%) (entry 7 vs. 6). No reactivity was observed when strongly electron-withdrawing substituents (e.g. *m*-CF3 or *p*-CN) were incorporated.[65]

A correlation between enantioselectivity and substrate electronics was then evaluated. Enantioselectivity was converted to the difference in activation energies for the formation of two enantiomers ($\Delta\Delta G^{\ddagger}$ in kcal/mol) for the substrates in Table 3.9. Calculated $\Delta\Delta G^{\ddagger}$'s were then plotted against Hammett σ-parameters for the substituents on acetals revealing a linear correlation between substrate electronics and enantioselectivity ($R^2 = 0.88$) with a $\rho>0$: electron-withdrawing substituents lead to higher enantioselectivity (Figure 3.3). We hypothesize that electron-withdrawing substituents destabilize the oxocarbenium intermediate that forms upon acetal ionization, leading to a more oxocarbenium-like (late) transition state according to Hammond postulate. Positive charge build-up results in tighter binding of the oxocarbenium to the triflate-catalyst complex and consequently leads to higher selectivity for one of the prochiral oxocarbenium faces exposed for nucleophilic attack.

[65] Substrates bearing electron-donating substituents (e.g. *p*-OMe or *p*-Me) were not synthetically accessible. Low reactivity towards dibenzyl acetal formation from p-anisaldehyde was previously reported: Watahiki, T.; Akabane, Y.; Mori, S.; Oriyama, T. *Org. Lett*. **2003**, *5*, 3045–3048.

Table 3.8. ***Acetal scope.***

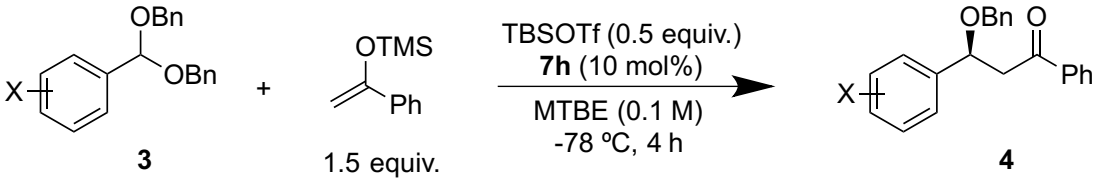

Entry	Product	Yield[a] (%)	ee[b] (%)
1	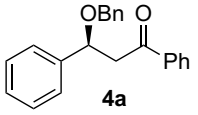 **4a**	95	51
2	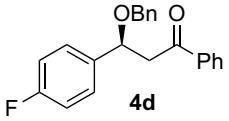 **4d**	96	58
3	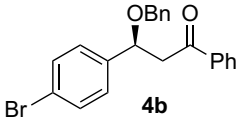 **4b**	95	88
4	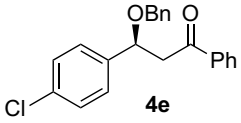 **4e**	96	79
5	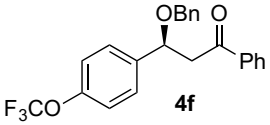 **4f**	97	88
6	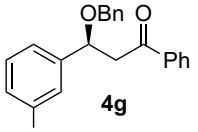 **4g**	50	96
7		97[c]	94[c]
8	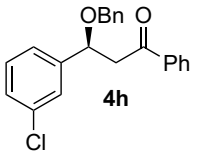 **4h**	55	97
9	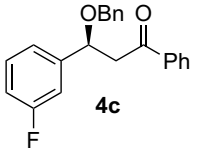 **4c**	72	93
10	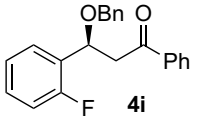 **4i**	53	96

a. Isolated yields after chromatographic purification are reported.
b. ee values determined by chiral HPLC analysis.
c. Reaction was run at -65° C for 24 h.

Table 3.9. ***Conversion of enantioselectivity to ΔΔG‡.***

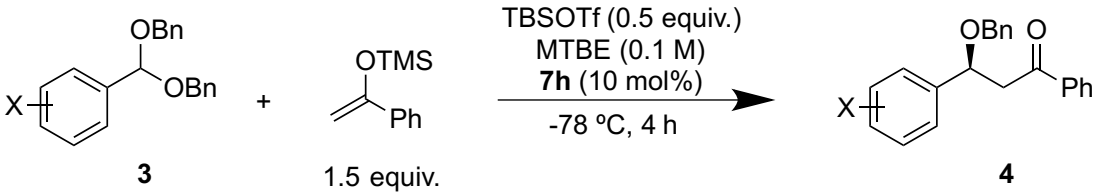

Entry	Substituent (X =)	ee (%)	$\sigma_{p \text{ or } m}$	$\Delta\Delta G^{\ddagger}$ (kcal/mol)
1	H (**4a**)	51	0	0.44
2	4-Br (**4b**)	88	0.232	1.07
3	4-Cl (**4e**)	79	0.227	0.83
4	3-Br (**4g**)	96	0.391	1.51
5	3-Cl (**4h**)	97	0.373	1.62
6	3-F (**4c**)	93	0.337	1.29
7	4-F (**4d**)	58	0.062	0.51
8	4-OCF3 (**4f**)	88	0.35	1.07

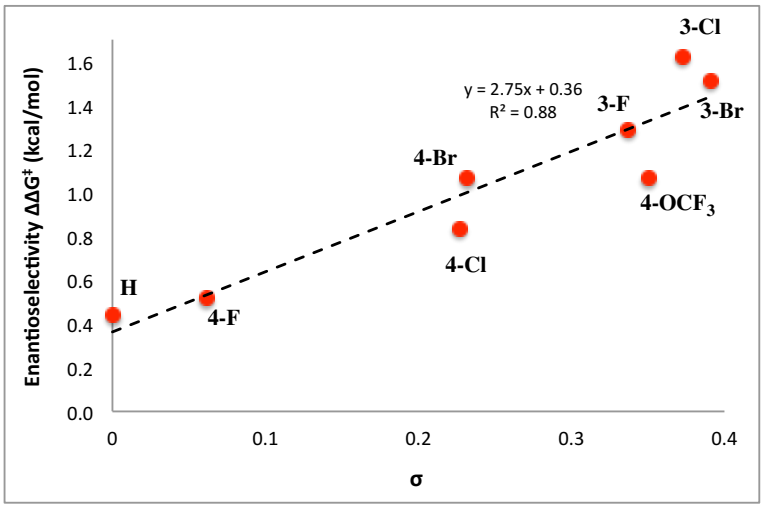

Figure 3.3. ***Correlation of enantioselectivities and Hammett σ-values.***

3.2.6. Nucleophile Scope

A number of nucleophiles were evaluated with the model acetal **3b** (Table 3.10). Substitution products were obtained in similar yields and enantioselectivities with nucleophiles ranging from methallyltrimethylsilane (nucleophilicity parameter of 4.41 (entry 3)) to methyl

trimethylsilyl dimethylketene acetal (nucleophilicity parameter of 9.00 (entry 5)).[66] Silyl enol ethers (entries 1, 2) and silyl ketene thioacetals (entry 4) were also well tolerated under the reaction conditions. Overall, the scope of compatible nucleophilic partners for this transformation spans almost five orders of magnitude in nucleophilicity. This finding, in combination with the positive effect that destabilizing the oxocarbenium intermediate has on enantioselectivity led us to conclude that nucleophilic addition is likely not the enantiodetermining step in this reaction. Rather, the formation of the chiral ion pair between oxocarbenium and catalyst-bound triflate anion is consistent with the above data as the enantiodetermining step.

[66] Nucleophilicities are reported according to the *N*-parameter from the Mayr's database of reactivity parameters: http://www.cup.lmu.de/oc/mayr/reaktionsdatenbank/

Table 3.10. ***Nucleophile scope.***

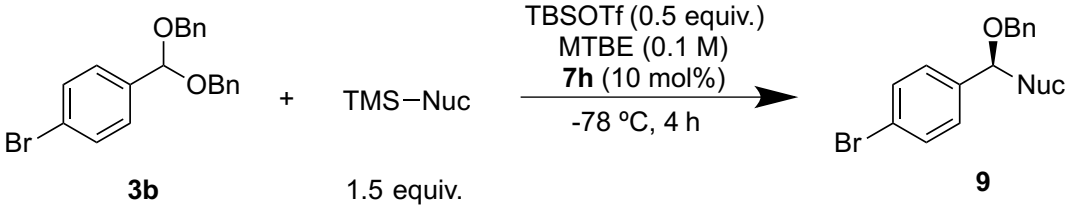

Entry	Nucleophile	Product	Yield[a] (%)	ee[b] (%)
1	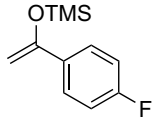	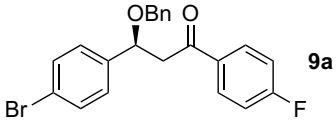 **9a**	97	89
2	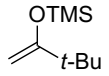	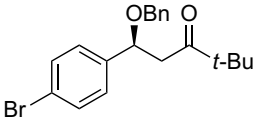 **9b**	96	93
3	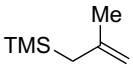	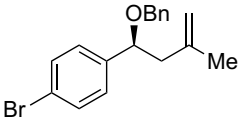 **9c**	97	88
4	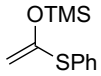	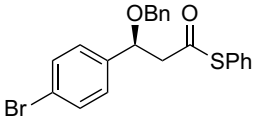 **9d**	94	95
5	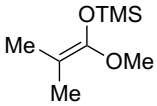	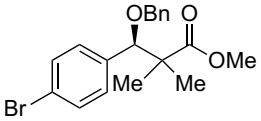 **9e**	98	90
6	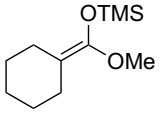	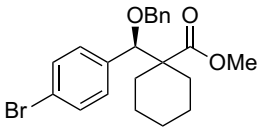 **9f**	80	91
7	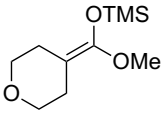	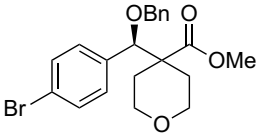 **9g**	92	94

a. Isolated yields after chromatographic purification are reported.
b. ee values determined by chiral HPLC analysis.

3.3. Conclusions

In conclusion, we have further applied the new concept of cooperative catalysis using squaramides and silyl triflates developed in Chapter 2 to a highly enantioselective nucleophilic substitution of acetals. This reaction displays an unprecedented nucleophile scope, wherein high yields and enantioselectivities are obtained with reaction partners spanning five orders of magnitude in nucleophilicity. This research represents a significant leap forward for methodologies targeting enantioselective additions to oxocarbenium ions. Investigation of other types of cationic intermediates that could be engaged in enantioselective transformations using this approach could drastically expand the limits of reactions amenable to catalysis by chiral dual hydrogen-bond donors.

3.4. Experimental Section

3.4.1. General Information

All reactions were performed in flame-dried 10 mL round-bottom flasks unless otherwise noted. The flasks were fitted with rubber septa and reactions were conducted under nitrogen. Stainless steel syringes were used to transfer air- and moisture-sensitive liquids. Flash chromatography was performed using silica gel 60 (230-400 mesh) from EM Science. Commercial reagents were purchased from Aldrich, Alfa Aesar, Strem or TCI, and used as received with the following exceptions: dichloromethane, tetrahydrofuran, toluene, ethyl ether, *t*-butyl methyl ether were dried by passing through columns of activated molecular sieves. Triethylamine was distilled from CaH_2 at 760 torr. Proton nuclear magnetic resonance (^{1}H NMR) spectra and carbon nuclear magnetic resonance (^{13}C NMR) spectra were recorded on Inova-500 (500 MHz) spectrometers. Chemical shifts for protons are reported in parts per million downfield from tetramethylsilane and are referenced to residual protium in NMR solvent ($CHCl_3$ = δ 7.27). Chemical shifts for carbon are reported in parts per million downfield from tetramethylsilane and are referenced to the carbon resonance of the solvent ($CDCl_3$ = δ 77.0). Data are represented as follows: chemical shift, multiplicity (br. = broad, s = singlet, d = doublet, t = triplet, q = quartet, m = multiplet), coupling constants in Hertz (Hz), integration. Infrared (IR) spectra were obtained using Bruker Optics Tensor 27 FTIR spectrometer. Optical rotations were measured using a 1mL cell with 0.5 dm path length on a Jasco DIP 370 digital polarimeter. The mass spectra were obtained on a Bruker micrOTOF-Q II time-of-flight LC/MS spectrometer. Chiral HPLC analysis was performed using an Agilent Technologies 1200 series instrument with commercial Chiralpak columns.

3.4.2. Characterization Data for Substrates 3a-3i

Dibenzyl acetals were prepared using a previously reported procedure[67] in 30-70% yield. These compounds could be subjected to column chromatography using davisil grade silica gel.

Benzaldehyde dibenzyl acetal (**3a**):

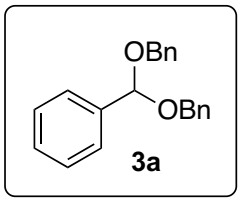

^{1}H NMR (500 MHz, $CDCl_3$) δ 7.59 (d, J=6.8 Hz, 2 H), 7.27 - 7.44 (m, 13 H), 5.79 (s, 1 H), 4.62 (d, *J*=1.0 Hz, 4 H);

^{13}C NMR (125 MHz, $CDCl_3$) δ 138.3, 138.1, 128.4, 128.3, 127.8, 127.6, 127.0, 126.9, 100.4, 67.0;

FTIR (neat, cm^{-1}) ν_{max} 1098, 1072, 1038, 1024, 734, 696 cm^{-1};

HRMS (ESI-TOF) calculated for $C_{21}H_{20}O_2$ $[M+Na]^+$: 327.1361, found: 327.1392.

[67] Gregg, B. T.; Golden, K. C.; Quinn, J. F. *Tetrahedron* **2008**, *64*, 3287–3295.

4-bromobenzaldehyde dibenzyl acetal (**3b**):

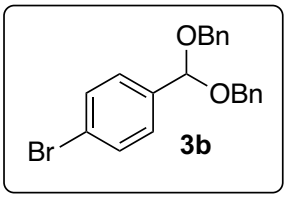

^{1}H NMR (500 MHz, $CDCl_3$) δ 7.49 (dd, J=37.1, 8.3 Hz, 4 H), 7.28 - 7.40 (m, 10 H), 5.73 (s, 1 H), 4.60 (d, *J*=3.4 Hz, 4 H);

^{13}C NMR (125 MHz, $CDCl_3$) δ 137.8, 137.4, 131.5, 128.7, 128.5, 127.8, 127.7, 122.6, 99.7, 67.1;

FTIR (neat, cm^{-1}) ν_{max} 1038, 1024, 1010, 729, 695 cm^{-1};

HRMS (ESI-TOF) calculated for $C_{21}H_{19}O_2Br$ $[M+Na]^+$: 405.0466, found: 405.0415.

3-fluorobenzaldehyde dibenzyl acetal (**3c**):

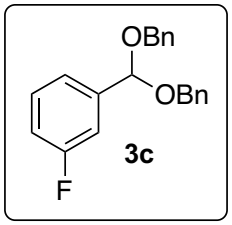

^{1}H NMR (500 MHz, $CDCl_3$) δ 7.35 - 7.39 (m, 10 H), 7.29 - 7.34 (m, 3 H), 7.02 - 7.09 (m, 1 H), 5.77 (s, 1 H), 4.62 (d, *J*=2.4 Hz, 4 H);

^{13}C NMR (125 MHz, $CDCl_3$) δ 162.9 (d, J = 244.1 Hz), 141.0, 137.8, 129.9, 128.5, 127.9, 127.8, 122.6, 115.5, 114.1, 99.5, 67.1;

FTIR (neat, cm^{-1}) ν_{max} 1039, 1024, 775, 729, 696, 681 cm^{-1};

HRMS (ESI-TOF) calculated for $C_{21}H_{19}O_2F$ $[M+Na]^+$: 345.1267, found: 345.1267.

4-fluorobenzaldehyde dibenzyl acetal (**3d**):

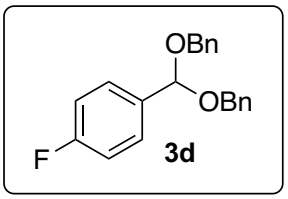

^{1}H NMR (500 MHz, $CDCl_3$) δ 7.51 - 7.59 (m, 2 H), 7.34 - 7.42 (m, 8 H), 7.28 - 7.34 (m, 2 H), 7.08 (m, J=8.3, 8.3 Hz, 2 H), 5.76 (s, 1 H), 4.60 (d, *J*=1.5 Hz, 4 H);

^{13}C NMR (125 MHz, $CDCl_3$) δ 162.9 (d, J = 245.1 Hz), 137.9, 134.2, 128.7, 128.6, 128.5, 127.8, 127.7, 115.3, 67.1;

FTIR (neat, cm^{-1}) ν_{max} 1509, 1222, 1090, 1039, 1025, 734, 697 cm^{-1};

HRMS (ESI-TOF) calculated for $C_{21}H_{19}O_2F$ $[M+Na]^+$: 345.1267, found: 345.1287.

4-chlorobenzaldehyde dibenzyl acetal (**3e**):

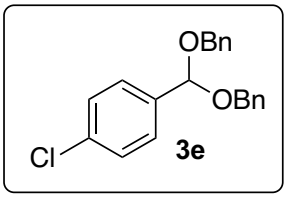

^{1}H NMR (500 MHz, $CDCl_3$) δ 7.51 (d, *J*=8.3 Hz, 2 H), 7.33 - 7.40 (m, 10 H), 7.28 - 7.33 (m, 2 H), 5.75 (s, 1 H), 4.59 (d, *J*=2.9 Hz, 4 H);

^{13}C NMR (125 MHz, $CDCl_3$) δ 137.8, 136.9, 134.4, 128.5, 128.4, 128.3, 127.8, 127.7, 99.7, 67.1;

FTIR (neat, cm^{-1}) ν_{max} 1087, 1037, 1024, 1013, 731, 695 cm^{-1};

HRMS (ESI-TOF) calculated for $C_{21}H_{19}O_2Cl$ $[M+Na]^+$: 361.0971, found: 361.0984.

4-(trifluoromethoxy)benzaldehyde dibenzyl acetal (**3f**):

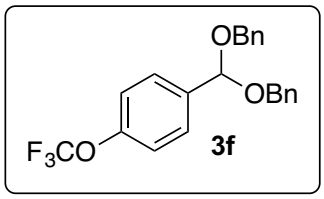

^{1}H NMR (500 MHz, $CDCl_3$) δ 7.60 (d, J=8.8 Hz, 2 H), 7.33 - 7.37 (m, 8 H), 7.28 - 7.33 (m, 2 H), 7.24 (d, J=8.3 Hz, 2 H), 4.61 (d, *J*=2.4 Hz, 4 H);

^{13}C NMR (125 MHz, $CDCl_3$) δ 149.3, 137.8, 137.1, 128.5, 127.9, 127.8, 120.5 (q, J = 256.3 Hz), 120.8 99.6, 67.2;

FTIR (neat, cm^{-1}) ν_{max} 1257, 1221, 1164, 1042, 1026, 1019, 697 cm^{-1};

HRMS (ESI-TOF) calculated for $C_{22}H_{19}O_3F_3$ $[M+Na]^+$: 411.1184, found: 411.180.

3-bromobenzaldehyde dibenzyl acetal (**3g**):

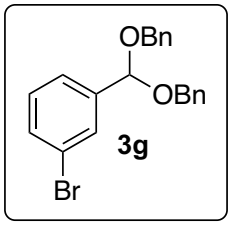

^{1}H NMR (500 MHz, $CDCl_3$) δ 7.77 (s, 1 H), 7.48 - 7.55 (m, 2 H), 7.23 - 7.43 (m, 12 H), 5.75 (s, 1 H), 4.62 (d, *J*=2.9 Hz, 4 H);

^{13}C NMR (125 MHz, $CDCl_3$) δ 140.7, 137.7, 131.7, 130.1, 130.0, 128.5, 127.9, 127.8, 125.6, 122.6, 99.4, 67.2;

FTIR (neat, cm^{-1}) ν_{max} 1197, 1038, 1023, 784, 728, 694, 678 cm^{-1};

HRMS (ESI-TOF) calculated for $C_{21}H_{19}O_2Br$ $[M+Na]^+$: 405.0466, found: 405.0464.

3-chlorobenzaldehyde dibenzyl acetal (**3h**):

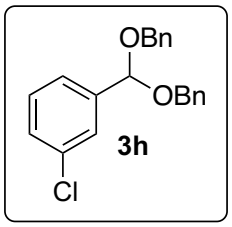

^{1}H NMR (500 MHz, $CDCl_3$) δ 7.58 (s, 1 H), 7.42 - 7.49 (m, 1 H), 7.28 - 7.41 (m, 12 H), 5.73 (s, 1 H), 4.60 (d, *J*=3.4 Hz, 4 H);

^{13}C NMR (125 MHz, $CDCl_3$) δ 140.4, 137.7, 134.4, 129.6, 128.7, 128.5, 127.9, 127.8, 127.2, 125.1, 99.5, 67.1;

FTIR (neat, cm^{-1}) ν_{max} 1202, 1104, 1076, 1042, 1025, 733, 697 cm^{-1};

HRMS (ESI-TOF) calculated for $C_{21}H_{19}O_2Cl$ $[M+Na]^+$: 361.0971, found: 361.0961.

2-fluorobenzaldehyde dibenzyl acetal (**3i**):

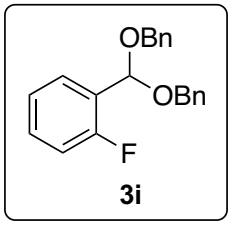

^{1}H NMR (500 MHz, $CDCl_3$) δ 7.77 (td, J=7.8, 2.0 Hz, 1 H), 7.29 - 7.40 (m, 11 H), 7.21 (td, J=7.8, 1.0 Hz, 1 H), 7.06 - 7.12 (m, 1 H), 6.02 (s, 1 H), 4.67 (br. s, 4 H);

^{13}C NMR (125 MHz, $CDCl_3$) δ 160.5 (d, J = 247.5 Hz), 137.8, 130.4, 130.3, 128.4, 127.9, 127.7, 125.7, 125.6, 124.0, 115.6, 95.9, 68.0;

FTIR (neat, cm^{-1}) ν_{max} 1455, 1042, 1023, 757, 731, 695 cm^{-1};

HRMS (ESI-TOF) calculated for $C_{21}H_{19}O_2F$ $[M+Na]^+$: 345.1267, found: 345.1285.

3.4.3. General Procedure for Squaramide-Catalyzed Nucleophilic Substitution of Acetals

Method A (reaction optimization): A 1-dram vial was equipped with a magnetic stir bar, closed with a cap containing a rubber septum, flame-dried and subsequently cooled under vacuum. The vial was placed under N_2 and charged with substrate **3b** (0.05 mmol, 1 equiv.), 1-phenyl-1-trimethylsiloxyethylene (15.4 μL, 0.075 mmol, 1.5 equiv.), **7h** (3.5 mg, 0.005 mmol, 10 mol%) and dry *t*-butyl methyl ether (0.5 mL). The mixture was then cooled to -78 ºC on the dry ice-acetone bath. TBSOTf (5.7 μL, 0.025 mmol, 0.5 equiv.) was added via syringe. The reaction was stirred for 4 h at -78 ºC, and then quenched via addition of 100 μL of a 6:1 MeOH:Et_3N solution via syringe.

Method B (preparative scale reactions): A 10 mL round-bottom flask was equipped with a magnetic stir bar, flame-dried and subsequently cooled under vacuum. The flask was placed under N_2 and charged with substrate **3b** (0.25 mmol, 1 equiv.), 1-phenyl-1-trimethylsiloxyethylene (76.9 μL, 0.38 mmol, 1.5 equiv.), **7h** (17.3 mg, 0.025 mmol, 10 mol%) and dry *t*-butyl methyl ether (2.5 mL). The mixture was then cooled to -78 ºC on the dry ice-acetone bath. TBSOTf (28.5 μL, 0.125 mmol, 0.5 equiv.) was added via syringe. The reaction was stirred for 4 h at -78 ºC, and then quenched via addition of 500 μL of a 6:1 MeOH:Et_3N solution via syringe. The crude reaction mixture was concentrated and purified by column chromatography with hexane/ethyl ether as eluent (1:0 to 4:1) to yield pure **4b**.

3.4.4. Characterization of Products 4a-9g

(*S*)-3-(benzyloxy)-1,3-diphenylpropan-1-one (**4a**):

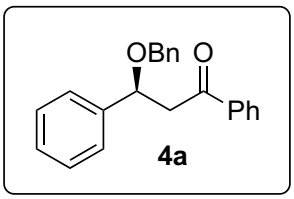

4a

According to general procedure (Method B), **3a** (0.125 mmol) was reacted to give **4a** in 37.6 mg (95% yield) as clear oil.

^{1}H NMR (500 MHz, $CDCl_3$) δ 7.89 (d, *J*=8.3 Hz, 2 H), 7.46 - 7.51 (m, 1 H), 7.31 - 7.45 (m, 6 H), 7.15 - 7.29 (m, 6 H), 5.07 (dd, *J*=8.3, 4.9 Hz, 1 H), 4.39 (d, *J*=11.7 Hz, 1 H), 4.32 (d, *J*=11.7 Hz, 1 H), 3.63 (dd, *J*=16.6, 8.3 Hz, 1 H), 3.10 (dd, *J*=16.1, 4.4 Hz, 1 H);

^{13}C NMR (125 MHz, $CDCl_3$) δ 197.6, 141.6, 138.1, 137.2, 133.0,128.6, 128.5, 128.2, 127.9, 127.7, 127.4, 126.8, 77.7, 70.9, 47.3;

FTIR (neat, cm^{-1}) ν_{max} 1685, 1094, 1072, 1057, 733, 688, 580 cm^{-1};

HRMS (ESI-TOF) calculated for $C_{22}H_{20}O_2$ $[M+Na]^+$: 339.1361, found: 339.1501;

$[\alpha]_D^{25}$ = –28.0° (c = 1, $CHCl_3$).

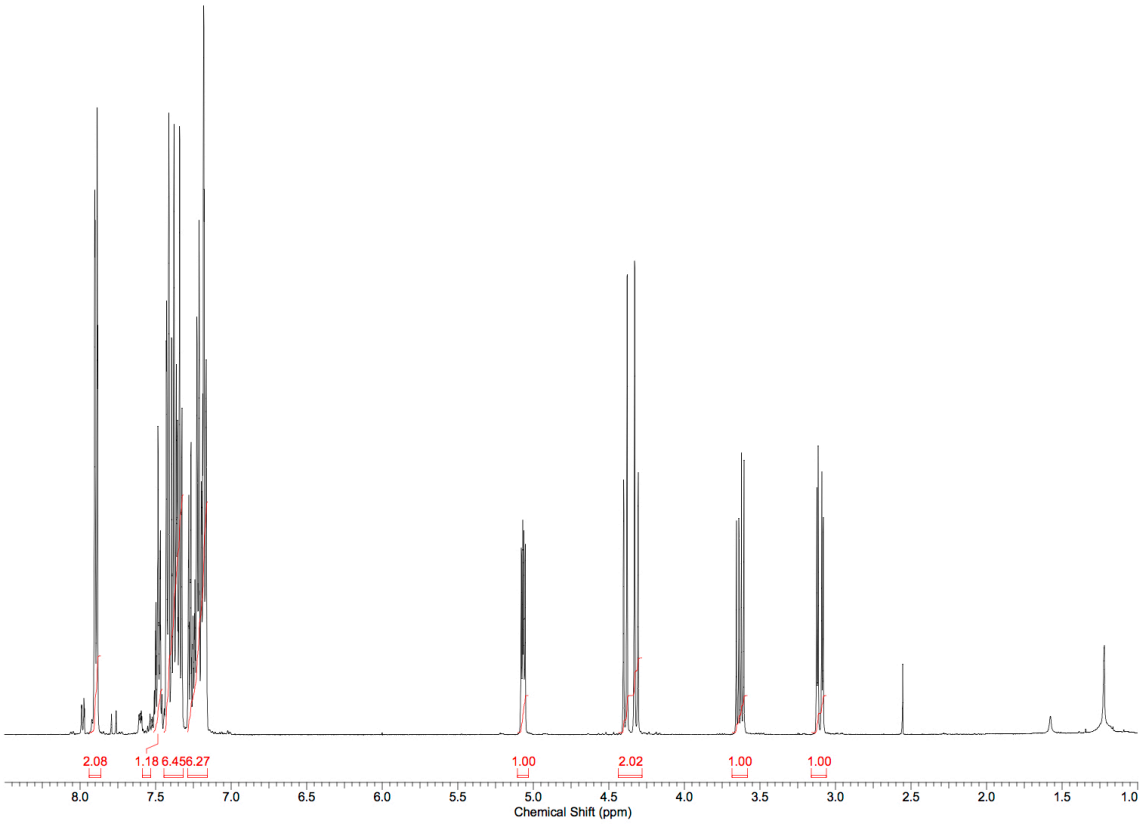
2.08
1.18
6.45
6.27
1.00
2.02
1.00
1.00
8.0
7.5
7.0
6.5
6.0
5.5
5.0
4.5
4.0
3.5
3.0
2.5
2.0
1.5
1.0
Chemical Shift (ppm)

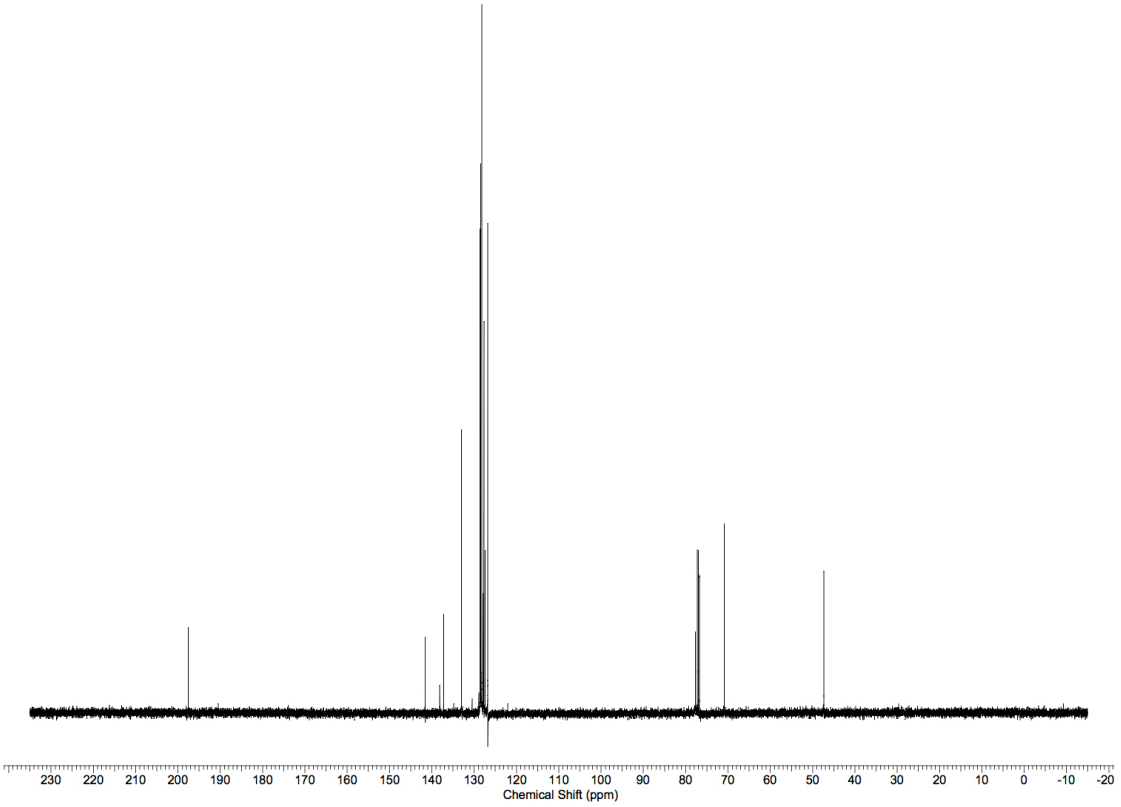
230
220
210
200
190
180
170
160
150
140
130
120
110
100
90
80
70
60
50
40
30
20
10
0
-10
-20
Chemical Shift (ppm)

Racemic sample: HPLC (ChiralPak AS-H, 2% IPA/hexanes, 1 mL/min, 210 nm)

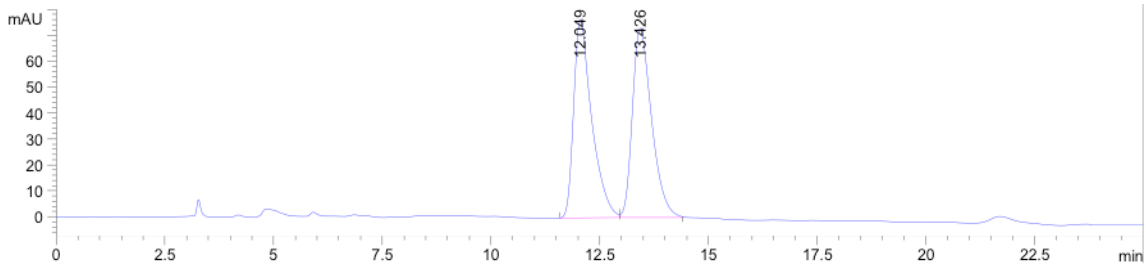

Peak #	RetTime [min]	Type	Width [min]	Area [mAU*s]	Height [mAU]	Area %
1	12.049	BV	0.4258	2214.81787	76.49049	49.6237
2	13.426	VB	0.4670	2248.40625	73.07730	50.3763

Enantioenriched Sample: HPLC (ChiralPak AS-H, 2% IPA/hexanes, 1 mL/min, 210 nm), 51% e.e.

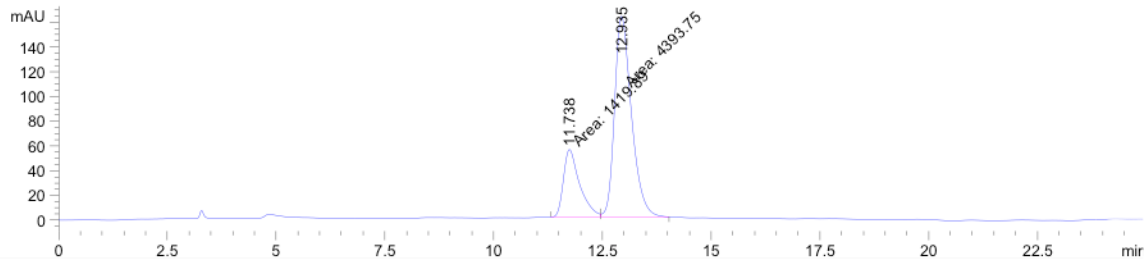

Peak #	RetTime [min]	Type	Width [min]	Area [mAU*s]	Height [mAU]	Area %
1	11.738	MF	0.4326	1419.89429	54.70115	24.4235
2	12.935	FM	0.4510	4393.75439	162.37103	75.5765

(*S*)-3-(benzyloxy)-3-(4-bromophenyl)-1-phenylpropan-1-one (**4b**):

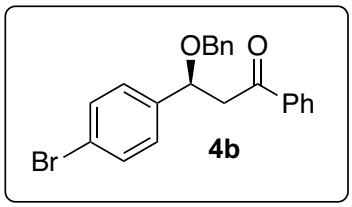

According to general procedure (Method B), **3b** (0.5 mmol) was reacted to give **4b** in 187.7 mg (95% yield) as clear amorphous solid.

^{1}H NMR (500 MHz, $CDCl_3$) δ 7.96 (dd, *J*=8.3, 1.0 Hz, 2 H), 7.51 - 7.61 (m, 3 H), 7.47 (t, *J*=8.3 Hz, 2 H), 7.38 (d, *J*=8.3 Hz, 2 H), 7.21 - 7.34 (m, 5 H), 5.11 (dd, *J*=5.4, 2.9 Hz, 1 H), 4.45 (d, *J*=11.7 Hz, 1 H), 4.39 (d, *J*=11.2 Hz, 1 H), 3.68 (dd, *J*=16.6, 7.8 Hz, 1 H), 3.17 (dd, *J*=16.6, 4.9 Hz, 1 H);

^{13}C NMR (125 MHz, $CDCl_3$) δ 197.3, 140.7, 137.9, 137.1, 133.2, 131.8, 128.7, 128.6, 128.4, 128.2, 127.8, 127.7, 121.8, 71.1, 47.2;

FTIR (neat, cm^{-1}) ν_{max} 1685, 1092, 1069, 1009, 984, 823, 732, 688 cm^{-1};

HRMS (ESI-TOF) calculated for $C_{22}H_{19}O_2Br$ $[M+Na]^+$: 417.0466, found: 417.0464;

$[\alpha]_D^{25}$ = –52.8° (c = 1, $CHCl_3$).

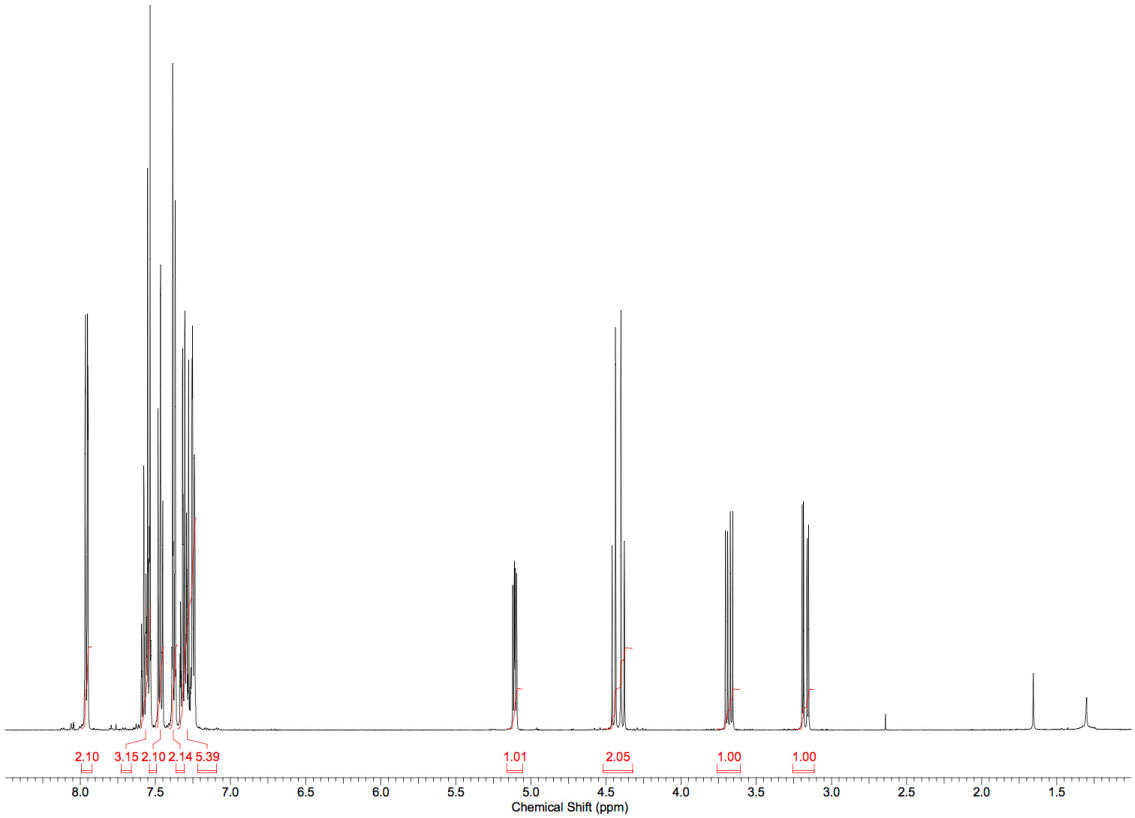
2.10
3.15
2.10
2.14
5.39
1.01
2.05
1.00
1.00
8.0
7.5
7.0
6.5
6.0
5.5
5.0
4.5
4.0
3.5
3.0
2.5
2.0
1.5
Chemical Shift (ppm)

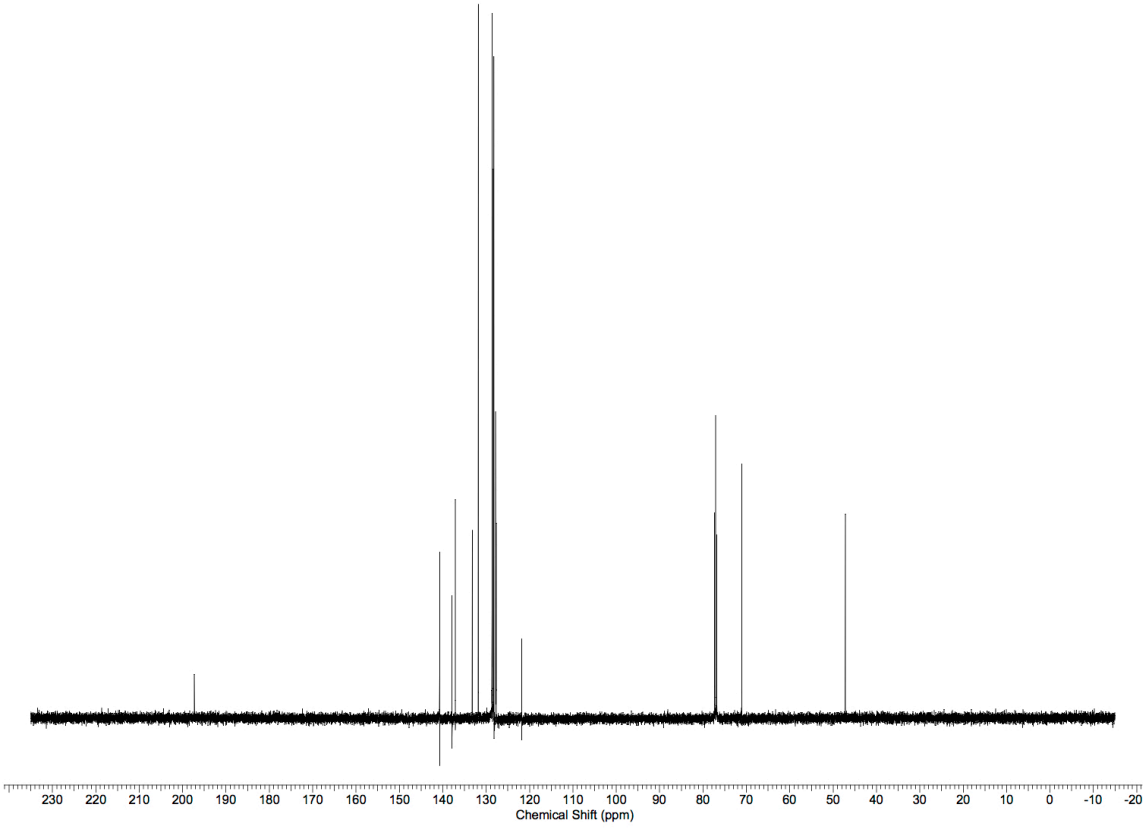
230
220
210
200
190
180
170
160
150
140
130
120
110
100
90
80
70
60
50
40
30
20
10
0
-10
-20
Chemical Shift (ppm)

Racemic sample: HPLC (ChiralPak IB, 2% IPA/hexanes, 1 mL/min, 210 nm)

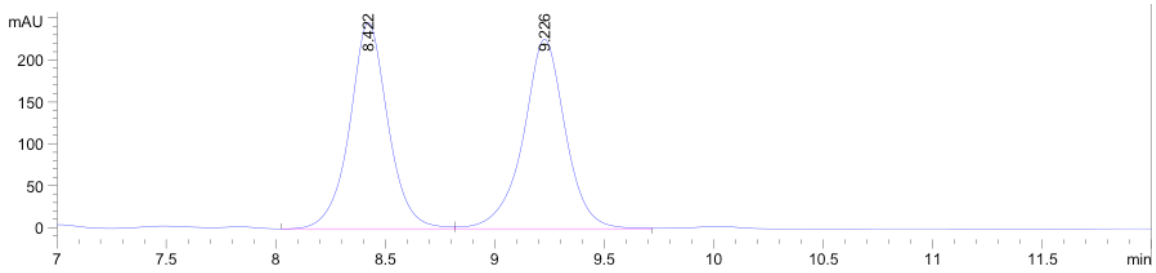

Peak #	RetTime [min]	Type	Width [min]	Area [mAU*s]	Height [mAU]	Area %
1	8.422	VV	0.1824	3005.87964	246.35075	49.7228
2	9.226	VB	0.1988	3039.39038	226.18246	50.2772

Enantioenriched Sample: HPLC (ChiralPak IB, 2% IPA/hexanes, 1 mL/min, 210 nm), 88% e.e.

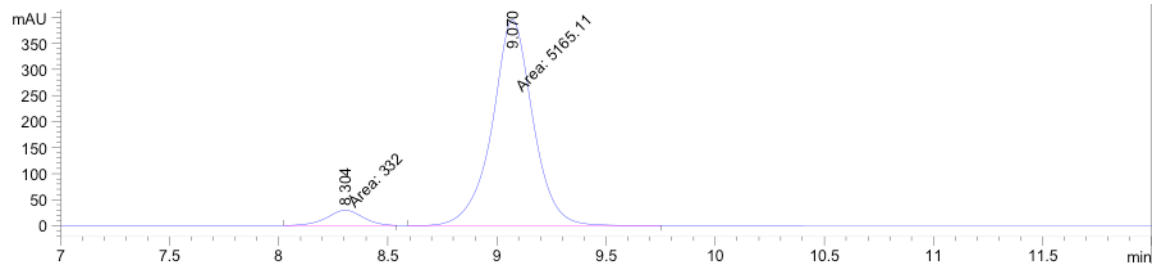

Peak #	RetTime [min]	Type	Width [min]	Area [mAU*s]	Height [mAU]	Area %
1	8.304	MM	0.1887	332.00049	29.31790	6.0395
2	9.070	MM	0.2173	5165.10596	396.10992	93.9605

(*S*)-3-(benzyloxy)-3-(3-fluorophenyl)-1-phenylpropan-1-one (**4c**):

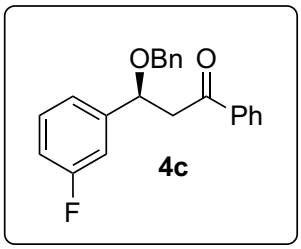

4c

According to general procedure (Method B), **3c** (0.25 mmol) was reacted to give **4c** in 60.0 mg (72% yield) as clear oil.

^{1}H NMR (500 MHz, $CDCl_3$) δ 7.97 (dd, *J*=8.3, 1.5 Hz, 2 H), 7.58 (t, *J*=7.3 Hz, 1 H), 7.47 (t, *J*=7.8 Hz, 2 H), 7.19 - 7.42 (m, 8 H), 7.03 (td, *J*=7.8, 2.4 Hz, 1 H), 5.15 (dd, *J*=4.4, 3.4 Hz, 1 H), 4.48 (d, *J*=11.2 Hz, 1 H), 4.41 (d, *J*=11.2 Hz, 1 H), 3.69 (dd, *J*=16.6, 8.3 Hz, 1 H), 3.17 (dd, *J*=16.6, 4.9 Hz, 1 H);

^{13}C NMR (125 MHz, $CDCl_3$) δ 197.3, 163.2 (d, J = 246.5 Hz), 144.6, 137.9, 137.1, 133.2, 130.2, 128.6, 128.2, 127.8, 122.5, 114.9, 114.8, 113.7, 113.5, 76.8, 71.2, 47.2;

FTIR (neat, cm^{-1}) ν_{max} 1685, 1448, 1094, 1072, 756, 733, 688 cm^{-1};

HRMS (ESI-TOF) calculated for $C_{22}H_{19}O_2F$ $[M+Na]^+$: 357.1267, found: 357. 1283;

$[\alpha]_D^{25}$ = –44.0° (c = 1, $CHCl_3$).

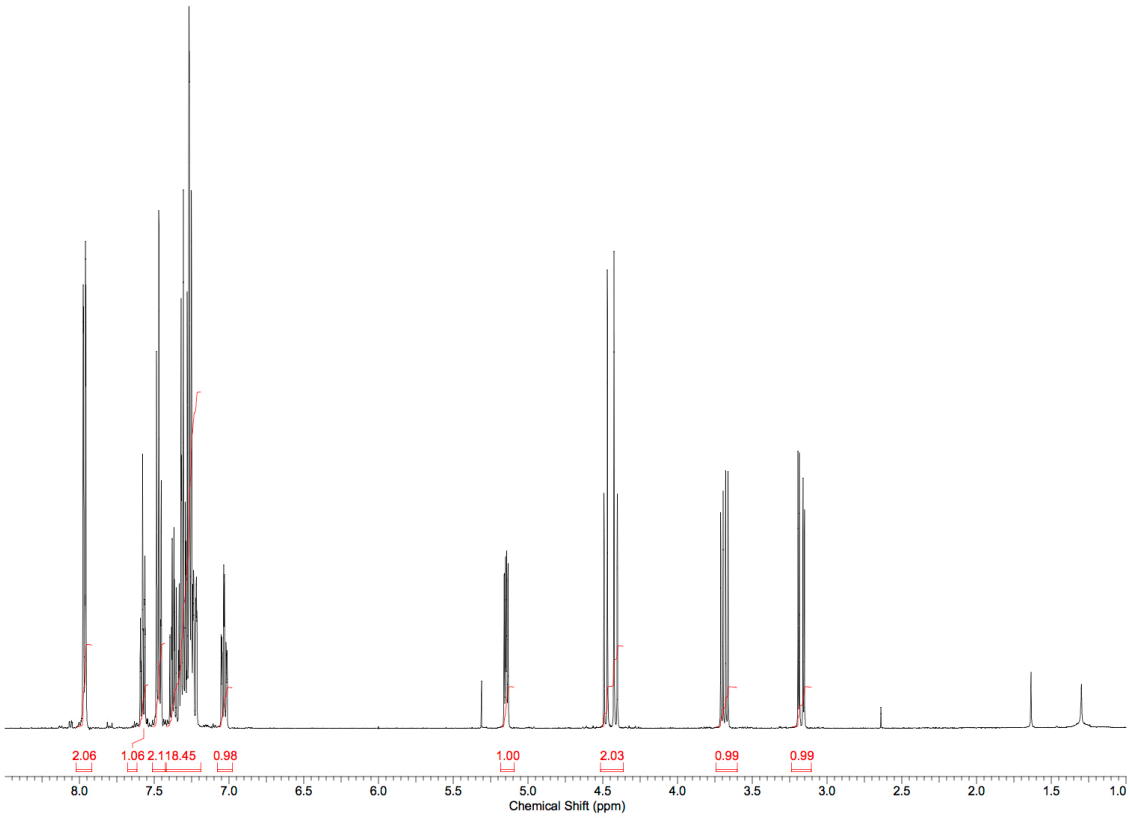
2.06
1.06
2.11
8.45
0.98
1.00
2.03
0.99
0.99
8.0 7.5 7.0 6.5 6.0 5.5 5.0 4.5 4.0 3.5 3.0 2.5 2.0 1.5 1.0
Chemical Shift (ppm)

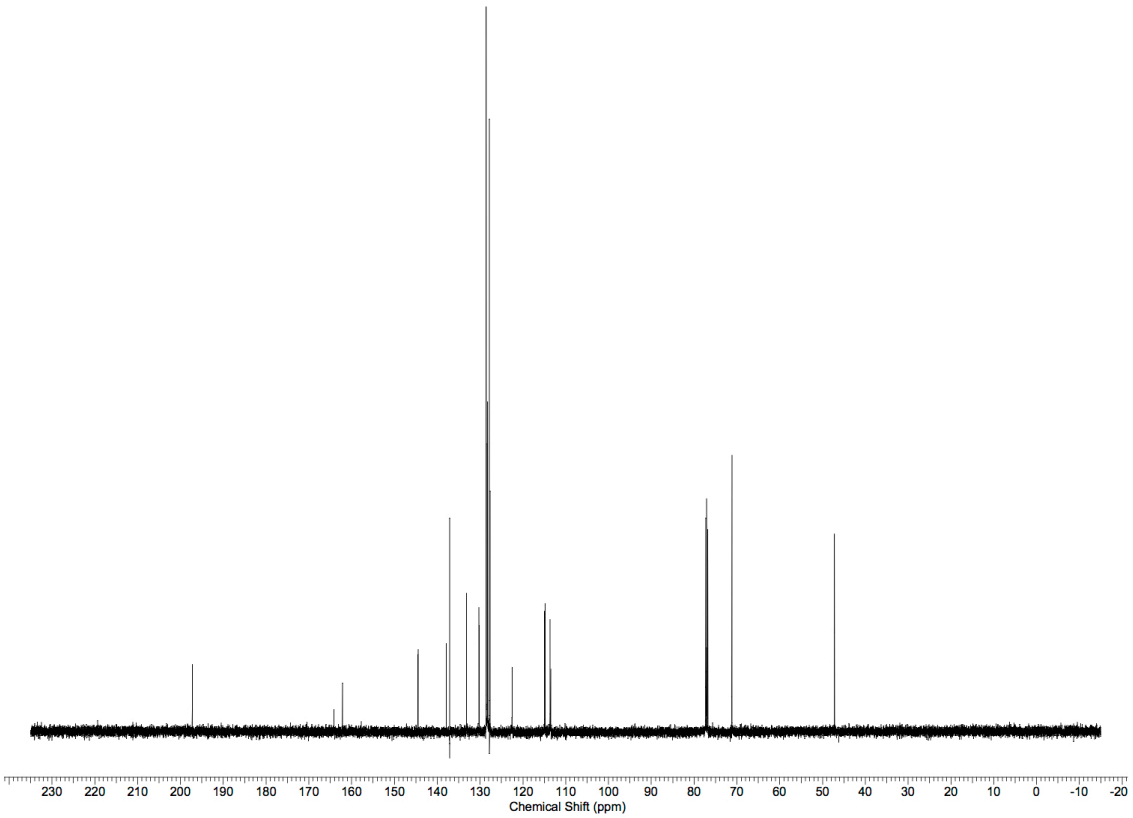
230 220 210 200 190 180 170 160 150 140 130 120 110 100 90 80 70 60 50 40 30 20 10 0 -10 -20
Chemical Shift (ppm)

Racemic sample: HPLC (ChiralPak AS-H, 2% IPA/hexanes, 1 mL/min, 230 nm)

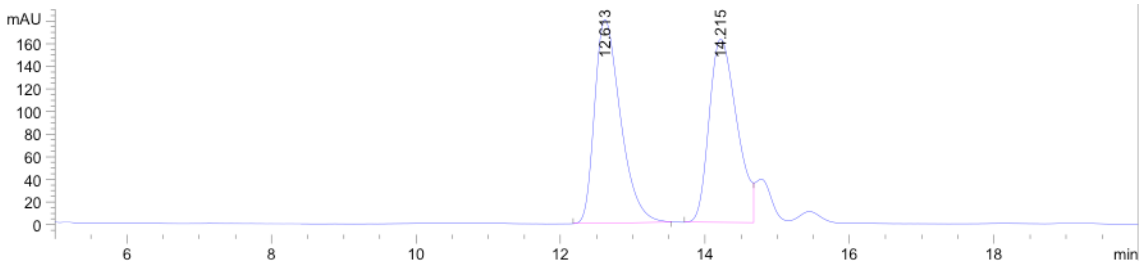

Peak #	RetTime [min]	Type	Width [min]	Area [mAU*s]	Height [mAU]	Area %
1	12.613	BB	0.3836	4506.09863	180.26205	50.9922
2	14.215	BV	0.4153	4330.74316	162.32893	49.0078

Enantioenriched Sample: HPLC (ChiralPak AS-H, 2% IPA/hexanes, 1 mL/min, 230 nm), 93% e.e.

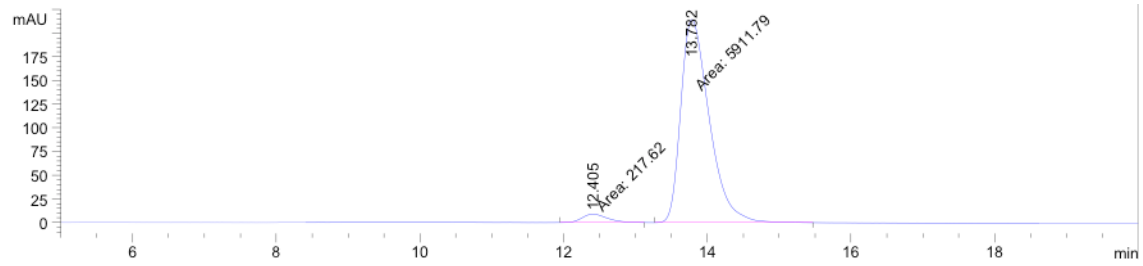

Peak #	RetTime [min]	Type	Width [min]	Area [mAU*s]	Height [mAU]	Area %
1	12.405	MM	0.4042	217.61993	8.97322	3.5504
2	13.782	MM	0.4596	5911.78711	214.40303	96.4496

(*S*)-3-(benzyloxy)-3-(4-fluorophenyl)-1-phenylpropan-1-one (**4d**):

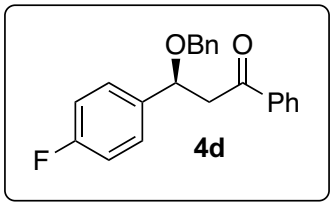

According to general procedure (Method B), **3d** (0.25 mmol) was reacted to give **4d** in 79.3 mg (95% yield) as clear oil.

^{1}H NMR (500 MHz, $CDCl_3$) δ 7.96 (d, J = 7.3 Hz, 2 H), 7.53 - 7.60 (m, 1 H), 7.42 - 7.50 (m, 4 H), 7.21 - 7.33 (m, 5 H), 7.06 - 7.14 (m, 2 H), 5.12 (dd, *J*=7.8, 4.9 Hz, 1 H), 4.42 - 4.47 (m, 1 H), 4.36 - 4.41 (m, 1 H), 3.69 (dd, *J*=16.6, 7.8 Hz, 1 H), 3.19 (m, *J*=16.1, 4.9 Hz, 1 H);

^{13}C NMR (125 MHz, $CDCl_3$) δ 197.5, 162.4 (d, J = 244.1 Hz), 138.0, 137.3, 137.2, 133.2, 128.7, 128.5, 128.3, 128.2, 127.8, 127.6, 115.5, 70.9, 47.3;

FTIR (neat, cm^{-1}) ν_{max} 1685, 1507, 1218, 1092, 835, 734, 689, 553 cm^{-1};

HRMS (ESI-TOF) calculated for $C_{22}H_{19}O_2F$ $[M+Na]^+$: 357.1269, found: 357.1422;

$[\alpha]_D^{25}$ = –33.6° (c = 1, $CHCl_3$).

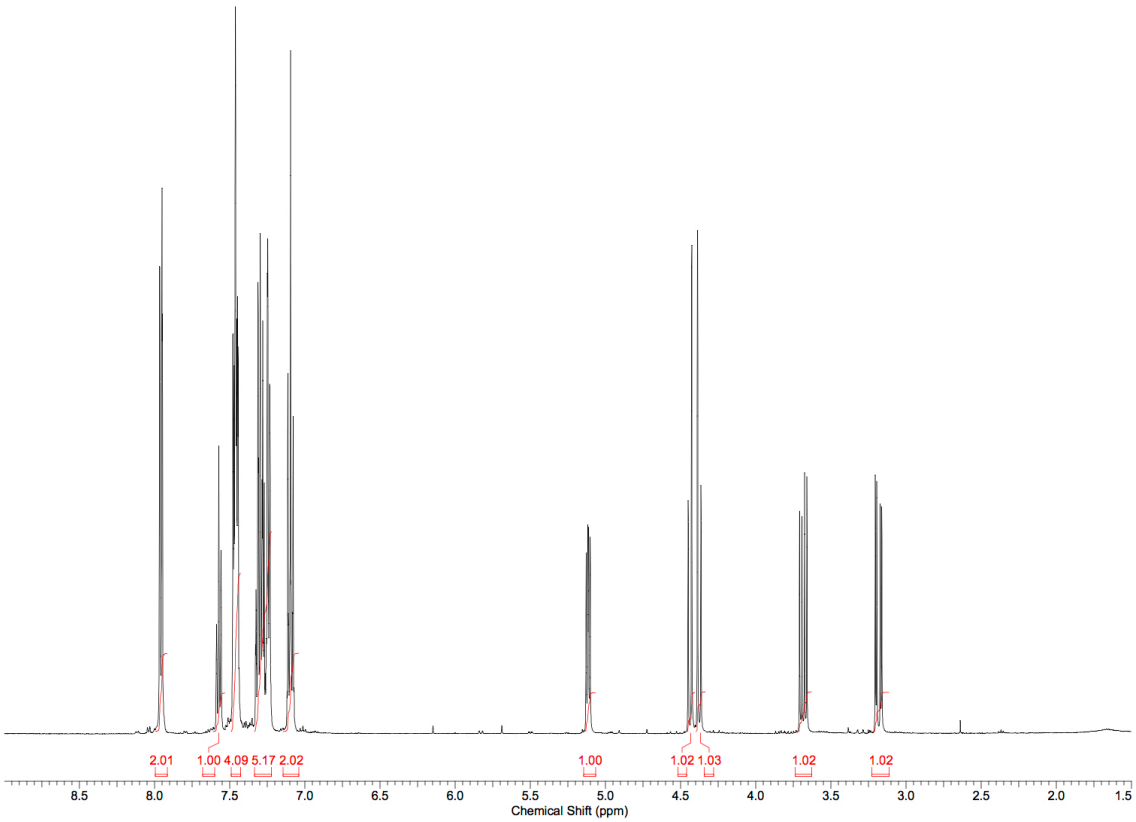
2.01
1.00
4.09
5.17
2.02
1.00
1.02
1.03
1.02
1.02
8.5
8.0
7.5
7.0
6.5
6.0
5.5
5.0
4.5
4.0
3.5
3.0
2.5
2.0
1.5
Chemical Shift (ppm)

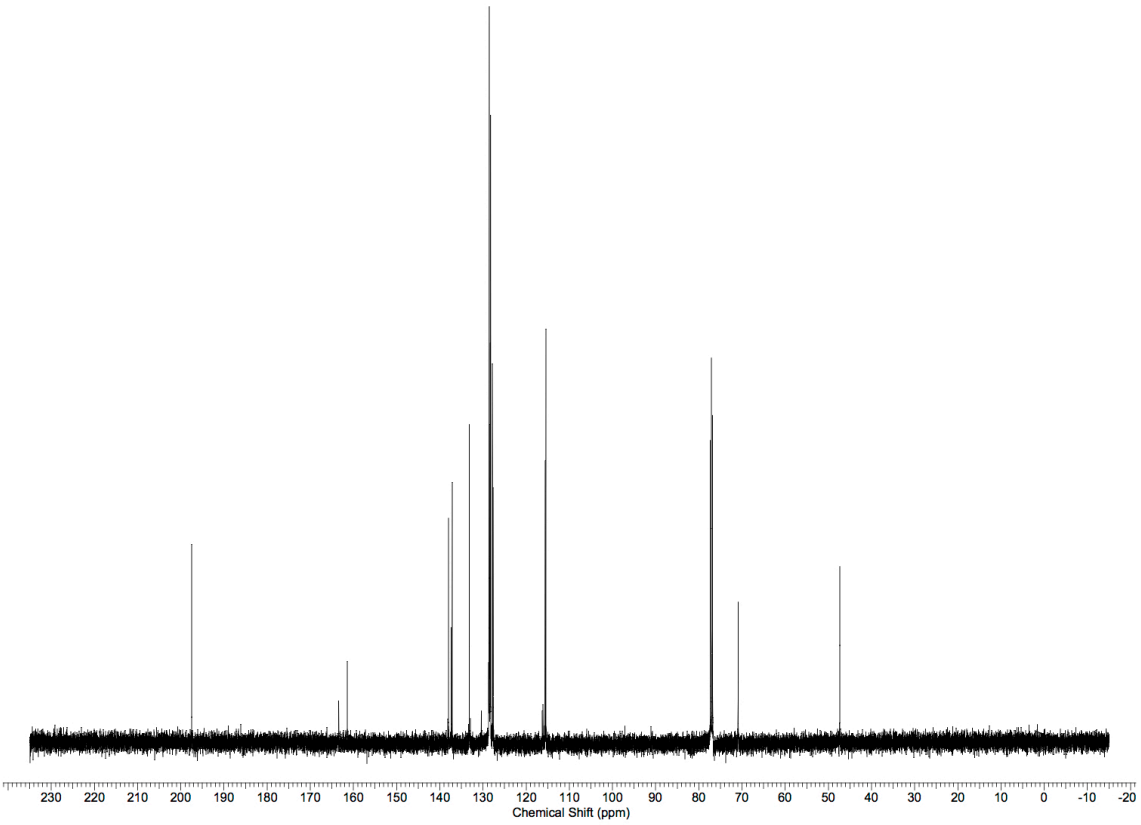
230
220
210
200
190
180
170
160
150
140
130
120
110
100
90
80
70
60
50
40
30
20
10
0
-10
-20
Chemical Shift (ppm)

Racemic sample: HPLC (ChiralPak AS-H, 2% IPA/hexanes, 1 mL/min, 210 nm)

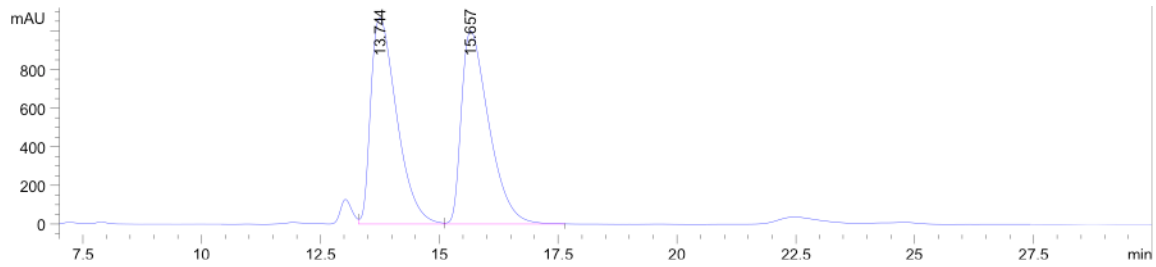

Peak #	RetTime [min]	Type	Width [min]	Area [mAU*s]	Height [mAU]	Area %
1	13.744	VV	0.5935	4.07314e4	1066.71155	50.2619
2	15.657	VB	0.6145	4.03068e4	999.38745	49.7381

Enantioenriched Sample: HPLC (ChiralPak AS-H, 2% IPA/hexanes, 1 mL/min, 210 nm), 58% e.e.

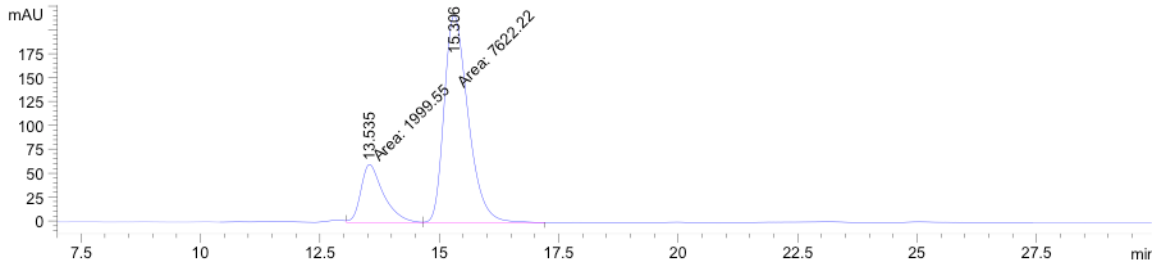

Peak #	RetTime [min]	Type	Width [min]	Area [mAU*s]	Height [mAU]	Area %
1	13.535	FM	0.5490	1999.54956	60.69805	20.7815
2	15.306	FM	0.5857	7622.22461	216.91263	79.2185

(*S*)-3-(benzyloxy)-3-(4-chlorophenyl)-1-phenylpropan-1-one (**4e**):

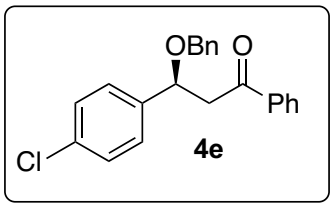

According to general procedure (Method B), **3e** (0.125 mmol) was reacted to give **4e** in 42.2 mg (96% yield) as pale yellow oil.

^{1}H NMR (500 MHz, $CDCl_3$) δ 7.96 (d, *J*=6.8 Hz, 2 H), 7.54 - 7.61 (m, 2 H), 7.41 - 7.50 (m, 4 H), 7.37 - 7.41 (m, 2 H), 7.23 - 7.33 (m, 5 H), 5.12 (dd, *J*=7.8, 4.9 Hz, 1 H), 4.43 - 4.47 (m, 1 H), 4.37 - 4.41 (m, 1 H), 3.65 - 3.72 (m, 1 H), 3.18 (dd, *J*=16.6, 5.4 Hz, 1 H);

^{13}C NMR (125 MHz, $CDCl_3$) δ 197.3, 140.2, 137.9, 137.1, 133.7, 133.2, 128.9, 128.6, 128.4, 128.3, 128.2, 127.8, 127.7, 77.1, 71.0, 47.2;

FTIR (neat, cm^{-1}) ν_{max} 1685, 1088, 1073, 1013, 826, 732, 688 cm^{-1};

HRMS (ESI-TOF) calculated for $C_{22}H_{19}O_2Cl$ $[M+Na]^+$: 373.0971, found: 373.1009;

$[\alpha]_D^{25}$ = –38.5° (c = 1, $CHCl_3$).

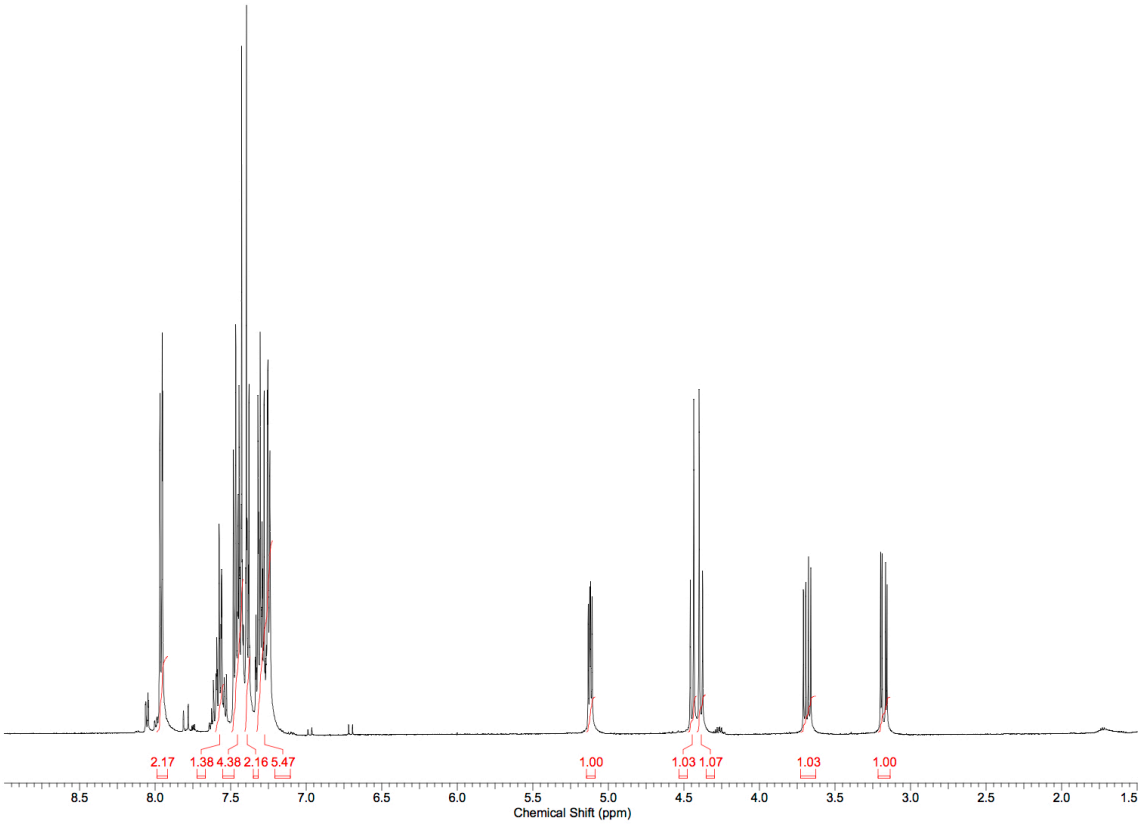
2.17
1.38
4.38
2.16
5.47
1.00
1.03
1.07
1.03
1.00
Chemical Shift (ppm)

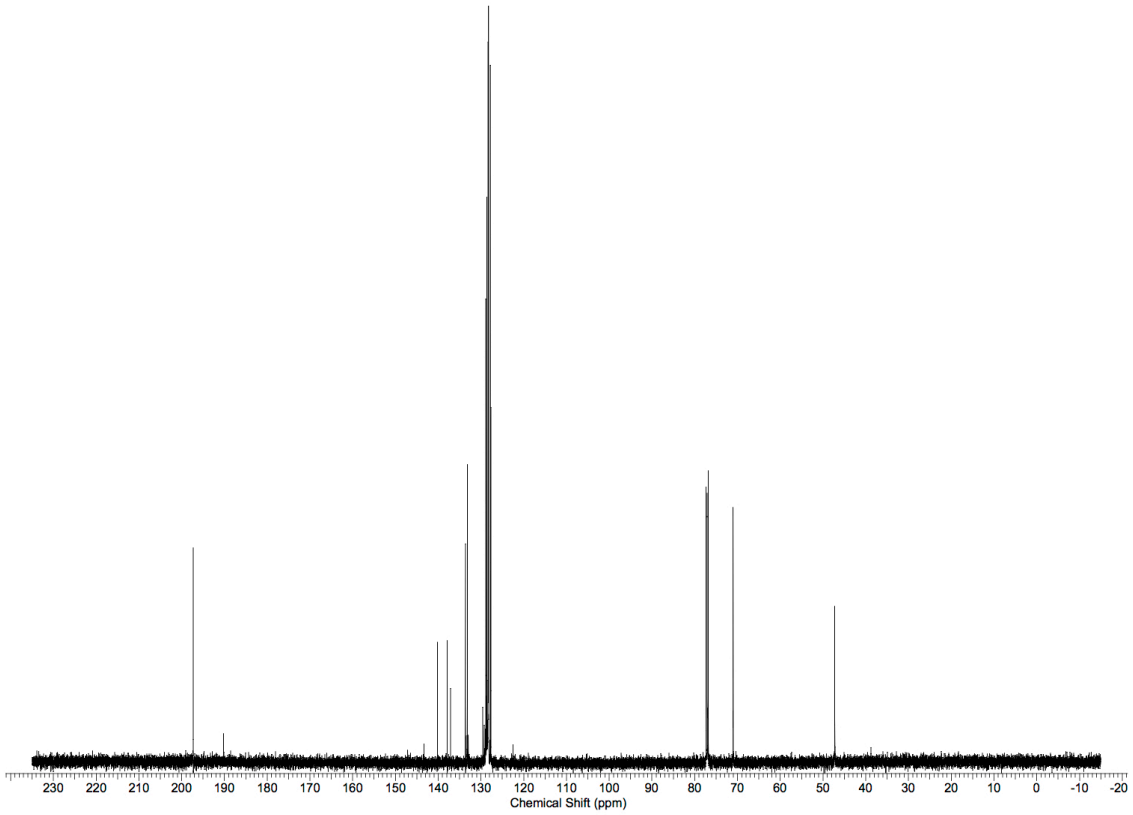
Chemical Shift (ppm)

Racemic sample: HPLC (ChiralPak OD-H, 2% IPA/hexanes, 1 mL/min, 210 nm)

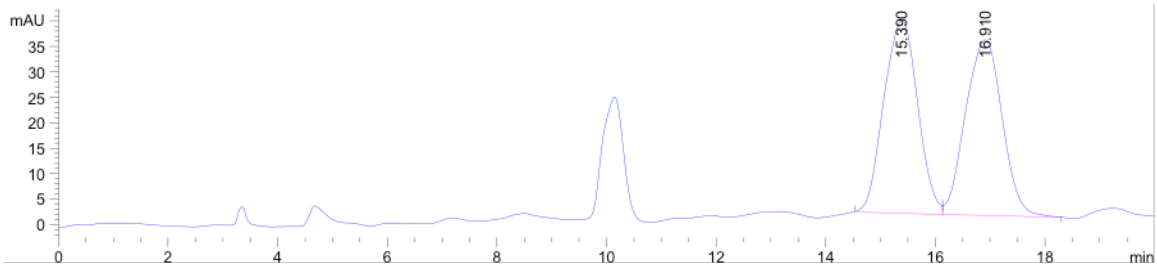

Peak #	RetTime [min]	Type	Width [min]	Area [mAU*s]	Height [mAU]	Area %
1	15.390	BV	0.6915	1633.03088	37.99159	50.3767
2	16.910	VB	0.7517	1608.60852	34.51785	49.6233

Enantioenriched Sample: HPLC (ChiralPak OD-H, 2% IPA/hexanes, 1 mL/min, 210 nm), 79% e.e.

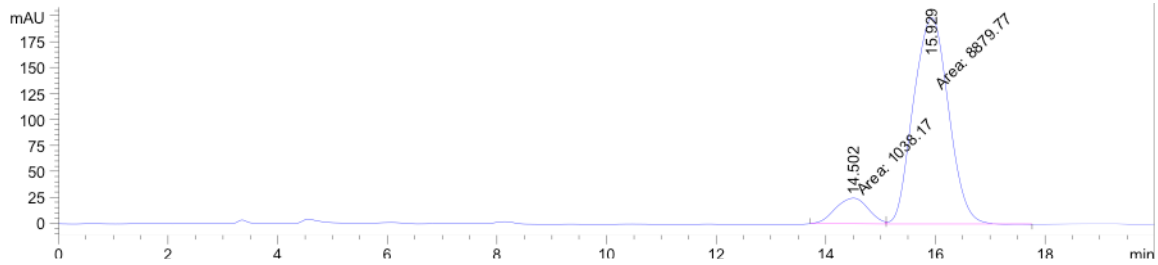

Peak #	RetTime [min]	Type	Width [min]	Area [mAU*s]	Height [mAU]	Area %
1	14.502	MF	0.6959	1038.17065	24.86362	10.4676
2	15.929	FM	0.7432	8879.77051	199.14661	89.5324

(*S*)-3-(benzyloxy)-1-phenyl-3-(4-(trifluoromethoxy)phenyl)propan-1-one (**4f**):

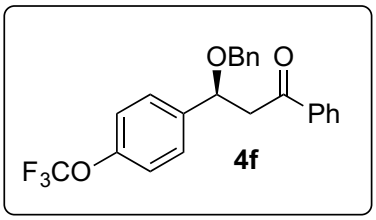

According to general procedure (Method B), **3f** (0.25 mmol) was reacted to give **4f** in 97.5 mg (97% yield) as clear oil.

^{1}H NMR (500 MHz, $CDCl_3$) δ 7.97 (d, *J*=7.8 Hz, 2 H), 7.58 (t, *J*=7.3 Hz, 1 H), 7.53 (d, *J*=8.3 Hz, 2 H), 7.47 (t, *J*=7.3 Hz, 2 H), 7.24 - 7.35 (m, 7 H), 5.17 (dd, *J*=7.8, 4.9 Hz, 1 H), 4.47 (d, *J*=11.2 Hz, 1 H), 4.42 (d, *J*=11.7 Hz, 1 H), 3.70 (dd, *J*=16.6, 7.8 Hz, 1 H), 3.19 (dd, *J*=16.6, 4.9 Hz, 1 H);

^{13}C NMR (125 MHz, $CDCl_3$) δ 197.3, 148.8, 140.5, 137.9, 137.1, 133.2, 128.6, 128.5, 128.4, 128.3, 128.2, 127.8, 127.7, 121.2, 76.8, 71.2, 47.3;

FTIR (neat, cm^{-1}) ν_{max} 1253, 1205, 1156, 1093, 736, 688 cm^{-1};

HRMS (ESI-TOF) calculated for $C_{23}H_{19}O_3F_3$ $[M+Na]^+$: 423.1184, found: 423.1188;

$[\alpha]_D^{25}$ = –37.2° (c = 1, $CHCl_3$).

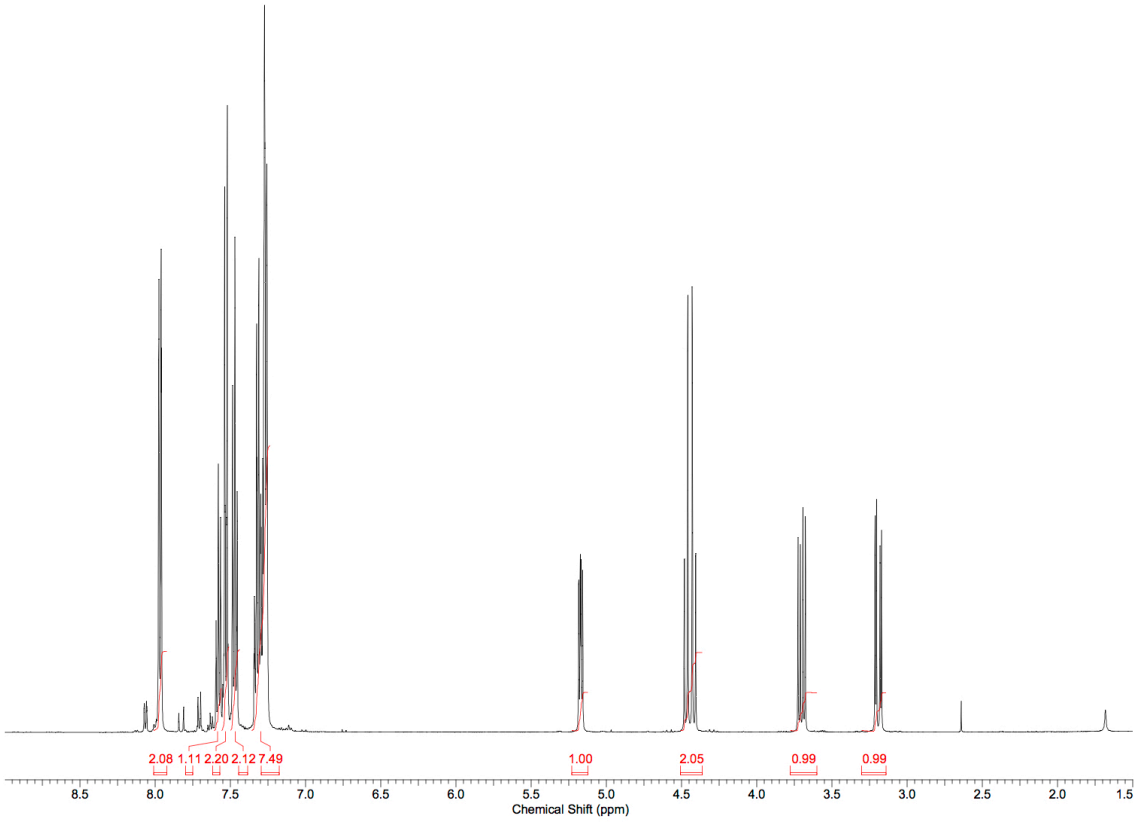
2.08
1.11
2.20
2.12
7.49
1.00
2.05
0.99
0.99
8.5
8.0
7.5
7.0
6.5
6.0
5.5
5.0
4.5
4.0
3.5
3.0
2.5
2.0
1.5
Chemical Shift (ppm)

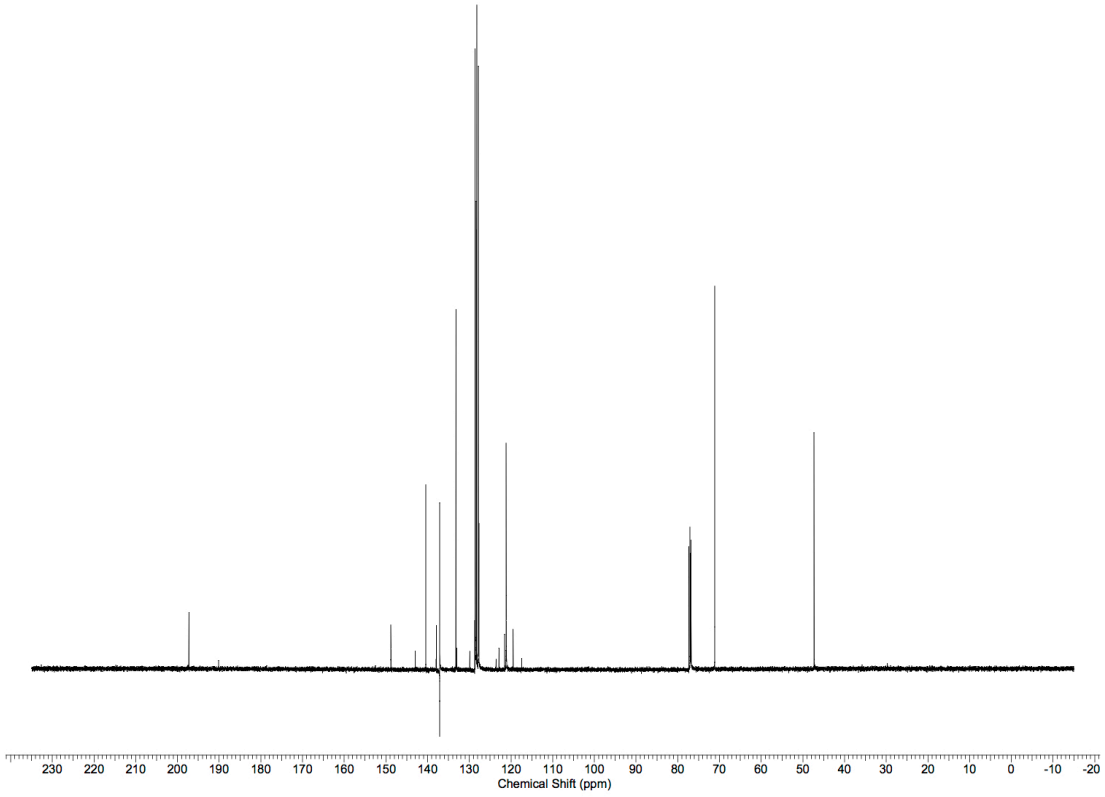
230
220
210
200
190
180
170
160
150
140
130
120
110
100
90
80
70
60
50
40
30
20
10
0
-10
-20
Chemical Shift (ppm)

Racemic sample: HPLC (ChiralPak IB, 2% IPA/hexanes, 1 mL/min, 210 nm)

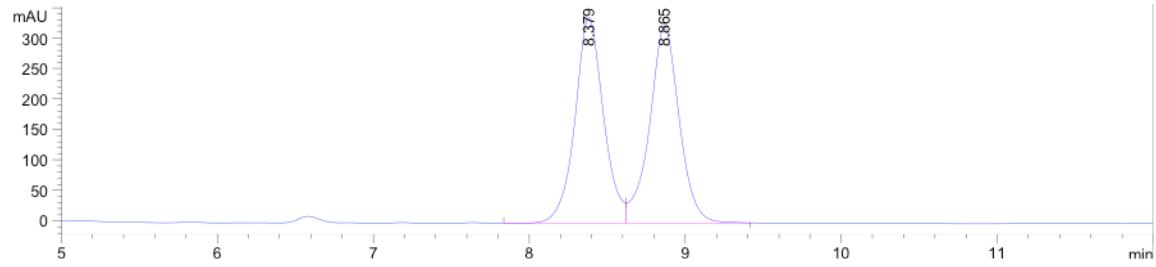

Peak #	RetTime [min]	Type	Width [min]	Area [mAU*s]	Height [mAU]	Area %
1	8.379	VV	0.1907	4313.43945	338.45700	49.9997
2	8.865	VB	0.1995	4313.49219	323.68427	50.0003

Enantioenriched Sample: HPLC (ChiralPak IB, 2% IPA/hexanes, 1 mL/min, 210 nm), 89% e.e.

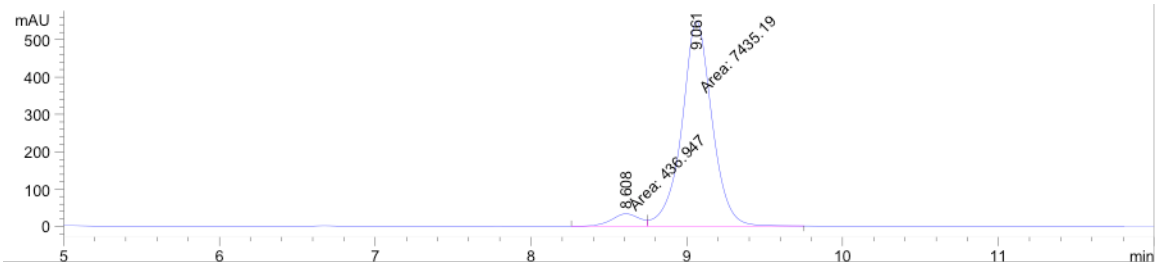

Peak #	RetTime [min]	Type	Width [min]	Area [mAU*s]	Height [mAU]	Area %
1	8.608	MF	0.2157	436.94669	33.75583	5.5505
2	9.061	FM	0.2253	7435.18652	549.91742	94.4495

(*S*)-3-(benzyloxy)-3-(3-bromophenyl)-1-phenylpropan-1-one (**4g**):

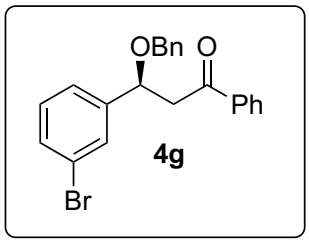

According to general procedure (Method B), **3g** (0.25 mmol) was reacted to give **4g** in 49.4 mg (50% yield) as clear oil.

^{1}H NMR (500 MHz, $CDCl_3$) δ 7.96 (d, *J*=6.8 Hz, 4 H), 7.65 (s, 2 H), 7.58 (t, *J*=7.3 Hz, 2 H), 7.43 - 7.51 (m, 6 H), 7.41 (d, *J*=7.8 Hz, 2 H), 7.21 - 7.36 (m, 13 H), 5.10 (dd, *J*=8.3, 4.9 Hz, 2 H), 4.46 (d, *J*=11.7 Hz, 1 H), 4.40 (d, *J*=11.2 Hz, 1 H), 3.68 (dd, *J*=16.6, 8.3 Hz, 2 H), 3.15 (dd, *J*=16.6, 4.9 Hz, 2 H);

^{13}C NMR (125 MHz, $CDCl_3$) δ 197.2, 144.2, 137.8, 137.1, 133.2, 131.1, 130.3, 129.8, 128.8, 128.6, 128.3, 127.8, 127.7, 125.6, 122.9, 76.8, 71.2, 47.2;

FTIR (neat, cm^{-1}) ν_{max} 1685, 1201, 1096, 1069, 985, 751, 689 cm^{-1};

HRMS (ESI-TOF) calculated for $C_{22}H_{19}O_2Br$ $[M+Na]^+$: 417.0466, found: 417.0491;

$[\alpha]_D^{25}$ = –44.4° (c = 1, $CHCl_3$).

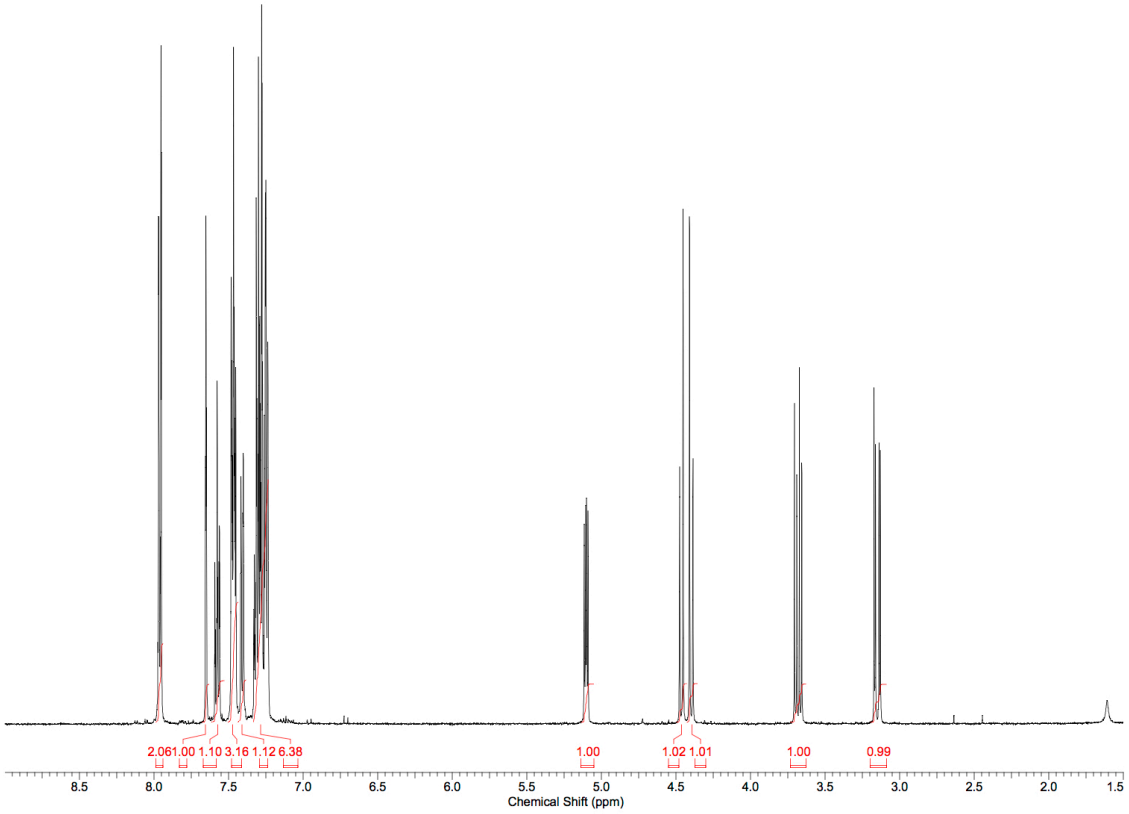
2.06 1.00 1.10 3.16 1.12 6.38
1.00
1.02 1.01
1.00
0.99
8.5 8.0 7.5 7.0 6.5 6.0 5.5 5.0 4.5 4.0 3.5 3.0 2.5 2.0 1.5
Chemical Shift (ppm)

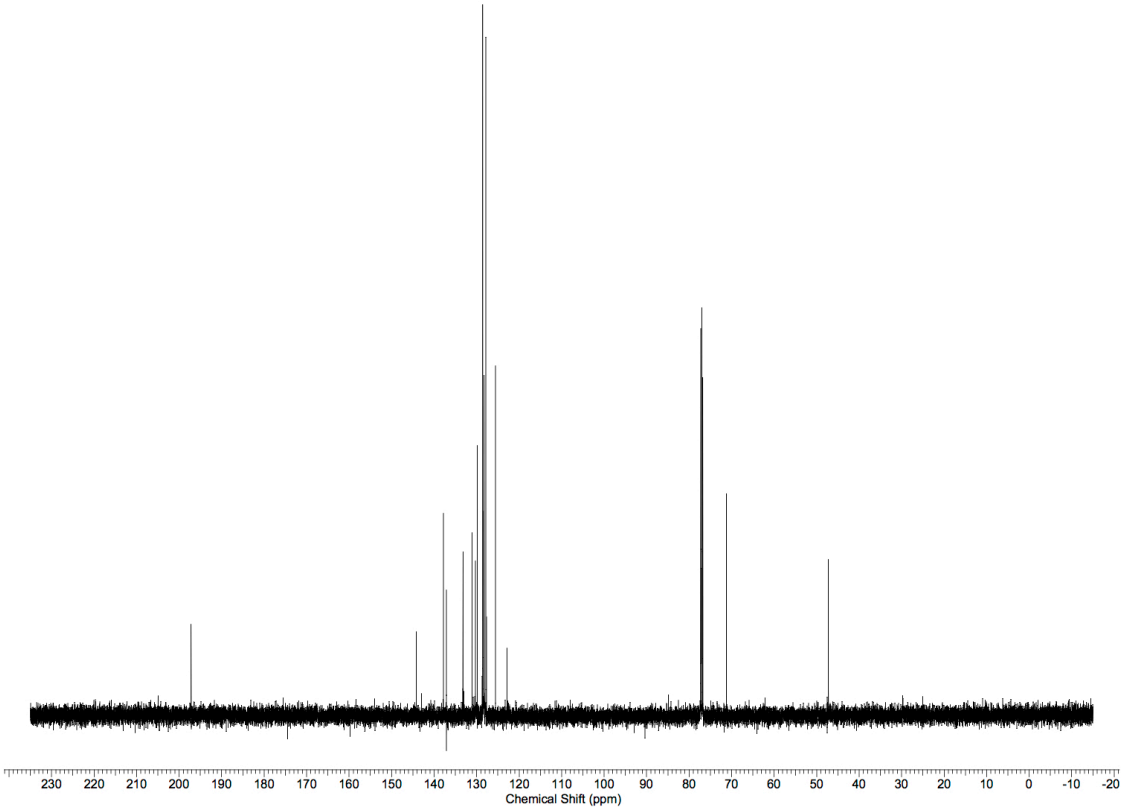
230 220 210 200 190 180 170 160 150 140 130 120 110 100 90 80 70 60 50 40 30 20 10 0 -10 -20
Chemical Shift (ppm)

Racemic sample: HPLC (ChiralPak AS-H, 2% IPA/hexanes, 1 mL/min, 210 nm)

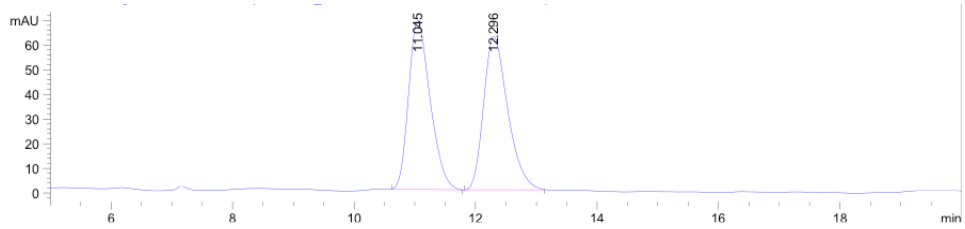

Peak #	RetTime [min]	Type	Width [min]	Area [mAU*s]	Height [mAU]	Area %
1	11.045	BB	0.3770	1699.53772	68.61494	49.6561
2	12.296	BB	0.4206	1723.08130	62.31678	50.3439

Enantioenriched Sample: HPLC (ChiralPak AS-H, 2% IPA/hexanes, 1 mL/min, 210 nm), 96% e.e.

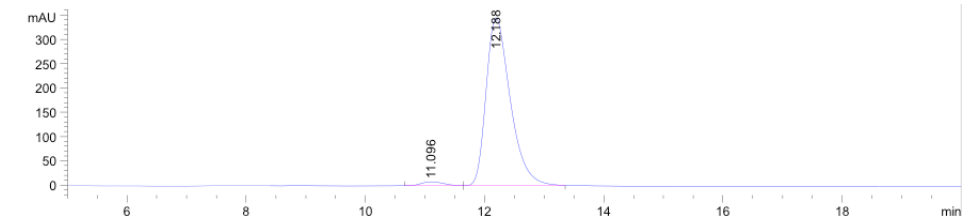

Peak #	RetTime [min]	Type	Width [min]	Area [mAU*s]	Height [mAU]	Area %
1	11.096	BV	0.4112	206.46085	8.05096	2.0817
2	12.188	VB	0.4302	9711.53223	345.20956	97.9183

Enantioenriched Sample for reaction at -65 ˚C: HPLC (ChiralPak AS-H, 2% IPA/hexanes, 1 mL/min, 210 nm), 94% e.e.

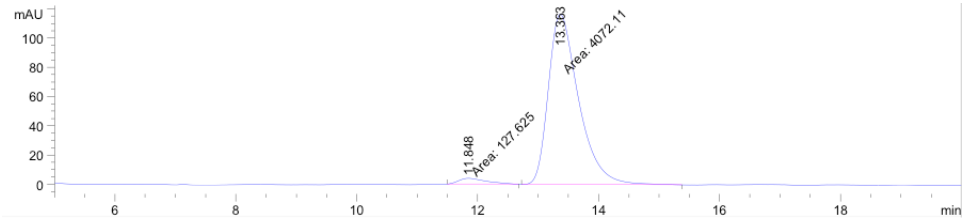

Peak #	RetTime [min]	Type	Width [min]	Area [mAU*s]	Height [mAU]	Area %
1	11.848	MM	0.5340	127.62542	3.98314	3.0389
2	13.363	FM	0.5814	4072.10718	116.72292	96.9611

(*S*)-3-(benzyloxy)-3-(3-chlorophenyl)-1-phenylpropan-1-one (**4h**):

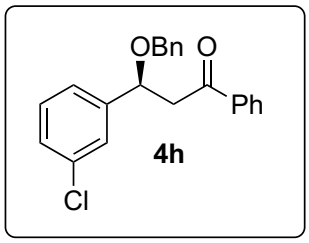

4h

According to general procedure (Method B), **3h** (0.25 mmol) was reacted to give **4h** in 48.1 mg (55% yield) as white amorphous solid.

^{1}H NMR (500 MHz, $CDCl_3$) δ 7.96 (dd, *J*=8.3, 1.0 Hz, 2 H), 7.58 (t, *J*=7.3 Hz, 1 H), 7.47 (dd, *J*=14.6, 6.8 Hz, 3 H), 7.22 - 7.38 (m, 8 H), 5.11 (dd, *J*=8.3, 4.9 Hz, 1 H), 4.47 (d, *J*=11.2 Hz, 1 H), 4.40 (d, *J*=11.2 Hz, 1 H), 3.68 (dd, *J*=16.6, 8.3 Hz, 1 H), 3.16 (dd, *J*=16.1, 4.4 Hz, 1 H);

^{13}C NMR (125 MHz, $CDCl_3$) δ 197.2, 143.9, 137.8, 137.1, 134.7, 133.2, 130.0, 128.6, 128.3, 128.2, 128.1, 127.8, 127.7, 126.9, 125.1, 76.8, 71.2, 47.2;

FTIR (neat, cm^{-1}) ν_{max} 1686, 1202, 1097, 1075, 754, 691 cm^{-1};

HRMS (ESI-TOF) calculated for $C_{22}H_{19}O_2Cl$ $[M+Na]^+$: 373.0971, found: 373.1018;

$[\alpha]_D^{25}$ = –27.2° (c = 1, $CHCl_3$).

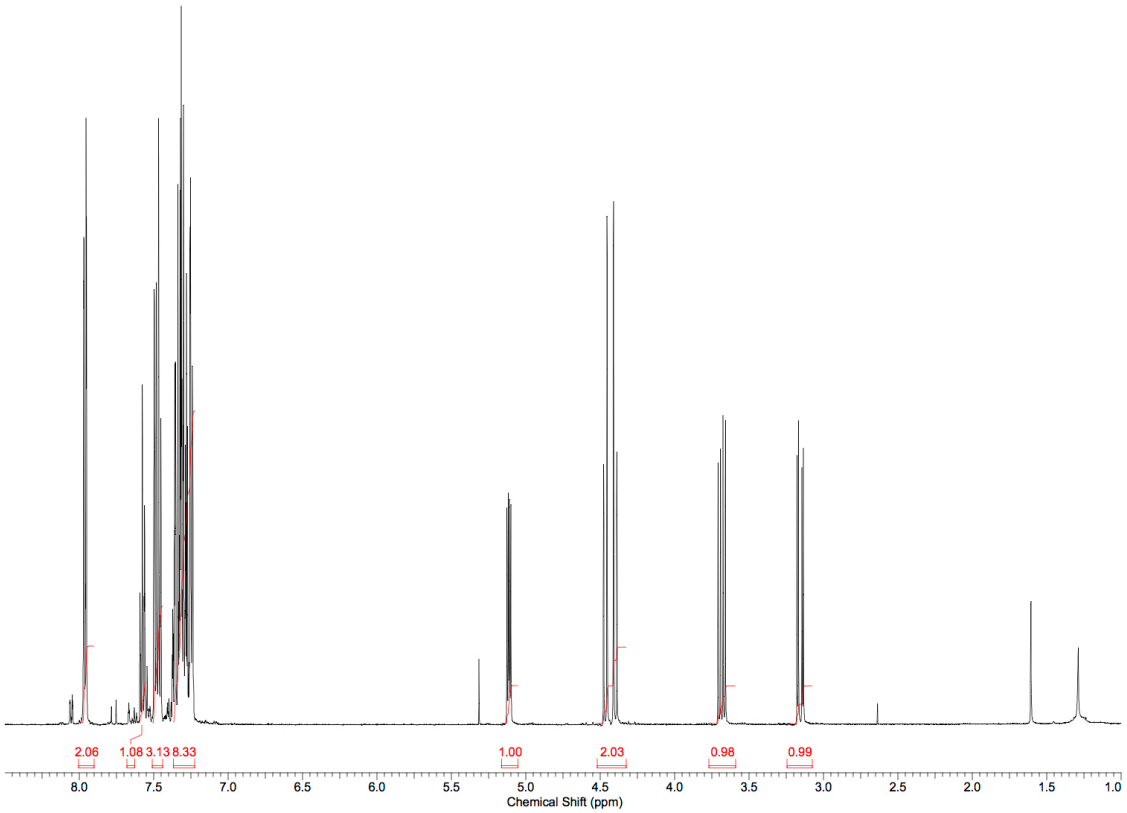
2.06
1.08
3.13
8.33
1.00
2.03
0.98
0.99
8.0
7.5
7.0
6.5
6.0
5.5
5.0
4.5
4.0
3.5
3.0
2.5
2.0
1.5
1.0
Chemical Shift (ppm)

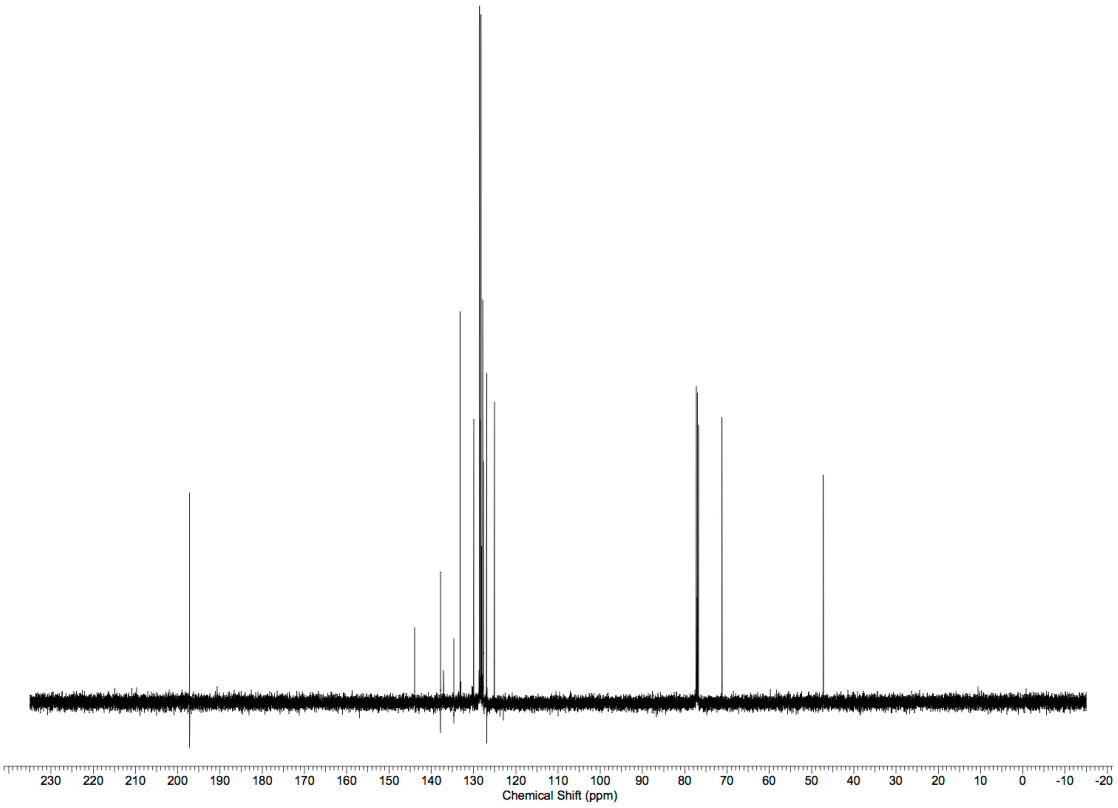
230
220
210
200
190
180
170
160
150
140
130
120
110
100
90
80
70
60
50
40
30
20
10
0
-10
-20
Chemical Shift (ppm)

Racemic sample: HPLC (ChiralPak AS-H, 2% IPA/hexanes, 1 mL/min, 210 nm)

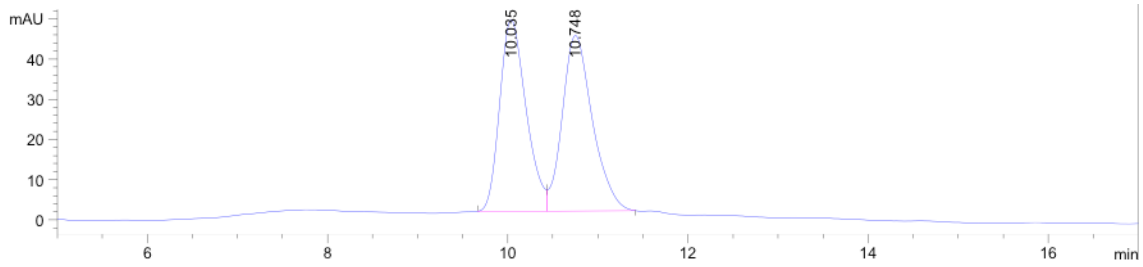

Peak #	RetTime [min]	Type	Width [min]	Area [mAU*s]	Height [mAU]	Area %
1	10.035	BV	0.3123	975.64996	47.76474	48.8281
2	10.748	VB	0.3527	1022.48236	43.74928	51.1719

Enantioenriched Sample: HPLC (ChiralPak AS-H, 2% IPA/hexanes, 1 mL/min, 210 nm), 97% e.e.

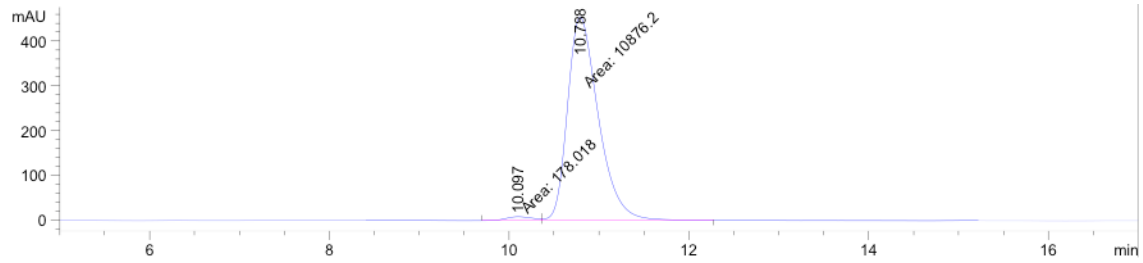

Peak #	RetTime [min]	Type	Width [min]	Area [mAU*s]	Height [mAU]	Area %
1	10.097	MF	0.3441	178.01784	8.62135	1.6104
2	10.788	FM	0.3990	1.08762e4	454.36133	98.3896

(*S*)-3-(benzyloxy)-3-(2-fluorophenyl)-1-phenylpropan-1-one (**4i**):

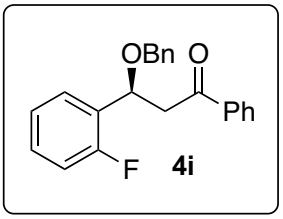

4i

According to general procedure (Method B), **3i** (0.25 mmol) was reacted to give **4i** in 44.5 mg (53% yield) as clear oil.

^{1}H NMR (500 MHz, $CDCl_3$) δ 7.99 (dd, *J*=8.3, 1.0 Hz, 2 H), 7.54 - 7.62 (m, 2 H), 7.47 (t, *J*=7.8 Hz, 2 H), 7.18 - 7.36 (m, 7 H), 7.10 (ddd, *J*=10.3, 8.3, 1.0 Hz, 1 H), 5.48 (dd, *J*=8.8, 3.9 Hz, 1 H), 4.43 - 4.52 (m, 2 H), 3.67 (dd, *J*=16.6, 8.8 Hz, 1 H), 3.26 (dd, *J*=16.1, 3.9 Hz, 1 H);

^{13}C NMR (125 MHz, $CDCl_3$) δ 197.2, 160.5 (d, J = 245.1 Hz), 137.9, 137.1, 133.1, 129.4, 129.3, 128.6, 128.4, 128.3, 128.2, 128.1, 128.2, 127.6, 124.5, 124.4, 115.7, 115.5, 71.8, 71.5, 45.9;

FTIR (neat, cm^{-1}) ν_{max} 1686, 1449, 1203, 1091, 1057, 756, 689 cm^{-1};

HRMS (ESI-TOF) calculated for $C_{22}H_{19}O_2F$ $[M+Na]^+$: 357.1267, found: 357.1206;

$[\alpha]_D^{25}$ = –47.8° (c = 1, $CHCl_3$).

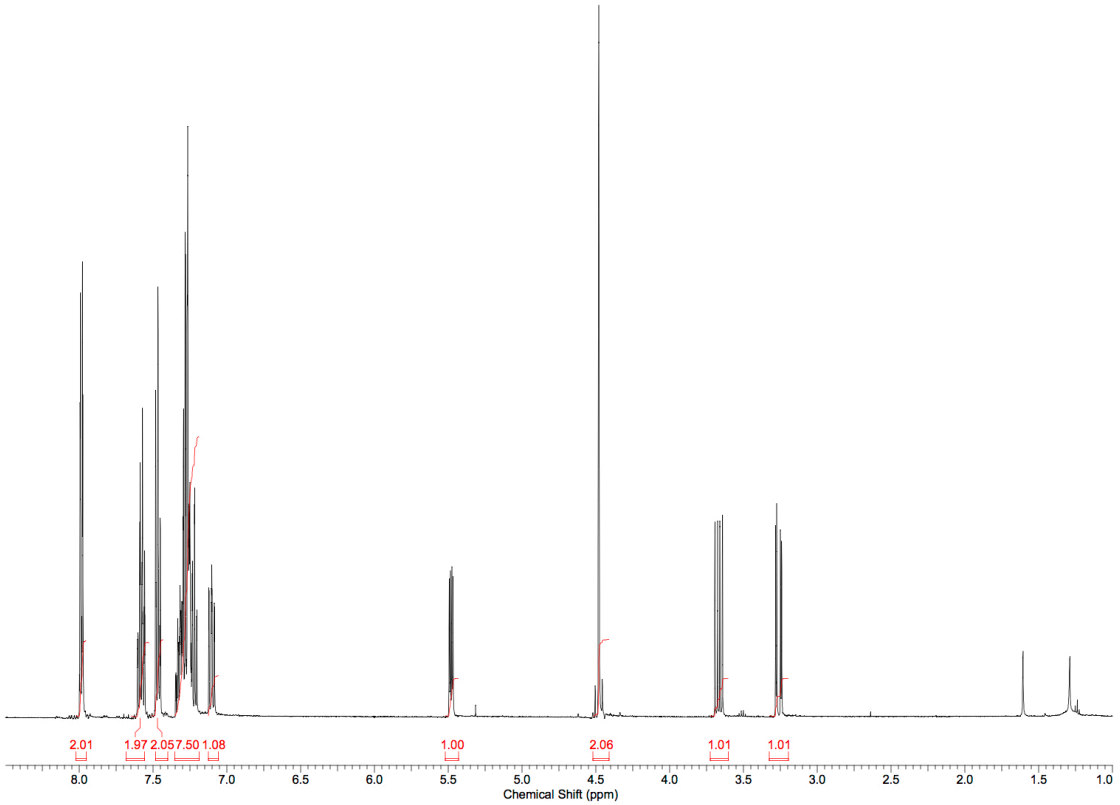
2.01
1.97
2.05
7.50
1.08
1.00
2.06
1.01
1.01
8.0
7.5
7.0
6.5
6.0
5.5
5.0
4.5
4.0
3.5
3.0
2.5
2.0
1.5
1.0
Chemical Shift (ppm)

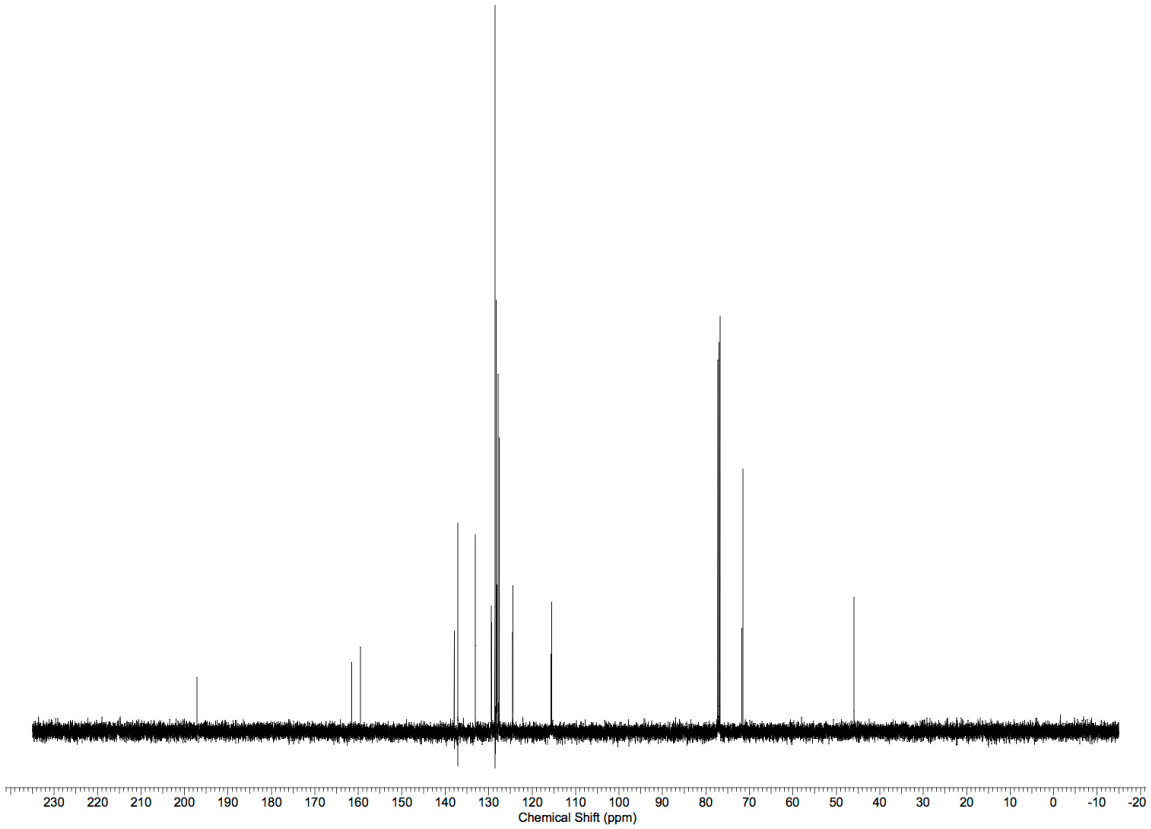
230
220
210
200
190
180
170
160
150
140
130
120
110
100
90
80
70
60
50
40
30
20
10
0
-10
-20
Chemical Shift (ppm)

Racemic sample: HPLC (ChiralPak IA, 2% IPA/hexanes, 1 mL/min, 210 nm)

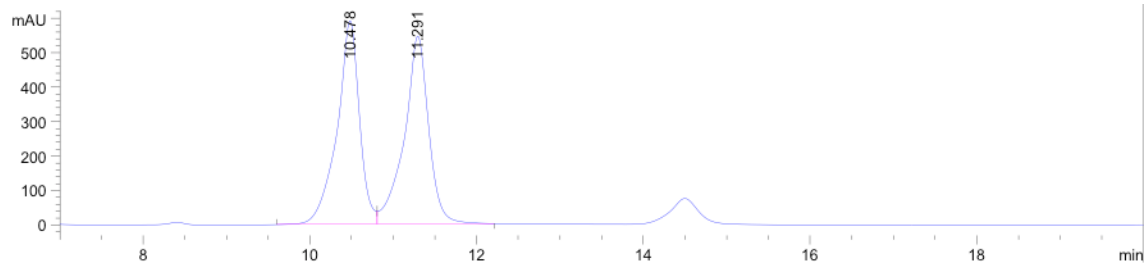

Peak #	RetTime [min]	Type	Width [min]	Area [mAU*s]	Height [mAU]	Area %
1	10.478	BV	0.2689	1.11007e4	591.52356	49.8176
2	11.291	VB	0.2928	1.11819e4	546.24030	50.1824

Enantioenriched Sample: HPLC (ChiralPak IA, 2% IPA/hexanes, 1 mL/min, 210 nm), 96% e.e.

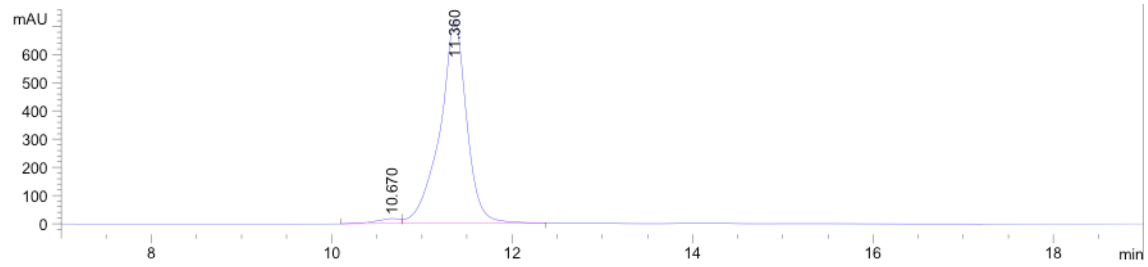

Peak #	RetTime [min]	Type	Width [min]	Area [mAU*s]	Height [mAU]	Area %
1	10.670	BV	0.2602	152.76578	8.24335	2.1276
2	11.360	VB	0.2902	7027.43994	344.13901	97.8724

(*S*)-3-(benzyloxy)-3-(4-bromophenyl)-1-(4-fluorophenyl)propan-1-one (**9a**):

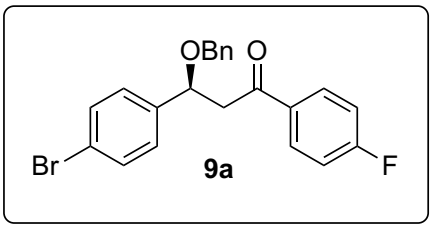

9a

According to general procedure (Method B), **3b** (0.25 mmol) was reacted to give **9a** in 100.2 mg (97% yield) as clear oil.

^{1}H NMR (500 MHz, $CDCl_3$) δ 7.98 (dd, *J*=8.8, 5.4 Hz, 2 H), 7.54 (d, *J*=8.3 Hz, 2 H), 7.36 (d, *J*=8.3 Hz, 2 H), 7.27 - 7.34 (m, 3 H), 7.21 - 7.25 (m, 2 H), 7.13 (t, *J*=8.3 Hz, 2 H), 5.08 (dd, *J*=7.8, 4.9 Hz, 1 H), 4.44 (d, *J*=11.7 Hz, 1 H), 4.37 (d, *J*=11.2 Hz, 1 H), 3.64 (dd, *J*=16.6, 7.8 Hz, 1 H), 3.11 (dd, *J*=16.1, 4.4 Hz, 1 H);

^{13}C NMR (125 MHz, $CDCl_3$) δ 195.7, 165.8 (d, J = 255.8 Hz), 140.6, 137.8, 133.6, 131.9, 131.0, 130.9, 128.6, 128.4, 127.8,121.9, 115.8, 115.6, 71.1, 47.1;

FTIR (neat, cm^{-1}) ν_{max} 1595, 1155, 1069, 1010, 819, 697 cm^{-1};

HRMS (ESI-TOF) calculated for $C_{22}H_{18}O_2FBr$ $[M+Na]^+$: 435.0372, found: 435.0382;

$[\alpha]_D^{25}$ = –42.0° (c = 1, $CHCl_3$).

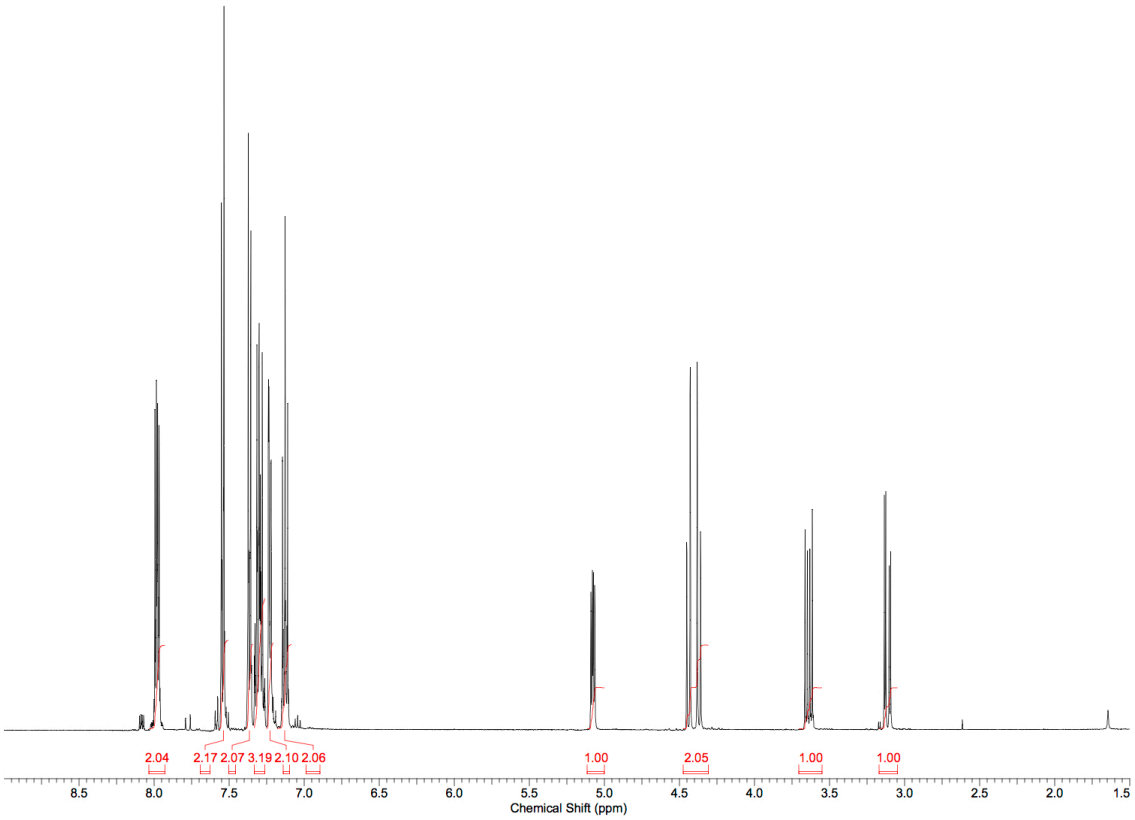
2.04
2.17
2.07
3.19
2.10
2.06
1.00
2.05
1.00
1.00
8.5
8.0
7.5
7.0
6.5
6.0
5.5
5.0
4.5
4.0
3.5
3.0
2.5
2.0
1.5
Chemical Shift (ppm)

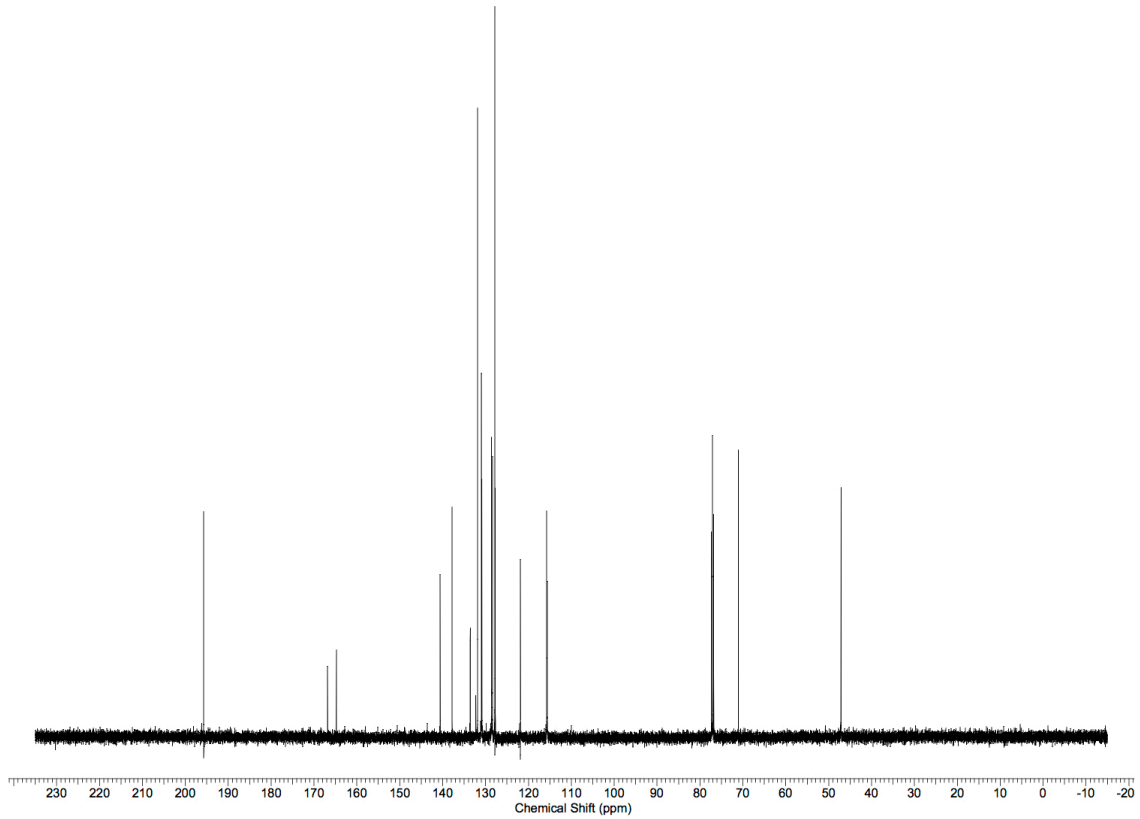
230
220
210
200
190
180
170
160
150
140
130
120
110
100
90
80
70
60
50
40
30
20
10
0
-10
-20
Chemical Shift (ppm)

Racemic sample: HPLC (ChiralPak OD-H, 2% IPA/hexanes, 1 mL/min, 210 nm)

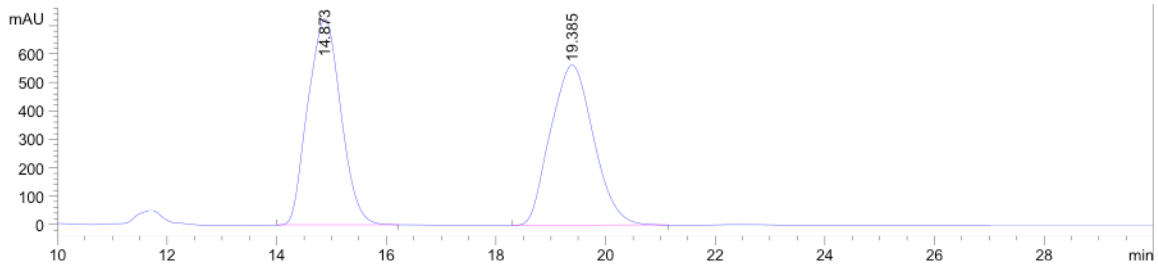

Peak #	RetTime [min]	Type	Width [min]	Area [mAU*s]	Height [mAU]	Area %
1	14.873	BB	0.6895	3.03474e4	726.25616	49.6059
2	19.385	BB	0.9016	3.08296e4	564.13690	50.3941

Enantioenriched Sample: HPLC (ChiralPak OD-H, 2% IPA/hexanes, 1 mL/min, 210 nm), 89% e.e.

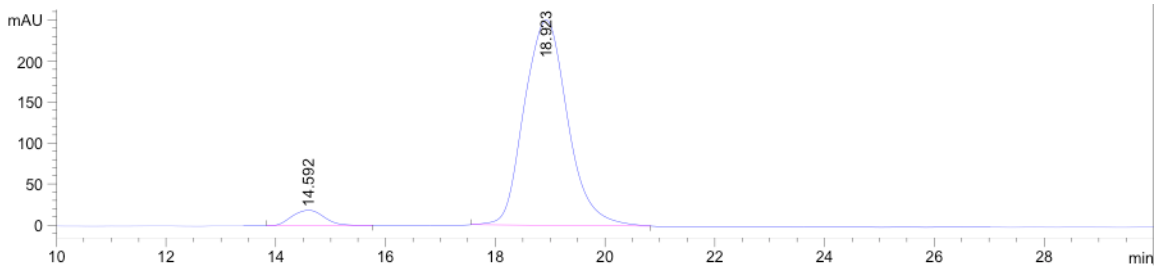

Peak #	RetTime [min]	Type	Width [min]	Area [mAU*s]	Height [mAU]	Area %
1	14.592	BB	0.6556	776.16931	18.87916	5.3266
2	18.923	BB	0.8840	1.37953e4	250.68062	94.6734

(*S*)-1-(benzyloxy)-1-(4-bromophenyl)-4,4-dimethylpentan-3-one (**9b**):

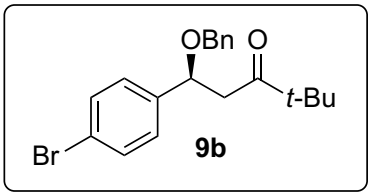

According to general procedure (Method B), **3b** (0.25 mmol) was reacted to give **9b** in 90.1 mg (96% yield) as clear oil.

^{1}H NMR (500 MHz, $CDCl_3$) δ 7.50 (d, *J*=8.3 Hz, 2 H), 7.23 - 7.35 (m, 8 H), 4.95 (dd, *J*=7.8, 5.4 Hz, 1 H), 4.35 (dd, *J*=20.5, 11.2 Hz, 2 H), 3.15 (dd, *J*=16.6, 7.8 Hz, 1 H), 2.67 (dd, *J*=16.6, 5.4 Hz, 1 H), 1.07 (s, 9 H);

^{13}C NMR (125 MHz, $CDCl_3$) δ 212.6, 140.9, 138.1, 131.7, 128.6, 128.3, 127.7, 127.6, 121.6, 76.8, 71.1, 45.4, 44.2, 25.9;

FTIR (neat, cm^{-1}) ν_{max} 1704, 1091, 1069, 1010, 822, 732, 696 cm^{-1};

HRMS (ESI-TOF) calculated for $C_{20}H_{23}O_2Br$ $[M+Na]^+$: 397.0779, found: 397.0939;

$[\alpha]_D^{25}$ = –23.0° (c = 1, $CHCl_3$).

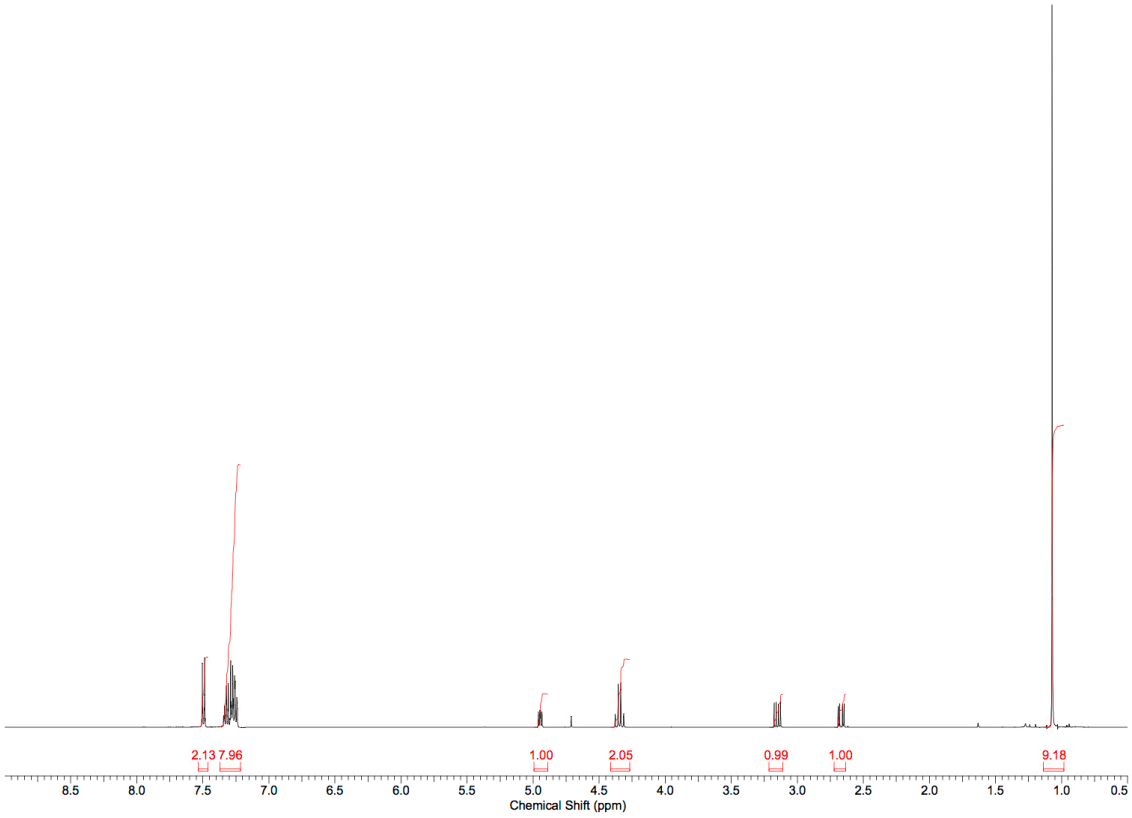
2.13
7.96
1.00
2.05
0.99
1.00
9.18
Chemical Shift (ppm)

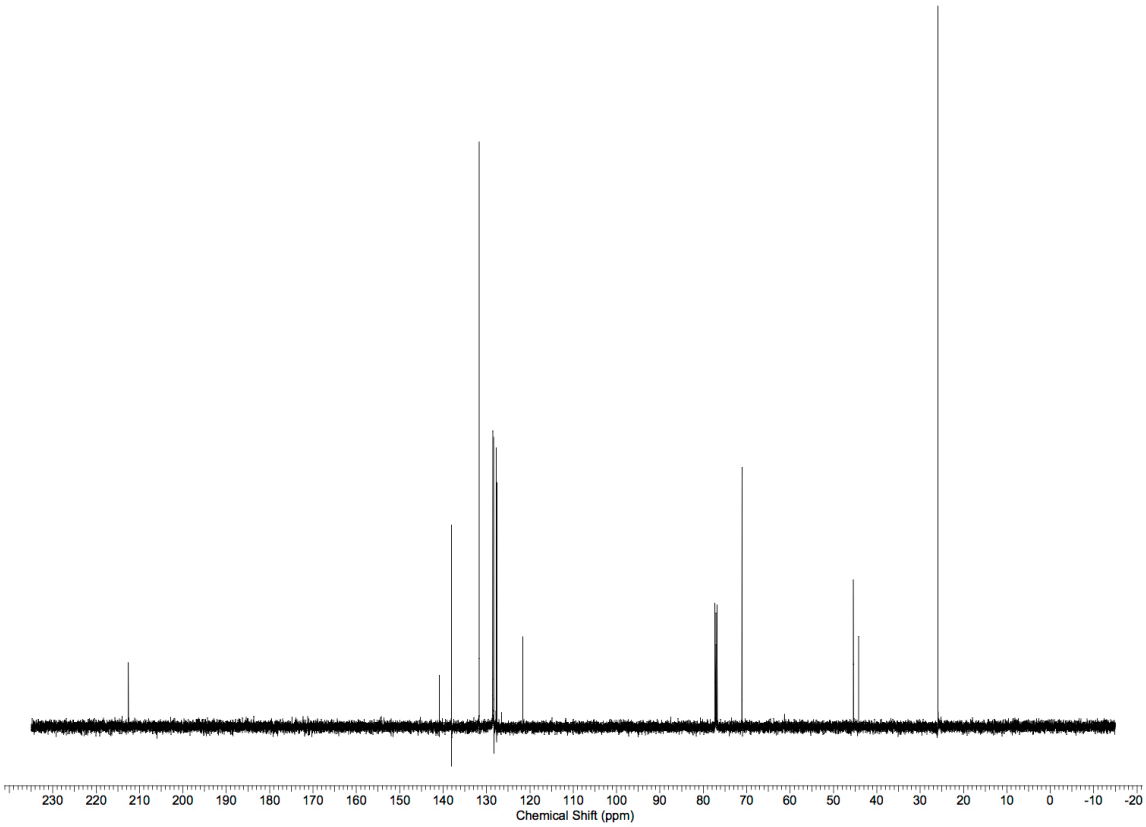
Chemical Shift (ppm)

Racemic sample: HPLC (ChiralPak OD-H, 2% IPA/hexanes, 1 mL/min, 230 nm)

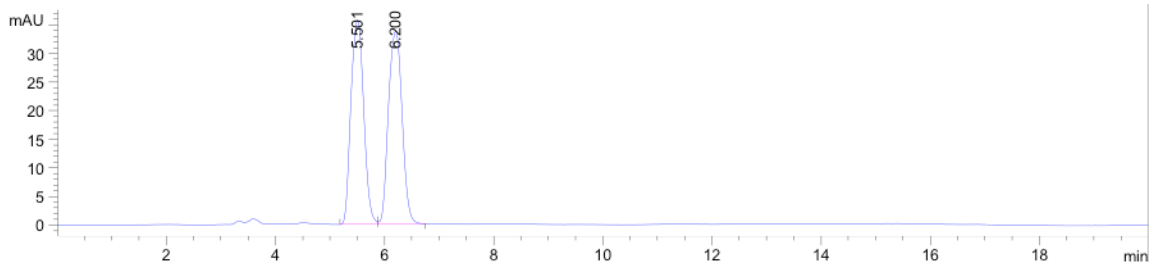

Peak #	RetTime [min]	Type	Width [min]	Area [mAU*s]	Height [mAU]	Area %
1	5.501	BV	0.2643	582.60980	35.71070	49.7673
2	6.200	VB	0.2831	588.05811	33.78712	50.2327

Enantioenriched Sample: HPLC (ChiralPak OD-H, 2% IPA/hexanes, 1 mL/min, 230 nm), 93% e.e.

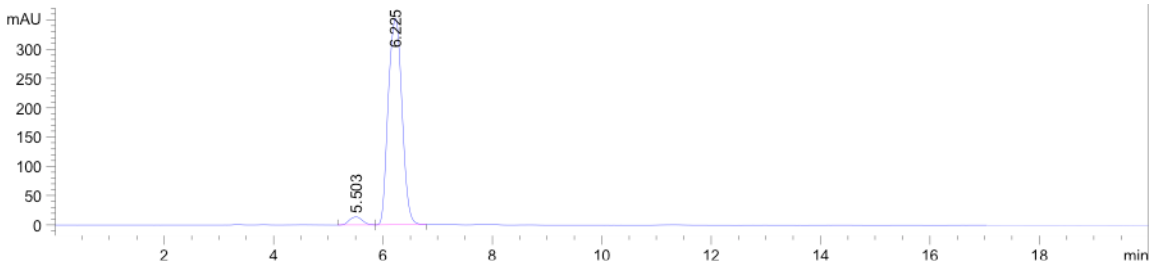

Peak #	RetTime [min]	Type	Width [min]	Area [mAU*s]	Height [mAU]	Area %
1	5.503	BV	0.2687	226.99588	13.74333	3.5480
2	6.225	VB	0.2862	6170.91113	352.50800	96.4520

(*S*)-1-(1-(benzyloxy)-3-methylbut-3-en-1-yl)-4-bromobenzene (**9c**):

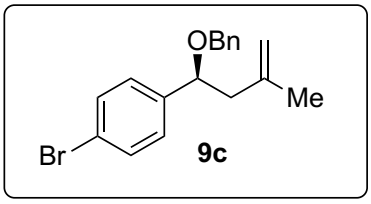

According to general procedure (Method B), **3b** (0.25 mmol) was reacted to give **9c** in 80.1 mg (97% yield) as clear oil.

^{1}H NMR (500 MHz, $CDCl_3$) δ 7.49 (d, *J*=8.3 Hz, 2 H), 7.31 - 7.36 (m, 2 H), 7.27 - 7.30 (m, 3 H), 7.23 (d, *J*=8.8 Hz, 2 H), 4.73 (d, *J*=49.8 Hz, 2 H), 4.41 - 4.47 (m, 2 H), 4.26 (d, *J*=12.2 Hz, 1 H), 2.59 (dd, *J*=14.6, 7.8 Hz, 1 H), 2.31 (dd, *J*=14.2, 4.4 Hz, 1 H), 1.68 (s, 3 H);

^{13}C NMR (125 MHz, $CDCl_3$) δ 141.9, 141.3, 138.2, 131.6, 128.6, 128.4, 127.8, 127.6, 121.4, 113.1, 79.5, 70.5, 46.5, 22.9;

FTIR (neat, cm^{-1}) ν_{max} 1486, 1454, 1091, 1070, 1010, 892, 824, 735, 697 cm^{-1};

HRMS (ESI-TOF) calculated for $C_{18}H_{19}OBr$ $[M+Na]^+$: 353.0517, found: 353.0528;

$[\alpha]_D^{25}$ = –48.6° (c = 1, $CHCl_3$).

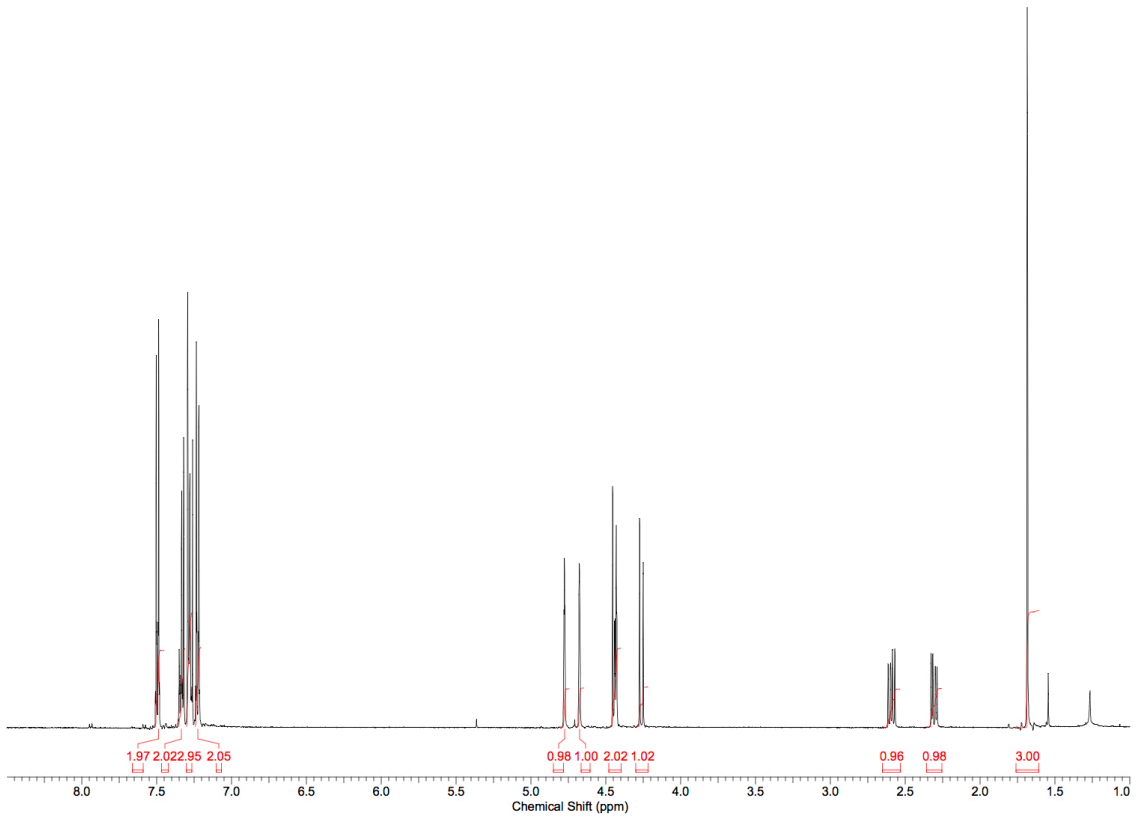
1.97 2.02 2.95 2.05
0.98 1.00 2.02 1.02
0.96 0.98
3.00
8.0 7.5 7.0 6.5 6.0 5.5 5.0 4.5 4.0 3.5 3.0 2.5 2.0 1.5 1.0
Chemical Shift (ppm)

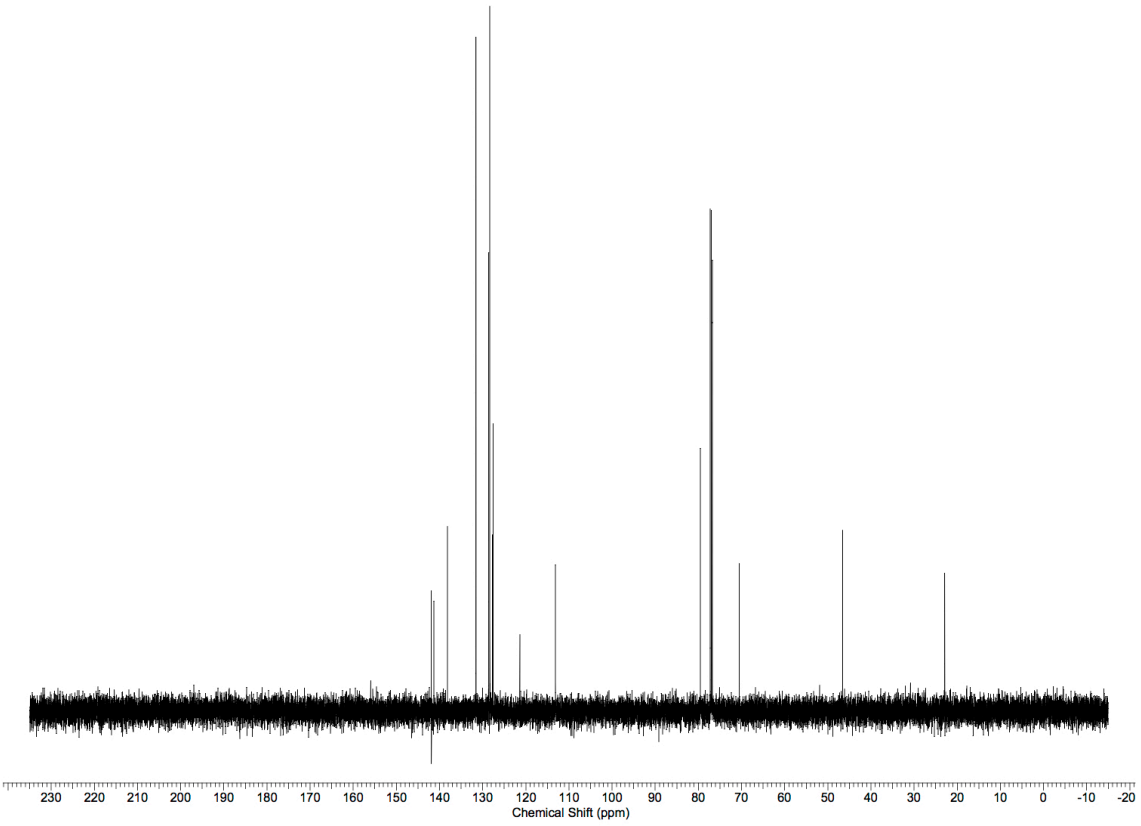
230 220 210 200 190 180 170 160 150 140 130 120 110 100 90 80 70 60 50 40 30 20 10 0 -10 -20
Chemical Shift (ppm)

Racemic sample: HPLC (ChiralPak AD-H, 1% IPA/hexanes, 1 mL/min, 230 nm)

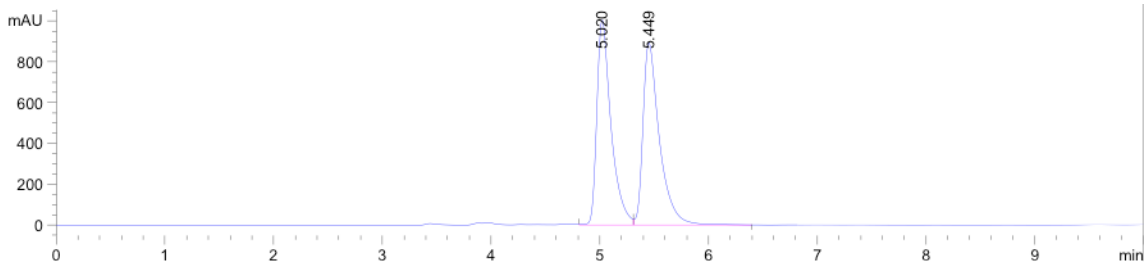

Peak #	RetTime [min]	Type	Width [min]	Area [mAU*s]	Height [mAU]	Area %
1	5.020	VV	0.1339	9129.24902	1005.66815	49.2556
2	5.449	VB	0.1568	9405.18066	893.72369	50.7444

Enantioenriched Sample: HPLC (ChiralPak AD-H, 1% IPA/hexanes, 1 mL/min, 230 nm), 87% e.e.

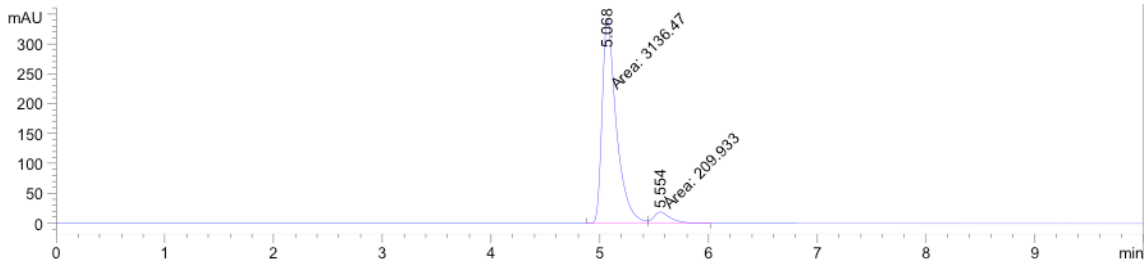

Peak #	RetTime [min]	Type	Width [min]	Area [mAU*s]	Height [mAU]	Area %
1	5.068	MF	0.1521	3136.47485	343.77988	93.7266
2	5.554	MF	0.1819	209.93343	19.23543	6.2734

S-phenyl (*S*)-3-(benzyloxy)-3-(4-bromophenyl)propanethioate (**9d**):

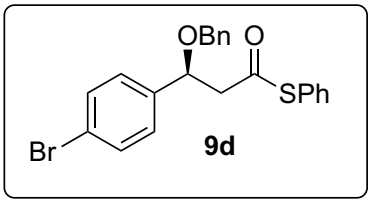

According to general procedure (Method B), **3b** (0.25 mmol) was reacted to give **9d** in 101.0 mg (94% yield) as pale yellow amorphous solid.

^{1}H NMR (500 MHz, $CDCl_3$) δ 7.54 (d, *J*=8.3 Hz, 2 H), 7.27 - 7.47 (m, 13 H), 4.91 (dd, *J*=8.8, 4.4 Hz, 1 H), 4.46 (d, *J*=11.2 Hz, 1 H), 4.35 (d, *J*=11.7 Hz, 1 H), 3.23 (dd, *J*=15.1, 8.8 Hz, 1 H), 2.90 (dd, *J*=15.1, 4.9 Hz, 1 H);

^{13}C NMR (125 MHz, $CDCl_3$) δ 194.6, 139.5, 137.7, 134.5, 131.9, 129.6, 129.3, 128.5, 128.4, 127.8, 127.6, 122.1, 77.4, 71.1, 51.7;

FTIR (neat, cm^{-1}) ν_{max} 1700, 1068, 1010, 974, 743, 689 cm^{-1};

HRMS (ESI-TOF) calculated for $C_{22}H_{19}O_2SBr$ $[M+Na]^+$: 449.1087, found: 449.0193;

$[\alpha]_D^{25}$ = –29.6° (c = 1, $CHCl_3$).

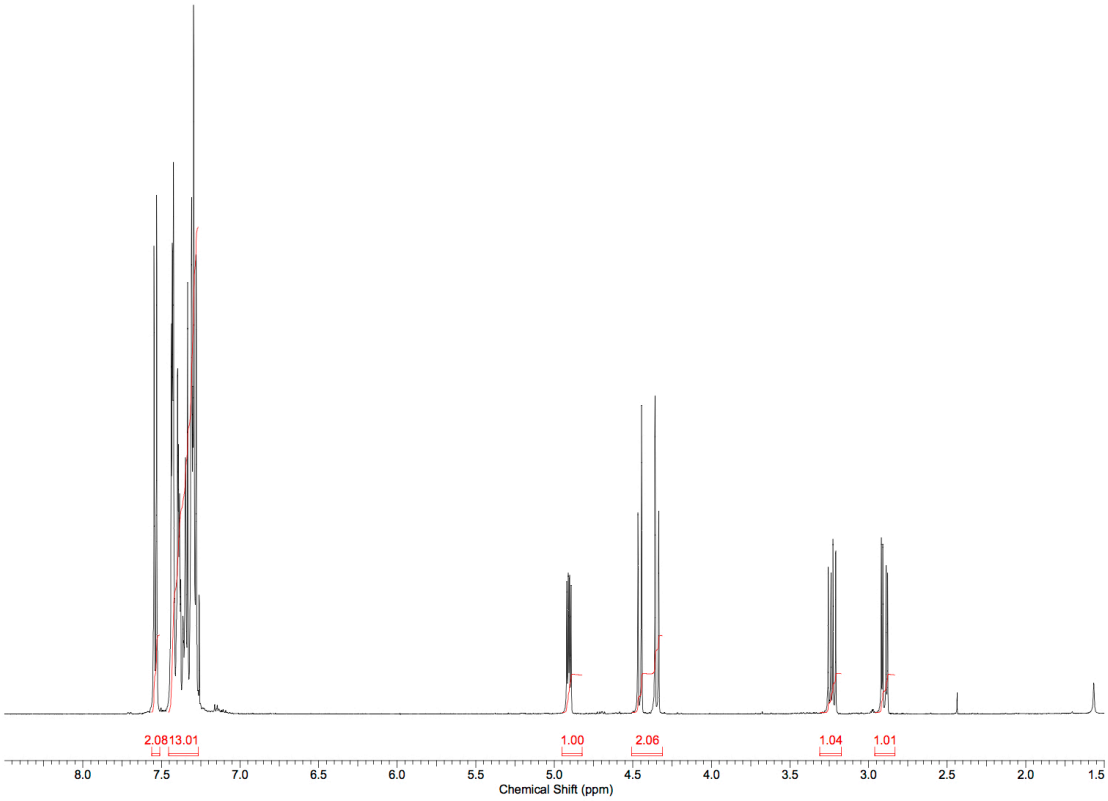
2.08
13.01
1.00
2.06
1.04
1.01
8.0
7.5
7.0
6.5
6.0
5.5
5.0
4.5
4.0
3.5
3.0
2.5
2.0
1.5
Chemical Shift (ppm)

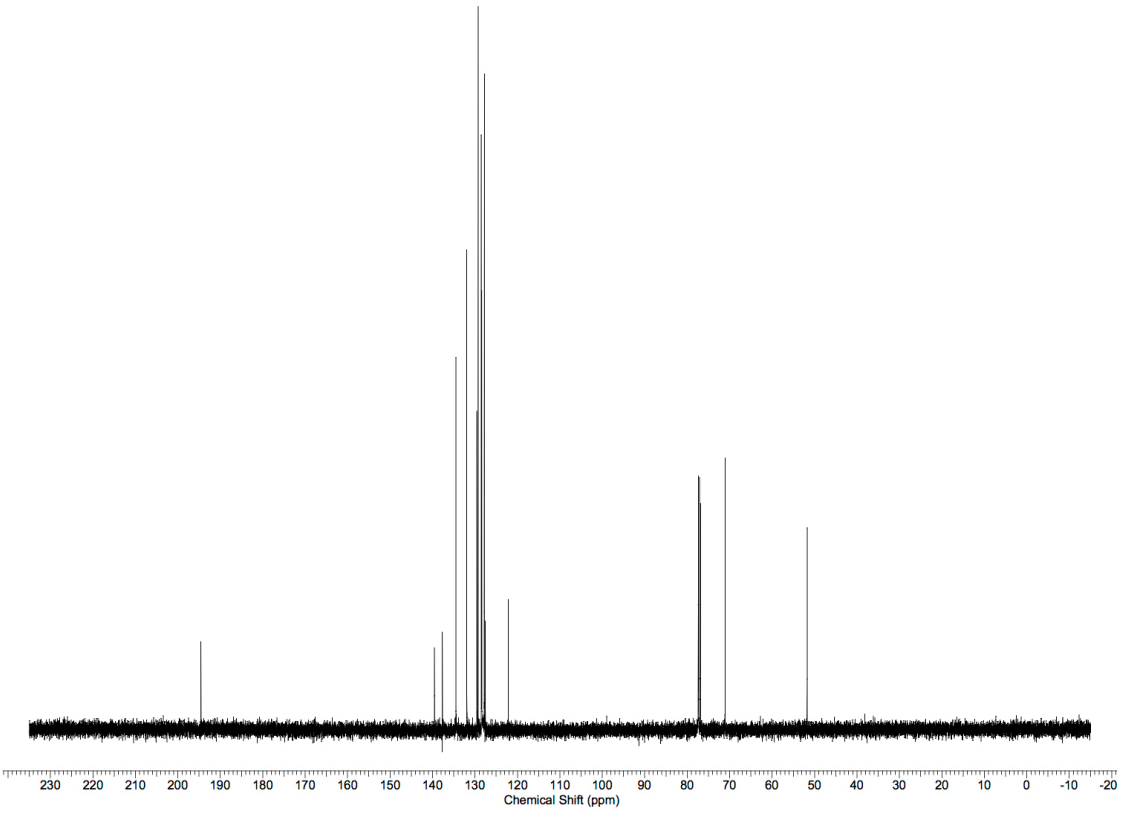
230
220
210
200
190
180
170
160
150
140
130
120
110
100
90
80
70
60
50
40
30
20
10
0
-10
-20
Chemical Shift (ppm)

Racemic sample: HPLC (ChiralPak AS-H, 2% IPA/hexanes, 1 mL/min, 210 nm)

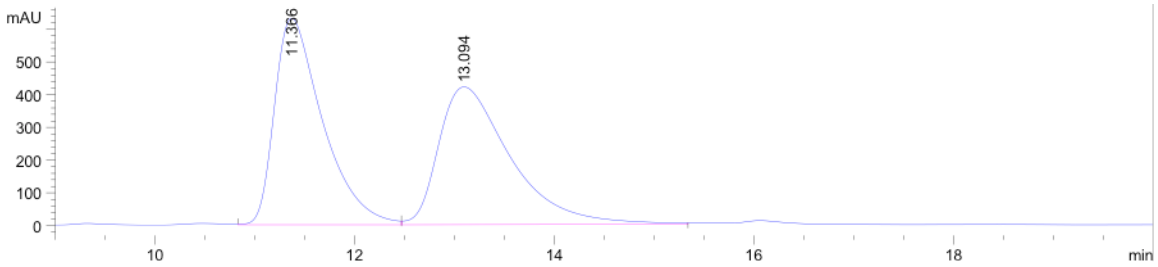

Peak #	RetTime [min]	Type	Width [min]	Area [mAU*s]	Height [mAU]	Area %
1	11.366	VV	0.5013	2.12223e4	632.74127	49.9792
2	13.094	VB	0.7576	2.12400e4	421.72116	50.0208

Enantioenriched Sample: HPLC (ChiralPak AS-H, 2% IPA/hexanes, 1 mL/min, 210 nm), 95% e.e.

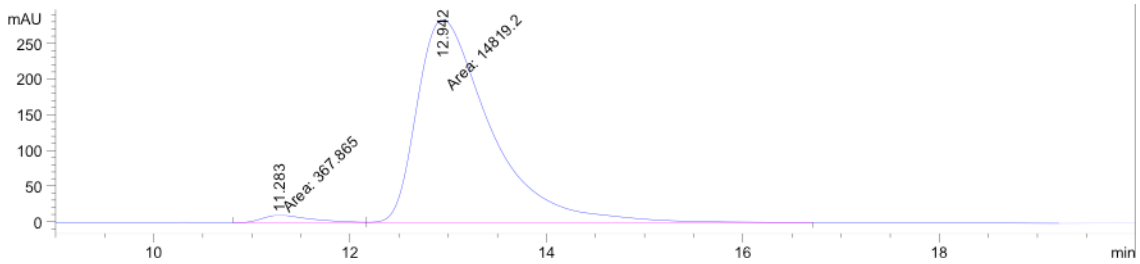

Peak #	RetTime [min]	Type	Width [min]	Area [mAU*s]	Height [mAU]	Area %
1	11.283	MF	0.5751	367.86514	10.66062	2.4222
2	12.942	FM	0.8687	1.48192e4	284.31815	97.5778

methyl (*R*)-3-(benzyloxy)-3-(4-bromophenyl)-2,2-dimethylpropanoate (**9e**):

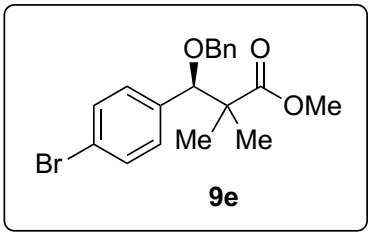

9e

According to general procedure (Method B), **3b** (0.25 mmol) was reacted to give **9e** in 92.2 mg (98% yield) as clear oil.

^{1}H NMR (500 MHz, $CDCl_3$) δ 7.52 (d, *J*=8.3 Hz, 2 H), 7.21 - 7.38 (m, 7 H), 4.70 (s, 1 H), 4.45 (d, *J*=11.7 Hz, 1 H), 4.26 (d, *J*=11.7 Hz, 1 H), 3.66 (s, 3 H), 1.19 (s, 3 H), 1.03 - 1.06 (m, 3 H);

^{13}C NMR (125 MHz, $CDCl_3$) δ 176.8, 138.0, 136.6, 131.1, 130.2, 128.3, 127.6, 127.5, 121.9, 84.8, 71.1, 51.9, 47.9, 22.3, 19.1;

FTIR (neat, cm^{-1}) ν_{max} 1736, 1132, 1071, 1010, 734, 698 cm^{-1};

HRMS (ESI-TOF) calculated for $C_{19}H_{21}O_3Br$ $[M+Na]^+$: 399.0572, found: 399.0705;

$[\alpha]_D^{25}$ = –51.2° (c = 1, $CHCl_3$).

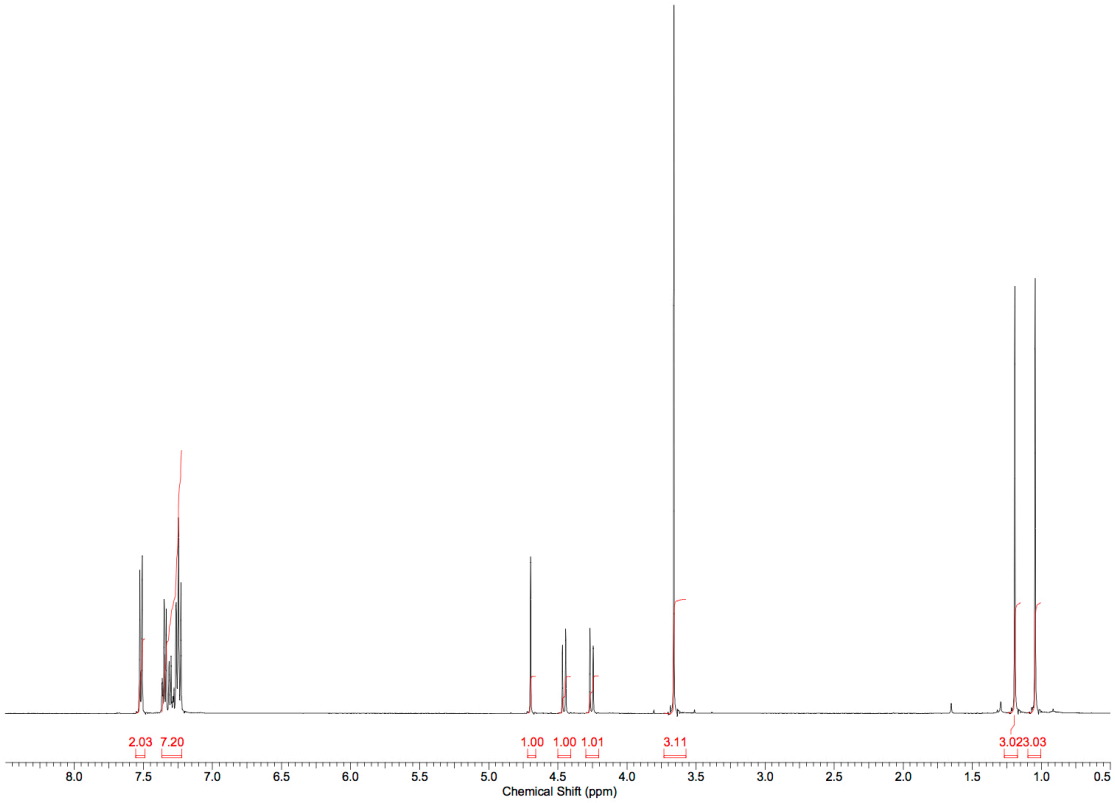
2.03
7.20
1.00
1.00
1.01
3.11
3.02
3.03
8.0
7.5
7.0
6.5
6.0
5.5
5.0
4.5
4.0
3.5
3.0
2.5
2.0
1.5
1.0
0.5
Chemical Shift (ppm)

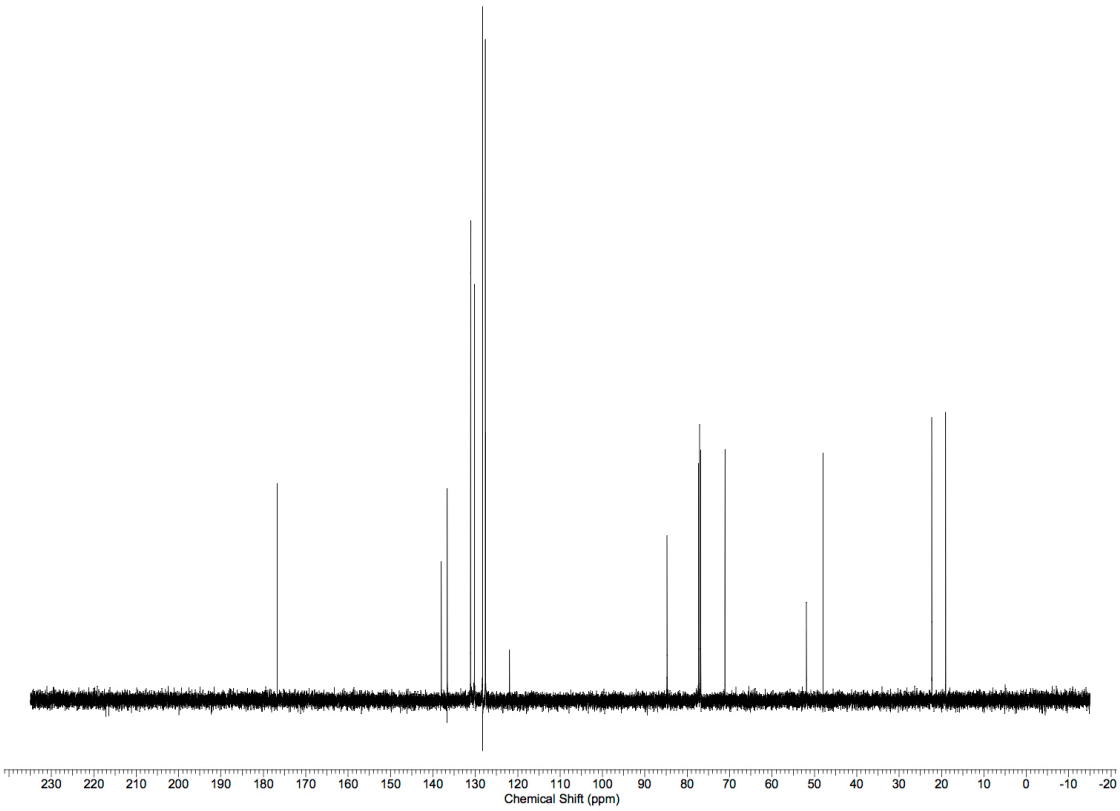
230
220
210
200
190
180
170
160
150
140
130
120
110
100
90
80
70
60
50
40
30
20
10
0
-10
-20
Chemical Shift (ppm)

Racemic sample: HPLC (ChiralPak OD-H, 2% IPA/hexanes, 1 mL/min, 230 nm)

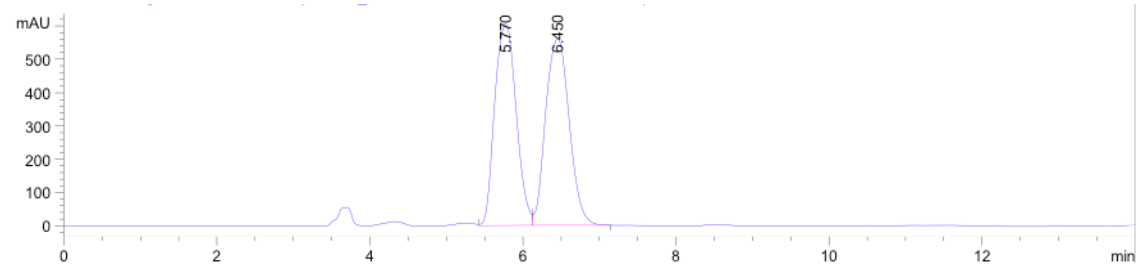

Peak #	RetTime [min]	Type	Width [min]	Area [mAU*s]	Height [mAU]	Area %
1	5.770	VV	0.3161	1.18618e4	606.82330	49.6163
2	6.450	VB	0.3479	1.20453e4	562.31506	50.3837

Enantioenriched Sample: HPLC (ChiralPak OD-H, 2% IPA/hexanes, 1 mL/min, 230 nm), 90% e.e.

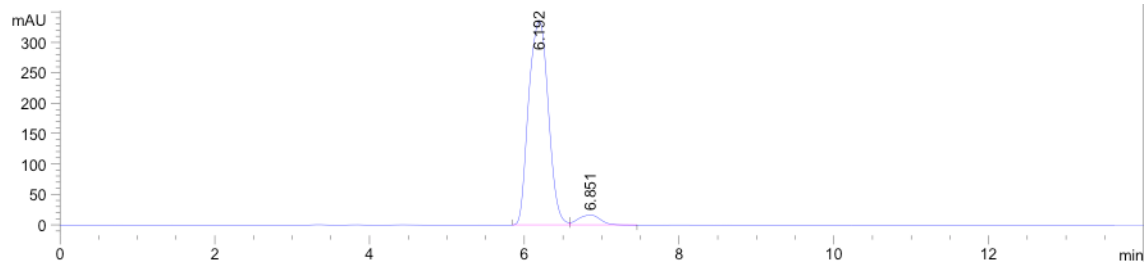

Peak #	RetTime [min]	Type	Width [min]	Area [mAU*s]	Height [mAU]	Area %
1	6.192	BV	0.2897	5930.29443	336.27844	94.8263
2	6.851	VB	0.3201	323.55215	16.40701	5.1737

methyl (*R*)-1-((benzyloxy)(4-bromophenyl)methyl)cyclohexane-1-carboxylate (**9f**):

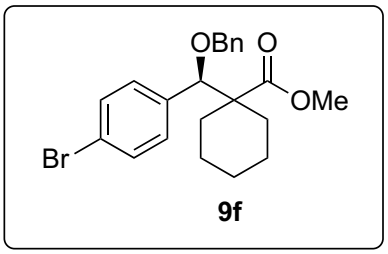

9f

According to general procedure (Method B), **3b** (0.25 mmol) was reacted to give **9f** in 83.3 mg (80% yield) as clear oil.

^{1}H NMR (500 MHz, $CDCl_3$) δ 7.50 (d, *J*=8.3 Hz, 2 H), 7.24 - 7.38 (m, 5 H), 7.17 (d, *J*=8.3 Hz, 2 H), 4.45 (d, *J*=11.7 Hz, 1 H), 4.42 (s, 1 H), 4.18 (d, *J*=11.7 Hz, 1 H), 3.63 (s, 3 H), 2.18 (d, *J*=12.7 Hz, 1 H), 2.06 (d, *J*=9.3 Hz, 1 H), 1.53 - 1.68 (m, 3 H), 1.13 - 1.48 (m, 4 H), 0.95 - 1.09 (m, 1 H);

^{13}C NMR (125 MHz, $CDCl_3$) δ 175.1, 138.0, 136.7, 131.0, 130.2, 128.3, 127.6, 127.5, 121.9, 86.0, 71.0, 53.4, 51.5, 30.1, 29.1, 25.7, 23.3, 23.1;

FTIR (neat, cm^{-1}) ν_{max} 1720, 1216, 1131, 1071, 1010, 906, 728, 697 cm^{-1};

HRMS (ESI-TOF) calculated for $C_{22}H_{25}O_3Br$ $[M+Na]^+$: 439.0885, found: 439.1060;

$[\alpha]_D^{25}$ = –34.0° (c = 1, $CHCl_3$).

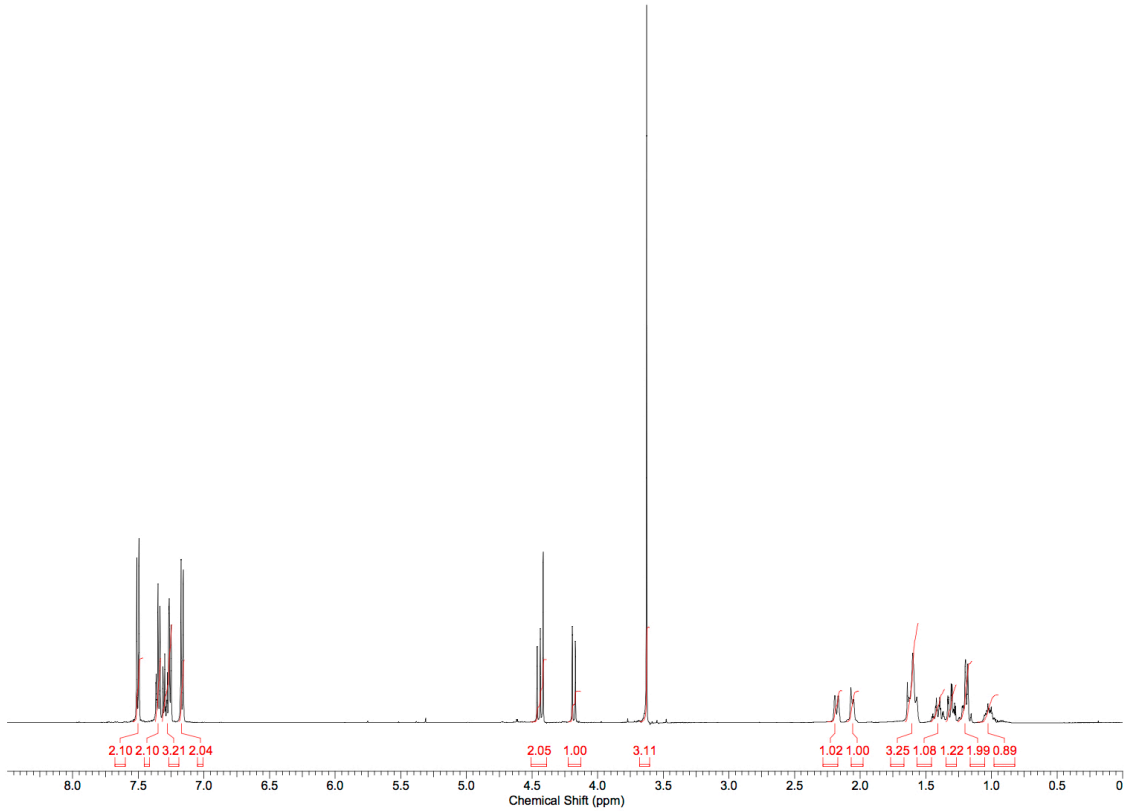
2.10 2.10 3.21 2.04
2.05 1.00 3.11
1.02 1.00 3.25 1.08 1.22 1.99 0.89
8.0 7.5 7.0 6.5 6.0 5.5 5.0 4.5 4.0 3.5 3.0 2.5 2.0 1.5 1.0 0.5 0
Chemical Shift (ppm)

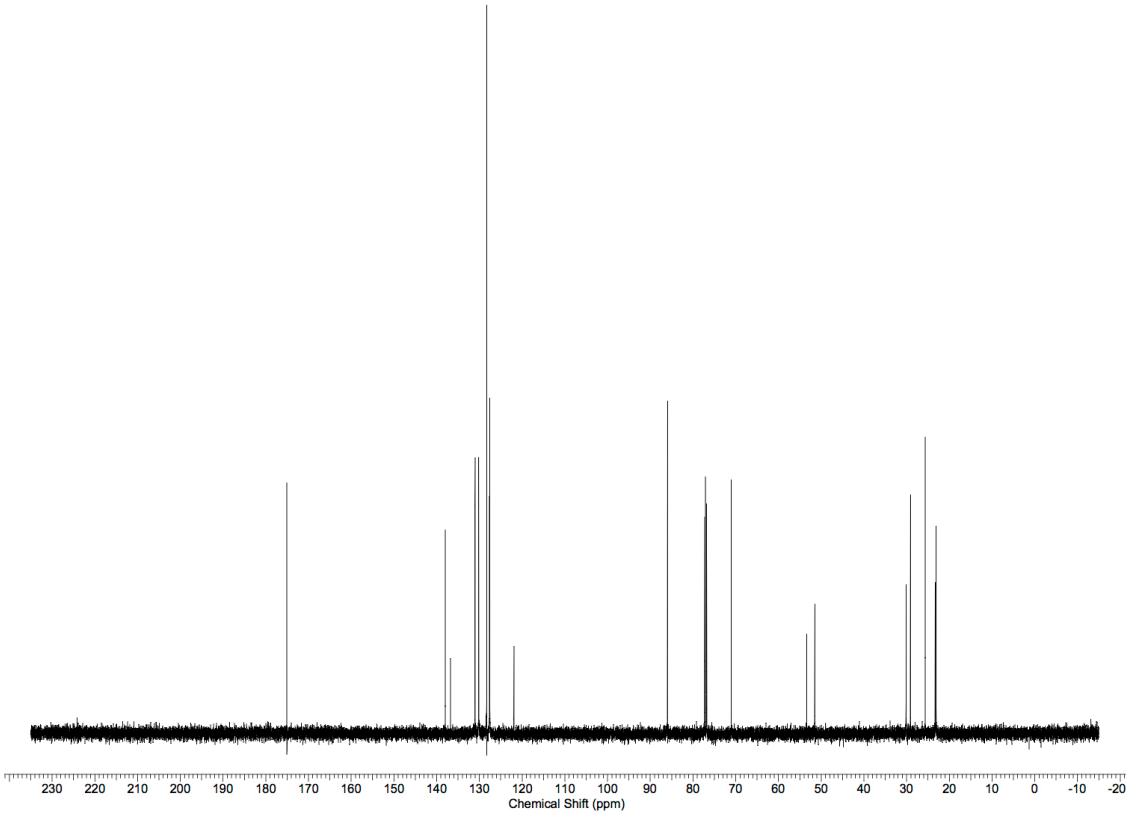
230 220 210 200 190 180 170 160 150 140 130 120 110 100 90 80 70 60 50 40 30 20 10 0 -10 -20
Chemical Shift (ppm)

Racemic sample: HPLC (ChiralPak AD-H, 2% IPA/hexanes, 1 mL/min, 230 nm)

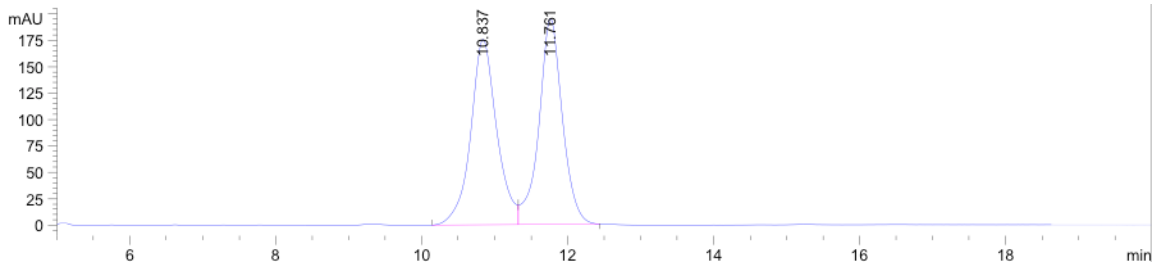

Peak #	RetTime [min]	Type	Width [min]	Area [mAU*s]	Height [mAU]	Area %
1	10.837	BV	0.3668	4375.83154	175.56119	50.0024
2	11.761	VB	0.3318	4375.41406	194.99959	49.9976

Enantioenriched Sample: HPLC (ChiralPak AD-H, 2% IPA/hexanes, 1 mL/min, 230 nm), 91% e.e.

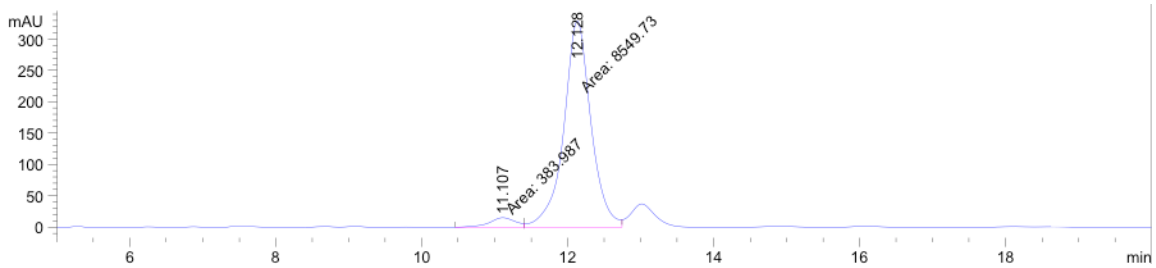

Peak #	RetTime [min]	Type	Width [min]	Area [mAU*s]	Height [mAU]	Area %
1	11.107	MF	0.4180	383.98734	15.31069	4.2982
2	12.128	FM	0.4336	8549.72559	328.64566	95.7018

methyl (*R*)-4-((benzyloxy)(4-bromophenyl)methyl)tetrahydro-2*H*-pyran-4-carboxylate (**9g**):

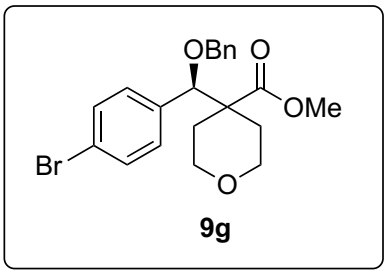

9g

According to general procedure (Method B), **3b** (0.25 mmol) was reacted to give **9g** in 96.7 mg (92% yield) as pale yellow oil.

^{1}H NMR (500 MHz, $CDCl_3$) δ 7.52 (d, *J*=8.3 Hz, 2 H), 7.24 - 7.40 (m, 5 H), 7.15 (d, *J*=8.3 Hz, 2 H), 4.47 (d, *J*=11.7 Hz, 1 H), 4.43 (s, 1 H), 4.19 (d, *J*=12.2 Hz, 1 H), 3.85 (td, *J*=11.7, 3.9 Hz, 2 H), 3.65 (s, 3 H), 3.45 (td, *J*=12.2, 2.0 Hz, 1 H), 3.32 (td, *J*=12.2, 2.0 Hz, 1 H), 1.99 (ddd, *J*=48.8, 13.7, 2.0 Hz, 2 H), 1.80 (td, *J*=12.7, 4.4 Hz, 1 H), 1.66 (td, *J*=13.2, 4.9 Hz, 1 H);

^{13}C NMR (125 MHz, $CDCl_3$) δ 174.2, 137.6, 136.0, 131.3, 130.0, 128.4, 127.8, 127.7, 122.3, 85.0, 71.0, 65.4, 65.3, 51.8, 51.3, 29.7, 29.5;

FTIR (neat, cm^{-1}) ν_{max} 1093, 1070, 1010, 907, 727, 698 cm^{-1};

HRMS (ESI-TOF) calculated for $C_{21}H_{23}O_4Br$ $[M+Na]^+$: 441.0677, found: 441.0716;

$[\alpha]_D^{25}$ = –38.8° (c = 1, $CHCl_3$).

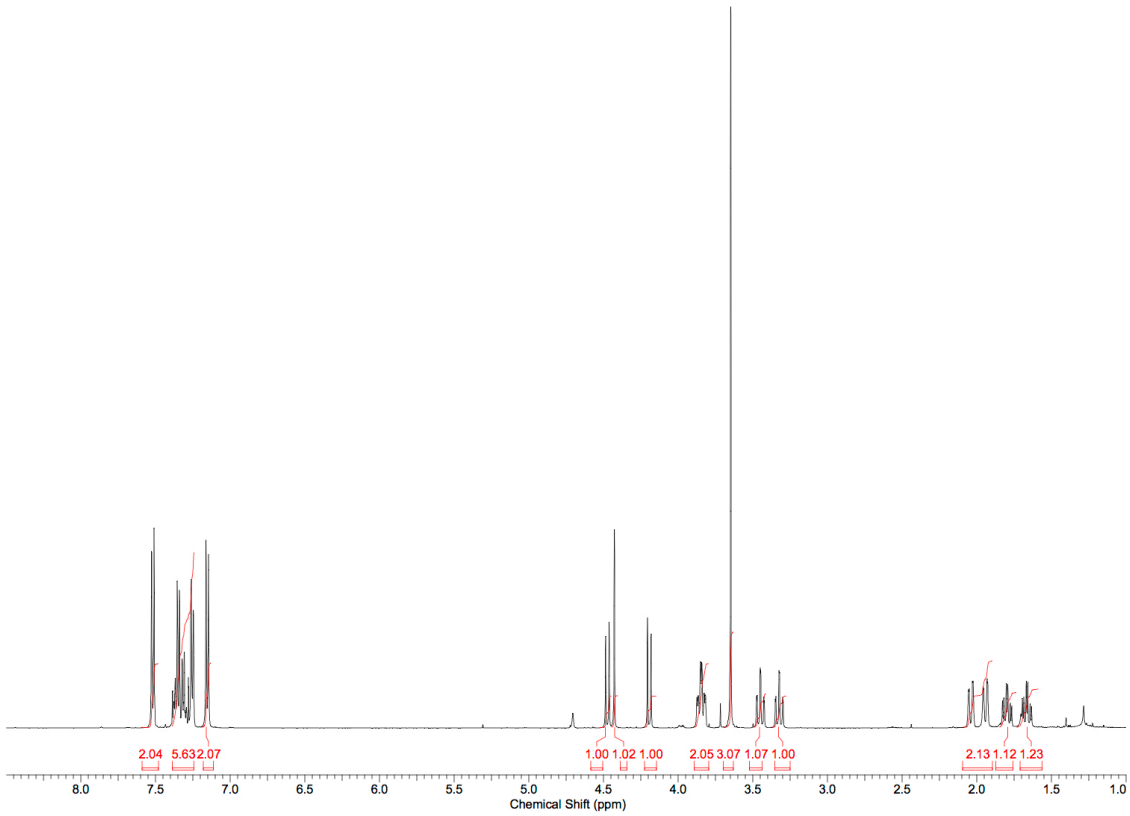
2.04
5.63
2.07
1.00
1.02
1.00
2.05
3.07
1.07
1.00
2.13
1.12
1.23
Chemical Shift (ppm)

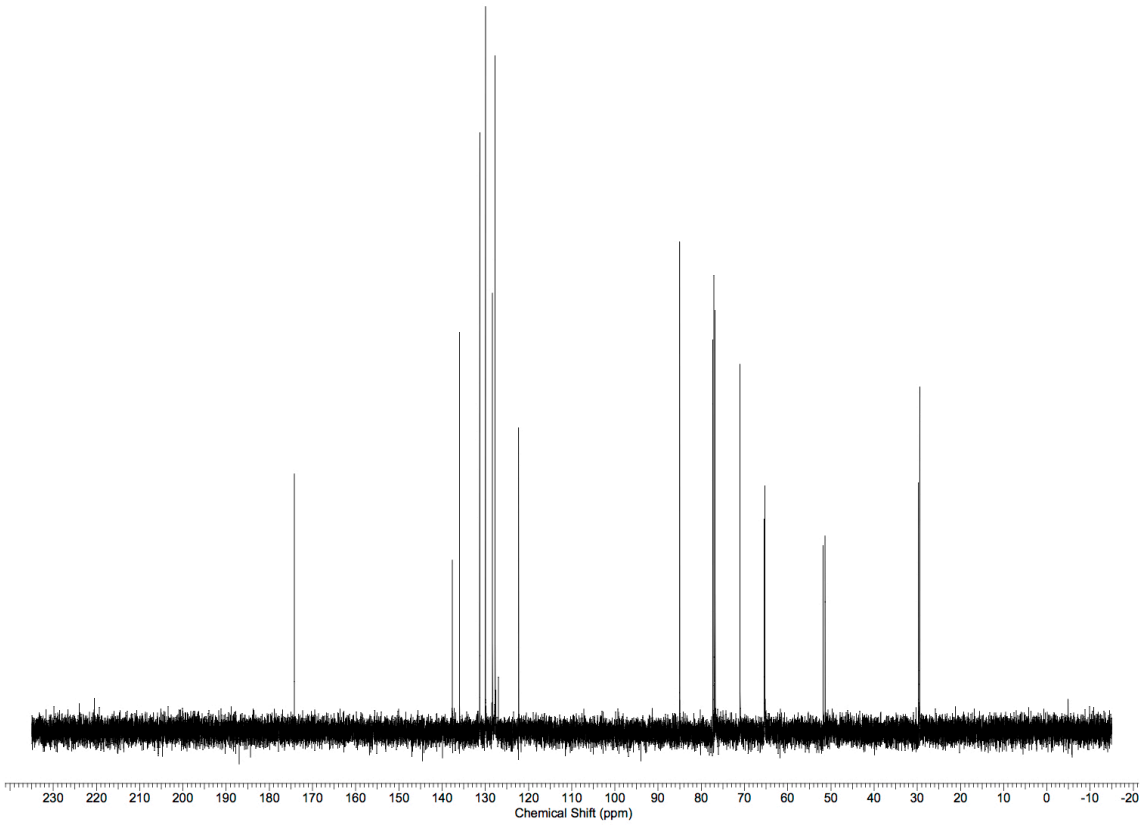
Chemical Shift (ppm)

Racemic sample: HPLC (ChiralPak OD-H, 2% IPA/hexanes, 1 mL/min, 210 nm)

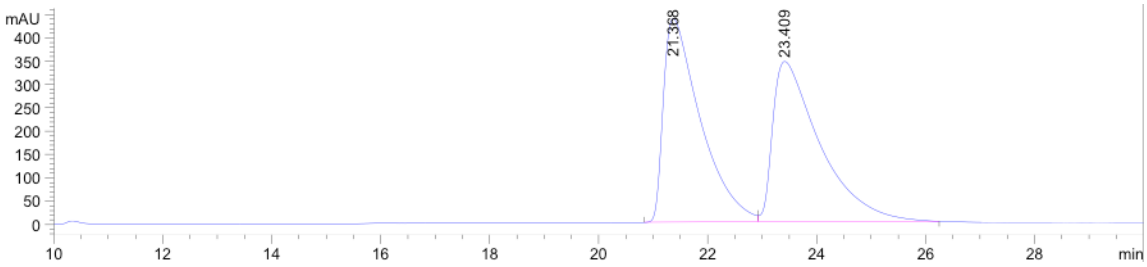

Peak #	RetTime [min]	Type	Width [min]	Area [mAU*s]	Height [mAU]	Area %
1	21.368	BV	0.6924	2.06593e4	436.29556	49.8716
2	23.409	VB	0.8286	2.07657e4	343.85229	50.1284

Enantioenriched Sample: HPLC (ChiralPak OD-H, 2% IPA/hexanes, 1 mL/min, 210 nm), 94% e.e.

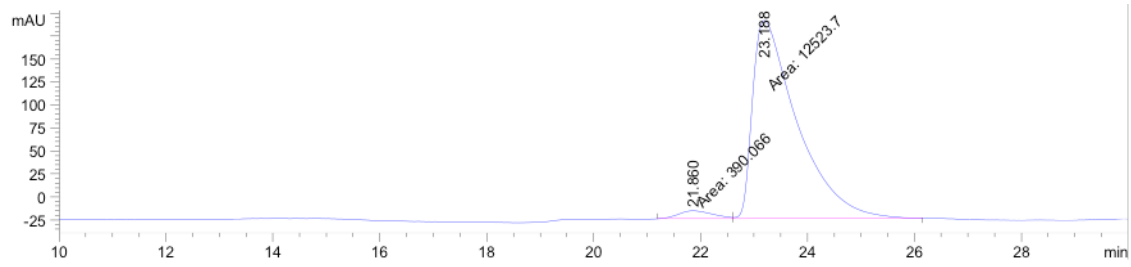

Peak #	RetTime [min]	Type	Width [min]	Area [mAU*s]	Height [mAU]	Area %
1	21.860	MF	0.7514	390.06622	8.65239	3.0205
2	23.188	FM	0.9683	1.25237e4	215.55536	96.9795

3.4.5. Additional Substrate Scope Studies

Table 3.11. ***Best results for ketone-derived acetals.***

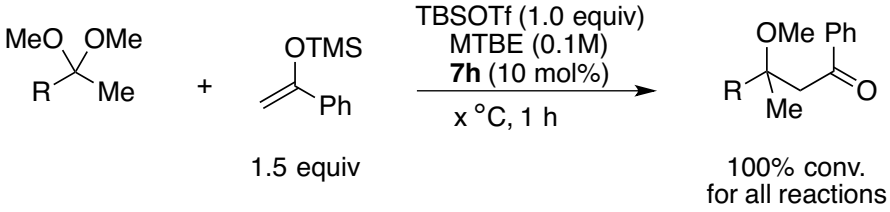

Entry	Substrate	Temperature (°C)	ee (%)
1	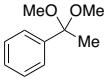	-78	40
2		-100	46
3	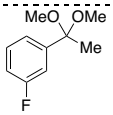	-78	33
4		-100	50
5	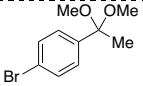	-78	40
6	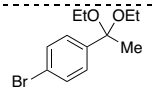	-78	10
7	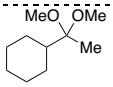	-78	30

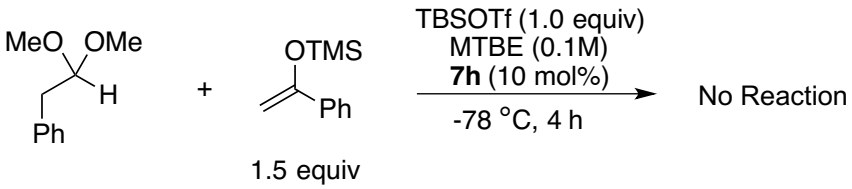

Scheme 3.5. No reaction was observed with dibenzyl acetal of alkyl aldehyde as a substrate.

Table 3.12. ***Limitations in the nucleophile scope.***

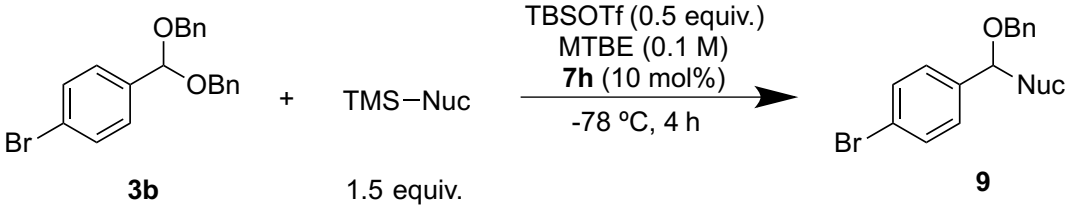

Entry	Nucleophile	Product	Conversion[a] (%)	ee[b] (%)
1	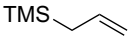	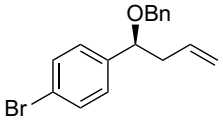	n.r.[c]	n.d.
2	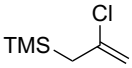	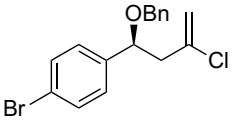	n.r.[c]	n.d.
3	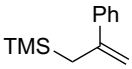	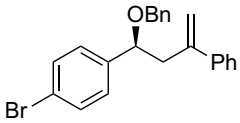	100	62
4[d]	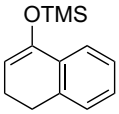	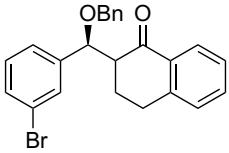	100	86

a. Conversions determined by ^{1}H NMR analysis of the crude reaction mixture are reported.
b. ee values determined by chiral HPLC analysis.
c. Irreproducible reactivity was observed with these substrates – we hypothesized that when reactivity was observed it was due to warming up of the reaction above -78 °C and likely contamination of TBSOTf with TfOH under highly humidity conditions.
d. Substrate **3g** was used in this entry. Product was obtained in 3:1 dr. Configuration of the major diastereomer was not determined.

3.4.6. Additional Reaction Optimization Data

Table 3.13. ***TESOTf loading investigation (part 1).***

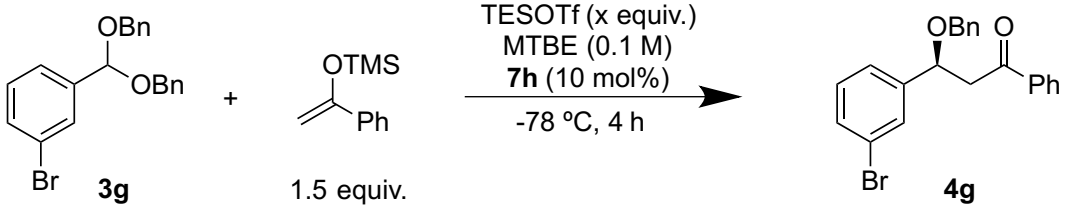

Entry	TESOTf Loading (equiv.)	Conversion[a] (%)	ee[b] (%)
1	0.1	10	n.d.
2	0.2	38	n.d.
3	0.5	51	96
4	1.0	50	96
5	1.5	48	n.d.
6	2.0	45	n.d.

a. Conversions determined by ^{1}H NMR analysis of the crude reaction mixture are reported.
b. ee values determined by chiral HPLC analysis.

Small positive effect was observed on enantioselectivity of electron-rich substrates with lower TBSOTf loading.

Table 3.14. ***TBSOTf loading investigation (part 2).***

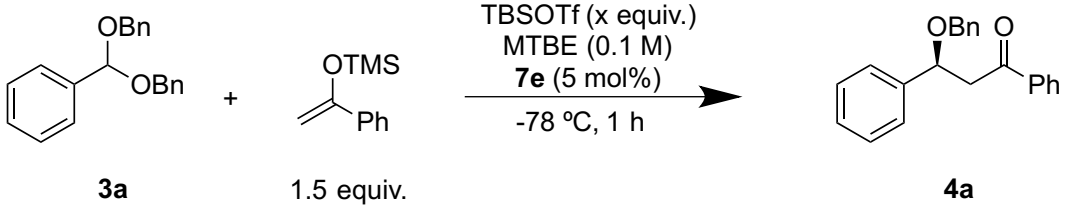

Entry	TBSOTf Loading (equiv.)	Conversion[a] (%)	ee[b] (%)
1	0.1	100	67
2	0.25	100	68
3	0.5	100	63
4	1.0	100	60
5	2.0	100	55

a. Conversions determined by ^{1}H NMR analysis of the crude reaction mixture are reported.
b. ee values determined by chiral HPLC analysis.

Table 3.15. ***TBSOTf loading investigation (part 3).***

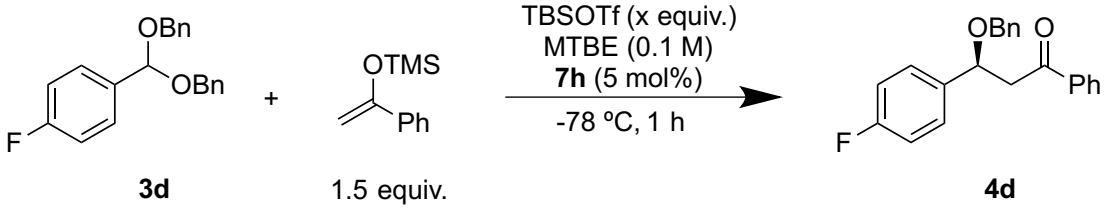

3d 1.5 equiv. **4d**

Entry	TBSOTf Loading (equiv.)	Conversion[a] (%)	ee[b] (%)
1	0.2	100	48
2	0.5	100	47
3	1.0	100	45

a. Conversions determined by ^{1}H NMR analysis of the crude reaction mixture are reported.
b. ee values determined by chiral HPLC analysis.

In order to balance reactivity of electron-poor substrates and selectivity of electron-rich substrates, 0.5 equivalents of TBSOTf was chosen as the optimal loading.

3.4.7. Absolute Configuration Determination

Absolute configuration was determined by benzylating enantioenriched products of known configuration of nucleophilic addition to aldehydes.

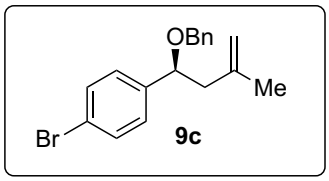

Absolute configuration of free-alcohol precursor of **9c** (shown below) was synthesized in 78% ee and absolute configuration assigned by comparison with reported experimental data.[68]

(*S*)-1-(4-bromophenyl)-3-methylbut-3-en-1-ol:

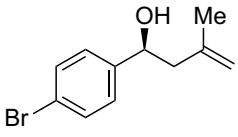

$[\alpha]_D^{25} = -46.0°$ (c=1.0, $CHCl_3$),

Williamson ether synthesis with (*S*)-1-(4-bromophenyl)-3-methylbut-3-en-1-ol and benzyl bromide provided **9c** in 78% ee in the same direction as **9c** obtained through method B of this chapter.

HPLC trace for **9c** obtained through benzylation of (*S*)-1-(4-bromophenyl)-3-methylbut-3-en-1-ol:

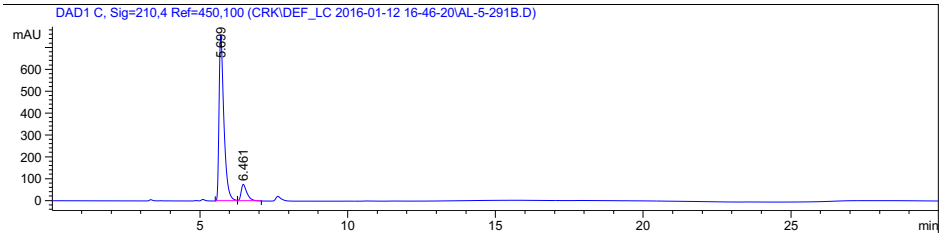

Signal 3: DAD1 C, Sig=210,4 Ref=450,100

Peak #	RetTime [min]	Type	Width [min]	Area [mAU*s]	Height [mAU]	Area %
1	5.699	BV	0.1690	8649.31250	758.64178	89.0810
2	6.461	VB	0.2048	1060.17810	75.97206	10.9190

[68] Sai, M.; Yamamoto, H. *J. Am. Chem. Soc.* **2015**, *137*, 7091–7094.

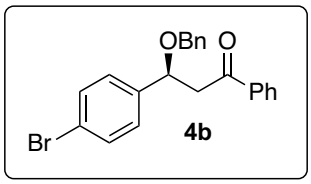

Absolute configuration of free-alcohol precursor of **4b** (shown below) was synthesized in 78% ee and absolute configuration assigned by comparison with reported experimental data.[69]

(*S*)-3-(4-bromophenyl)-3-hydroxy-1-phenylpropan-1-one:

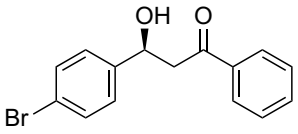

$[\alpha]_D^{25} = -35.3°$ (c=0.8, $CHCl_3$).

Following previously reported benzylation procedure[70] on (*S*)-3-(4-bromophenyl)-3-hydroxy-1-phenylpropan-1-one provided **4b** in 62% ee (some loss in enantioselectivity was observed) in the same direction as **4b** obtained through method B of this chapter.

HPLC trace for **4b** obtained through benzylation of (*S*)-3-(4-bromophenyl)-3-hydroxy-1-phenylpropan-1-one:

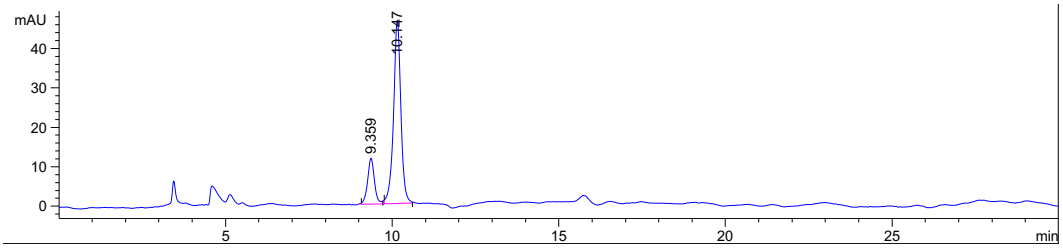

Peak #	RetTime [min]	Type	Width [min]	Area [mAU*s]	Height [mAU]	Area %
1	9.359	BB	0.2173	166.98981	11.64719	18.9334
2	10.147	BB	0.2275	714.99683	46.46915	81.0666

The absolute configurations of all other products were assigned by analogy.

[69] Cheon, C. H.; Yamamoto, H. *Org. Lett.* **2010**, *12*, 2476–2479.

[70] Poon, K. W. C.; Dudley, G. B. *J. Org. Chem.* **2006**, *71*, 3923–3927.

Chapter 4

Squaramide and Silyl Trifluoromethanesulfonate co-Catalyzed Asymmetric Mukaiyama Aldol[71]

4.1. Introduction

Having established that cooperative reactivity between squaramides and silyl triflates can promote acetal ionization and control enantioselectivity in the subsequent nucleophilic addition in Chapters 2 and 3 of this thesis, we sought to investigate whether this mode of catalysis could be applied to aldehyde substrates as well (Figure 4.1). Asymmetric additions of nucleophiles to aldehydes are powerful and fundamental organic reactions.[72] In particular, the catalytic asymmetric Mukaiyama aldol reaction has captured the interest of the scientific community.[73] A Mukaiyama version of the aldol reaction involves the use of silyl enol ethers as enolate equivalents to react with aldehydes. In this chapter we discuss our research towards the development of an squaramide and silyl triflate co-catalyzed enantioselective Mukaiyama aldol reaction.

[71] This work was done in collaboration with Nina Shevzov-Zebrun.

[72] For a review on catalytic asymmetric allylation of aldehydes and ketones, see: Denmark, S. E.; Fu. J. *Chem. Rev*. **2003**, *103*, 2763–2793.

[73] For examples of asymmetric Mukaiyama aldol reactions, see: (a) Sai, M.; Yamamoto, H. *J. Am. Chem. Soc*. **2015**, *137*, 7091–7094. (b) McGilvra, J. D.; Unni, A. K.; Modi, K.; Rawal, V. H. *Angew. Chem., Int. Ed.* **2006**, *45*, 6130–6133. (c) Zhuang, W.; Poulsen, T. B.; Jørgensen, K. A. *Org. Biomol. Chem*. **2005**, *3*, 3284–3289. (d) García-García, P.; Lay, F.; García-García, P.; Rabalakos, C.; List, B. *Angew. Chem., Int. Ed*. **2009**, *48*, 4363–4366. (e) Cheon, C. H.; Yamamoto, H. *Org. Lett.* **2010**, *12*, 2476–2479. (f) Denmark, S. E.; Heemstra, J. R. *Org. Lett*. **2003**, *5*, 2303–2306.

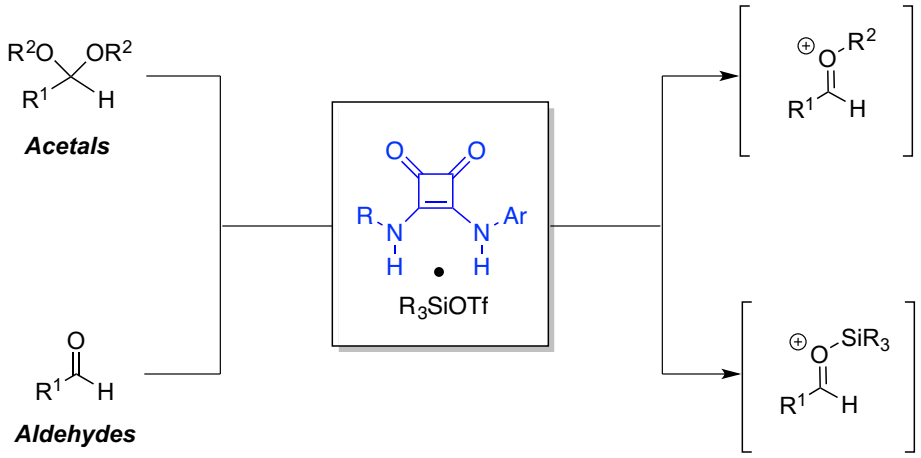

Figure 4.1. ***Oxocarbenium ion intermediates resulting from activation of acetals and aldehydes.***

4.2. Results and Discussion

4.2.1. Catalyst Optimization

We began our investigation into the feasibility of catalyzing a Mukaiyama aldol reaction via cooperative catalysis with squaramide and silyl triflate by assessing reactivity between 3-bromo benzaldehyde (**1a**) and trimethyl((1-phenylvinyl)oxy)silane under conditions similar to those found in Chapters 2 and 3. Chiral urea, thiourea and squaramide catalysts were examined in this reaction (Table 4.1). Significant reactivity was observed in the absence of H-bond donor catalyst (entry 1). Urea (**3a**) and thiourea (**3b**) catalysts provided no meaningful acceleration over background and only trace levels of enantioselectivity (entries 2,3). Consistent with our findings in Chapters 2 and 3 of this thesis, squaramide catalyst (**3c**) resulted in full conversion and a promising level of enantioselectivity (entry 4).

Table 4.1. ***Identification of the optimal hydrogen-bond donor motif.***

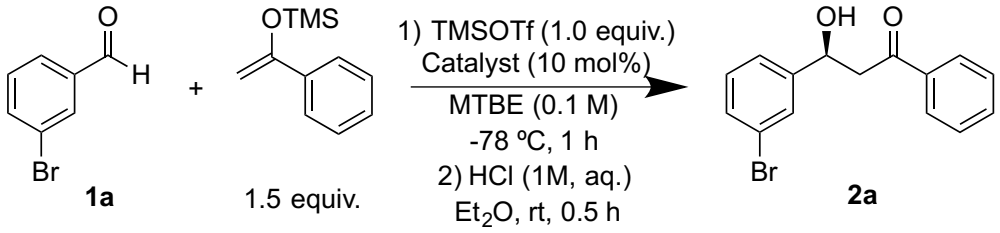

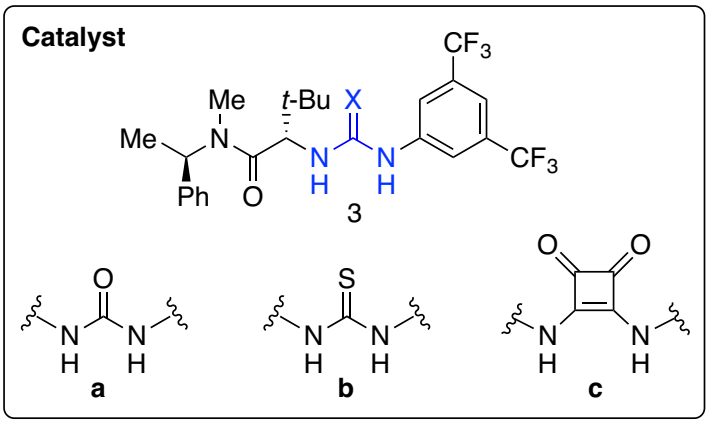

Entry	Catalyst	Conversion[a] (%)	ee[b] (%)
1	-	65	n/a
2	**3a**	64	0
3	**3b**	68	6
4	**3c**	100	43

a. Conversions determined by ^{1}H NMR analysis of the crude reaction mixture are reported.
b. ee values determined by chiral HPLC analysis.

Having established that squaramides were the optimal hydrogen-bond donor motif for this reaction, we examined the effect of structural variations in the left-hand amide portion of the catalyst on the reaction (Table 4.2). Promising lead results of enantioselectivities above 50% were obtained with three classes of catalyst: *N*-methyl-1-phenylmethanamine catalyst **3d** (entry 2), prolinol catalyst **3f** (entry 4), and indoline catalyst **3g** (entry 5). Upon extensive investigation of catalyst structure under optimal reaction conditions, squaramide catalyst **3g** was chosen for further studies and preparative scale reactions.[74]

[74] Detailed catalyst optimization studies are described in the Experimental Section. Catalyst **3g** is also practical due to its ease of synthesis.

Table 4.2. ***Investigation of squaramide catalyst structure.***

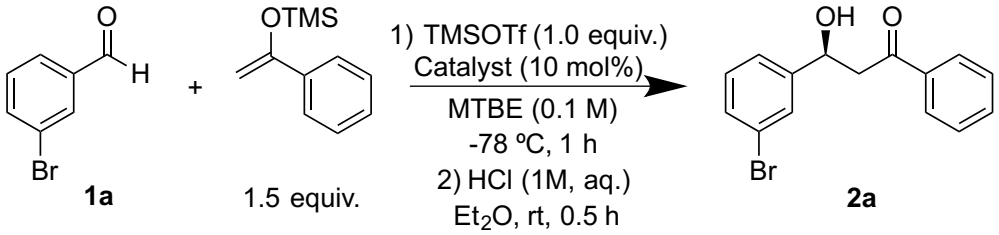

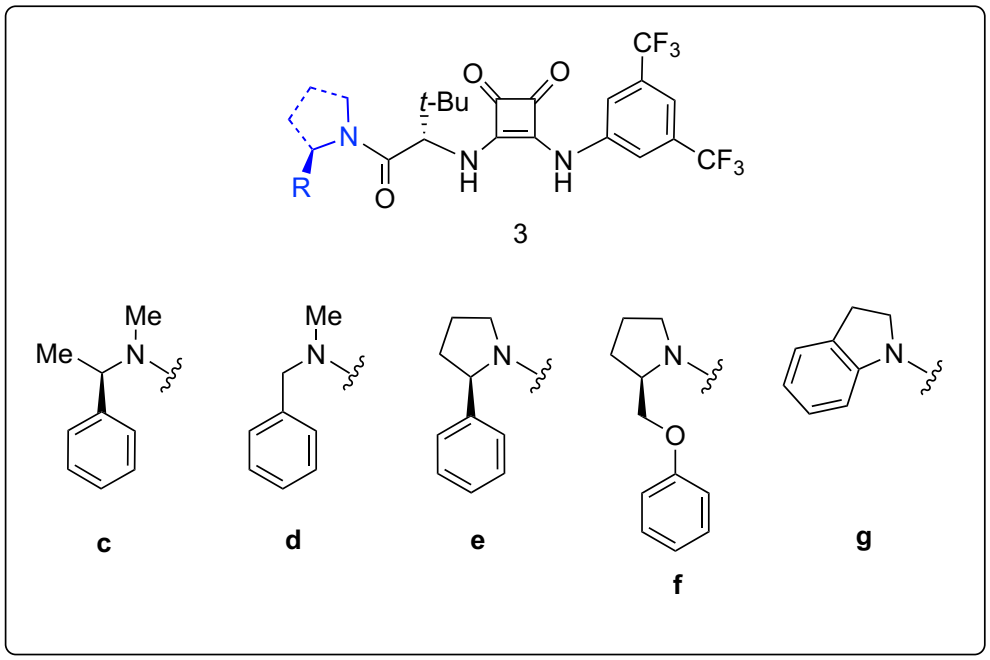

Entry	Catalyst	Conversion[a] (%)	ee[b] (%)
1	**3c**	100	43
2	**3d**	100	61
3	**3e**	100	29
4	**3f**	100	56
5	**3g**	100	55

a. Conversions determined by ^{1}H NMR analysis of the crude reaction mixture are reported.
b. ee values determined by chiral HPLC analysis.

4.2.2. Optimization of Reaction Conditions

Having established **3g** as the optimal squaramide catalyst for the Mukaiyama aldol reaction, we investigated the effects of other parameters on the reaction outcome. Solvent proved a particularly useful handle in improving the enantioselectivity of this transformation (Table 4.3). In contrast to acetal reactions discussed in Chapters 2 and 3, ethyl ether (entry 4) provided higher levels of enantioselectivity than t-butyl methyl ether (entry 1) in the Mukaiyama aldol reaction (81% ee vs. 55% ee).

Table 4.3. ***Investigation of solvent effect.***

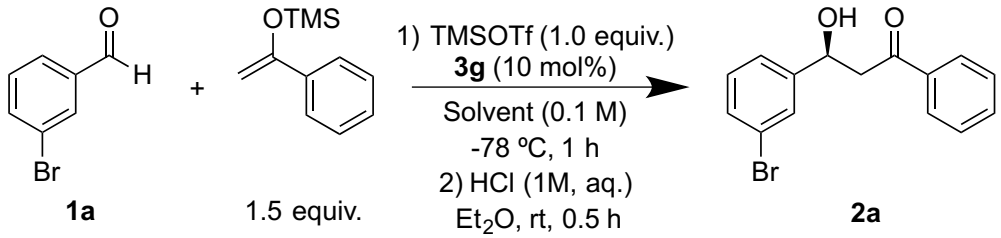

Entry	Solvent	Conversion[a] (%)	ee[b] (%)
1	MTBE	100	55
2	CPME	100	78
3	O(*i*Pr)$_2$	100	70
4	Et$_2$O	100	81
5	THF	78	0
6	Toluene	100	66
7	DCM	100	3

a. Conversions determined by ^{1}H NMR analysis of the crude reaction mixture are reported.
b. ee values determined by chiral HPLC analysis.

We observed that catalyst **3g** was not fully soluble in the reaction mixture, which led us to investigate if lower catalyst loading could be used to provide the same levels of reactivity and enantioselectivity for this transformation. We observed that lowering catalyst loading from 10 mol% (entry 7, Table 4.4) to 1 mol% (entry 4, Table 4.4) resulted in no loss of conversion or selectivity for the Mukaiyama aldol reaction. However, lowering catalyst loading below 1 mol%

did result in a gradual loss of selectivity and reactivity (entries 1-3). A catalyst loading of 1 mol% was thus chosen for further investigations.

Table 4.4. ***Investigation of squaramide catalyst loading.***

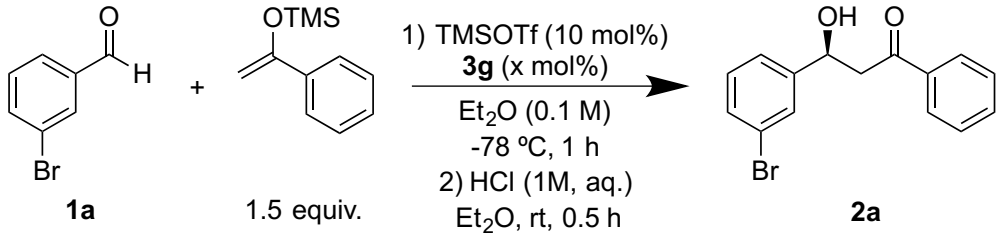

Entry	Catalyst Loading (mol%)	Conversion[a] (%)	ee[b] (%)
1	0.1	37	21
2	0.2	96	77
3	0.3	100	77
4	1	100	81
5	2	100	81
6	5	100	81
7	10	100	81

a. Conversions determined by ^{1}H NMR analysis of the crude reaction mixture are reported.
b. ee values determined by chiral HPLC analysis.

Given the high levels of background reactivity, we investigated the effect of the loading of TMSOTf promoter on the reaction outcome. Varying TMSOTf loading over two orders of magnitude, from 2 mol% (entry 4, Table 4.5) to 200 mol% (entry 8, Table 4.5), had only a negligible effect on enantioselectivity of the reaction (79% vs. 81%). The small effects that both the squaramide catalyst and TMSOTf promoter loadings had on the reaction outcome led us to conclude that the observed enantioselectivity was intrinsic to the catalyst and was not eroded by a competing background reaction. The fact that background reactivity has negligible effect on the outcome of the reaction under a wide range of the catalyst and TMSOTf loadings speaks to the power and efficiency of the squaramide-silyl triflate co-catalytic system.

Table 4.5. ***Investigation of TMSOTf promoter loading*****.**

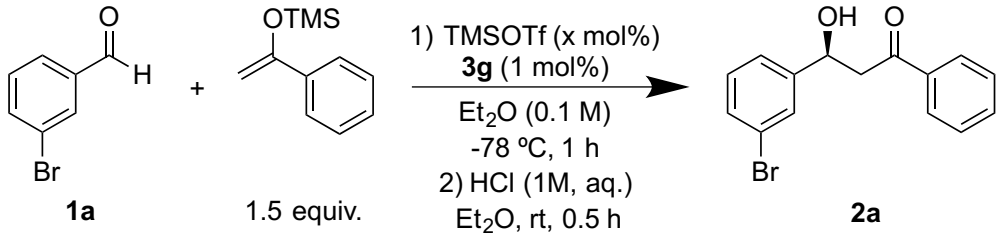

Entry	TMSOTf Loading (mol%)	Conversion[a] (%)	ee[b] (%)
1	0.1	n.r.	n.d.
2	0.5	71	73
3	1	91	79
4	2	100	79
5	5	100	81
6	10	100	81
7	50	100	81
8	200	100	81

a. Conversions determined by ^{1}H NMR analysis of the crude reaction mixture are reported.
b. ee values determined by chiral HPLC analysis.

4.2.3. Aldehyde Scope

With the optimal catalyst and reaction conditions in hand, we investigated the scope of the Mukaiyama aldol reaction with respect to the aldehyde. Electron-poor aryl aldehydes were viable substrates for this reaction with enantioselectivity varying between 78% and 82% for a range of substrates (entries 1-6, Table 4.6). Benzaldehyde provided product with 100% conversion, but in slightly lower enantioselectivity of 71% (entry 7). Electron-rich *p*-tolualdehyde resulted in further decrease in enantioselectivity to 52% (entry 8). In this case, it appears that the reaction outcome is less dependent on the electronics of the oxocarbenium intermediate (as compared to the nucleophilic substitution of acetals in Chapter 3). This suggests that the oxocarbenium ion pair arising from aldehyde silylation is lower in energy than the corresponding oxocarbenium arising from acetal ionization, resulting in an earlier transition state with less charge build-up and less sensitivity to electronic perturbations. Alternatively, a change in the enantioselectivity-determining step from the oxocarbenium complex formation with acetal substrates to nucleophilic addition with aldehydes could be at play here.

Sterically encumbered aldehydes resulted in lower reactivity as well as selectivity in this transformation (entries 9, 10). Heteroaromatic substrate, 5-chlorofuran-2-carbaldehyde, resulted in low levels of both enantioselectivity and reactivity (entry 12). Aliphatic aldehydes resulted in enantioselectivities below 5% under a variety of conditions. Ketones were unreactive under various reaction conditions, even at temperatures as high as 0 °C.

Table 4.6. ***Aldehyde scope.***

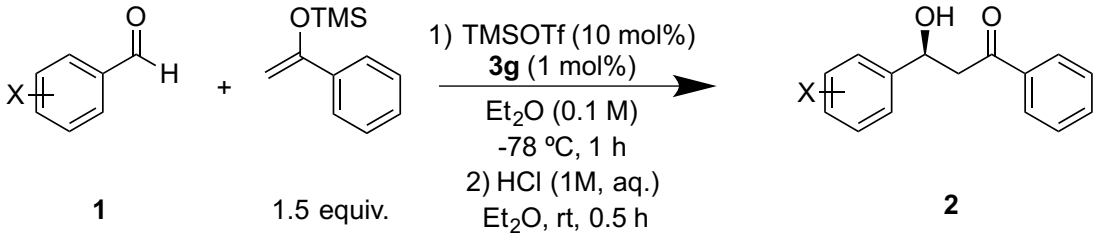

1 1.5 equiv. **2**

Entry	Aldehyde	Product		Conversion[a] (%)	ee[b] (%)
1	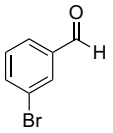	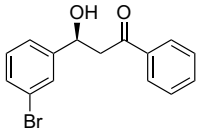	**2a**	100	82
2	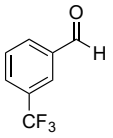	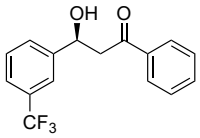	**2b**	100	79
3	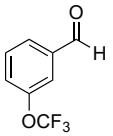	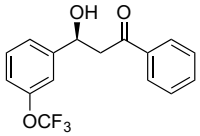	**2c**	100	82
4	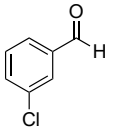	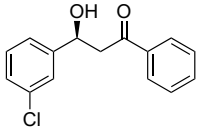	**2d**	100	81
5	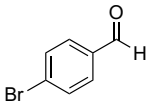	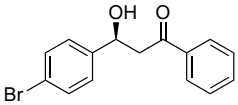	**2f**	100	78
6	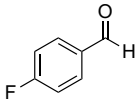	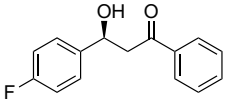	**2g**	100	78
7	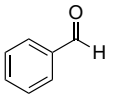	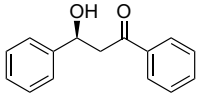	**2e**	100	71
8	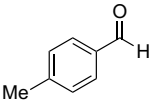	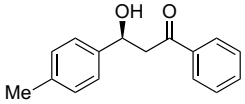	**2h**	100	52
9	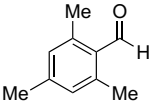	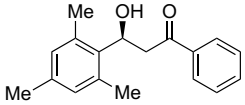	**2i**	100	19
10	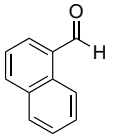	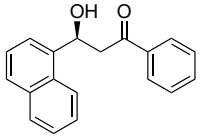	**2j**	74	23

Table 4.6. (Continued).

11	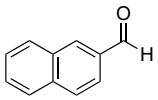	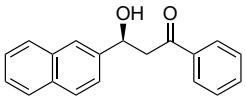	**2k**	94	71
12	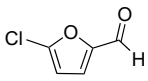	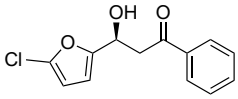	**2l**	57	33

a. Conversions determined by ^{1}H NMR analysis of the crude reaction mixture are reported.
b. ee values determined by chiral HPLC analysis.

4.2.4. Nucleophile Scope

Given the wide range of nucleophiles that are compatible with nucleophilic substitution of acetals described in Chapter 3, we investigated the scope of nucleophiles compatible with the Mukaiyama aldol reaction. In contrast to the acetal chemistry, this reaction displays a strong sensitivity towards the nucleophile structure (Table 4.7). Structurally different silyl enol ethers, either derived from substituted acetophenones or aliphatic ketones, performed worse than the trimethyl((1-phenylvinyl)oxy)silane nucleophile used in reaction optimization studies (entries 1-5, Table 4.7 vs. entry 1, Table 4.6). Methallyltrimethylsine resulted in clean product formation in 76% ee (entry 6). Silyl ketene acetals provided products in lower enantioselectivity, which is likely due to the high nucleophilicity of these compounds relative to silyl enol ethers and allyl silanes, resulting in a less selective attack on the oxocarbenium-catalyst complex. This reaction's strong dependence on both nucleophile structure and nucleophilicity as compared to the nucleophilic substitution of acetals described in Chapter 3 suggests that nucleophilic addition is likely the enantiodetermining step.

Table 4.7. ***Nucleophile scope.***

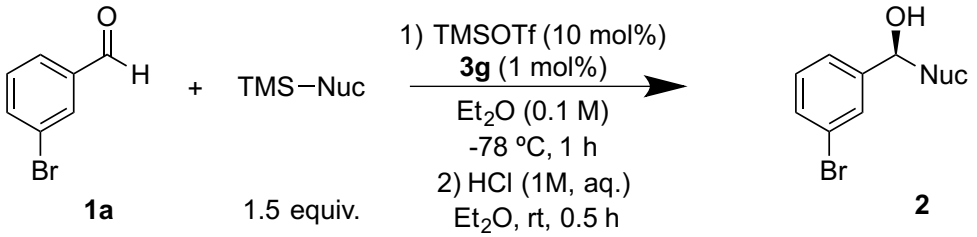

Entry	Nucleophile	Product		Conversion[a] (%)	ee[b] (%)
1	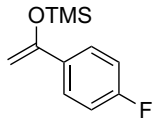	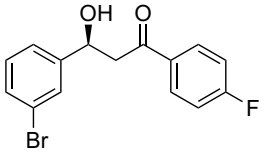	**2m**	85	71
2	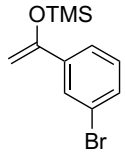	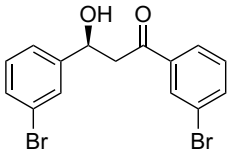	**2n**	54	61
3	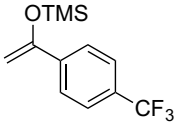	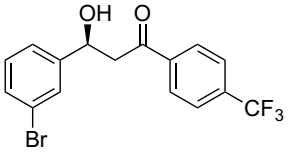	**2o**	<10	n.d.
4	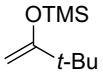	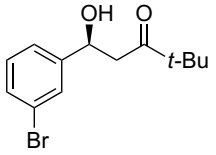	**2p**	n.r.	n.d.
5		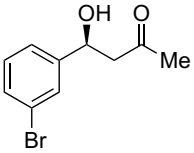	**2q**	93	42
6	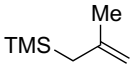	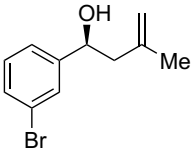	**2r**	100	76
7	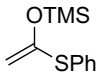	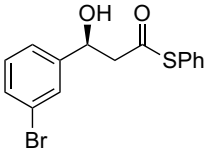	**2s**	74	28
8	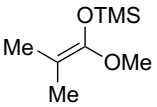	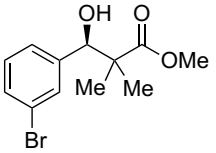	**2t**	82	11

a. Conversions determined by ^{1}H NMR analysis of the crude reaction mixture are reported.
b. ee values determined by chiral HPLC analysis.

4.2.5. Preparative scale reactions

While our aldehyde and nucleophile scope studies were done on 0.05 mmol scale, we also briefly investigated reactions on preparative scale (0.5 mmol) with optimized reaction conditions (Schemes 4.1 and 4.2). Only 2.7 mg of catalyst **3g** were used to afford more than 100 mg of products in good yields and enantioselectivities.

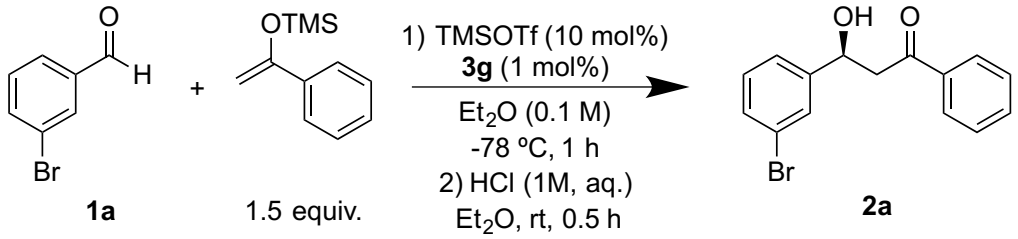

Scheme 4.1. ***Preparative scale reaction with silyl enol ether nucleophile.*** 80% yield, 82% ee.

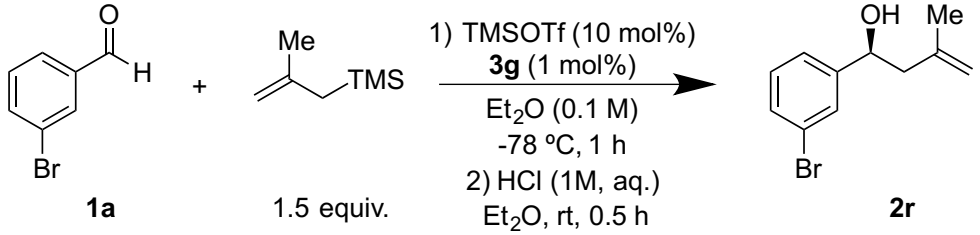

Scheme 4.1. ***Preparative scale reaction with methallyltrimethylsine nucleophile.*** 84% yield, 79% ee.

4.3. Conclusion

The new mode of cooperative catalysis with squaramides and silyl triflates was applied to the asymmetric addition of silyl enol ether and allylsilane nucleophiles to aldehydes. While we were not able to afford products with synthetically useful enantioselectivities using current catalyst scaffolds, future developments in catalyst structures could enable these reactions to proceed in a highly enantioselective fashion. This research extends starting material scope for asymmetric reactions of oxocarbenium ions using squaramide and silyl triflate co-catalysts from acetals to aldehydes and lays the groundwork for applying this new mode of catalysis to other cationic intermediates in the future.

4.4. Experimental Section

4.4.1. General Information

All reactions were performed in flame-dried 10 mL round-bottom flasks unless otherwise noted. The flasks were fitted with rubber septa and reactions were conducted under nitrogen. Stainless steel syringes were used to transfer air- and moisture-sensitive liquids. Flash chromatography was performed using silica gel 60 (230-400 mesh) from EM Science. Commercial reagents were purchased from Aldrich, Alfa Aesar, Strem or TCI, and used as received with the following exceptions: dichloromethane, tetrahydrofuran, toluene, ethyl ether, *t*-butyl methyl ether were dried by passing through columns of activated molecular sieves. Triethylamine was distilled from CaH_2 at 760 torr. Proton nuclear magnetic resonance (^{1}H NMR) spectra and carbon nuclear magnetic resonance (^{13}C NMR) spectra were recorded on Inova-500 (500 MHz) spectrometers. Chemical shifts for protons are reported in parts per million downfield from tetramethylsilane and are referenced to residual protium in NMR solvent ($CHCl_3$ = δ 7.27). Chemical shifts for carbon are reported in parts per million downfield from tetramethylsilane and are referenced to the carbon resonance of the solvent ($CDCl_3$ = δ 77.0). Data are represented as follows: chemical shift, multiplicity (br. = broad, s = singlet, d = doublet, t = triplet, q = quartet, m = multiplet), coupling constants in Hertz (Hz), integration. Infrared (IR) spectra were obtained using Bruker Optics Tensor 27 FTIR spectrometer. Optical rotations were measured using a 1mL cell with 0.5 dm path length on a Jasco DIP 370 digital polarimeter. The mass spectra were obtained on a Bruker micrOTOF-Q II time-of-flight LC/MS spectrometer. Chiral HPLC analysis was performed using an Agilent Technologies 1200 series instrument with commercial Chiralpak columns.

4.4.2. Synthesis and Characterization of Catalyst 3g

3g was synthesized according to general procedure for catalyst synthesis described in Chapter 1 in 44% yield over 3 steps.

(*S*)-3-((3,5-bis(trifluoromethyl)phenyl)amino)-4-((1-(indolin-1-yl)-3,3-dimethyl-1-oxobutan-2-yl)amino)cyclobut-3-ene-1,2-dione (**3g**):

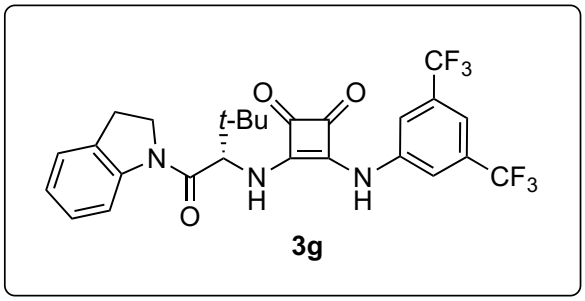

3g

^{1}H NMR (500 MHz, DMSO-d_6) δ 10.43 (s, 1 H), 8.42 (d, *J*=9.8 Hz, 1 H), 8.16 (d, *J*=7.8 Hz, 1 H), 8.08 (s, 2 H), 7.66 (s, 1 H), 7.27 (d, *J*=7.3 Hz, 1 H), 7.19 (t, *J*=7.3 Hz, 1 H), 7.03 - 7.09 (m, 1 H), 7.06 (t, *J*=7.8 Hz, 1 H), 5.08 (d, *J*=9.8 Hz, 1 H), 4.29 (ddd, *J*=38.6, 18.1, 9.8 Hz, 2 H), 3.19 (t, *J*=9.3 Hz, 2 H), 1.07 (s, 9 H); (rotamer ration in DMSO >20:1);

^{13}C NMR (125 MHz, $CDCl_3$) δ 184.9, 180.94, 169.6, 168.8, 163.0, 142.5, 141.5, 133.1, 132.0, 131.7, 127.5, 125.5, 124.7, 122.5, 118.5, 117.2, 115.2, 62.2, 49.2, 36.5, 27.9, 26.2;

FTIR (neat, cm^{-1}) ν_{max} 1595, 1554, 1478, 1437, 1409, 1377, 1278, 1175, 1131, 699, 680 cm^{-1};

HRMS (ESI-TOF) calculated for $C_{26}H_{23}F_6N_3O_3$ $[M+Na]^+$: 562.1541, found: 562.1547;

$[\alpha]_D^{25}$ = –44.2° (c = 1, $CHCl_3$).

4.4.3. General Procedure for Squaramide-Catalyzed Mukaiyama Aldol Reaction

Method A (reaction optimization): A 1-dram vial was equipped with a magnetic stir bar, closed with a cap containing a rubber septum, flame-dried and subsequently cooled under vacuum. The vial was placed under N_2 and charged with substrate **1a** (0.05 mmol, 1 equiv.), 1-phenyl-1-trimethylsiloxyethylene (15.4 μL, 0.075 mmol, 1.5 equiv.), **3g** (2.7 mg, 0.005 mmol, 10 mol%) and dry ethyl ether (0.5 mL). The mixture was then cooled to -78 ºC on the dry ice-acetone bath. TMSOTf (9 μL, 0.05 mmol, 1 equiv.) was added via syringe. The reaction was stirred for 4 h at -78 ºC, and then quenched via addition of 100 μL of a 6:1 MeOH:Et_3N solution via syringe. Crude reaction mixture was then concentrated and conversion determined by ^1H NMR. Crude mixture was then re-dissolved in ethyl ether and HCl (2 mL, 1M, aq.) was added. The mixture was allowed to stir at room temperature for 0.5 h at room temperature, after which layers were separated and organic layer was used to determine enantioselectivity.

Method B (preparative scale reactions): A 25 mL round-bottom flask was equipped with a magnetic stir bar, flame-dried and subsequently cooled under vacuum. The flask was placed under N_2 and charged with substrate **1a** (0.5 mmol, 1 equiv.), 1-phenyl-1-trimethylsiloxyethylene (153.8 μL, 0.75 mmol, 1.5 equiv.), **3g** (2.7 mg, 0.005 mmol, 1.0 mol%) and dry ethyl ether (5 mL). The mixture was then cooled to -78 ºC on the dry ice-acetone bath. TMSOTf (9 μL, 0.05 mmol, 10 mol%) was added via syringe. The reaction was stirred for 1 h at -78 ºC, and then quenched via addition of 100 μL of a 6:1 MeOH:Et_3N solution via syringe. The reaction mixture was warmed up to room temperature and HCl (10 mL, 1M, aq.) was added. The reaction mixture was allowed to stir for 0.5 h at room temperature, after which layers were separated and aqueous layer was washed with DCM (3 x 10 mL). Combined organic layers were

dried over $MgSO_4$, filtered and concentrated. Product was then purified by column chromatography with hexane/ethyl ether as eluent (1:0 to 3:1) to yield pure **2a**.

4.4.4. Characterization of Products 2a, 2r and (*S*)-1-(4-bromophenyl)-3-methylbut-3-en-1-ol

(*S*)-3-(3-bromophenyl)-3-hydroxy-1-phenylpropan-1-one (**2a**):

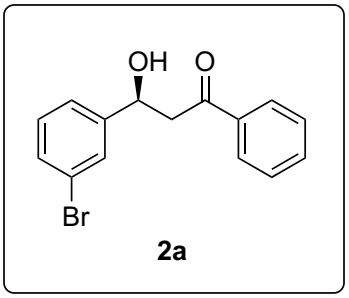

2a

According to general procedure (Method B), **1a** (0.5 mmol) was reacted to give **2a** in 121.2 mg (79.4% yield) as a yellow oil.

^{1}H NMR (500 MHz, $CDCl_3$) δ 7.94 (d, *J*=8.3 Hz, 2 H), 7.56 - 7.66 (m, 2 H), 7.47 (t, *J*=7.8 Hz, 2 H), 7.42 (d, *J*=6.8 Hz, 1 H), 7.36 (d, *J*=7.8 Hz, 1 H), 7.20 - 7.26 (m, 1 H), 5.32 (dd, *J*=7.8, 4.4 Hz, 1 H), 5.15 - 5.45 (m, 1 H), 3.75 (s, 1H), 3.27 - 3.45 (m, 2 H);

^{13}C NMR (125 MHz, $CDCl_3$) δ 199.8, 145.4, 136.4, 133.8, 130.7, 130.1, 129.0, 128.6, 172.3, 124.5, 122.7, 69.3, 47.3;

FTIR (neat, cm^{-1}) ν_{max} 1677, 1597, 1448, 1213, 1180, 1069, 781, 754, 688 cm^{-1};

HRMS (ESI-TOF) calculated for $C_{15}H_{13}BrO_2$ $[M+Na]^+$: 326.9997, found: 327.0045;

$[\alpha]_D^{25}$ = –34.4° (c = 1, $CHCl_3$).

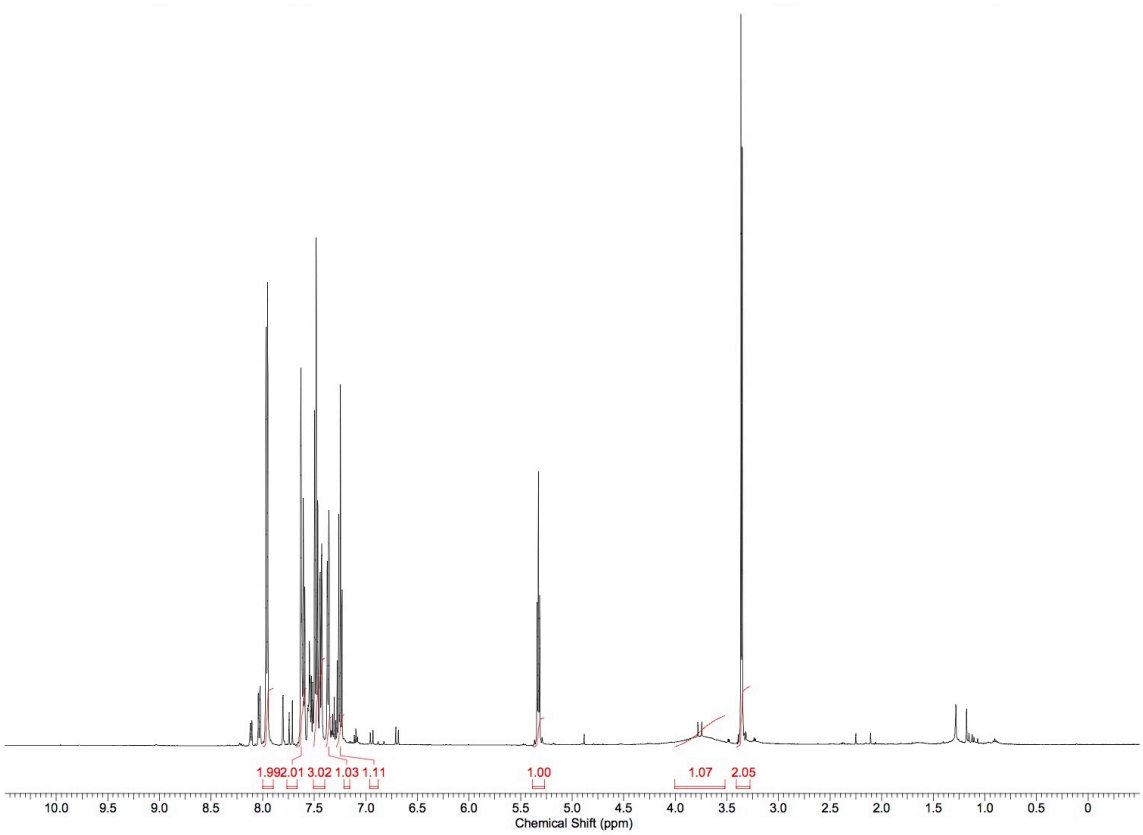
1.99
2.01
3.02
1.03
1.11
1.00
1.07
2.05
10.0 9.5 9.0 8.5 8.0 7.5 7.0 6.5 6.0 5.5 5.0 4.5 4.0 3.5 3.0 2.5 2.0 1.5 1.0 0.5 0
Chemical Shift (ppm)

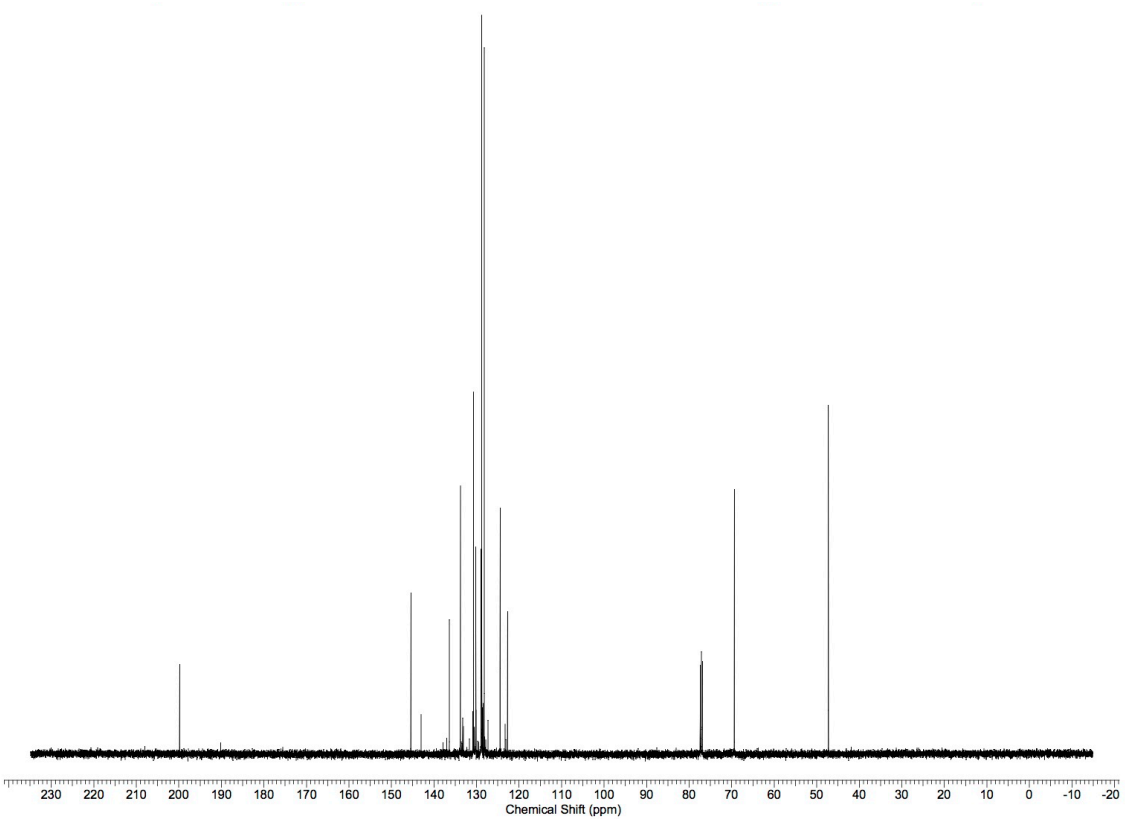
230 220 210 200 190 180 170 160 150 140 130 120 110 100 90 80 70 60 50 40 30 20 10 0 -10 -20
Chemical Shift (ppm)

Racemic sample: HPLC (ChiralPak AS-H, 10% IPA/hexanes, 1 mL/min, 210 nm)

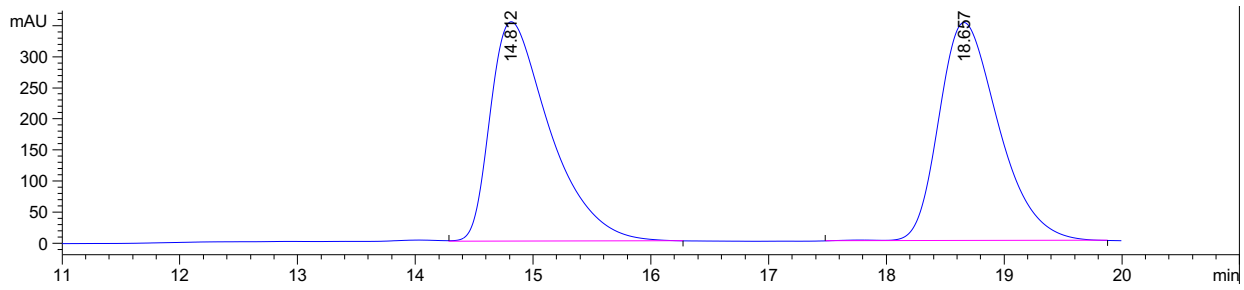

Peak #	RetTime [min]	Type	Width [min]	Area [mAU*s]	Height [mAU]	Area %
1	14.812	VB	0.5334	1.24325e4	352.54868	50.0912
2	18.657	BB	0.5441	1.23872e4	350.70255	49.9088

Enantioenriched Sample: HPLC (ChiralPak AS-H, 10% IPA/hexanes, 1 mL/min, 210 nm),

82% e.e.

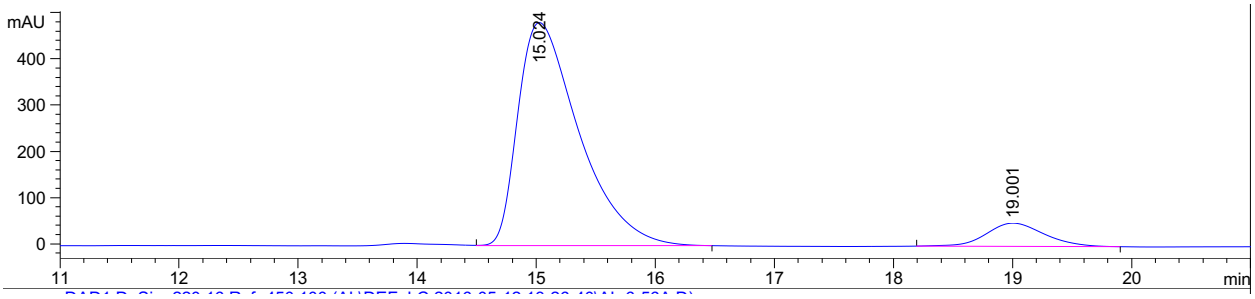

Peak #	RetTime [min]	Type	Width [min]	Area [mAU*s]	Height [mAU]	Area %
1	15.024	VB	0.5428	1.72522e4	482.95331	90.8216
2	19.001	BB	0.5232	1743.51074	50.70445	9.1784

(*S*)-1-(3-bromophenyl)-3-methylbut-3-en-1-ol (**2r**):

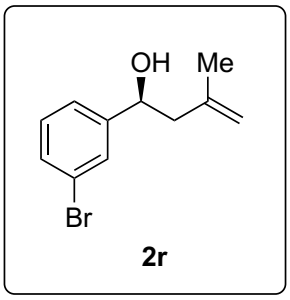

2r

According to general procedure (Method B), **1a** (0.25 mmol) was reacted to give **2r** in 101.2 mg (84% yield) as clear oil.

^{1}H NMR (500 MHz, $CDCl_3$) δ 7.52 - 7.57 (m, 1 H), 7.41 (d, *J*=7.8 Hz, 1 H), 7.29 (d, *J*=7.8 Hz, 1 H), 7.22 (t, *J*=7.8 Hz, 1 H), 4.94 - 4.97 (m, 1 H), 4.86 (s, 1 H), 4.76 (dd, *J*=8.3, 4.9 Hz, 1 H), 2.37 - 2.41 (m, 3 H), 1.80 (s, 3 H);

^{13}C NMR (125 MHz, $CDCl_3$) δ 146.5, 141.9, 130.5, 130.0, 128.9, 124.4, 122.5, 114.5, 70.7, 48.4, 22.3;

FTIR (neat, cm^{-1}) ν_{max} 1570, 1428, 1194, 1070, 997, 888, 781, 693, 672 cm^{-1};

HRMS (ESI-TOF) calculated for $C_{11}H_{13}BrO$ $[M+Na]^+$: 263.0047, found: 263.0088;

$[\alpha]_D^{25}$ = –45.0° (c = 1, $CHCl_3$).

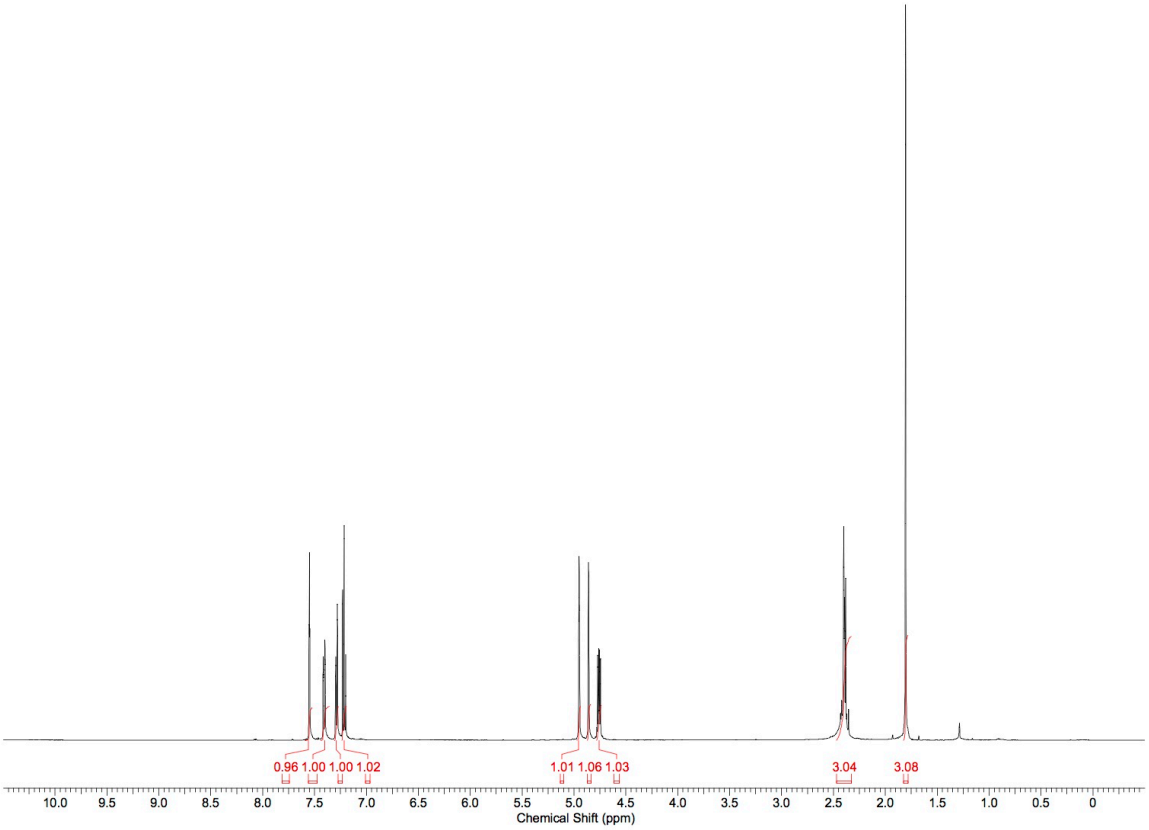
0.96 1.00 1.00 1.02
1.01 1.06 1.03
3.04
3.08
10.0 9.5 9.0 8.5 8.0 7.5 7.0 6.5 6.0 5.5 5.0 4.5 4.0 3.5 3.0 2.5 2.0 1.5 1.0 0.5 0
Chemical Shift (ppm)

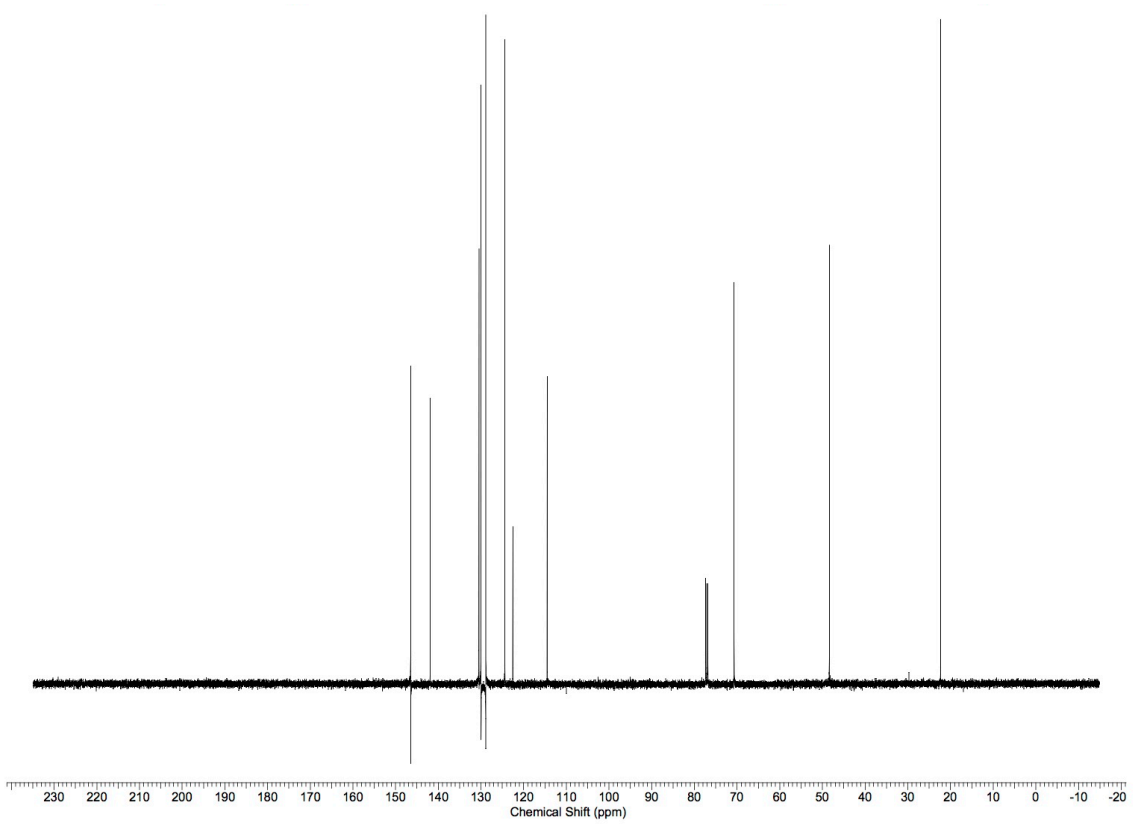
230 220 210 200 190 180 170 160 150 140 130 120 110 100 90 80 70 60 50 40 30 20 10 0 -10 -20
Chemical Shift (ppm)

Racemic sample: HPLC (ChiralPak OD-H, 10% IPA/hexanes, 1 mL/min, 210 nm)

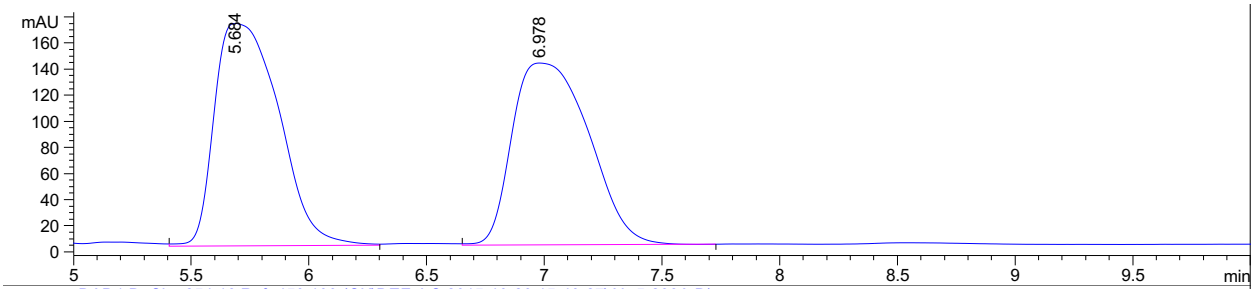

Peak #	RetTime [min]	Type	Width [min]	Area [mAU*s]	Height [mAU]	Area %
1	5.684	VV	0.3184	3255.30151	170.77275	50.8172
2	6.978	BB	0.3757	3150.60278	139.37738	49.1828

Enantioenriched Sample: HPLC (ChiralPak OD-H, 10% IPA/hexanes, 1 mL/min, 210 nm),

79% e.e.

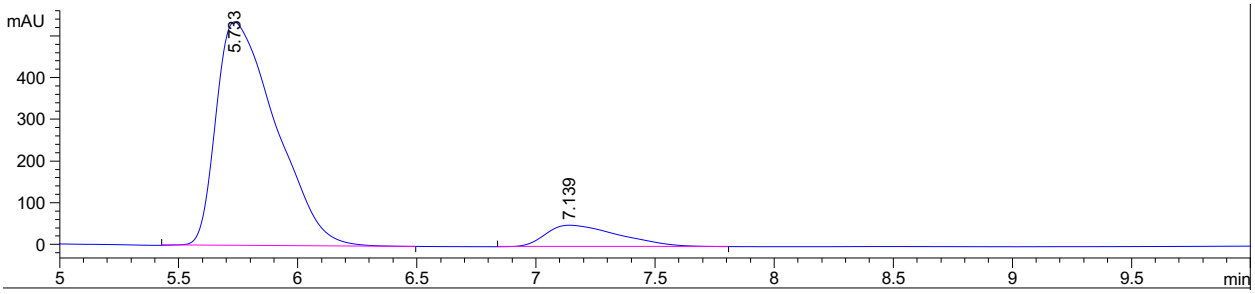

Peak #	RetTime [min]	Type	Width [min]	Area [mAU*s]	Height [mAU]	Area %
1	5.733	BB	0.2670	9334.43945	536.34875	89.4130
2	7.139	BB	0.3303	1105.24719	51.52133	10.5870

(*S*)-1-(4-bromophenyl)-3-methylbut-3-en-1-ol:

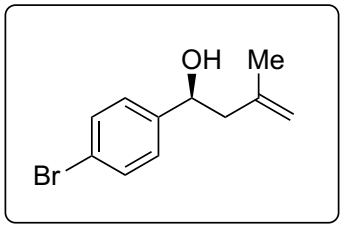

According to general procedure (Method B), **1a** (0.25 mmol) was reacted to give (*S*)-1-(4-bromophenyl)-3-methylbut-3-en-1-ol in 118.00 mg (98% yield) as a white solid.

^{1}H NMR (500 MHz, $CDCl_3$) δ 7.47 (d, *J*=8.3 Hz, 2 H), 7.25 (d, *J*=8.3 Hz, 2 H), 4.94 (s, 1 H), 4.82 - 4.89 (m, 1 H), 4.68 - 4.79 (m, 1 H), 2.39 (d, *J*=6.3 Hz, 2 H), 1.79 (s, 3 H);

^{13}C NMR (125 MHz, $CDCl_3$) δ 143.1, 142.0, 131.5, 127.5, 121.2, 144.4, 70.8, 48.3, 22.4;

FTIR (neat, cm^{-1}) ν_{max} 1487, 1404, 1375, 1070, 1010, 893, 826, 552 cm^{-1};

HRMS (ESI-TOF) calculated for $C_{11}H_{13}BrO$ $[M+Na]^+$: 263.0047, found: 263.0097;

$[\alpha]_D^{25}$ = –52.2° (c = 1, $CHCl_3$).

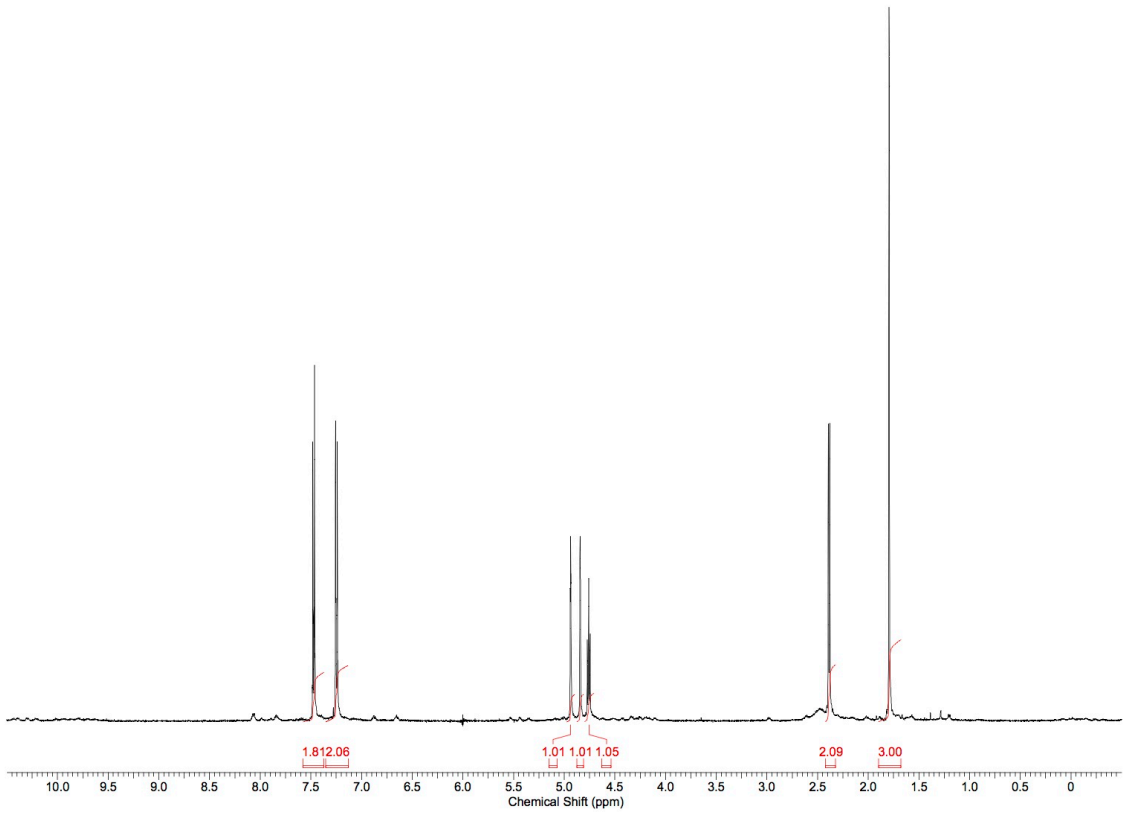
1.81
2.06
1.01
1.01
1.05
2.09
3.00
10.0 9.5 9.0 8.5 8.0 7.5 7.0 6.5 6.0 5.5 5.0 4.5 4.0 3.5 3.0 2.5 2.0 1.5 1.0 0.5 0
Chemical Shift (ppm)

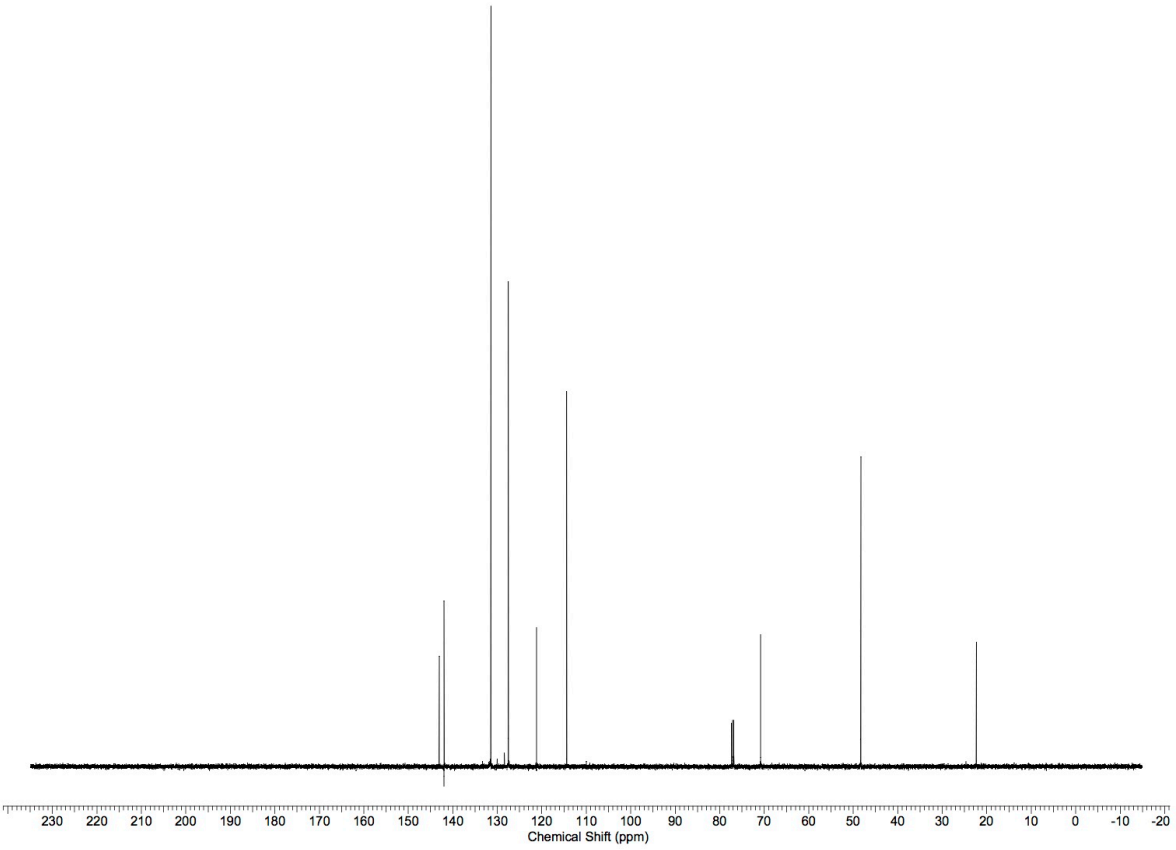
230 220 210 200 190 180 170 160 150 140 130 120 110 100 90 80 70 60 50 40 30 20 10 0 -10 -20
Chemical Shift (ppm)

Racemic sample: HPLC (ChiralPak IC, 2% IPA/hexanes, 1 mL/min, 220 nm)

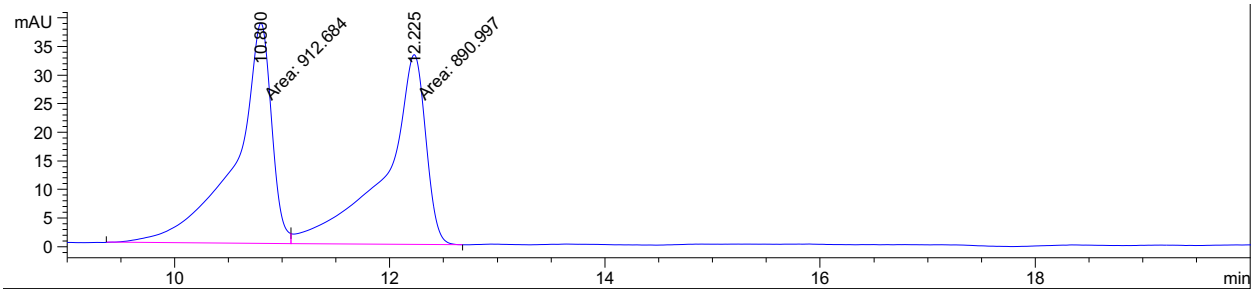

Peak #	RetTime [min]	Type	Width [min]	Area [mAU*s]	Height [mAU]	Area %
1	10.800	MF	0.3943	912.68433	38.57579	50.6012
2	12.225	FM	0.4466	890.99750	33.25454	49.3988

Enantioenriched Sample: HPLC (ChiralPak IC, 2% IPA/hexanes, 1 mL/min, 220 nm), 76% e.e.

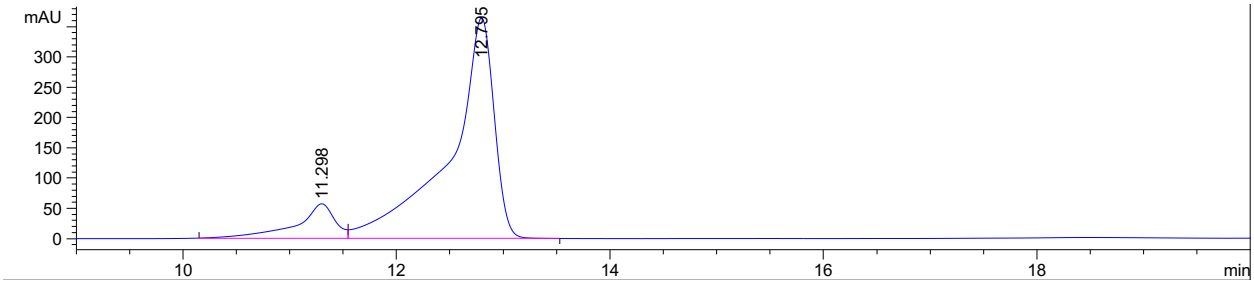

Peak #	RetTime [min]	Type	Width [min]	Area [mAU*s]	Height [mAU]	Area %
1	11.298	BV	0.3517	1459.59973	57.19541	12.2402
2	12.795	VB	0.3949	1.04651e4	364.57053	87.7598

4.4.5. Absolute Configuration Determination

The absolute configurations of (*S*)-1-(4-bromophenyl)-3-methylbut-3-en-1-ol and (*S*)-3-(4-bromophenyl)-3-hydroxy-1-phenylpropan-1-one were assigned by comparison with experimental data provided in references 73a and 73e. The absolute configurations of all other products were assigned by analogy.

4.4.6. Catalyst Optimization Studies

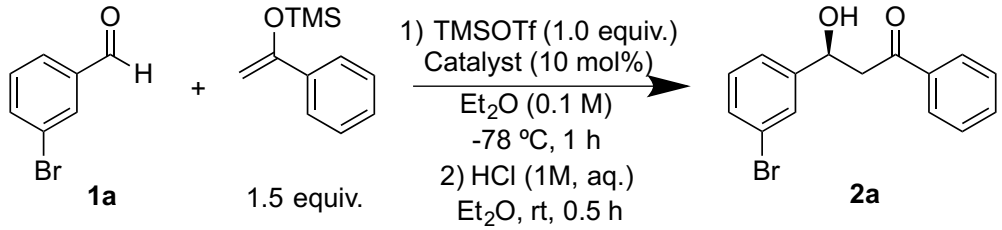

Scheme 4.3. ***Reaction used for catalyst optimization studies.***

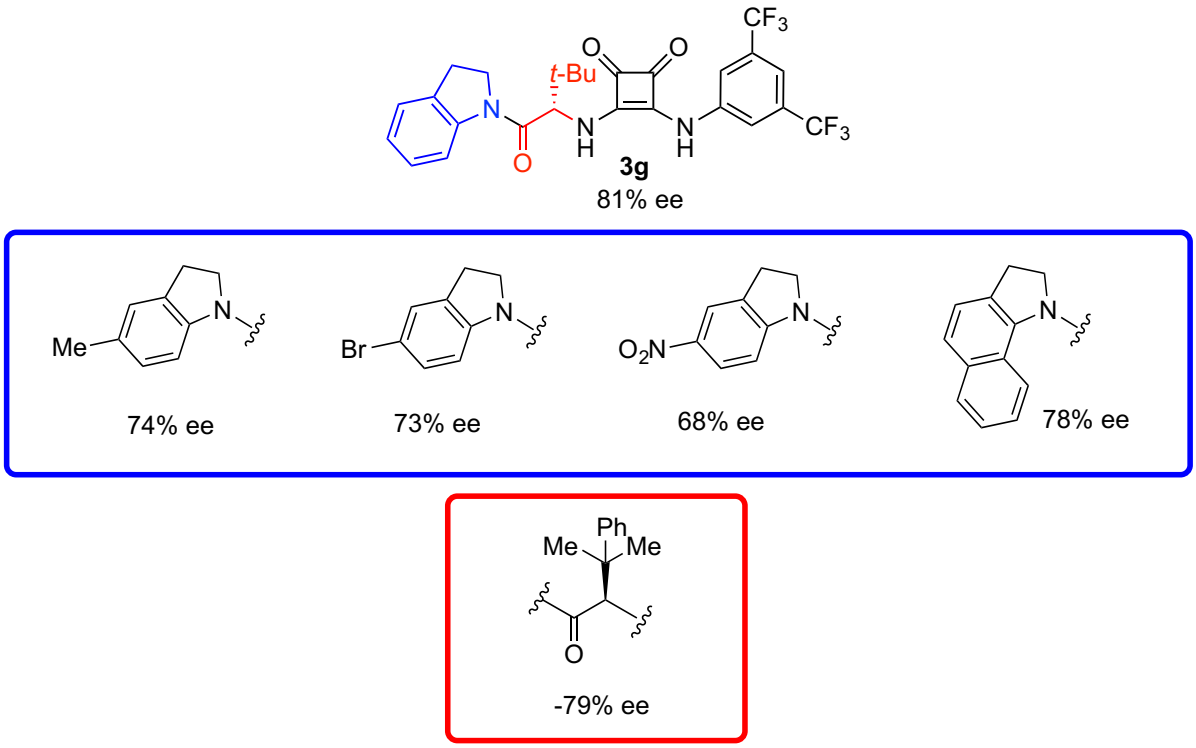

Figure 4.2. ***Variation in structure of catalyst 3g.***

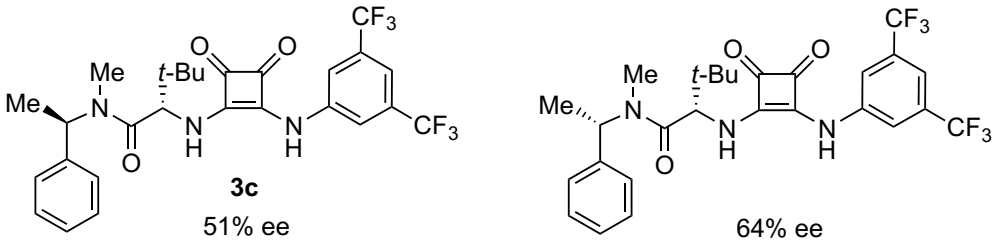

Figure 4.3. ***Investigation of diastereomers of catalyst 3c.***

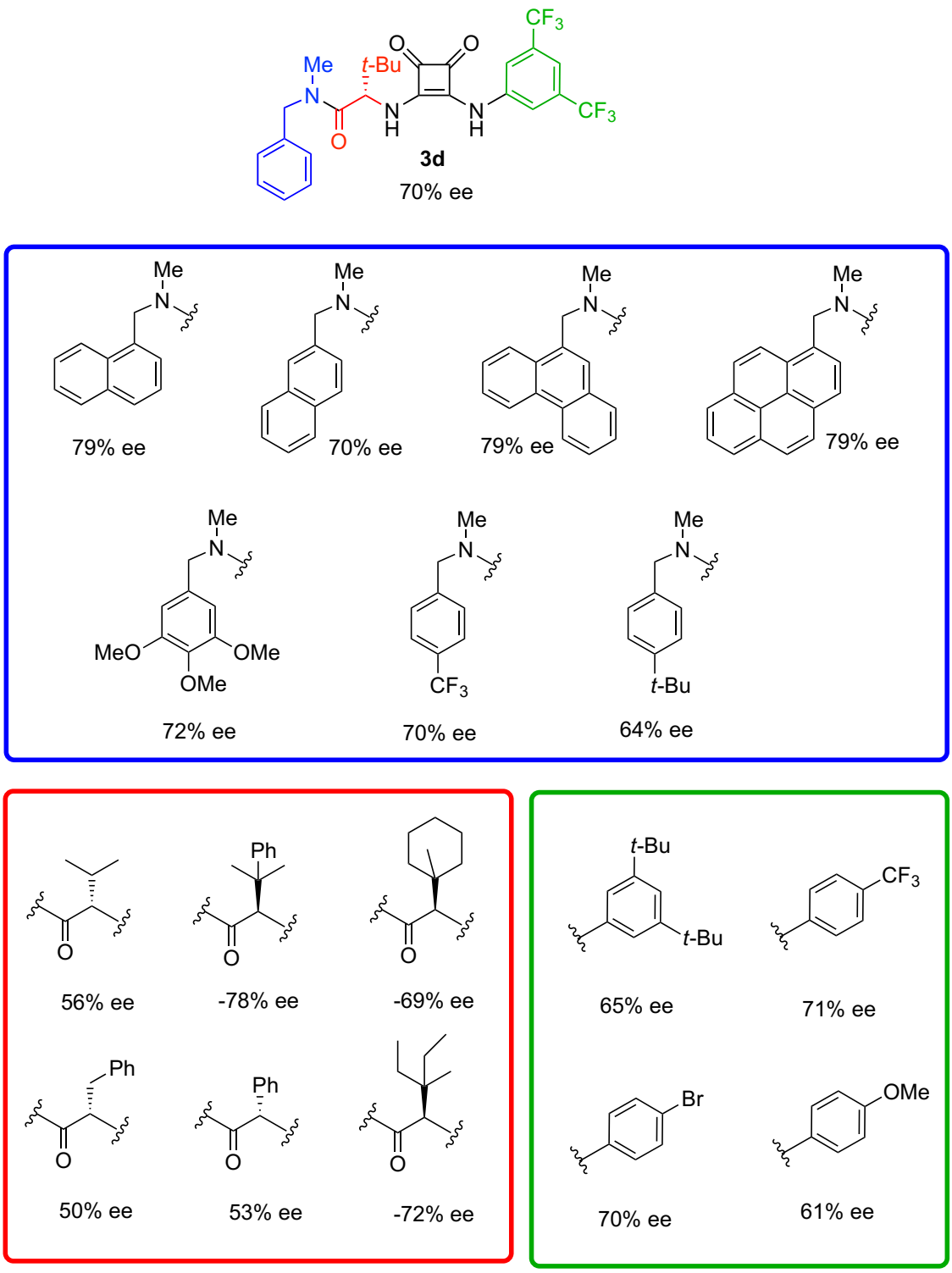

Figure 4.4. ***Variation in structure of catalyst 3d.***

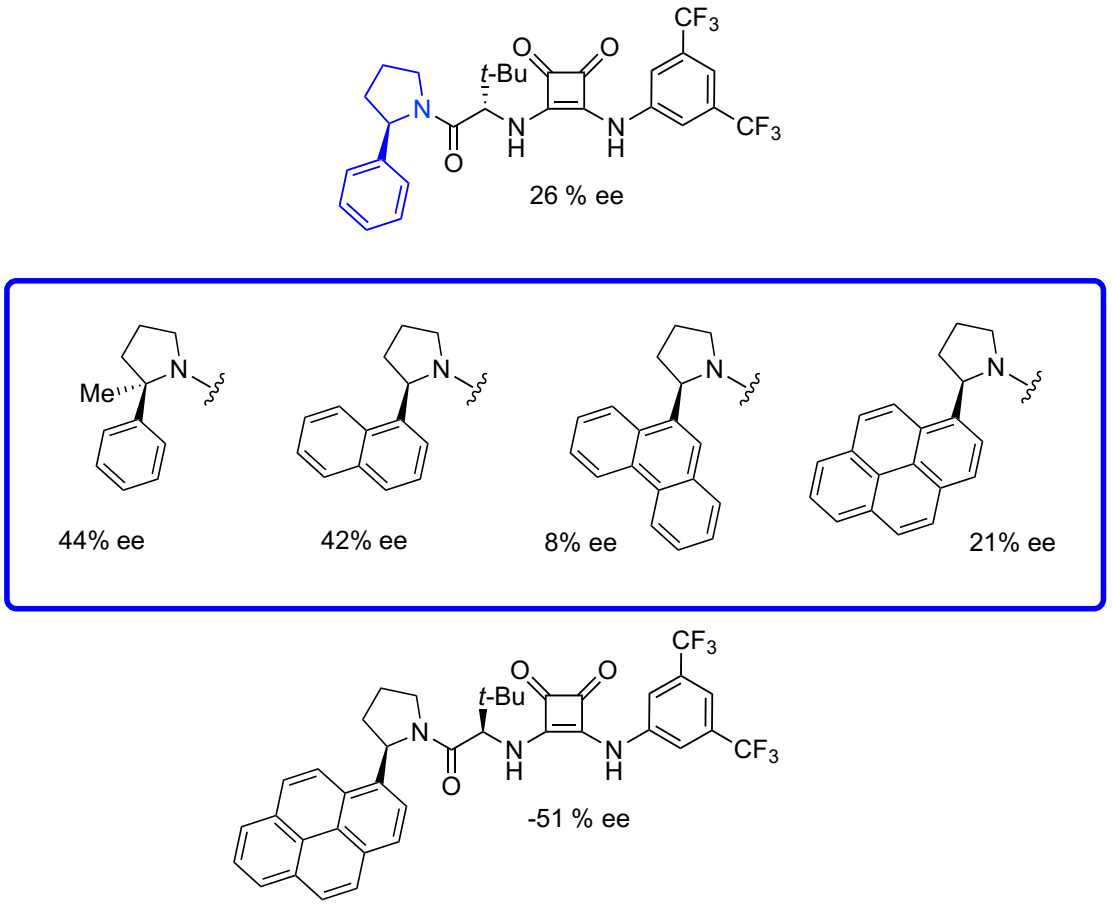

Figure 4.5. ***Variation in structure of catalyst 3e.***

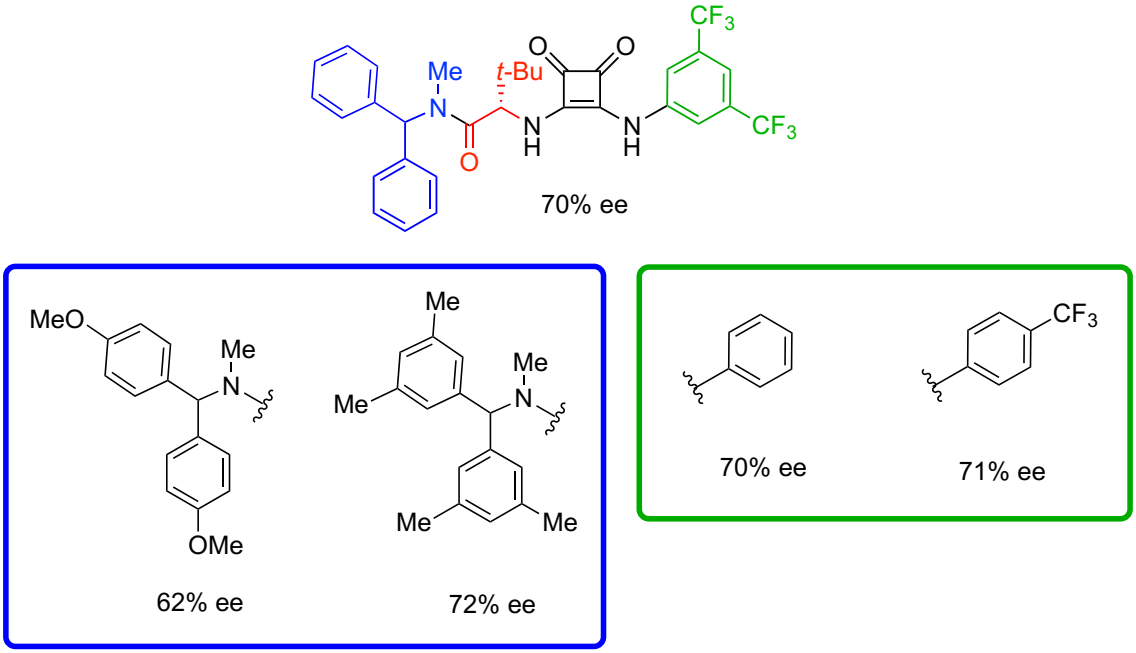

Figure 4.6. ***Variation in structure of benzhydrylamine-derived catalyst.***

4.4.7. Reaction Optimization Studies

Table 4.8. ***Investigation of the protecting group on nucleophile.***

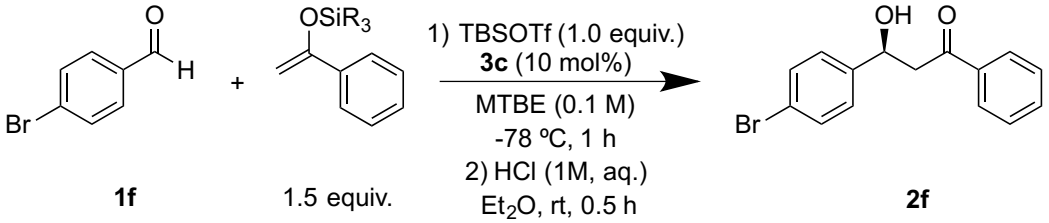

1f 1.5 equiv. **2f**

Entry	Nucleophile	Conversion[a] (%)	ee[b] (%)
1	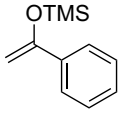	100	43
2	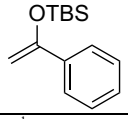	100	13

a. Conversions determined by ^{1}H NMR analysis of the crude reaction mixture are reported.
b. ee values determined by chiral HPLC analysis.

Table 4.9. ***Investigation of the promoter.***

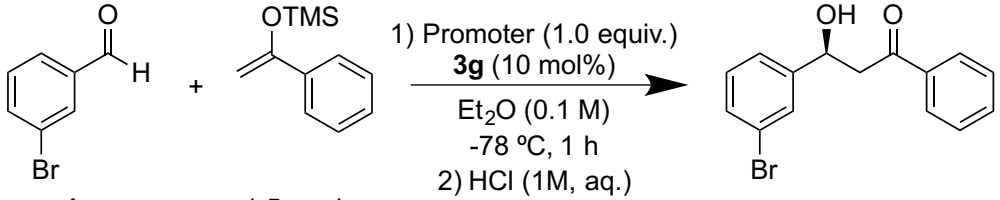

1a 1.5 equiv. **2a**

Entry	Promoter	Conversion[a] (%)	ee[b] (%)
1	TBSOTf	100	72
2	TESOTf	100	n.d.
3	TIPSOTf	100	79
4	TMSBr	n.r.	-
5	HCl[c]	n.r.	-

a. Conversions determined by ^{1}H NMR analysis of the crude reaction mixture are reported.
b. ee values determined by chiral HPLC analysis.
c. 2M HCl solution in Et_2O was used in this reaction.

Table 4.10. ***Investigation of the reaction concentration.***

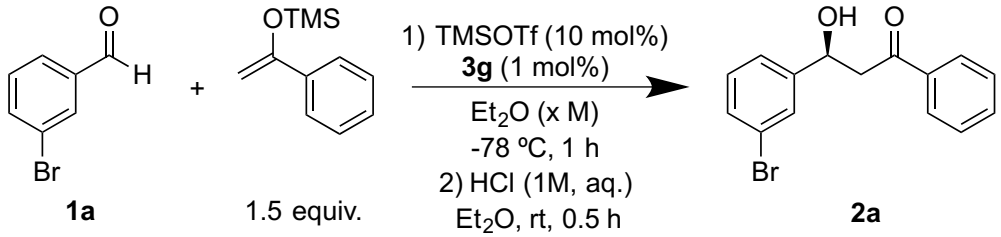

Entry	Concentration (M)	Conversion[a] (%)	ee[b] (%)
1	0.025	58	80
2	0.05	98	80
3	0.1	100	81
4	0.2	100	71
5	0.5	100	57

a. Conversions determined by ^{1}H NMR analysis of the crude reaction mixture are reported.
b. ee values determined by chiral HPLC analysis.